Einsatz humaner Stammzellen für die kardiale und osteogene Geweberegeneration

DISSERTATION

der Mathematisch-Naturwissenschaftlichen Fakultät
der Eberhard Karls Universität Tübingen
zur Erlangung des Grades eines
Doktors der Naturwissenschaften
(Dr. rer. nat.)

vorgelegt von
M.Sc. Marbod Christian Weber
aus Villingen-Schwenningen

Tübingen
2022

Gedruckt mit Genehmigung der Mathematisch-Naturwissenschaftlichen Fakultät der Eberhard Karls Universität Tübingen.

Tag der mündlichen Qualifikation:	02.08.2022
Dekan:	Prof. Dr. Thilo Stehle
1. Berichterstatter/-in:	Prof. Dr. Meltem Avci-Adali
2. Berichterstatter/-in:	Prof. Samuel Wagner, PhD

Danksagung

In erster Linie möchte ich mich bei Frau Prof. Dr. Meltem Avci-Adali und Herrn Prof. Dr. Hans-Peter Wendel für die Ermöglichung der Promotion im klinischen Forschungslabor der Thorax-, Herz- und Gefäßchirurgie am Universitätsklinikum Tübingen bedanken. Mein besonderer Dank gebührt hierbei Frau Prof. Avci-Adali, für die stets gute Betreuung, konstruktive Kritik und das mir entgegengebrachte Vertrauen während der gesamten Zeit. Ebenfalls möchte ich meinen Dank an Prof. Wagner für die Betreuung und die Begutachtung der Dissertation aussprechen.

Mein weiterer Dank gilt allen Mitarbeitern und Studenten des klinischen Forschungslabors der THG Chirurgie, sowie allen Kooperationspartnern, welche die gesamte Zeit durch ihre freundliche Art, ihre Hilfsbereitschaft und ihr Engagement zum Gelingen dieser Arbeit einen wesentlichen Teil beigetragen haben. Insbesondere möchte ich mich hier bei Dr. Heidrun Steinle für die ausgezeichnete Projektübergabe, die Einarbeitung und die erfolgreiche Zusammenarbeit bedanken.

Ganz besonders danken möchte ich außerdem meiner lieben Frau und Kollegin Josefin, die mich seit über 10 Jahre unterstützt und durch ihre Zielstrebigkeit, gemeinsame Forschungsprojekte maßgeblich vorangebracht hat.

Zu guter Letzt möchte ich meine tiefe Dankbarkeit meiner Familie und meinen Schwiegereltern ausdrücken, welche mich jeder Zeit unterstützt haben und immer beratend zur Seite standen.

Inhaltsverzeichnis

Abkürzungsverzeichnis

ALPL	Alkaline phosphatase L
AP-1	Activator protein 1
bFGF	Basic fibroblast growth factor
C3 / C3a /C5a	Komplementfaktor C3 / C3a / C5a
CAM	Chorio-allantoic membrane
CPCs	Cardiac progenitor cells
DNA	Desoxyribose nucleic acid
pDNA	Plasmid DNA
eGFP	Enhanced green fluorescent protein
ELISA	Enzyme-linked immunosorbent assay
ESC	Embryonic stem cells
hESC	Human ESCs
FACS	Fluorescence-activated cell sorting
FII / FIIa	Factor II / Iia / XII / XIIa
GSK-3	Glycogen synthase kinase 3
IFN	Interferon
iPSC	Induced pluripotent stem cells
hiPSC	Human iPSCs
IRES	Internal ribosome entry site
IRF	Interferon-regulating-factor
ISG	Interferon-stimulated gene
IVIS	In vivo imaging system
IVT	In vitro transcription
JAK	Janus kinase
JPC	Jaw periosteal cells
Klf4	Kruppel-like factor 4
LGP2	Laboratory of genetics and physiology 2
MACS	Magnetic-activated cell sorting
MAVS	Mitochondrial antiviral-signaling protein
MDA5	Melanoma differentiation-associated protein 5
MRT	Magnetresonanztomographie
MSC	Mesenchymal stem cells
hMSC	Human MSCs
MyD88	Myeloid differentiation primary response 88
NF-κB	Nuclear-factor κB
NLR	NOD-like-receptor
NLRP3	NLR family pyrin domain containing 3
NOD2	Nucleotide-binding oligomerization domain-containing protein 2
nsP	Non-structural Protein
NuFF	Newborn Foreskin Fibroblasts
Oct4	Octamer-binding transcription factor 4
OKSM	Oct4, Klf4, Sox2 und c-Myc
ORF	Open reading frame
PAC	Puromycin N-acetyltransferase
PAMP	Pathogen-associated molecular pattern

PBMC	Peripheral blood mononuclear cells
PCL	Polycaprolacton
PDGF	Platelet-derived growth factor
PLGA	Polylactid-co-Glycolid
PMN-Elastase	Polymorphonuklear-Elastase
PRR	Pattern recognition receptors
qRT-PCR	Quantitative reverse transcription polymerase chain reaction
RBP	RNA-binding proteins
REC	Renal epithelial cells
REM	Rasterelektronenmikrokopie
RIG-I	Retinoic acid inducible gene I
RLR	RIG-I-like-receptor
RNA	Ribonucleic acid
dsRNA	Double stranded RNA
mRNA	Messenger RNA
srRNA	Self replicating RNA
ssRNA	Single stranded RNA
tRNA	Transfer RNA
SIRPα	Signal regulating protein α
SC5b-9	Soluble membrane attack complex
Sox2	Sex determining region Y
STAT	Signal transducer and activator of transcription proteins
TAT	Thrombin-Antithrombin-III-Komplex
TF	Tissue factor
TGF-β	Transforming Growth Factor
TLR	Toll-like-receptor
TRIF	TIR-domain-containing adapter-inducing interferon-β
VEE	Venezuelan equine encephalitis
VEGF	Vaskulärer endothelialer Wachstumsfaktor
Wnt	Wingless-related integration site
β-TCP	β-Tri-Calcium-Phosphat
β-TG	β-thromboglobuline

Zusammenfassung

Die Regenerative Medizin ist eines der vielversprechendsten Forschungsgebiete für die zukünftige Behandlung von Krankheiten, für die bisher noch keine oder nicht ausreichende Behandlungsmöglichkeiten zur Verfügung stehen. Ziel der regenerativen Medizin ist, einen durch Krankheit oder Gendefekt ausgelösten Funktionsverlust von einzelnen Zellen, Geweben oder ganzen Organen zu kompensieren oder gänzlich zu therapieren. Ein limitierender Faktor war hierbei der Mangel an patientenspezifischen Zellen, sowie die Nachbildung dreidimensionaler Gewebestrukturen, die eine erfolgreiche Integration der eingesetzten Implantate gewährleistet. Durch die Kombination verschiedener Fachgebiete, wie der Molekular- und Zellbiologie mit dem Tissue Engineering und der Biomaterialforschung, konnten in den letzten Jahrzehnten jedoch enorme Fortschritte erzielt werden. Insbesondere die Entdeckung und die Forschung an mesenchymalen- und pluripotenten Stammzellen, sowie die Möglichkeit aus somatischen Zellen iPSCs (Induced pluripotent stem cells) zu generieren, hat eine nahezu unerschöpfliche Quelle an patientenspezifischen Zellen hervorgebracht. Damit hiPSCs (human iPSCs) in einer klinischen Anwendung zum Einsatz kommen können, muss die Sicherheit der Zellen jedoch gewährleistet und eine Reaktivierung der Reprogrammierungsfaktoren nach der Implantation im Patienten ausgeschlossen werden.

Im Rahmen dieser Arbeit, wurde eine nicht-integrative synthetische srRNA (Self replicating RNA) verwendet, um RECs (Renal epithelial cells) zu hiPSCs zu reprogrammieren. Die Behandlung mit B18R Protein ermöglichte eine gezielte Steuerung der zellulären Typ-I-IFN (Interferon) Antwort und die erfolgreiche Reprogrammierung der Zellen. In den generierten hiPSCs konnten keine srRNA-Rückstände oder chromosomale Aberrationen festgestellt werden. Zudem wiesen sie typische Charakteristika pluripotenter Stammzellen auf, wie unter anderem die Fähigkeit in Zellen der drei Keimbahnen Mesoderm, Endoderm und Ektoderm zu differenzieren. Neben in vitro Untersuchungen konnte dies in einem erstmals hierfür eingesetzten alternativen Tiermodell auf der CAM (Chorion-allantoic membran) von befruchteten Hühnereiern gezeigt werden. Im weiteren Verlauf dieser Arbeit, konnten die aus RECs generierten hiPSCs zu kontrahierenden Kardiomyozyten differenziert werden. Nach einer ausführlichen Charakterisierung der differenzierten Kardiomyozyten über spezifische Marker-Proteine und das Ansprechen auf die Kalziumkanal-Modulatoren Nifedipin und Isoproterenol, wurde die Applikation der Zellen für einen potenziellen Einsatz nach einem Myokardinfarkt ex-vivo in Schweineherzen untersucht. Hierbei konnte gezeigt werden, dass eine neuartige wasserstrahlbasierte Zellapplikationsmethode zu einer verbesserten

räumlichen Verteilung im Myokard, bei einem ausschließlich geringen Verlust an Viabilität der applizierten Zellen, im Vergleich zu einer Nadelinjektion führt. Des Weiteren konnte mittels wasserstrahlbasierter Applikationsmethode eine unterwünschte Verteilung der Zellen in den Koronararterien deutlich reduziert werden. Dadurch könnte die Gefahr einer Stenose, die bei einer Injektion der Kardiomyozyten in die Herzkranzgefäße gegeben ist, gesenkt werden.

Ein vielversprechendes Einsatzgebiet in der regenerativen Medizin von mesenchymalen Stammzellen ist die Regeneration von Knochen im Bereich der Mund-, Kiefer- und Gesichtschirurgie. Um die osteogene Regeneration zu unterstützen, werden diese Zellen in Kombination mit Biomaterialien eingesetzt. Teil dieser Arbeit war, aus dem Kieferperiost isolierte mesenchymale Stammzellen, sogenannte JPCs (Jaw periosteal cells), auf einem β-TCP (β-Tri-Calcium-Phosphat)-Trägermaterial auszusäen und ihre osteogene Differenzierungskapazität zu analysieren. Zusätzlich sollte nach dem Kontakt mit Blut ein möglicher Einfluss der zellbesiedelten Konstrukte auf die Hämostase untersucht werden. Die Untersuchungen zeigten, dass PLGA (Polylactid-co-Glycolid)-beschichtete und unbeschichtete β-TCP-Gerüste mit JPCs besiedelt und weiter in osteogene Zellen differenziert werden können. Die Inkubation dieser Konstrukte mit humanem Vollblut zeigten eine Erhöhung des Gerinnungsmarkers TAT (Thrombin-Antithrombin-III-Komplex) sowie eine Anhäufung von Fibrinfasern auf den mit JPC besiedelten β-TCP-Gerüsten im Vergleich zu den Gerüsten ohne Zellen. Diese Studie zeigte, dass neben dem Biomaterial auch die darauf ausgesäten Zellen die Hämostase beeinflussen und somit die osteogene Regeneration beeinflussen können.

Der Einsatz von patientenspezifischen mesenchymalen und pluripotenten Stammzellen eröffnet enorme Möglichkeiten im Bereich der regenerativen Medizin. So können mesenchymale und mittels srRNA generierte pluripotente Stammzellen zu autologen Gewebezellen differenziert werden und zur Zelltherapie oder Generierung 3-dimensionaler Gewebekonstrukte eingesetzt werden. Dadurch kann zukünftig die Regeneration von Geweben und eine Behandlung von bisher nicht oder nicht vollständig heilbaren Krankheiten ermöglicht werden.

Abstract

Regenerative medicine is one of the most promising fields of research to treat diseases for which no or insufficient options of therapy are currently available. The aim of regenerative medicine is to compensate or completely heal loss of function of individual cells, tissues or entire organs caused by diseases or genetic defects. A limiting factor has been the lack of patient-specific cell material, as well as the generation of three-dimensional tissue structures for a successful tissue integration. However, by combining different disciplines, such as molecular and cellular biology with tissue engineering and biomaterial research, enormous progress has been made in the last decades. In particular, the discovery and research on mesenchymal and pluripotent stem cells, as well as the possibility to generate iPSCs from somatic cells, has revealed an almost inexhaustible source of patient-specific cells. However, for clinical application, the safety of hiPSCs must be ensured and reactivation of the reprogramming factors after implantation in the patient must be excluded.

Therefore, in this work, a srRNA was used to reprogram RECs into hiPSCs. By targeting the cellular type-I-IFN immune response using B18R protein, selective srRNA degradation was achieved after reprogramming. No srRNA residues or chromosomal aberrations were detected in the hiPSCs generated with this method. Moreover, the cells exhibited typical characteristics of pluripotent stem cells, such as the ability to differentiate into cells of the three germlines mesoderm, endoderm, and ectoderm. In addition to in vitro studies, this could be confirmed in an alternative animal model on the CAM of fertilized chicken eggs.

In addition, RECs based hiPSCs could be differentiated into contracting cardiomyocytes. After a detailed characterization of the differentiated cardiomyocytes by analyzing specific marker proteins and the response to the calcium channel modulators nifedipine and isoproterenol, the application of the cells was investigated ex-vivo in porcine hearts to investigate the use after myocardial infarction. It was shown that a novel waterjet-based cell application method leads to an improved spatial distribution in the myocardium with only a small loss of viability of the applied cells compared to a 23 G needle. In addition, the waterjet-based delivery method was shown to be a blood vessel gentle method. The risk of a further stenosis could be significantly reduced when cardiomyocytes did not enter the coronary vessels.

A promising field of application in regenerative medicine of mesenchymal stem cells is the regeneration of bone in the field of oral and maxillofacial surgery. To support osteogenic regeneration, biomaterials are often used in this application. Part of this work

was to seed JPCs on a β-TCP biomaterial and to analyze their osteogenic differentiation capacity. Additionally, after contact with blood, a possible influence of the cell-seeded constructs on hemostasis should be investigated. The studies showed that JPCs could be seeded on PLGA-coated and uncoated β-TCP scaffolds and further differentiated into osteogenic cells. Incubation with human whole blood showed no significant increase in most hemocompatibility markers analyzed (β-TG, Sc5B-9, PMN-elastase). However, an increase in TAT complexes and an accumulation of fibrin fibers were observed on the JPC-seeded β-TCP scaffolds compared with native scaffolds. Thus, this study suggests that in addition to the biomaterial, the cells seeded on the scaffold may also affect hemostasis and could influence osteogenic regeneration.

The use of mesenchymal and pluripotent stem cells opens enormous possibilities in the field of regenerative medicine. Mesenchymal and srRNA-generated pluripotent stem cells can be differentiated into autologous tissue cells and used for cell therapy or generation of 3-dimensional tissue constructs. Thus, enabling the future regeneration of tissues and treatment of previously incurable or incompletely curable diseases.

1 Einleitung

1.1 Regenerative Medizin

Die Geweberegeneration ist eine fundamentale Eigenschaft aller Lebewesen und kann als Fähigkeit bezeichnet werden, tote Zellen durch neu gebildete zu ersetzen, ohne dabei die ursprüngliche Zellzusammensetzung, Architektur und Funktion des Gewebes zu verändern. Die früheste bekannte Quelle, die sich mit der Geweberegeneration befasste, stammt aus der antiken griechischen Mythologie. Hierbei wurde überliefert, dass sich der Kopf der Hydra, ein mehrköpfiges Ungeheuer, nach Abtrennung an derselben Stelle erneut bildete. Herkules besiegte die Hydra schließlich, indem er ihren Hals verbrannte, bevor sich ein neuer Kopf ausbildete. Ein ähnliches regeneratives Potential wurde in einer Veröffentlichung von Spallazani 1769 bei der erstmaligen ausführlichen Beschreibung der Regeneration von Salamander Gliedmaßen festgehalten [1]. Wird beispielsweise durch Amputation bei einem zu den Schwanzlurchen gehörenden Axolotl ein Bein abgetrennt, kommt es, je nach alter des Tieres, über einen Zeitraum mehreren Wochen oder einiger Monate zu einer vollständigen Regeneration eines funktionsfähigen Beines [2]. Die postnatale Regenerationskapazität von Säugetieren unterscheidet sich jedoch grundlegend von der der Salamander [3]. Es wird vermutet, dass in Säugetieren die Fähigkeit der narbenlosen Regeneration möglicherweise zugunsten der Strategie aufgegeben wurde, mit einer größeren Bandbreite von Krankheitserregern umgehen zu können [4, 5].

Die moderne Regenerative Medizin ist ein multidisziplinäres Forschungsgebiet der Biomedizin und verbindet die Fachgebiete der Molekular- und Zellbiologie mit denen der Gewebezüchtung / des Tissue Engineerings und der Biomaterialforschung [6]. Ziel ist die Wiederherstellung von Zellen, Geweben oder ganzen Organen, deren Funktion durch angeborene und erworbene Erkrankungen, Traumata oder natürliche Alterungsprozesse eingeschränkt wurden oder diese gänzlich verloren haben. Dabei beschäftigt sich die Regenerative Medizin sowohl mit dem biologischen Ersatz [7] als auch mit der Anregung körpereigener Regenerations- und Reparaturprozesse [8]. Durch die Möglichkeit von Genom- und Transkriptomanalysen sowie der Stammzellforschung hat sich das Wissen zu den der Geweberegeneration zugrunde liegenden molekularen Mechanismen in den letzten drei Dekaden vervielfacht [9]. Dadurch hat sich die Rege-

nerative Medizin zu einem der vielversprechendsten Therapieansätze für Erkrankungen entwickelt, für die bisher nur unzureichende Behandlungs- bzw. Therapiemöglichkeiten zur Verfügung standen.

Der Funktionsverlust ganzer Organe als Folge verschiedenster Erkrankungen ist nach wie vor eine der häufigsten Todesursachen in jeglichen Altersgruppen. Durch mechanischen Ersatz, wie beispielsweise durch Dialysegeräte, chirurgische Rekonstruktion oder Organtransplantation, konnten im vergangenen Jahrhundert unzählige Leben gerettet werden. Dennoch bleiben diese Therapien unvollkommene oder nur temporäre Lösungen. Therapien mit mechanischen Vorrichtungen oder chirurgische Rekonstruktionen stehen häufig nur für spezifische Krankheitsbilder zur Verfügung und können meist nicht die gesamte Funktion eines Organs ersetzen oder können zu Folgeerkrankungen führen [10]. Ebenso ist die Transplantation von Organen durch einen permanenten Spendermangel stark eingeschränkt. Selbst Patienten, die eine Organtransplantation erhalten, müssen mit immunologischen Abstoßungsreaktionen rechnen und sind lebenslang auf die Einnahme von immunsuppressiven Medikamenten angewiesen. Anders als die Organtransplantation, strebt die Regenerative Medizin eine frühere Intervention an. Durch die Applikation von Stamm- oder Progenitorzellen, die in vitro oder in vivo zu der gewünschten Zellart differenzieren, der Stimulation endogener Reparaturmechanismen durch den Einsatz bioaktiver Materialien und das Freisetzen von Wachstumsfaktoren, oder durch Transplantation von biotechnologisch hergestellten Gewebestücken kann die Regeneration von erkranktem oder geschädigtem Gewebe eingeleitet werden, bevor es zum Organversagen kommt [11].

1.1.1 Tissue Engineering

Die Generierung dreidimensionaler funktioneller Gewebekonstrukte wird als „Tissue Engineering“ bezeichnet und setzt sich aus drei grundlegenden Komponenten zusammen [12]: 1. Gewebetypspezifische Zellen, die die benötigte Funktion erfüllen können; 2. Biomoleküle, die den Zellen gewebespezifische Signale vermitteln und gegebenenfalls eine weitere Differenzierung zur Zielzelle ermöglichen und 3. ein strukturelles Gerüst, das sowohl biologische als auch mechanische Funktionen der jeweiligen extrazellulären Matrix des Gewebes nachahmen kann [12, 13]. Dies erlaubt eine zielgerichtete und lokale Applikation der Zellen und stellt sicher, dass die vordefinierte dreidimensionale Struktur bis zur Integration in das Zielgewebe erhalten bleibt [14]. Für die Kultivierung der Gewebekonstrukte kommen meist Bioreaktoren zum Einsatz, die in

der Lage sind, mechanische Kräfte (Scherspannung, Dehnung und Kompression sowie Druckbelastungen) gewebespezifisch in vitro nachzuahmen und eine Kultivierung unter möglichst physiologischen Bedingungen ermöglichen [15].

Die im Tissue Engineering häufig eingesetzten Biomaterialien lassen sich in natürliche Materialien (Alginat, Kollagen), dezellularisierte Extrazellulärmatrices (Herzklappen, Blutgefäße), synthetische Polymere (PLGA, PCL (Polycaprolacton)) oder Keramiken (Hydroxylapatit, Calcium-Phosphat) einteilen [14, 16]. Mit verschiedenen Herstellungs- und Verarbeitungstechniken, wie Elektrospinning, Phasentrennung, Gefriertrocknung oder Selbstorganisation von Polymeren (z.B. in Hydrogelen), können einerseits die Architektur der extrazellulären Matrix des jeweiligen Gewebes auf Nanoebene nachgeahmt und andererseits biologische und mechanische Eigenschaften imitiert werden [17]. Darüber hinaus können die Oberflächen der Trägermatrices, auch als Scaffolds bezeichnet, modifiziert (z. B. Plasmabestrahlung) werden und mit funktionellen Gruppen (z. B. Arg-Gly-Asp-Peptid) und bioaktiven Faktoren (z.B. Wachstumsfaktoren) beschichtet werden. Dadurch können Adhäsion, Proliferation und Migration der Zellen ermöglicht oder gesteigert und somit die Integration des dreidimensionalen Gewebegerüsts ins umliegende Gewebe ermöglicht bzw. signifikant verbessert werden [14, 17]. Für den Einsatz im Menschen, sollte das ideale Biomaterial jedoch biologisch abbaubar und bioresorbierbar sein und keine Immunreaktionen auslösen. Abbauprodukte der Biomaterialien sollten über Stoffwechselwege ausgeschieden werden können, um die physiologischen Bedingungen im Gewebe aufrechtzuerhalten. Inkompatible Materialien, die durch Abbauprodukte Entzündungen oder Fremdkörperreaktionen hervorrufen, können zu Nekrosen oder Abstoßungsreaktionen führen [14].

Als funktionelle Einheit kommen beim Tissue Engineering humane Zellen zum Einsatz. Um die Hürden der Organtransplantationen durch Abstoßungsreaktionen und die damit verbundene Einnahme von Immunsuppressiva zu vermeiden, wird in der Regel auf patienteneigene (autologe) Zellen zurückgegriffen. Hierfür stehen neben bereits ausdifferenzierten Zellen und Progenitorzellen adulte und pluripotente Stammzellen zur Verfügung. Auf Grund der limitierten Verfügbarkeit von autologen gewebespezifischen Zellen sind insbesondere Stammzellen für die Regenerative Medizin von großem Interesse.

1.2 Stammzellen

Grundsätzlich werden drei Arten von Stammzellen unterschieden. Alle drei teilen die wichtige Eigenschaft der Selbsterneuerung sowie die Fähigkeit zur weiteren Differenzierung in verschiedene Zellarten. Eine hierarchische Unterteilung findet nach dem Fortschritt ihrer Spezialisierung in totipotente, pluripotente oder multipotente bzw. adulte Stammzellen statt (Abbildung 1) [18].

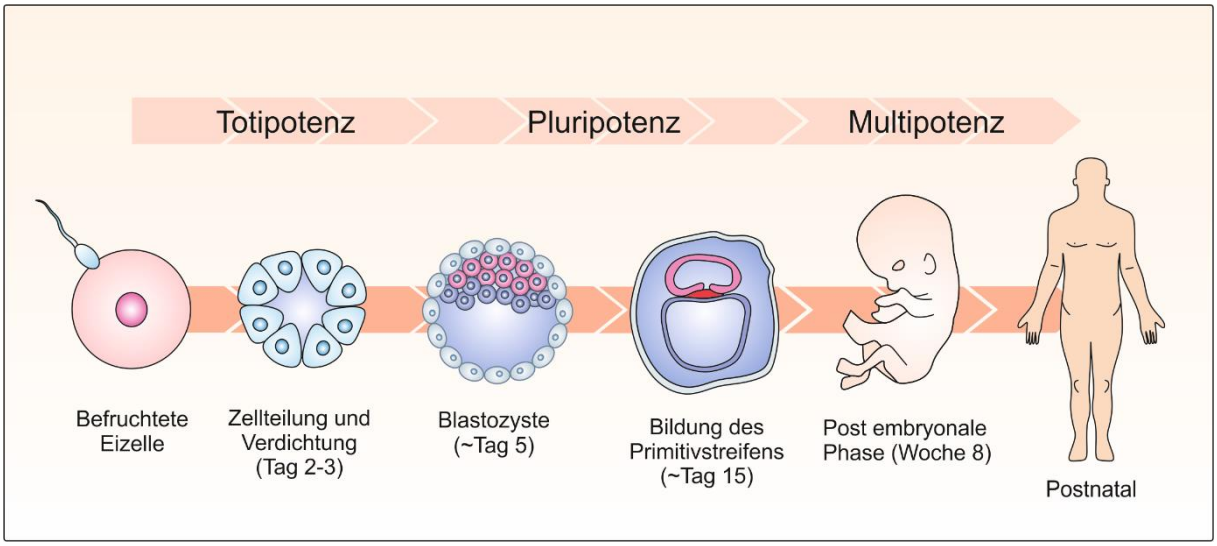

Abbildung 1: Embryogenese und hierarchische Einteilung von Stammzellen
Schematische Darstellung der Embryogenese. Mit zunehmender Spezialisierung geht die Differenzierungsfähigkeit der Stammzellen verloren. Ausgehend von einer befruchteten Eizelle kommt es über Teilung und Verdichtung der Zellen zur Ausbildung einer Blastozyste, womit die totipotente Eigenschaft verloren geht. Die pluripotenten Zellen bilden den Primitivstreifen und können sich in die Meso-, Endo- und Ektoderme Keimbahn differenzieren. Mit der weiteren Spezialisierung in der post-embryonalen Phase, bis hin zur Geburt, werden die Stammzellen multipotent und können sich ausschließlich in Zellen einer bestimmten Keimbahn differenzieren. Multipotente Stammzellen sind auch in ausgewachsenen Individuen zu finden und sind maßgeblich an der physiologischen Geweberegeneration beteiligt.

Totipotente Stammzellen sind die am wenigsten entwickelten Stammzellen. In dem Zeitraum nach der Befruchtung der Eizelle bis zum Stadium von vier bis acht Zellteilungen besitzen sie die Fähigkeit sich zu einem vollständigen Embryo zu entwickeln und das extra-embryonale Gewebe zu bilden [19]. Anschließend durchlaufen die Zellen weitere Teilungen bis zum Erreichen des Blastozystenstadiums, in dem sie eine pluripotente Identität annehmen und ab diesem Zeitpunkt ausschließlich in die drei embryonalen Keimbahnen (Mesoderm, Endoderm und Ektoderm) differenzieren können. Mit weiteren Teilungen und dem Eintritt in die postembryonale Phase steigt der Grad der Spezialisierung, was mit dem Verlust der Pluripotenz einhergeht. Die Diffe-

renzierungsfähigkeit dieser multipotenten Stammzellen ist auf Zellarten einer bestimmten Keimbahn bzw. einer Gewebeart beschränkt. Da diese Stammzellen auch in ausgewachsenen Individuen zu finden sind, spricht man hierbei auch von „adulten Stammzellen“ [19].

1.2.1 Multipotente / Adulte Stammzellen

Adulte multipotente Stammzellen befinden sich in einem metabolisch ruhenden Zustand in fast allen spezialisierten Körpergeweben und sind aktiv an der Geweberegeneration nach Verletzungen aber auch bei der physiologischen Erneuerung von Zellen beteiligt. Auf Grund ihres Vorkommens in jedem Individuum und der Möglichkeit eines autologen Einsatzes, werden adulte Stammzellen häufig als Goldstandard bei stammzellbasierten Therapien bezeichnet [20, 21]. Eine weitere Unterteilung der multipotenten Stammzellen kann je nach ihrem Gewebevorkommen und ihrer Spezialisierung beispielsweise in hämatopoetische, mesenchymale, Nerven- und Hautstammzellen stattfinden [18].

Mesenchymale Stammzellen

MSCs (Mesenchymal stem cells) wurden erstmals 1966 von Friedenstein et al. aus dem Knochenmark isoliert und im Verlauf der Forschungsarbeit als Fibroblasten-ähnliche koloniebildende Zellen mit Differenzierungspotential zu Osteoblasten, Chondrozyten und Adipozyten beschrieben [22-24]. Bis heute konnten mesenchymale Stammzellen aus zahlreichen anderen Geweben, wie Skelettmuskelgewebe [25], Fettgewebe [26], Synovialmembranen [27], Kieferperiost [28], Nabelschnur [29] und Nabelschnurblut [30], Lungengewebe [31], Lebergewebe [26] und aus Hautgewebe [25] isoliert werden. Zusätzlich zum osteogenen, chondrogenen und adipogenen Differenzierungspotential, konnte eine Differenzierung der MSCs zu Tenozyten [32], Skeletmuskelzellen [33] und Fibroblasten [34], sowie in vitro, eine Transdifferenzierung zu nichtmesodermen Zellen wie Neuronen-ähnlichen Zellen [35], Hepatozyten [36] und pankreatische Inselzellen [37] nachgewiesen werden.

Das therapeutische Potential dieser Zellen beruht, neben der Eigenschaft sich in verschiedene Zellarten zu differenzieren, auf der Fähigkeit, chemotaktisch an den Ort von Verletzung zu wandern [38] und mit der Sezernierung parakriner Faktoren [39] und der Modulation der Immunantwort [40] das Überleben und die Proliferation von umliegenden Gewebezellen positiv zu beeinflussen. Diese regenerativen und protektiven Ei-

genschaften sowie das natürliche Vorkommen in vielen Geweben führten zu den Ansätzen, hMSCs (human MSCs) für die Behandlung von diversen Krankheiten, wie Diabetes, neurologische- und Autoimmunerkrankungen, Leber-, Nieren- und Lungenerkrankungen, verschiedener inflammatorische, neurologische und kardiovaskuläre Erkrankungen sowie für die Regeneration von Knochen und Knorpelgewebe einzusetzen [41].

1.2.2 Pluripotente Stammzellen

Im Gegensatz zu adulten Stammzellen, die einer gewissen Seneszenz unterliegen und somit ein limitiertes Proliferations- und Differenzierungspotential aufweisen [42], besitzen pluripotente Stammzellen die Fähigkeiten der Selbsterneuerung und die Potenz, in nahezu alle Zelltypen der drei Keimbahnen (Mesoderm, Endoderm und Ektoderm) zu differenzieren [43]. Lediglich die Differenzierung in Keimzellen und somit die Fähigkeit zur Bildung eines neuen Individuums bleibt ihnen verwehrt. Diese Eigenschaften ermöglichen eine unbegrenzte Kultivierung und die Generierung gewebespezifischer Zellen für verschiedene medizinische Anwendungen.

Embryonale Stammzellen

ESCs (Embryonic stem cells) werden nach den ersten acht Zellteilungen der fötalen Entwicklung aus der inneren Zellmasse von Blastozysten extrahiert (Abbildung 1). Die anschließende Kultivierung unter genau definierten Bedingungen, ermöglicht den Stammzellen, sich unbegrenzt zu teilen, ohne dabei in andere Zellen auszudifferenzieren. Trotz zahlreicher Einsatzmöglichkeiten, die vor allem hESCs (human ESCs) für die Forschung und Medizin eröffnen, gibt es eine Reihe von technischen und ethischen Problemen, die die Verwendung von hESC einschränken [44]. Da die Isolation von hESCs aus der Blastozyste mit der Zerstörung des Embryos einhergeht („verbrauchende Embryonenforschung“), wirft dies ethische Bedenken auf [45]. In Deutschland wird insbesondere die Frage diskutiert, ab wann der Embryo als menschliches Wesen gilt und somit unter dem Würdeschutz des Grundgesetzes steht [46]. Internationale rechtliche Regelungen, welche Großteiles auf der Beurteilung dieser ethischen Bedenken beruhen, variieren und schränken die Verwendung von hESCs für Forschung und Medizin in den jeweiligen Ländern unterschiedlich stark ein [47]. Zusätzlich zur ethischen Problematik und der allgemeinen Gefahr der Teratombildung durch undifferenzierte pluripotente Stammzellen im Patienten, handelt es sich bei hESCs um eine sel-

tene und ausschließlich allogen verfügbare Zellart. Immunreaktionen mit einem ausgeprägten Risiko der Abstoßung sowie die schlechte Verfügbarkeit von embryonalem Gewebe beschränken klinische Anwendungen. Um diese Problematik zu umgehen, arbeitet die Stammzellforschung an alternativen Möglichkeiten. Seit einigen Jahren ist beispielsweise die Umwandlung vollständig differenzierter adulter somatischer Zellen in PSCs möglich.

Induzierte Pluripotente Stammzellen

Das Konzept der Generierung von PSCs durch eine gezielte Umwandlung (=Reprogrammierung) von somatischen Zellen wurde bereits 1958 von Gordon nach dem erfolgreichen Zellkerntransfer einer Darmzelle einer Xenopus-Kaulquappe in ein enukleiertes Froschei entdeckt [48]. Die Annahme, dass das Zytoplasma des Froscheis Faktoren enthält, die das Genom der differenzierten Zelle in einen totipotenten Embryo im Ein-Zell-Stadium umprogrammiert, wurde von Shinya Yamanaka aufgegriffen und 2006 mit der gezielten Einbringung der vier Transkriptionsfaktoren (Abbildung 2) Oct4 (octamer-binding transcription factor 4), Klf4 (Krüppel-like factor), Sox2 (sex determining region Y-box 2) und c-Myc in den Zellkern, erstmals ohne Zellkerntransfer, iPSCs aus murinen und wenig später aus humanen Fibroblasten generiert [49, 50]. Im Vergleich zu hESCs und dem somatischen Zellkern Transfer ist die Generierung von hiPSCs aus patienteneigenen Zellen ethisch unbedenklich und ermöglicht die autologe Generierung von nahezu allen Zellarten (ausgenommen Keimzellen) in vitro, welche anschließend zum Erforschen von Krankheiten, neuen Medikamenten und deren Wechselwirkungen oder als Quelle für den Gewebeersatz in der regenerativen Medizin eingesetzt werden können. Aktuell sind 57 klinische Studien gemeldet (in Planung, Patientenrekrutierung und Abgeschlossen), die eine Behandlung von diversen Krankheitsbildern mit hiPSCs anstreben (Stand Jan. 2022; https://www.clinicaltrials.gov).

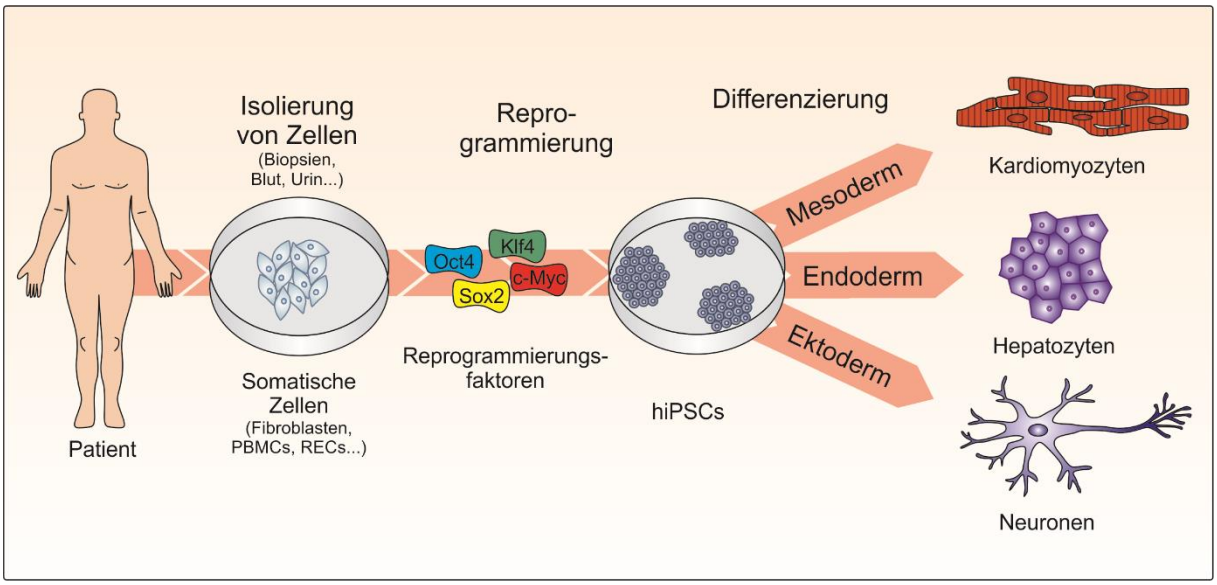

Abbildung 2: Reprogrammierung somatischer Zellen zu hiPSCs und anschließende Differenzierung zu gewebespezifischen Zellen
Schematische Darstellung der Reprogrammierung von humanen somatischen Zellen. Anders als bei ESCs geht die Gewinnung von hiPSCs von adulten Zellen aus (vgl.: Abbildung 1). Gängige somatische Zellarten sind hierbei Fibroblasten, oder RECs, welche über Hautbiopsien, Blutentnahme oder Urinproben entnommen, isoliert und gegebenenfalls in vitro expandiert werden. Durch das Einschleusen oder die erzwungene Expression von Reprogrammierungsfaktoren (z.B. Klf4, Oct4, Sox2, c-Myc) können hiPSCs generiert werden, welche anschließend wieder zu gewebetypischen Zellen differenziert werden können und somit für die Regenerative Medizin, die Erforschung von Krankheiten oder pharmakologische Untersuchungen bereitstehen.

1.3 Generierung von iPSCs

Die Reprogrammierung von somatischen Zellen basiert auf der gezielten Aktivierung von Genen durch Transkriptionsfaktoren, welche für die Aufrechterhaltung der Pluripotenz im embryonalen Stadium zuständig sind. Als zentrale Pluripotenzfaktoren werden neben Oct4, meist Sox2 und Nanog aufgeführt, da diese sowohl in murinen als auch humanen ESCs am stärksten exprimiert werden [51, 52] und nachweislich zur Generierung von iPSCs eingesetzt werden können [53]. Trotz der zentralen Bedeutung für die Aufrechterhaltung der Pluripotenz, hat sich gezeigt, dass der Transkriptionsfaktor Nanog für die Induktion der Pluripotenz von murinen und humanen somatischen Zellen durch die Faktoren Klf4 und c-Myc ersetzt werden kann [49, 50]. Eine weiterführende Studie legt jedoch nahe, dass Klf4 dies über eine Regulation von Nanog erreicht [54]. Zusätzlich zu den Transkriptionsfaktoren ist mittlerweile bekannt, dass auch epigenetische Faktoren wie die kovalente Modifikation von Histonen, die Methylierung und Acetylierung von DNA (Desoxyribonukleinsäuren) sowie nicht-kodierende RNAs (Ribonucleinsäuren) eine wichtige Rolle bei der Aufrechterhaltung der Pluripotenz von Stammzellen besitzen [55, 56] und während der Reprogrammierung zumindest teilweise an die Modifikationen von ESCs angepasst werden [57]. Trotz dieser Erkenntnis

sind über die genauen Abläufe des Reprogrammierungsprozesses noch wenig detailliertere Forschungsergebnisse verfügbar. Dies liegt maßgeblich an der sehr geringen Reprogrammierungseffizienz von meist deutlich unter 1%, was eine Transkriptom- und Proteomanalyse zu definierten Zeitpunkten deutlich erschwert.

Nach der erfolgreichen Generierung von iPSCs ist eine detaillierte Charakterisierung der Zellen notwendig. Neben dem Ausschluss genomischer Aberrationen und der Expression von Proteinen, die mit Stammzelleigenschaften assoziiert sind, ist die Bestätigung der Pluripotenz erforderlich. Der Nachweis der Pluripotenz findet weitestgehend in immundefizienten Mäusen durch die Injektion und der anschließenden Bildung eines Teratoms statt. Durch das Abhandensein von Abstoßungsreaktionen führt die subkutane oder intramuskuläre Injektion von iPSCs zu einer spontanen Differenzierung und der damit verbundenen Bildung eines Teratoms, welches nach der Explantation und Sektion auf Zellenarten der drei verschiedenen Keimbahnen untersucht werden kann [58].

1.3.1 Somatische Zellquellen

Nach der erstmaligen Generierung aus humanen Fibroblasten, konnte die erfolgreiche Generierung von iPSCs bereits aus vielen verschiedenen somatischen Zellquellen wie PBMCs (Peripheral blood mononuclear cells) [59], Keratinozyten aus Haarwurzeln [60] und RECs (Renal epithelial cells) aus dem Urin [61] dokumentiert werden. Im Vergleich zu Fibroblasten, für deren Isolation eine Hautbiopsie und somit ein invasiver Eingriff benötigt wird, stellt die Isolation von RECs einen einfachen und Pateientenfreundlichen Ansatz dar. Aufgrund der physiologischen Selbsterneuerung des Epithelgewebes im Harntrakt werden täglich ca. 2.000 bis 7.000 Epithelzellen des proximalen Nierentubulus abgelöst und mit dem Urin ausgeschieden [62]. Die Isolation von RECs aus Urin ist somit eine einfache und nicht-invasive Strategie zur Gewinnung patienteneigener somatischer Zellen.

1.3.2 Reprogrammierungsmethoden

Grundsätzlich können für die Induktion der Pluripotenz in somatischen Zellen integrierende und nicht-integrierende Reprogrammierungsmethoden eingesetzt werden. Bei der Generierung von iPSCs mittels Genom-integrierenden viralen Vektoren (z.B. Retroviren) werden die gewünschten Transgene, die für die Reprogrammierungsfaktoren kodieren, mit Hilfe der Viren in die Zielzelle geschleust und zufällig ins Genom integriert. Neben einer erhöhten Immunogenität der integrierenden Vektoren [63], kann die

permanente Präsenz im Genom auch nach der erfolgreichen Reprogrammierung zu einer Reaktivierung der Transkriptionsfaktoren und somit zu einer Änderung der Genexpression oder der DNA-Methylierung führen [64]. Insbesondere bei der Verwendung des Proto-Onkogens c-Myc als Verstärker der Pluripotenzfaktoren, wurde hierdurch eine deutlich gesteigerte Tumorentstehung in Mäusen beobachtet [65, 66]. Eine gezielte Exzision der viralen Vektorsequenzen nach der Reprogrammierung kann durch die Erweiterung der Vektorsequenz, wie beispielsweise durch einen für das Cre-Lox oder PiggyBac System kodierenden Bereich, erreicht werden [67]. Die Bedenken einer Reaktivierung der Transkriptionsfaktoren bei einer nicht erfolgreichen Deletion der viralen Vektorsequenz bleiben jedoch bestehen. Mittlerweile sind eine Reihe von nicht-integrierenden Reprogrammierungsmethoden, wie Sendai- [68] und Adenoviren [69], Proteinen [70], pDNA (Plasmid DNA) [71], niedermolekulare Verbindungen [72] oder die Verwendung von synthetischer mRNA (Messenger RNA) [73] etabliert und haben die Bedenken hinsichtlich einer genomischen Integration reduziert.

RNA basierte Reprogrammierung

In den letzten Jahren hat vor allem die Verwendung von synthetischer mRNA als eine vielversprechende Alternative zu integrierenden und nicht-integrierenden Methode an Bedeutung gewonnen [74]. mRNAs, die beispielsweise für die OKSM Reprogrammierungsfaktoren (Oct4, Klf4, Sox2 und c-Myc) und Lin28 kodieren, können mittels in IVT (In vitro transcription) synthetisiert und durch die Transfektion mittels Lipid-basierter Vehikel zur Induktion der Pluripotenz von somatischen Zellen eingesetzt werden [73, 75]. Die Ergänzung einer mRNA, die für ein fluoreszierendes Reporterprotein kodiert, kann eine fluoreszenzmikroskopisch Beurteilung der Transfektionseffizienz ermöglichen [75].

Der größte Vorteil von mRNA ist, dass sie im Zytoplasma verbleibt und auf Grund ihrer Unterschiede im molekularen Aufbau zu DNA nicht ins Genom integriert werden kann. Die Gefahr einer Integrationsmutagenese kann somit ausgeschlossen werden. Ein weiterer Vorteil besteht in den transienten Eigenschaften der mRNA. Durch natürliche Abbauprozesse werden die mRNA Moleküle nach etwa 2-3 Tagen degradiert [73, 76]. Eine Reaktivierung der Reprogrammierungsfaktoren zu einem späteren Zeitpunkt ist somit ausgeschlossen. Ein Vorteil gegenüber pDNA ist, dass das Umschreiben der DNA in mRNA, bereits während der IVT durchgeführt wurde. Die Translation der

mRNA in das jeweilige Protein kann somit direkt nach dem Einbringen durch die zelleigenen Ribosomen im Zytoplasma stattfinden. Im Vergleich dazu muss pDNA zunächst im Zellkern transkribiert werden. Da die intakte Zellkernmembran jedoch nicht überwunden werden kann, kann pDNA nur in Zellen translatiert werden, die zum Zeitpunkt der Exposition eine Mitose durchlaufen und die Kernmembran nicht vorhanden ist [77]. Zusätzlich wird die Transfektionsrate der Zielzellen durch die Größe der pDNA beeinträchtig [78]. Neben einer verzögerten Proteinexpression ist somit auch die Expressionseffizienz gegenüber einer mRNA basierten Transfektion deutlich geringer [79, 80]. Durch die transienten Eigenschaften der mRNA kann die kontinuierliche Expression der Proteine über den gesamten Reprogrammierungsprozess von etwa zwei Wochen nur durch eine tägliche Transfektion der Zellen mit dem gesamten mRNA Cocktail erreicht werden [73]. Dies verstärkt die Aktivierung des angeborenen Immunsystem, was zu erhöhtem zellulärem Stress, dem Abbau der RNA und zum Zelltod führen kann [81, 82]. Die Reduktion der Immunogenität der mRNA ist somit zwingend notwendig und kann mit dem Einbau von modifizierten RNA Nukleotiden, während der IVT erreicht werden [83]. Zusätzlich besteht die Möglichkeit, mit der Zugabe eines Typ I-IFN-Inhibitors in Form einer weiteren mRNA oder direkt als Protein, die Immunreaktionen zu inhibieren [84, 85]. Die gewonnene Sicherheit und Effizienz der mRNA basierten Reprogrammierung, geht jedoch mit erhöhten Kosten und erhöhtem Zeit- und Arbeitsaufwand einher. Um diese Aspekte zu umgehen, wurden die Vorteile viraler Vektoren mit denen der mRNA in sogenannten srRNAs vereint.

srRNA basierte Reprogrammierung

Die Verwendung einer srRNA für die Generierung von iPSCs wurde erstmals von Yoshioka et al. im Jahr 2013 veröffentlicht [86]. Ziel dieser Studie war die Entwicklung einer einzelnen RNA, die in der Lage ist, sich für eine begrenzte Anzahl von Zellteilungen selbst zu replizieren und dadurch die Anzahl der Transfektionen zu reduzieren. Mit mindestens vier ORFs (Open reading frame) sollte die Integration der Sequenzen und die konsistente Expression der Reprogrammierungsfaktoren (Oct4, Klf4, Sox2 und c-Myc) über mehrere Zellteilungen hinweg ermöglicht werden und dennoch ein kontrollierter Abbau der srRNA nach dem Reprogrammierungsprozess möglich sein. Als Ausgangskonstrukt wurde hierfür ein nicht infektiöses, aber selbstreplizierendes RNA Replikon, basierend auf Genabschnitten des VEE (Venezuelan Equine Encephalitis) Virus gewählt [87]. Das VEE Virus gehört zu den Alphaviren und ist somit ein positives

ssRNA (Single stranded RNA)-Virus. Wie typisch für Alphaviren bringt es die Information für eine RNA Polymerase in Form der nsPs 1-4 (Non-structural proteins 1-4) mit (Abbildung 3A) [88-90]. Durch die Expression der nsPs, die durch die Translationsmaschinerie der Wirtszelle gewährleistet wird, ist das Virus in der Lage, über den Zwischenschritt eines negativen RNA Strangs, seine genomische RNA zu replizieren und über den 26S Promotor eine subgenomische RNA zu generieren (Abbildung 3B). Die subgenomische RNA kodiert hierbei für die viralen Strukturproteine, wie des Kapsid (C) und die Glykoproteine (E2 und E1), welche im Anschluss an die Translation ko- und posttranslational modifiziert werden und nach dem Transport zur Wirtszellmembran neue Viruspartikel bilden [89].

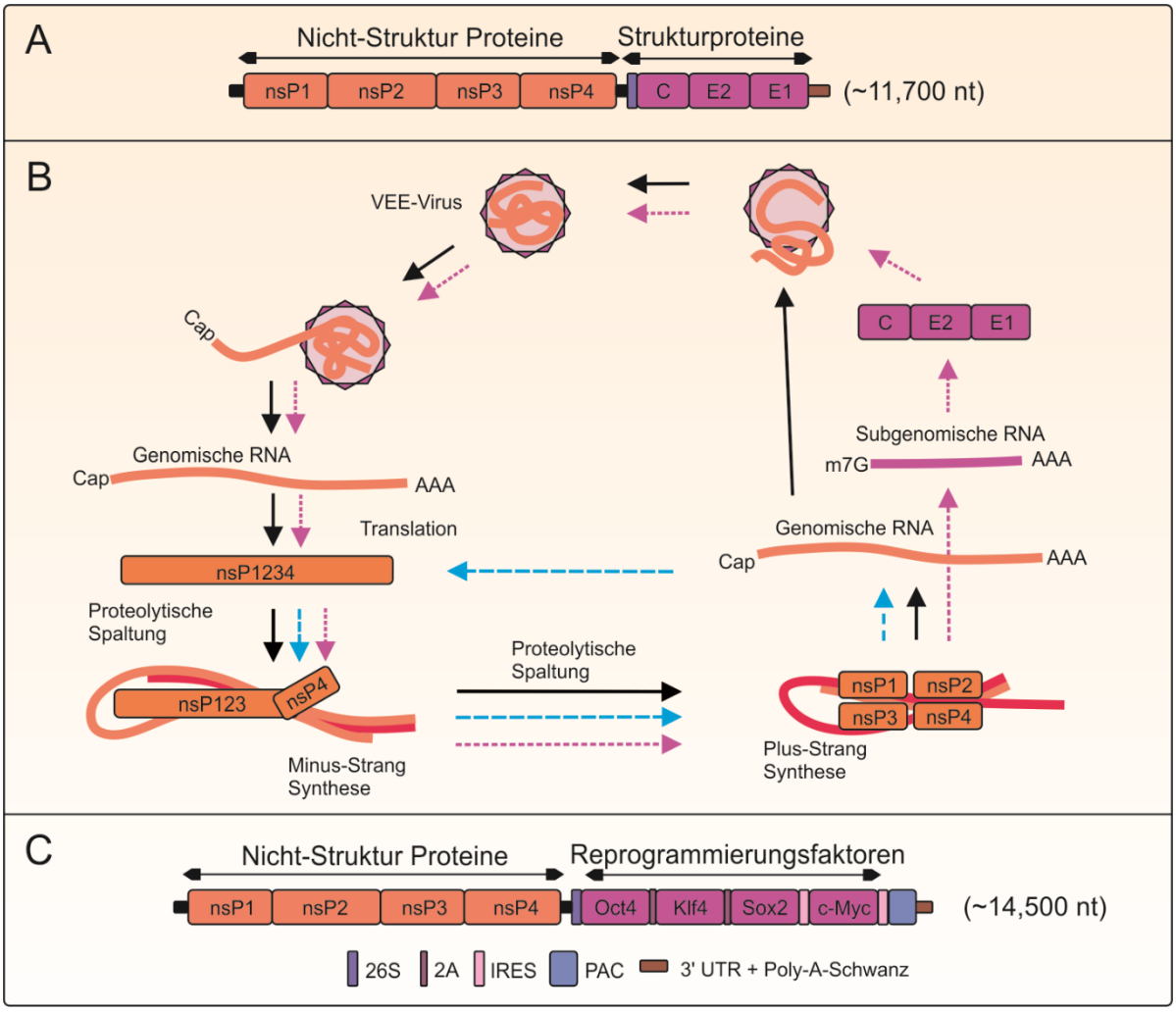

Abbildung 3: Struktur und Zyklus des VEE Virus und der VEE srRNA
A) Schematische Darstellung des VEE-Virus Genoms mit den nsP1-4 und der Strukturproteine C, E2 und E1. B) Darstellung eines schematischen Replikationszyklus eines VEE-Virus im Wirt. Durch die Freisetzung der genomischen RNA im Wirt kommt es zur Translation der nsP1-4. Damit wird die Minus-Strang-Synthese eingeleitet. Der Minus-Strang dient als Matrize für die genomischen sowie der subgenomischen RNA und wird nach einer erneuten proteolytischen Spaltung der nsPs generiert. Die Translation der subgenomischen RNA führt zur Bildung der Strukturproteine (C, E2 und E1) und zur Bildung neuer Virus-Kapside (Lila Zyklus). Die genomische RNA kann in einer Amplifikationsschleife (blauer

Zyklus) entweder erneut translatiert werden oder als Minus-Strang Matrize für die Generierung weiter genomischer RNAs dienen. Die genomische RNA kann anschließend, durch das Verlassen der Amplifikationsschleife, zusammen mit dem aus der subgenomischen RNA gebildeten Virus Kapsid zu einem funktionellen Virus verpackt und freigesetzt werden (schwarzer Zyklus). C) Schematische Darstellung der VEE-OKSiM-srRNA mit den nsP1-4 die für die Selbstreplikation der srRNA in der Wirtszelle sorgen. Die Strukturproteine wurden durch die Reprogrammierungsfaktoren Oct4, Klf4, Sox2 und c-Myc sowie einer PAC ersetzt.

Die VEE srRNA basiert auf dem VEE Replikon, das mit einem 5′-Cap und Poly(A)-Schwanz zelluläre mRNA nachahmt [87]. Die nicht-Struktur-Proteine (nsP1-4) kodieren wie beim VEE Virus für den Selbstrelikationskomplex der RNA (vgl. Abbildung 3A-C). Die Sequenz der Strukturproteine (S, E2 und E1) wurden jedoch durch die der Reprogrammierungsfaktoren Oct4, Klf4, Sox2 und c-Myc bzw. Glis1 ersetzt [86]. Die Erweiterung der Sequenz um virale 2A Peptide oder IRES (Internal ribosome entry site) ermöglicht eine Trennung der einzelnen Reprogrammierungsfaktoren nach der Translation bzw. die Cap-Struktur-unabhängige Translation der Proteine [86]. Zusätzlich wurde die Sequenz für eine PAC (Puromycin N-acetyltransferase) ergänzt, um eine Positivselektion der transfizierten Zellen mit dem zytotoxischen Puromycin zu ermöglichen. In nicht transfizierten Zellen kann Puromycin mit seiner Ähnlichkeit zu einer Tyrosin kodierenden tRNA (Transfer RNA) an der Bindungsstelle der Ribosomen eintreten und kovalente an mRNA mit GGU Kodon binden [91]. Dadurch kommt es zur frühzeitigen Termination der Proteinsynthese und die Zelle stirbt aufgrund der Anhäufung von Fehlerhaften Proteinen. PAC acetyliert und blockiert die reaktive Aminogruppe in Puromycin, wodurch die Bildung von Peptidbindungen verhindert und die Wirkung inhibiert wird [91].

Da die Replikation der srRNA unter Verwendung der zelleigenen Nukleotide im Zytoplasma der Wirtszelle stattfindet, ist eine einzige Transfektion ausreichend, was den zellulären Stress und die Immunogenität zunächst reduzieren. Auf Grund ihrer Ähnlichkeit zu Alphaviren mit einem doppelsträngigen RNA (dsRNA)-Zwischenprodukt, der starken Replikation und ihrer Größe von etwa 14.500 Nukleotiden, wird die srRNA dennoch als fremd erkannt und eine Immunreaktion eingeleitet [92, 93]. Im Fall der srRNA kann diese Eigenschaft genutzt werden, um die Selbstreplikation der srRNA zu unterbrechen und rückstandsfreie iPSCs zu generieren.

Selektive (sr)RNA Degradierung

Um sich vor Pathogenen wie Viren schützen zu können, haben sich bereits früh in der Entwicklung von Eukaryoten Mechanismen etabliert, mit denen Pathogene möglichst schnell und unspezifisch unschädlich gemacht werden können. Die Erkennung der

Krankheitserreger erfolgt über PRRs (pathogen recognition receptors), die PAMPs (Pathogen-associated molecular patherns) wie beispielsweise exogene RNA erkennen und Immunreaktionen einleiten. Für die Erkennung der Fremd-RNA sind insbesondere die zu den PRRs gehörenden TLR (Toll-like-receptors) sowie die RLRs (RIG-I-like receptors) und NLRs (NOD-like receptors) zuständig (Abbildung 4) [94]. Eine Aktivierung der in Endosomen lokalisierten TLR3 [95], TLR7 [96] und TLR8 [97] mittels ssRNA (TLR7/8) oder dsRNA (TLR3) löst den MyD88 (Myeloid differentiation primary response 88)- bzw. TRIF (TIR-domain-containing adapter-inducing interferon-β)-abhängigen Signalweg aus und führt zur Aktivierung der IRF 3/7 (Interferon-regulierenden Faktoren) bzw. IRF5/7, des NF-κB (Nuclear-factor κB) und des AP-1 (Activator protein-1), welche in Folge eine Typ I-IFN (IFN-α und IFN-β) abhängige antivirale Immunreaktion und die Freisetzung von proinflammatorischen Zytokinen und Chemokinen auslösen (Abbildung 4C) [98, 99]. Anders als TLRs sind RLRs mit ihren drei bekannten Vertretern RIG-I (Retinoic acid-inducible gene I), MDA5 (Melanoma differentiation-associated protein 5) und LGP2 (Laboratory of Genetics and Physiology 2) direkt im Zytosol lokalisiert. Während RIG-I hauptsächlich nicht verkappte 5'-Triphosphat Enden von ssRNA und dsRNA erkennt [100, 101], bevorzugt LGP2 die Bindung an abgeschnittene dsRNA Enden sowie an MDA5, wodurch dessen Signalweiterleitung nach der Bindung von großen dsRNAs (>2000 bp) verstärkt wird [92]. Während noch nicht vollständig geklärt ist, ob LGP2 auch zu einer direkten Signalweiterleitung ohne MDA5 fähig ist [102], mündet die Aktivierung von RIG-I und MDA5 über den MAVS (Mitochondrial antiviral-signaling protein)-abhängigen Signalweg, wie bei TLR7/8, in der Aktivierung der Transkriptionsfaktoren IRF 3/7 und NF-κB und einer Typ-I-IFN Antwort [103, 104]. Die ebenfalls im Zytoplasma lokalisierten NLRs sind mit ihren 20 Vertretern hauptsächlich auf die Erkennung von bakteriellen Toxinen sowie Zellwandbestandteilen spezialisiert [105]. Die zu den NLRs gehörenden NOD2 (Nucleotide-binding oligomerization domain-containing protein 2) und NLRP3 (NLR family pyrin domain containing 3) sind jedoch zusätzlich auch bei der intrazellulären Erkennung von viraler ssRNA bzw. dsRNA beteiligt. Diese führen wiederum unter Beteiligung von MAVS und IRF3 zu einer Typ-I-IFN Antwort [106] oder aber über die Induktion von Caspase-1 zur Freisetzung weiterer proinflammatorischer Signalmoleküle wie IL-1β und IL-18 [107].

Die zentrale Komponente der Immunreaktion gegen Fremd-RNA ist somit die Einleitung einer Typ-I-IFN Antwort. Die Freisetzung und Bindung von IFN-α und IFN-β an

IFN-Rezeptoren auf der Zellmembran von betroffenen und umliegenden Zellen (Abbildung 4D) führt über die JAK-STAT (Janus kinase; Signal transducer and activator of transcription)-Signalkaskade zur Aktivierung von mehr als 300 ISGs (Interferon-stimulated genes) [108]. Dazu gehört die Expression von RBPs (RNA binding proteins), die zu einer Reduktion der Proteinbiosynthese, der Degradierung von RNA und der Einleitung apoptotischer Prozesse in den Zellen zur Beseitigung viraler oder exogen eingebrachter RNA beitragen (Abbildung 4E) [108] führt. Mit dem Einsatz eines Typ-I-IFN Inhibitors, wie beispielsweise das aus dem Vaccina Virus stammende B18R Protein, können die Immunreaktionen während der Reprogrammierung auf ein geringes Maß reduziert werden. Somit kann einer vorzeitigen RNA Degradierung vorgebeugt werden [84, 85]. Durch das Ausschleichen des Typ-I-IFN Inhibitors, nach der erfolgreicher iPSC Generierung, kann die Immunreaktion wieder in Gang gesetzt werden und eine selektive Degradierung der srRNA erfolgen [86].

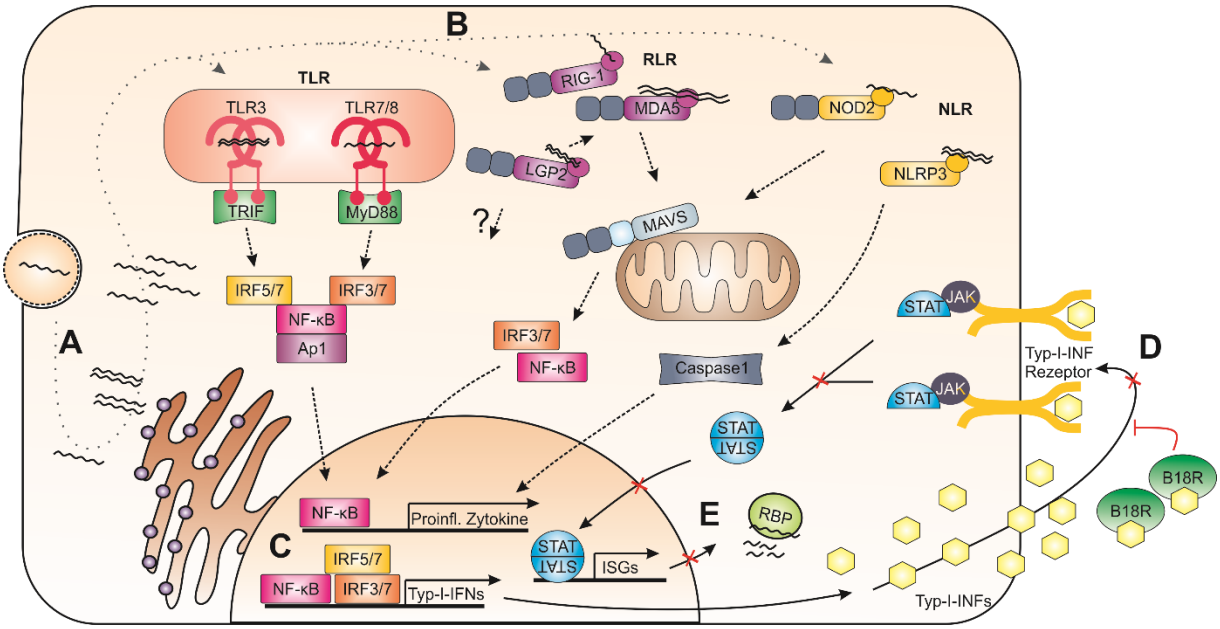

Abbildung 4: RNA vermittelte Typ-I-IFN Immunantwort und Inhibierung mittels B18R
Schematischer Ablauf der Aktivierung einer Typ-I-IFN Immunantwort in der Zelle. Nach der Einschleusung von exogener RNA **(A)** wird diese über PRRs (TLRs: TLR3, TLR7/8; RLRs: RIG-1, LGP2, MDA5; NLRs: NOD2 oder NLRP3) erkannt **(B)** und führen über IRF, NF-κB, AP1 und der Caspase 1 zur Expression von proinflammatorischen Zytokinen und Typ-I-IFNs **(C)**. Die Sekretion der Typ-I-IFNs führt zur Bindung dieser an Typ-I-IFN-Rezeptoren **(D)** welche über den JAK/STAT Signalweg zur Expression von verschiedenen ISGs wie RBPs führt und die Degradierung der Fremd-RNA zur Folge hat **(E)**. Die Behandlung der Zellen mit B18R führt zur Bindung der Typ-I-IFNs, so dass keine Typ-I-IFN-Rezeptor vermittelte Signalweiterleitung stattfinden kann und die RNA Degradierung inhibiert wird **(D&E)**.

1.4 Stammzell-basierte Geweberegeneration

In den letzten Jahren haben sich sowohl pluripotente, aber auch multipotente Stammzellen auf Grund ihrer Fähigkeit zur Differenzierung in diverse Körperzellen zu einem

der vielversprechendsten und fortschrittlichsten wissenschaftlichen Forschungsthemen in der regenerativen Medizin entwickelt. Die Differenzierung von gewebespezifischen Zellen wie Neuronen [109], Pankreas β-Zellen [110], Skelett-[111] und Kardiomyozyten [112], Osteoblasten [113] und Hepatozyten [114, 115] beruht dabei großteiles auf der Zugabe von Wachstumsfaktoren, Zytokinen oder chemischen Substanzen, die wiederum Signalproteine imitieren [116].

1.4.1 Regeneration von Knochen

Ein mögliches Anwendungsgebiet von Stammzellen ist hierbei die Regeneration von Knochendefekten, wie zum Beispiel im Bereich der Mund-, Kiefer- und Gesichtschirurgie. Die Ursachen dieser Knochendefekte können angeborene Anomalien [117], Allgemeinerkrankungen [118], Entzündungen [119], traumatische Verletzungen bei Unfällen [120], Folgen von Zahnextraktionen [121] oder die chirurgische Resektion gutartiger oder bösartiger Tumoren [122] sein. Übersteigt ein Knochendefekt eine kritische Größe, findet keine vollständige körpereigene Regeneration (maximal 10% des verlorenen Knochengewebes) mehr statt [123]. Um bei Patienten Knochendefekte kritischen Ausmaßes wiederherzustellen, sind somit chirurgische Rekonstruktionen erforderlich. Autologe Transplantate gelten hierbei auf Grund der wesentlichen Kombination von osteogenen, osteoinduktiven und osteokonduktiven Eigenschaften als Goldstandard [124]. Neben der Morbidität an der Entnahmestelle des Ersatzgewebes ist die Menge an Transplantatgewebe jedoch äußerst begrenzt [124].

Die Kombination von autologen Zellen mit Biomaterialien im Knochen Tissue Engineering versprechen jedoch eine bessere Verfügbarkeit und Behandlungsmöglichkeit von Knochendefekten in der Zukunft. Grundsätzlich werden zwei verschiedene Ansätze im Knochen Tissue Engineering unterschieden. In der in situ Knochenzüchtung werden autologe MSCs und/oder Osteoprogenitorzellen auf einem Gerüst/Scaffold ausgesät und an die Stelle des Knochendefekts implantiert [125, 126]. Das Scaffold dient hierbei als Gerüst und die Zellen unterstützen die Knochenregeneration durch die Sekretion von Zytokinen und Wachstumsfaktoren und/oder der Differenzierung zu Osteoblasten [127, 128]. Der zweite Ansatz besteht in der Transplantation von MSCs, die nach der Isolation, in vitro expandiert, auf Gerüsten ausgesät und unter kontrollierten Kulturbedingungen, unter der Zugabe von Dexamethason, Ascorbinsäure und β-Glycerophosphat [129], osteogen differenziert werden [130]. Hierbei dient das Scaffold

als Stützstruktur, bis die Zellen eine extrazelluläre Matrix aufgebaut und direkt als Knochenersatze implantiert werden können. MSCs aus dem Kieferperiost (JPCs) stellen für die Ansätze des Knochen Tissue Engineering eine vielversprechende Zellquelle dar. Im Vergleich zu MSCs anderen Ursprungs, wie Knochenmark MSCs, sind JPCs im Kieferperiost leicht zugänglich und weisen in vitro eine gute Proliferationsrate und ein starkes osteogenes Differenzierungspotential auf [131, 132].

Biomaterialien zur Knochenregeneration

Neben einer geeigneten Zellquelle und der passenden Handhabung, ist die Wahl des Scaffolds beim Knochen Tissue Engineering von entscheidender Bedeutung und sollte die Lebensfähigkeit, Anhaftung, Proliferation sowie die osteogene Differenzierung von Zellen ermöglichen. Zusätzlich muss die Struktur eine Vaskularisierung und die Integration in den Wirt ermöglichen. Verschiedene Biomaterialien wie Hydroxylapatit [14], Niedertemperatur-Kalziumphosphatzement [133], bioaktives Glas [134], Polylactidsäure [135] und β-TCP [136] wurden in dieser Hinsicht bereits für das Knochen Tissue Engineering untersucht. Insbesondere Biokeramiken aus Kalziumphosphat wie β-TCP erfüllen mit ihrer hohen strukturellen und chemischen Ähnlichkeit zu Knochengewebe diese Anforderungen. Durch die Freisetzung von große Mengen an wichtigen anorganischen Salzen wie Ca^{2+} und PO_4^{2-} während der Resorption kann die Knochenneubildung zusätzlich unterstützt werden [137]. An Stellen eines Knochendefekts mit stärkeren Belastungen kann durch eine dünne Beschichtung aus PLGA eine zusätzliche mechanische Stabilität erreicht werden [138].

1.4.2 Regeneration des Myokards

Ein weiteres Einsatzgebiet stellt die Verwendung von Stammzellen zur Regeneration von Herz-Kreislauf-Erkrankungen dar. Mit über 17 Millionen Todesfällen pro Jahr machen diese Erkrankungen etwa 30 % aller Todesfälle weltweit aus. Eine epidemiologische Studie belegt, dass auf Grund der sich weiter verschlechternden Lebensumstände wie steigender Fettleibigkeit, ungesunder Ernährung und Bewegungsmangel diese Zahl bis 2030 um weitere 40 % auf 23,6 Millionen Todesfälle pro Jahr ansteigen wird [139-141]. Da das Myokard nur ein äußerst begrenztes endogenes Potential für die Proliferation von Kardiomyozyten im Erwachsenenalter aufweist (<1 % pro Jahr), kann keine physiologisch relevante Regeneration in Folge eines Myokardinfarktes stattfinden [142]. Dabei werden die abgestorbenen kontraktilen Zellen hauptsächlich

durch Fibroblasten und Myofibroblasten ersetzt und bilden ein fibrotisches Narbengewebe. Dies wiederum führt zu einer Verdickung (Hypertrophie) und Versteifung (Fibrose) des Herzmuskels und zu einer Beeinträchtigung der Herzfunktion (Herzinsuffizienz) [143]. Im weiteren Verlauf kann es neben einer eingeschränkten körperlichen und geistigen Leistungsfähigkeit zur Einlagerung von Wasser in den Beinen und Lungen (rechtsseitige Herzinsuffizienz) oder den Nieren (linksseitige Herzinsuffizienz) kommen, was wiederum zu ersthaften Begleiterkrankungen wie Atemnot und Niereninsuffizienz führen kann [144]. Einem Patienten im Endstadium einer Herzinsuffizient kann meist nur eine Organtransplantation das Überleben sichern. Um den Mangel an Spenderorganen für eine Transplantation zu überwinden, wurden bereits mehrere stammzellbasierte Therapieansätze mit MSCs [145, 146], CPCs (Cardiac progenitor cells) [147, 148], ESCs [149] und iPSCs [150] in vitro, in vivo und auch bereits in klinischen Studien getestet.

Insbesondere mit der Entdeckung von iPSCs haben sich, neue Möglichkeiten für eine autologe Regeneration von Herz-Kreislauf-Erkrankungen aufgetan. Obwohl die Kardiogenese in der Embryonalentwicklung ein streng regulierter und komplexer Prozess ist, konnte sie in iPSCs in vitro über die gezielte Aktivierung bzw. Inhibierung des kanonischen Wnt/GSK3 (Wingless-related integration site / Glykogensynthase-Kinase 3)- Signalwegs nachgeahmt und durch Separation nahezu reine Kardiomyozyten Kulturen generiert werden [151, 152]. Eine Studie in immunsupprimierten Schweinen zeigte, dass eine Transplantation von allogenen Kardiomyozyten nach einem Myokardinfarkt zur Regeneration des Herzmuskels und einer verbesserten Herzleistung führt [153]. Aktuellere Studien konnten diesen positiven Effekt auch bei der Transplantation von aus iPSCs generierten Kardiomyozyten in Schweinen und Primaten belegen [154-156].

Applikation von Kardiomyozyten

Die Wirksamkeit der stammzellbasierten Myokardregeneration hängt in hohem Maße davon ab, ob die Zellen erfolgreich und möglichst ohne Verlust ihrer Viabilität in die Infarktregion gelangen. Sowohl traditionelle Methoden wie die Intramyokardiale (transendokardial, transepikardial) Injektion von Zellsuspensionen (Abbildung 5) als auch Tissue Engineering-Anwendungen kommen hierfür zum Einsatz [157, 158]. Die intravaskuläre Verabreichung (intravenös, intrakoronar, Koronarsinus), findet bei der

Kardiomyozyten Verabreichung auf Grund der Zellgröße und der hohen Zellkonzentration und der damit verbundenen Gefahr einer Okklusion und eines Mikroinfarktes allerdings kaum Verwendung [158]. Auch intramyokardiale und Tissue Engineering-Applikationen weisen trotz ihrer gut erprobten Anwendung Nachteile und Schwierigkeiten auf, welche vor einem möglichen klinischen Einsatz noch behoben werden müssen.

Bei kardialen Tissue Engineering Anwendungen werden meist Biopolymere wie beispielsweise Fibrin [159], dezellularisierte Extrazellulärmatrix [160], Alginat [161], PCL [162], oder Gelatine-Methacrylat [163, 164] mit ausschließlich Kardiomyozyten [162] oder mit zusätzlichen unterstützenden Zellarten [156] besiedelt und als sogenannte kardiale Pflaster auf das Epikard des Herzes transplantiert. Als funktionaler Gewebeersatz sollte das kardiale Pflaster eine ähnliche Kontraktilität wie das menschliche Myokard mit etwa 50 mN/mm^2 aufweisen [165]. Eine zu geringe Anzahl an Kardiomyozyten und eine nicht ausreichende Ausreifung und Ausrichtung der Sarkomere und der Myofilamentproteine können die Funktionalität somit beeinflussen [166]. Zusätzlich besteht die Gefahr, dass durch Narbenbildung und die Transplantation auf das Epikard, eine mangelhafte oder keine elektromechanische und vaskuläre Anbindung an das Patientenmyokard stattfinden könnte [167]. Neben einer schlechten Nährstoffversorgung der Zellen und einer eingeschränkten kontraktilen Funktion des kardialen Pflasters können durch die unzureichende Synchronisation zusätzlich Arrhythmien auftreten [168]. Im Gegensatz dazu findet bei der intramyokardialen Injektion von Kardiomyozyten-Suspensionen durch die Überwindung des Epikards leichter eine elektromechanische Integration der Zellen in das Empfängergewebe statt [167, 169]. Auf Grund der geringen Verteilung im Gewebe muss jedoch auf Kanülen mit großem Durchmesser oder auf multiple Injektionen zurückgegriffen werden, was zu einer zusätzlichen Schädigung des Gewebes und darin verlaufenden Nerven und Blutgefäßen führen kann [170]. Aus diesem Grund ist die Erforschung und Weiterentwicklung der zur Verfügung stehenden Transplantationsmethoden für eine effiziente Regeneration des Herzmuskels ein zentraler Punkt in der kardialen Regenerativen Medizin.

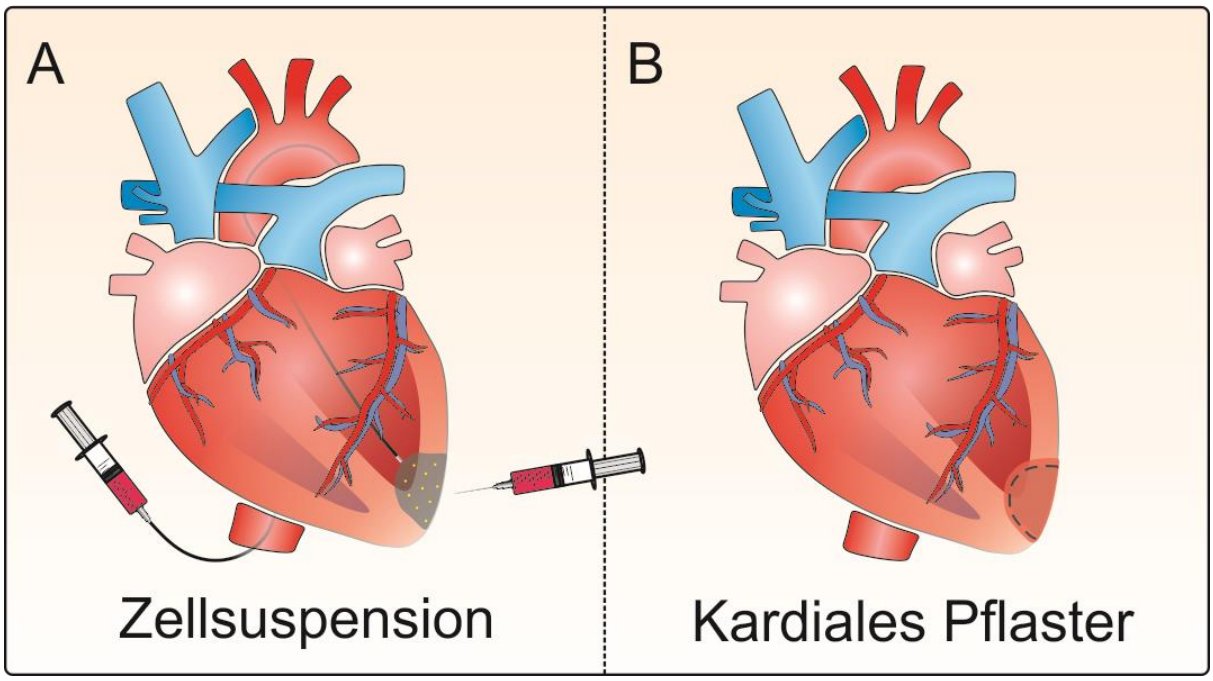

Abbildung 5: Gängige Applikationsmethoden für hiPSC abgeleiteter Kardiomyozyten
Schematsiche Darstelltung der transendokardialen und transepikardialen Injektion einer Zellsuspension mittels Herzkatheter bzw. einer Kanüle **(A)** und ein funktioneller Ersatz des geschädigten Myokardgewebes über ein epikardiales Pflaster **(B)**. Während die Injektion der Zellsuspension eine gute elektromechanische Kopplung der Zellen ermöglicht, jedoch mehrere Injektionen benötigt, decken kardiale Pflaster den gesamten infarzierten Bereich ab, bergen jedoch die Gefahr einer unzureichenden elektromechanischen und vaskulären Anbindung an das Patientenmyokard [167, 169].

1.5 Hämokompatibilität

Biomaterialien stellen in der Regenerativen Medizin, insbesondere im Bereich des Knochen Tissue Engineering, eine zentrale Komponente dar. Bei der Implantation kommen Biomaterialien häufig direkt, durch die Implantation in Blutgefäße, oder indirekt, durch die Verletzung des umliegenden Gewebes mit Blut in Kontakt. Neben der Verträglichkeit mit dem umliegenden Gewebe stellt somit die Hämokompatibilität des Biomaterials eine der wichtigsten Kriterien für ihre erfolgreiche klinische Anwendbarkeit dar. Mit diversen zellulären (44 % Erythrozyten, 1 % Leukozyten und 1 % Thrombozyten) und im Plasma gelösten Bestandteilen (7 % Plasmaproteinen, 1 % Mineralsalze) kann es zu zahlreichen Wechselwirkungen zwischen dem Blut und den Biomaterialien kommen. Der initiale Schritt ist hierbei die Adsorption und Kontaktaktivierung von Plasmaproteinen an Fremdoberflächen [171]. Durch eine Reihe von Folgereaktionen kann dies zu Gewebeschäden, akuten Entzündungen und thrombotischen Komplikationen führen [172].

Eine der wichtigsten unerwünschten biologischen Reaktionen, die bei blutkontaktierenden Biomaterialien beobachtet werden, ist die Aktivierung des Gerinnungsprozesses [173]. Der plasmatische Gerinnungsprozess ist eine Kaskade, bei der das in einer Reaktion gebildete Enzym die nächste Reaktion katalysiert. Letztlich entsteht FIIa (Thrombin/Factor IIa), eine Serinprotease, die das Fibrinogen hydrolysiert. Die Fibrinmonomere vernetzen sich anschließend zu einem Fibrinnetz und bilden zusammen mit aggregierten Thrombozyten ein stabilisiertes Aggregat [174]. Grundsätzlich kann eine extrinsische und eine intrinsische Aktivierung der Blutgerinnung unterschieden werden. Der extrinsische Weg ist in erster Linie für die Hämostase verantwortlich und wird nach einer Gefäßverletzung durch die Freisetzung von TF (Tissue factor) eingeleitet. Der intrinsische Weg dagegen, wird im Körper selbst durch die Aktivierung von FXII zu FXIIa durch den Kontakt mit subendothelialem Kollagen ausgelöst. Aber auch Fremdoberflächen, wie beispielsweise Biomaterialien, können zu der Aktivierung des intrinischen Koagulationsweges führen, weshalb hier auch von Kontaktaktivierung gesprochen wird. Die pathologische Ausbildung eines Thrombus an den Biomaterialien ist ein erhebliches klinisches Problem, das zum Funktionsversagen der Implantate und durch das Ablösen des Thrombus zu Gefäßverschlüssen und Infarkten führen kann.

Die Gerinnungskaskade ist zudem eng mit der Thrombozyten-Aktivierung vernetzt. Während Thrombozyten unter physiologischen Bedingungen hauptsächlich an der Hämostase beteiligt sind und nach Gefäßverletzungen und der Freisetzung des von-Willebrand Faktors aktiviert werden, können auch Fibrinablagerungen sowie Plasmaproteine, die an die Biomaterialien gebunden haben, zur Aktivierung von Thrombozyten führen [175, 176]. Durch die Sezernierung von in ihren Granula gespeicherten Chemokinen werden Leukozyten rekrutiert [177] und durch die Freisetzung von negativ geladenen Polyphosphatketten wird die Gerinnungskaskade über den intrinsischen Signalweg (FXII) aktiviert [178].

Die Adsorption von Plasmaproteinen an der Oberfläche von Biomaterialien schafft zudem eine neue Schnittstelle zwischen dem Material und dem umgebenden Gewebe, wodurch eine starke Komplementaktivierung auslösen werden kann [179, 180]. Neben der Opsonierung der Biomaterialien durch den Komplementfaktor C3 [181] werden über die Freisetzung der Spaltprodukte C3a und C5a weitere Granulozyten, Monozyten und Mastzellen rekrutiert. Durch die Sekretion von proinflammatorischen Zytokinen

und TF, findet ebenfalls eine Aktivierung der Gerinnungskaskade über den extrinsischen Signalweg statt [182, 183].

Ob Biomaterialien eine Aktivierung von Blut auslösen, kann über die Veränderungen von Blutplättchen, Erythrozyten und Leukozyten, über die Bildung von Aktivierungsprodukten im Plasma und Ablagerungen von Proteinen und Zellen auf der Materialoberfläche analysiert werden [184]. Hierzu werden Blut und Oberflächen von Biomaterialien vor und nach der Inkubation analysiert. Um die jeweilige Situation im Körper bestmöglich nachstellen zu können, stehen unterschiedliche Inkubationsmethoden zur Verfügung, wie eine statische Inkubation [185], eine dynamisch Inkubation auf Schüttelinkubatoren [186, 187] oder Scherströmungsmodelle [188-191]. Für eine einheitliche Prüfung der Testmaterialien ist das Vorgehen in der „ISO10993-4 - Biologische Beurteilung von Medizinprodukten - Teil 4: Auswahl von Tests für Wechselwirkungen mit Blut“ festgehalten [192].

2 Zielsetzung

Die Regenerative Medizin hat sich mit ihrem breiten Anwendungsspektrum zu einer der vielversprechendsten Therapiemöglichkeit zur Behandlung von weit verbreiteten Krankheitsbildern, wie beispielsweise Diabetes mellitus und koronare Herzkrankheiten, entwickelt. Durch die Anregung körpereigener Regenerations- und Reparaturprozesse aber auch durch den Ersatz von geschädigtem oder in seiner Funktionalität eingeschränktem Gewebe, ermöglicht sie im Vergleich zu den meisten aktuell verfügbaren Behandlungsmöglichkeiten eine gänzliche Heilung diverser Krankheiten.

Der große Bedarf an autologen Zellen, der lange Zeit als limitierender Faktor galt, kann mit Hilfe der Stammzellbiologie umgangen werden. Insbesondere die Entdeckung und Weiterentwicklung der Reprogrammierung von somatischen Zellen zu hiPSCs, bietet die Grundlage zur Generierung einer nahezu unerschöpflichen Anzahl an autologen Zellen. Nicht-integrative Reprogrammierungsmethoden, wie beispielsweise die mRNA basierte Expression der Reprogrammieungsfaktoren, erlaubt die rückstandsfreie Differenzierung klinisch einsetzbarer Zellen. Auf Grund ihrer transienten Eigenschaften besitzt synthetische mRNA eine sehr geringe Halbwertszeit in der Zelle. Daher ist der Reprogrammierungsprozess mit einer täglichen Transfektion der Zellen verbunden.

Ziel dieser Arbeit war die Generierung und Charakterisierung von rückstandsfreien hiPSCs, sowie deren gezielte Differenzierung zu Kardiomyozyten. Die Isolierung von RECs aus Mittelstrahlurin sollte hierbei als nicht invasive Quelle somatischer Zellen auf ihre Anwendbarkeit untersucht werden. Um die Nachteile der mRNA-basierten Reprogrammierung zu umgehen, sollte zudem eine selbstreplizierende RNA etabliert werden, die für die bekannten Reprogrammierungsfaktoren Oct4, Klf4, Sox2 und c-Myc sowie für eine PAC kodiert. Um die Sicherheit und die Pluripotenz der mit dieser srRNA generierten hiPSCs zu bestätigen, sollte zu der gängigen in vitro Charakterisierung, untersucht werden, ob durch die Abwandlung des CAM Assays eine kosten- und zeitsparende sowie Tierleid-reduzierende Alternative zum Maus-Teratoma-Modell zur in vivo Bestimmung der Pluripotenz eingesetzt werden kann.

Im weiteren Verlauf dieser Arbeit, sollte eine neuartige, wasserstrahlbasierte Methode etabliert werden, um aus hiPSCs abgeleitete Kardiomyozyten möglichst gewebeschonend und mit einer guten räumlichen Verteilung in Herzgewebe zu applizieren. Hierbei

sollte vor allem die Verteilung im Gewebe und die Viabilität der Zellen nach der Applikation mit der Wasserstrahl-basierten Methode mit der Injektion einer herkömmlichen 27 G Kanüle verglichen werden.

Ein weiteres Ziel dieser Arbeit war die Untersuchung der osteogenen Differenzierung von adulten Stammzellen in Kombination mit β-TCP Scaffolds für die Knochenregeneration. Anschließend sollten Effekte des Scaffolds auf die Koagulation / Hämostase des Patienten untersucht werden. Hierzu wurden neben wichtigen Blutaktivierungsmarkern wie TAT, β-TG, SC5b-9 und PMN-Elastase die Oberflächen der Scaffolds auf Blutzell- und Fibrinablagerungen mit Hilfe der REM (Rasterelektronenmikrokopie) untersucht werden.

3 Ergebnisse

3.1 Publikation I: Reprogramming of Urine-Derived Renal Epithelial Cells into iPSCs Using srRNA and Consecutive Differentiation into Beating Cardiomyocytes

Heidrun Steinle*, Marbod Weber*, Andreas Behring, Ulrike Mau-Holzmann, Christiane von Ohle, Aron-Frederik Popov, Christian Schlensak, Hans Peter Wendel, Meltem Avci-Adali

** gleichermaßen beigetragen*

Molecular Therapy - Nucleic Acids

Akzeptiert am 22. Juli 2019

Zusammenfassung:

Die Generierung von hiPSCs aus somatischen Patientenzellen und deren anschließende Differenzierung in unterschiedlichste Zelltypen eröffnet zahlreiche Möglichkeiten in der regenerativen Medizin. Auf Grund der äußerst geringen Selbsterneuerungsrate adulter Kardiomyozyten von weniger als 1 % pro Jahr, ist die effiziente und rückstandsfreie Generierung autologer Kardiomyozyten von großem Interesse für die Behandlung von geschädigtem Gewebe in Folge eines Myokardinfarktes.

In dieser Studie wurden mit Hilfe einer srRNA erfolgreich rückstandsfreie hiPSCs generiert, welche aus renalen Epithelzellen aus Spender-Urin reprogrammiert wurden. Die Pluripotenz wurde über die Expression stammzellspezifischer Marker und der Differenzierungsfähigkeit in die drei Keimbahnen (Mesoderm, Endoderm und Ektoderm) in vitro sowie in vivo nachgewiesen. Darüber hinaus konnten nach der erfolgreichen Generierung der hiPSCs keine srRNA Rückstände, sowie karyotypische Aberrationen festgestellt werden. Die kardiale Differenzierung der hiPSCs führte nach 10 Tagen zu kontrahierenden Kardiomyozyten, die spezifische Kardiomyozytenmarker exprimierten. Zusätzlich konnte der interzelluläre Ca^{2+}-Fluss und das Ansprechen auf die Calciumkanalmodulatoren Isoproterenol und Nifidipin, mittels Erhöhung bzw. Inhibierung der Schlagfrequenz nachgewiesen werden. Die Verwendung von Urin als nicht-invasive Zellquelle und die Verwendung von srRNA zur Generierung von patientenspezifischen hiPSCs kann zukünftig für die Erzeugung klinisch anwendbarer autologer Kardiomyozyten verwendet werden und somit eine Regeneration nach einem Myokardinfarkt ermöglichen.

3.2 Publikation II: An Alternative In Vivo Model to Evaluate Pluripotency of Patient-Specific hiPSCs

Josefin Weber*, Marbod Weber*, Heidrun Steinle, Christian Schlensak,
Hans-Peter Wendel, Meltem Avci-Adali

** gleichermaßen beigetragen*

ALTEX - Alternatives to animal experimentation

Akzeptiert am 20. Januar 2021

Zusammenfassung:

Die Gewinnung autologer hiPSCs aus Körperzellen des Patienten und die anschließende Differenzierung dieser Zellen in die gewünschten Zelltypen bieten innovative Behandlungsmöglichkeiten für die Geweberegeneration. Für eine Prüfung der Pluripotenz werden die generierten hiPSCs in der Regel in immundefiziente Mäuse implantiert und 4 bis 6 Wochen später auf Teratombildung analysiert.

In dieser Studie wurde ein alternatives In-vivo-Modell auf Grundlage der CAM von Hühnereiern entwickelt, um die Pluripotenz neu erzeugter hiPSC-Linien zu untersuchen. Für die Ermittlung der idealen Versuchsparameter, wurden verschiedene Mengen (0,5, 1, 2 und 4 x 10^6 Zellen) hiPSCs auf die CAM appliziert und für 9 Tage inkubiert. Die höchste Effizienz der Teratombildung konnte bei 2 x 10^6 Zellen (70 %) und 4 x 10^6 Zellen (100 %) festgestellt werden. Die gebildeten Teratome wurden anschließend auf das Vorhandensein der drei Keimschichten (Mesoderm, Endoderm und Ektoderm) über histochemische und Immunfluoreszenzfärbungen sowie eine Genexpressionsanalyse von keimschichtspezifischen Markern untersucht. Neben typischen Gewebestrukturen der drei Keimbahnen zeigten alle Teratome vaskuläre Strukturen und bestätigen somit die Eignung der CAM als Alternative zu immundefizienten Mäusen. Die uneingeschränkte Anwendbarkeit des CAM-Modells wurde durch die Verwendung von zwei weiteren hiPSC-Linien (aus Fibroblasten und Kieferperiostzellen stammend) bestätigt.

Das CAM-basierte In-vivo-Modell bietet eine optimale Testumgebung für die Bewertung der Pluripotenz von neu erzeugten hiPSC-Linien. Darüber hinaus reduziert diese einfache, schnelle, kostengünstige und reproduzierbare Methode das Leiden der Tiere und setzt damit die Prinzipien der 3R (Replacement, Reduction und Refinement) um.

3.3 Publikation III: Hydrojet-based delivery of footprint-free iPSC-derived cardiomyocytes into porcine myocardium

Marbod Weber, Andreas Fech, Luise Jäger, Heidrun Steinle, Louisa Bühler, Regine Mariette Perl, Petros Martirosian, Roman Mehling, Dominik Sonanini, Wilhelm K. Aicher, Konstantin Nikolaou, Christian Schlensak, Markus D. Enderle, Hans Peter Wendel, Walter Linzenbold, Meltem Avci-Adali

Scientific Reports

Akzeptiert am 14. September 2020

Zusammenfassung:

Die Reprogrammierung von somatischen patienteneigenen Zellen in hiPSCs und die anschließende Differenzierung in Kardiomyozyten eröffnet neue Möglichkeiten für die Regeneration des Herzmuskels nach einem Myokardinfarkt.

In dieser Studie wurde die Anwendbarkeit einer Wasserstrahl-basierten Injektionsmethode für hiPSC abgeleitete Kardiomyozyten in das Myokard untersucht. Hierfür wurde ein System entwickelt, das mit einem hohen Wasserstrahldruck das Gewebe schonend aufweiten und unmittelbar im Anschluss mit einem niedrigen Druck die Zellen injizieren kann. Die Anwendungsparameter wurden ex vivo in Schweineherzen mit Eisenoxid-beschichteten Mikropartikeln getestet und mittels MRT (Magnetresonanztomographie) analysiert. Anschließend wurde der Einfluss der Parameter auf die Wiederfindung und die Viabilität von hiPSC-abgeleiteten Kardiomyozyten durch eine Injektion in Medium analysiert und mit der Injektion mit einer 27 G Kanüle verglichen. Sieben Tage nach der Injektion zeigte ausschließlich der höchste Druck (E20) der Wasserstrahl-basierten Methode eine signifikant niedrigere Viabilität als die Injektion mit einer 27 G Kanüle. Die niedrigeren Drücke (E5 und E10) zeigten dagegen keine signifikanten Unterschiede zur Kanülen-Injektion. Die Verteilung im Gewebe wurde ex vivo im Schweinemyokard mit Hilfe fluorszenzmarkierter Kardiomyozyten in einem In-vivo-Bildgebungssystem analysiert und mit einer 27 G Kanüle verglichen. Neben einer deutlich besseren Verteilung im Gewebe konnte eine signifikant geringere Verteilung der Zellen in Blutgefäßen festgestellt werden, was auf eine schonendere Injektion hinsichtlich der umgebenden Stuktur hindeutet.

Diese Studie demonstriert die Anwendbarkeit der Wasserstrahl basierten Injektionsmethode für die intramyokardiale Verabreichung von hiPSC-abgeleiteten Kardiomyozyten. Die effiziente und schonende Applikation von Kardiomyozyten in das infarzierte Myokard könnte in Zukunft die Regeneration des Herzmuskels deutlich verbessern.

3.4 Publikation IV: Influence of human jaw periosteal cells seeded β-tricalcium phosphate scaffolds on blood coagulation

Marbod Weber, Felix Umrath, Heidrun Steinle, Lukas-Frank Schmitt, Lin Tzu Yu, Christian Schlensak, Hans Peter Wendel, Siegmar Reinert, Dorothea Alexander*, Meltem Avci-Adali*

** gleichermaßen beigetragen*

MDPI - International Journal of Molecular Sciences

Akzeptiert am 10. September 2021

Zusammenfassung:

Das Heilen von kleinen, aber auch großen Knochendefekten ist ein zentrales Anliegen im Bereich der Mund-, Kiefer- und Gesichtschirurgie. Für die Regenration von größeren Knochendefekten stellt die Kombination von JPCs mit Biomaterialien einen vielversprechenden Ansatz dar.

In dieser Studie wurde der Einfluss von unbeschichteten und mit PLGA beschichteten β-TCP Gerüsten auf die Besiedelung mit JPC und die anschließende osteogene Differenzierung untersucht. Da die Tissue Engineering Gerüste bei der Transplantation direkt in Kontakt mit Blut kommen, wurde der Einfluss der zellbesiedelten Gerüste mit humanem Vollblut unter dynamischen Bedingungen analysiert. Hierbei konnte gezeigt werden, dass PLGA-beschichtete und unbeschichtete β-TCP-Gerüste gute Eigenschaften für die Zelladhäsion der JPCs bieten, ohne dabei die Fähigkeit zur osteogenen Differenzierung zu beeinträchtigen. Eine mögliche Aktivierung der Gerinnung, des Komplementsystems und der Blutzellen wurde mittels ELISA (Enzyme-linked Immunosorbent Assay) und REM analysiert. Neben einer dichten JPC Besiedelung zeigte die Analyse der Gerüste und des Bluts keine relevante Anheftung von Blutzellen und keinen signifikanten Anstieg der meisten analysierten Zellaktivierungsmarker (β-TG, SC5b-9, PMN-Elastase). Jedoch zeigte die Analyse von TAT einen deutlichen Anstieg nach der Inkubation von zellbesiedelten β-TCP Scaffolds.

Dies lässt darauf schließen, dass neben den Biomaterialien auch die besiedelten Zellen zu einer Aktivierung von Blutbestandteilen führen und die Hämostase beeinflussen können. Da hierdurch eine direkte Beeinflussung der Knochenregeneration möglich ist, sollte dieser Aspekt vor einer klinischen Anwendung weiter untersucht werden.

4 Diskussion

Ein zentraler Punkt der Regenerativen Medizin und des Tissue Engineering ist die Generierung von einer ausreichenden Zellzahl autologer Zellen, die für die Regeneration geschädigter Gewebe eingesetzt werden können. Die Möglichkeit der Generierung von patientenspezifischen hiPSCs hat hierfür eine ideale Zellquelle geschaffen. Neben verschiedenen Reprogrammierungsmethoden zur Generierung von Rückstandsfreien autologen hiPSCs, sind die Differenzierung und die Charakterisierung der generierten Zellen, aber auch Implantationsmethoden und die Untersuchung unterschiedlicher Biomaterialien als Trägermaterialien in den Fokus des Tissue Engineerings gerückt.

4.1 srRNA basierte Reprogrammierung von Urinzellen

In dieser Arbeit konnte die erfolgreiche srRNA-basierte Generierung von hiPSCs aus RECs nachgewiesen werden. Eine einmalige Transfektion der Zellen war hierbei ausreichend, um innerhalb von 21-30 Tagen erste hiPSC Kolonien zu generieren. Die verwendete synthetische srRNA kodierte hierbei für nsP1-4, die Reprogrammierungsfaktoren Oct4, Klf4, Sox2 und c-Myc, sowie dem eGFP (Enhanced green fluorescent protein) und einer PAC, die eine Positivselektion der transfizierten Zellen ermöglicht. Um eine vorzeitige RNA Degradierung zu verhindern, wurden die Zellen während des gesamten Reprogrammierungsprozesses mit dem Typ-I-IFN Inhibitor B18R behandelt.

Die ersten iPSCs wurden durch die Reprogrammierung von murinen und wenig später von humanen Fibroblasten generiert [49, 50]. Auch heute sind Fibroblasten auf Grund ihrer hohen Verfügbarkeit, ihrer geringen Ansprüche an die Nährstoffanforderungen und der einfachen Kultivierung, Vermehrung und Kryokonservierung die am häufigsten verwendete Zellquelle [193]. Darüber hinaus sind sie einfach zu transfizieren und die Reprogrammierung verläuft schnell und effizient [75]. Ein Nachteil dagegen ist die Gewinnung der Zellen durch Hautbiopsien. Da es sich hierbei um einen invasiven Eingriff handelt, ist dies mit der Verletzung des gesunden Gewebes, mit Schmerzen, einem Infektionsrisiko und einer zusätzlichen Belastung des Patienten verbunden.

Eine alternative Quelle für somatische Zellen, ist die Isolation von PBMCs aus Patientenblut [59, 194]. Die Blutentnahme ist minimalinvasiv und ein klinisches Standardverfahren. Zusätzlich konnte von Tan und Kollegen gezeigten werden, dass aus einem einzigen Tropfen Blut (10 µl) genug PBMCs isoliert werden können, um daraus hiPSCs

zu generieren [195]. Der Reprogrammierungserfolg ist auf Grund der geringen Effizienz der bisher zur Verfügung stehenden Transfektionsmethoden jedoch im Vergleich zu anderen somatischen Zellarten äußerst gering [196].

Mit der erfolgreichen Reprogrammierung von RECs präsentierten Zhou und Kollegen erstmals eine einfache, nicht-invasive, kostengünstige und für den Spender schmerzfreie Methode zur Isolation somatischer Zellen zur Generierung von humanen iPSCs [61]. Während der physiologischen Selbsterneuerung des Epithelgewebes im Urinaltrakt werden ca. 2.000 bis 7.000 Zellen pro Tag abgelöst und über den Urin ausgeschieden [62]. Hierbei können hauptsächlich die drei Zellarten: Nieren-, Übergangs- und Plattenepithelzellen unterschieden werden [197]. Übergangszellen sind hierbei eher selten und werden hauptsächlich nach einer Katheterisierung der Harnröhre oder des Harnleiters gefunden [197]. Sie unterscheiden sich durch ihre Größe und Form von RECs [197]. Plattenepithelzellen kleiden die Harnröhre und die Vagina aus und sind am häufigsten im weiblichen Urin zu finden. Das Plattenepithel verbleibt jedoch nach der Inkulturnahme in Suspension und kann somit einfach entfernt werden. Bei RECs handelt es sich um Nierenepithelzellen, die das Nephron als Einzelschicht auskleiden [197]. Eine deutlich erhöhte Anzahl oder Zusammensetzung der im Urin gefundenen Zellen, wie beispielsweise ein hoher Anteil an Leukozyten deuten auf eine Infektion oder Erkrankung im Nieren und Harntrakt hin [197, 198]. In dieser Arbeit konnten bereits aus 100-200 ml Urin eine ausreichende Menge an RECs isoliert werden, um nach einer Expansion humane iPSCs zu generieren. Durch das kontinuierliche Auswaschen der Zellen über mehrere Tage konnte das Plattenepithel entfernt werden, so dass etwa 3 - 6 REC-Kolonien im Kulturgefäß übrigblieben, welche nach einer etwa 14-tägigen Kultivierung für die Reprogrammierung bereit waren. Die Isolierten Zellen wurden durch die Untersuchung auf den Epithelzellmarker β-Catenin und den renalen proximalen tubulären Marker CD13 charakterisiert und die Herkunft der Zellen bestätigt. Durch die Verwendung von größeren Mengen Urin oder der Isolation aus erstem Morgenurin kann die Anzahl der isolierten Zellen erhöht werden, wodurch die Expansionszeit der Zellen verringert und die Reprogrammierung schneller gestartet werden kann.

Für eine klinische Anwendbarkeit der hiPSCs sind nicht-integrative Reprogrammierungsmethoden von besonderem Interesse. DNA basierte Methoden gelten zwar

grundsätzlich als sicher, bergen aber dennoch die Gefahr einer genomischen Integration und einer Insertionsmutagenese [73]. Die Verwendung von rekombinanten Proteinen oder nicht-integrativen viralen Vektoren wie Sendai Viren ist mit einem hohem Aufwand und Kosten bei der Herstellung und Aufreinigung der Proteine [199] bzw. mit einer Behandlung nach der Reprogrammierung zur Entfernung der replizierenden Viren verbunden [68, 200]. Die Verwendung von synthetischen RNAs bietet gegenüber diesen Methoden den Vorteil einer höheren Reprogrammierungseffizienz [73]. Auf Grund der transienten Eigenschaften führt die Transfektion mit mRNA jedoch nur zu einer vorübergehenden Expression der Proteine von 2-3 Tagen und muss daher täglich wiederholt werden [73, 76]. Im Vergleich dazu kann mit der srRNA durch das Mitführen der Sequenz der nsP1-4 [87] die Proteinexpression mit einer einzigen Transfektion über den gesamten Reprogrammierungszeitraum aufrechterhalten werden [86]. Verglichen mit mRNA ist die srRNA-basierte Reprogrammierung somit mit deutlich weniger Arbeitsaufwand, Kosten und zellulärem Stress verbunden und bietet zusätzlich eine verbesserte Reprogrammierungseffizienz [73]. Der Einbau der srRNA mit der eGFP Sequenz erlaubte die Überwachung der Translation und somit der Transfektionseffizienz unmittelbar nach der Transfektion. Der Einfluss verschiedener Parameter, wie beispielsweise die RNA Menge, verschiedene Transfektionsreagenzien und das eingesetzte Verhältnis dieser, können somit untersucht werden. Außerdem liefert die eGFP Expression erste Hinweise auf eine erfolgreiche srRNA-Degradierung nach dem Absetzen des IFN-Inhibitors durch den Rückgang der Fluoreszenzintensität.

Wie bei anderen synthetischen RNAs, wird durch die Transfektion mit srRNA eine Typ-I-IFN Immunantwort ausgelöst. Deshalb ist die Behandlung mit einem IFN-Inhibitor B18R erforderlich, um einen vorzeitigen Abbau der srRNA zu verhindern [73, 86, 201, 202]. Nach dem Erscheinen erster iPSC-Kolonien kann der Entzug von B18R aus dem Medium zum gezielten Abbau und zur Eliminierung der srRNA verwendet werden, um rückstandsfreie iPSCs zu generieren [86, 201]. Neben dem Einsatz des rekombinanten Proteins B18R, konnte in weiteren Studien gezeigt werden, dass ebenfalls die Co-Transfektion mit B18R mRNA sowie der Gabe von B18R konditioniertem Medium, das durch die Transfektion von Fibroblasten mit B18R mRNA hergestellt wird, die Typ-I-IFN vermittelte Immunantwort nach der Transfektion mit Fremd-RNA inhibiert und die Expression der Reprogrammierungsfaktoren ermöglicht [75, 85, 86, 201, 203]. Durch dieses Verfahren könnten die Kosten für die Reprogrammierung weiter gesenkt werden. Da die B18R Konzentration in dem konditionierten Medium jedoch stark von der

Translation und Sezernierung der transfizierten Zellen abhängt, muss die Menge, die bei der Reprogrammierung eingesetzt wird bei jeder Charge und für jede Zellart neu eingestellt werden.

4.2 In vitro und in vivo Charakterisierung der REC-hiPSCs

Die Fähigkeit zur Selbsterneuerung und zur Differenzierung in nahezu jegliche Zellart hat in der Regenerativen Medizin großes Interesse und Aufmerksamkeit der hiPSCs erregt. Eine Analyse von 186 pluripotenten Zelllinien ergab jedoch, dass diese, im Vergleich zu nicht pluripotenten Zellen, häufiger zu chromosomalen Aberrationen neigen. Während hESCs hauptsächlich eine Vervielfachung von Chromosomen zeigten, waren bei hiPSCs eher Deletionen nachweisbar [204]. Um die Identität und Sicherheit der generierten hiPSCs zu bestätigen, wird somit eine ausführliche Charakterisierungsprozedur über mehrere Stufen empfohlen [205]. Eine initiale Charakterisierung der generierten hiPSCs erfolgte in vitro über den Nachweis Stammzell-spezifischer Proteine, die mit der Aufrechterhaltung der Pluripotenz und der Fähigkeit der Selbsterneuerung in Verbindung stehen, sowie über den Nachweis der Differenzierungsfähigkeit in die drei Keimbahnen (Mesoderm, Endoderm und Ektoderm).

Um die Sicherheit der generierten hiPSCs auf chromosomaler Ebene zu untersuchen, wurde eine ausführliche Karyotypisierung durchgeführt. Hierbei konnten bei keiner der generierten Linien chromosomale Vervielfältigungen, Deletionen oder andere strukturelle Veränderungen festgestellt werden. Zusätzlich wurde die Abwesenheit der srRNA auf Nukleinsäure-Ebene in einer frühen Phase (Passage 3) der generierten hiPSCs untersucht. Die qRT-PCR (Quantitative reverse transcription polymerase chain reaction)-Analyse mit spezifischen Primerpaaren, die für Sequenzen in den nsP2 und nsP4 Region kodieren, zeigte keine Rückstände der srRNA im Vergleich zu unmittelbar mit srRNA transfizierten Zellen. Da es sich hierbei um eine äußerst sensitive Methode handelt, welche bereits sehr geringe Mengen detektieren kann [206], eignet sich diese besonders gut, um Rückstände in den generierten iPSCs zu detektieren. Ebenfalls deutet die Abnahme der c-Myc und Klf4 Expression auf einen Rückgang der srRNA im Zytoplasma hin. Obwohl die Expression dieser Proteine für die Reprogrammierung erforderlich ist, sollten sie nach der Reprogrammierung herunterreguliert werden, da eine dauerhafte Überexpression mit einer erhöhten Tumorgenese und der möglichen Entstehung von Krebs in Verbindung gebracht wird [66, 207-209].

4.2.1 CAM Assay als alternative in vivo Methode zu immundefizienten Mäusen

Trotz zahlreicher in vitro Charakterisierungsmethoden ist die spontane in vivo Bildung von Teratomen die beständigste Eigenschaft von iPSCs und wird deshalb immer noch als Goldstandard für den Nachweis der Pluripotenz angesehen [58]. Teratome sind gutartige Tumore, welche in vivo zu einem schnellen Wachstum und durch ihre pluripotenten Eigenschaften Zellen aus allen drei Keimbahnen enthalten können.

Um in Bezug auf das 3R-Prinzip Tierversuche und das Leiden der Tiere zu verringern, wurde in dieser Arbeit die Anwendbarkeit des CAM-Assays als neues in vivo Modell für die Bewertung der Pluripotenz von hiPSCs getestet. Für die Analyse der explantierten Teratome wurden neben Hämatoxylin und Eosin Färbungen immunhistochemische und -zytochemische Färbungen sowie Genexpressionsanalysen mittels qRT-PCR angewendet.

Die in vivo Teratombildung wird üblicherweise in immundefizienten Mäusen durchgeführt. Hierbei werden gewöhnlich 15 bis 20 Mäusen im Alter von 6 bis 10 Wochen [58, 210] die Stammzellen subkutan [211] oder intramuskulär [212] injiziert. Nach etwa 4 bis 6 Wochen haben sich meistens deutlich sicht- und ertastbare Teratome gebildet [213]. Die Bildung des Teratoms ist hierbei jedoch häufig mit dem Leiden der Tiere verbunden und kann auf Grund der Größe und des Gewichts zu einer erheblichen eingeschränkten Beweglichkeit oder durch Schmerzen und Ängsten zu einem veränderten Verhalten oder einer eingeschränkten Futter- und Wasseraufnahme der Tiere führen [58].

Die CAM wird durch die Verschmelzung der mesodermalen Schicht der Allantois mit der mesodermalen Schicht des Chorions bis zum dritten Tag der Entwicklung des Hühnerembryos gebildet [214, 215]. Die stark vaskularisierte CAM stellt eine optimale Umgebung für die Zelltransplantation dar und kann die applizierten Zellen ausreichend versorgen [216]. Ein ethischer Vorteil gegenüber immundefizienten Mäusen besteht darin, dass die CAM nicht innerviert ist, wodurch keine Schmerzen oder Beeinträchtigungen für den Embryo entstehen [214] und die 3R-Prinzipien („Reduction, Replacement, Refinement“) umgesetzt werden können [217]. Außerdem ist durch die natürliche Immundefizienz der CAM die Transplantation von Artfremden (xenogenen) Zellen möglich, ohne dass die Zellen abgestoßen werden.

Für den Test auf Eignung des CAM-Assays als alternatives in vivo Modell zur Teratombildung in immundefizienten Mäusen wurde die CAM befruchteter Hühnereier so freipräpariert, dass die Hühnereier nach der Applikation der hiPSCs weiter bebrütet werden konnten. Die Inkubation der implantierten hiPSCs für 9 bis 10 Tage war hierbei ausreichend, um charakteristische Gewebestrukturen aller drei Keimschichten nachweisen zu können. Das etablierte CAM-Modell ist somit deutlich kostengünstiger und weniger zeitaufwändig als die Nagetiermodelle.

Obwohl der CAM-Assay mehrere Vorteile gegenüber dem in vivo Mausmodell hat, hat diese Methode den Nachteil, dass die Brutdauer der Küken auf 21 Tage limitiert ist. Da die CAM erst an Tag 3 bis 4 der Bebrütung gebildet wird und erst ab Tag 7 eine ausreichende Vaskularisierung für die Nährstoffversorgung der Zellen vorhanden ist, sollte die Inkubationszeit auf maximal 12 Tage ausgedehnt werden. Im Gegensatz dazu wird die Teratombildung bei Mäusen etwa 4 bis 6 Wochen lang durchgeführt [58]. Durch eine weitere Verlängerung der Inkubationszeit kann die Größe oder die Gewebereifung des Teratoms erhöht werden. Daher muss davon ausgegangen werden, dass die Gewebestrukturen, die sich in den Teratomen auf der CAM bilden, weniger ausgereift sind als die in Mäusen mit einer deutlich längeren Wachstumsphase. Dennoch konnte durch die Detektion von Gewebearten der drei Keimbahnen gezeigt gezeigt werden, dass der CAM-Assay geeignet ist. Die Robustheit der Methode wurde durch die erfolgreiche Teratombildung drei verschiedener hiPSC-Linien, die aus RECs, NuFFs (Human newborn foreskin fibroblasts) oder JPCs abstammen, nachgewiesen.

Neben der Inkubationszeit spielt die verwendete Zellzahl eine entscheidende Rolle bei der erfolgreichen Teratombildung. 1 x 10^6 PSCs pro Injektion sind eine gängige Zellmenge im Nagermodell [58]. Da die Wachstums- und Differenzierungsrate je nach pluripotenter Stammzell-Linie variieren kann, kann eine Anpassung der Zellzahl an die jeweilige Zelllinie erforderlich sein [58]. So führte die Erhöhung der hiPSC Anzahl von 0,5 x 10^6 auf 2 x 10^6 hiPSCs in dem hier etablierten CAM-Assay zu einer Steigerung der Teratombildungseffizienz von 30% auf 70%. Mit der weiteren Erhöhung auf 4 x 10^6 Zellen konnten auf allen CAMs Teratome detektiert werden. Die Verwendung von 2 x 10^6 hiPSCs war jedoch bereits ausreichend, um allen drei Keimbahnen in den explantierten Teratomen mittels H&E Färbung, spezifischer Antikörperfärbung (Immunhistochemie & Immuncytochmie) sowie durch den Nachweis der Expression mittels qRT-PCR nachzuweisen. Das etablierte CAM-Assay Modell bietet sich somit als Zeit- und

kostengünstige Alternative zu immundefizienten Mäusen zur in vivo Bestätigung der Differenzierungsfähigkeit von neu generierten hiPSC-Linien an. Eine Abwandlung diese Methode kann zusätzlich für die Überprüfung von Differenzierungsprotokollen auf verbliebene hiPSCs angewendet werden. Die Implantation von verbleibenden, nicht vollständig ausdifferenzierten hiPSCs kann zur Bildung von Teratomen führen und muss für den klinischen Einsatz durch eine effiziente Differenzierung oder Separationsschritte verhindert werden. Die Entstehung von atypischem Gewebe nach der Transplantation und Inkubation von ausdifferenzierten Zellen auf der CAM, würden hierbei auf verbliebene hiPSC und eine unvollständige und nicht ausreichende Differenzierung bzw. Separation für eine klinische Anwendung hindeuten.

4.3 Differenzierung und Verabreichung von hiPSCs-abgeleiteten Kardiomyozyten

Nach der erfolgreichen Reprogrammierung von RECs zu sicheren und rückstandsfreien hiPSCs mittels srRNA wurden die hiPSCs zu Kardiomyozyten differenziert. Der Fokus liegt hierbei auf der Regeneration von geschädigtem Myokard nach einem Herzinfarkt, um Folgeerkrankungen, die mit einer eingeschränkten Kontraktilität einhergehen, zu reduzieren. Hierfür ist neben der Expression kardialer Proteine und der Ausbildung von funktionellen Sarkomeren die elektromechanische Kopplung der Zellen von großer Bedeutung. In einer früheren Studie konnte bereits gezeigt werden, dass die elektromechanische Reizweiterleitung von hiPSC-abgeleiteten Kardiomyozyten ebenso wie im Myokard über „gap junctions“ und dem anschließenden schlagartigen Einstrom von Ca^{2+}-Ionen, die im sarkoplasmatischem Retikulum und dem Extrazellulärraum gespeichert sind, stattfindet [218]. Zusätzlich konnte gezeigt werden, dass die Erregungsweiterleitung bei funktionalen hiPSC-abgeleiteten Kardiomyozyten, durch die pharmakologische Modulation der Calciumkanäle beeinflusst werden kann [219].

In dieser Arbeit konnten bereits 7 Tage nach Beginn der Differenzierung erste spontan kontrahierende Zellen detektiert werden. Im weiteren Verlauf der Differenzierung kam es zur Synchronisierung einzelner kontrahierender Bereiche und letztlich zur Ausbildung kontraktiler Einheiten bis hin zu einer einzelnen kontraktilen Einheit über das gesamte Kulturgefäß. Die elektromechanische Kopplung und die Ausbildung eines Synzytiums konnte durch die Oszillation der Kontraktion sowie durch die fluoreszenzbasierte Detektion des pulsierenden Calciumeinstroms nachgewiesen werden.

Zusätzlich konnte das Ansprechen auf die gängigen Calciumkanal-Modulatoren Nifedipin und Isoproterenol/Isoprenalin nachgewiesen werden. Bei Nifedipin handelt es ich um einen Calciumkanalantagonisten, der zur Blockade des Ca^{2+} Einstroms und somit zur Verringerung der Kontraktilität der Kardiomyozyten im Herzen führt [220]. Isoprenalin ist dagegen ein Adrenalin-Abkömmling und ein β-Adrenozeptor-Agonist, der im Herzen zu einem verstärkten Einstrom von Ca^{2+} Ionen führt. Dadurch wird der Schwellenwert des Aktionspotentials schneller erreicht, was wiederum eine erhöhte Kontraktilität und Schlagfrequenz der Kardiomyozyten zur Folge hat [221, 222]. Bei der pharmakologischen Modulation der hiPSC-Kardiomyozyten mit Isoprenalin konnte vor dem Erreichen eines Plateaus eine konzentrationsabhängige Steigerung der Schlagfrequenz festgestellt werden. Im Gegensatz dazu führte die Behandlung der hiPSC-abgeleiteten Kardiomyozyten mit Nifedipin ab einer Konzentration von 0,1 µM zu einer kompletten Inhibierung der spontanen Kontraktionen, die jedoch nach Absetzen des Medikaments wieder einsetzte. Mit der Ausbildung eines Synzytiums sowie dem Ansprechen auf gängige Calciumkanal-Modulatoren konnte somit die elektromechanische Funktionalität aus REC-hiPSCs ausdifferenzierten Kardiomyozyten nachgewiesen werden.

Die klinische Anwendung der generierten Kardiomyozyten zur Reparatur von geschädigtem Herzgewebe erfordert jedoch neben der Funktionalitätsprüfung die Produktion einer reinen Kardiomyozyten-Kultur im großen Maßstab. Um vollständig ausdifferenzierte Kardiomyozyten-Kulturen zu erhalten, kann auf eine Positiv- oder Negativselektion zurückgegriffen werden. Hierzu können die generierten Kardiomyozyten über Oberflächenrezeptoren wie SIRPα (Signal-regulatory protein α) [223], mit Fluorophoren oder mit magnetischen Beads funktionalisierten Antikörpern markiert und mittels FACS (Fluorescent activated cell sorting) [223] oder MACS (Magnetic assisted(activated-cell sorting) [224] von nicht-Kardiomyozyten separiert werden (= Positivselektion). Ob die Antikörpermarkierungen jedoch einen Einfluss in klinischen Anwendungen haben können, ist bislang nicht vollständig geklärt. Alternativ können die Kardiomyozyten mit Hilfe eines nicht Glucose-haltigen Mediums mit Lactat angereichert werden. Glukose ist für die meisten Säugetierzellen die Hauptenergiequelle. Sie wird während der Glykolyse über Glucose-6-Phosphat zu Pyruvat und/oder Laktat umgewandelt, wobei geringe Mengen Energie frei werden. Das Pyruvat wird anschließend in den Mitochondrien im Citratzyklus durch oxidative Phosphorylierung zur hauptsächlichen Energiegewinnung umgesetzt. Kardiomyozyten sind dagegen in der Lage neben

Glukose auch Fettsäuren und Laktat durch die oxidative Phosphorylierung zur Energiegewinnung heranzuziehen [225, 226]. Durch die Kultivierung von Kardiomyozyten in lactathaltigem Medium ohne Glucose, können somit nicht differenzierte Zellen und nicht-Kardiomyozyten eliminiert werden (= Negativselektion) [227]. Im Rahmen dieser Arbeit konnte mit der Selektion über 4 bis 6 Tage in einem Lactat-haltigen Medium ohne Glucose eine nahezu reine Kardiomyozyten-Kultur generiert werden, die etwa zu 90 % kardiales Troponin exprimierten**.**

Eine weitere Methode, die auf der gezielten Stimulation der Proliferation von Kardiomyozyten basiert, wurde aktuell von Buikema und Kollegen präsentiert [112]. Mit dem Ablösen und Aussäen der Kardiomyozyten in einer geringen Zelldichte (~10.000/cm²) und der Zugabe des GSK-3 Inhibitors CHIR99021 konnten die Ausreifung unterbrochen und die hiPSC-Kardiomyozyten zur verstärkten Proliferation angeregt werden [112, 228]. Über mehrere Passagen hinweg können so fast reine Kardiomyozyten-Kulturen (>92 % α-Actinin positiv) generiert werden [228]. Zusätzlich kann hierdurch eine Expansion der Kardiomyozyten-Kultur von bis zu 30.000 % über 5 Passagen erreicht werden [112]. Da es sich hierbei um eine reversible Modulation verschiedener Signalwege handelt, können mit dem Entzug von CHIR99021 die proliferationsfördernden Signalwege abgeschaltet und die Ausreifung der Kardiomyozyten fortgesetzt werden [112]. Dies erlaubt die massive Generierung funktionaler Kardiomyozyten, die je nach Einsatzgebiet mit einer spezifische Subdifferenzierung zu nodalen, atrialen oder ventrikulären Kardiomyozyten in Ihrer Funktionsweise an das Zielgewebe angepasst werden können [229, 230].

4.3.1 Wasserstrahl-basierte Injektion von Kardiomyozyten

Im weiteren Verlauf dieser Forschungsarbeit wurde eine neuartige Wasserstrahl-basierte Injektionsmethode für die Anwendung von hiPSC-Kardiomyozyten ex vivo in Schweineherzen untersucht. Das aus der Wasserstrahlchirurgie abgeleitete System wurde erstmals von Jäger und Kollegen für die schnelle und präzise Injektion von MSCs in den Schließmuskel beschrieben [231]. Die Verwendung von zwei unmittelbar nacheinander geschalteten Wasserstrahlen mit unterschiedlich einstellbaren Drücken ermöglicht das nerven- und blutgefäßschonende Eröffnen des Gewebes und unmittelbar im Anschluss die großflächige Verteilung der Zellen im Gewebe.

Für die Stammzell-basierte Regeneration von geschädigtem kardialem Gewebe wurden bereits verschiedene Methoden, wie beispielsweise die intravenöse Infusion [232],

die Perfusion über die Herzarterien [233] oder Mehrfachinjektionen in das Myokard [234] getestet. Bei der Verabreichung von pluripotenten Stammzellen-abgeleiteten Kardiomyozyten stellt die intramyokardiale Injektion mit einer einzelnen Kanüle die häufigste Verabreichungsmethode dar [154, 234-236]. Trotz des häufigen Einsatzes bringt die Injektion über einzelne Kanülen eine Reihe von Nachteilen mit sich. Während kleine Kanülen auf Grund höherer Scherspannungen und Drücke, die während der Injektion erzeugt werden, zu einem höheren Verlust der Viabilität der Kardiomyozyten führen können, bergen Kanülen mit einem größeren Durchmesser dagegen ein erhöhtes Risiko für Gewebe- und Blutgefäßverletzungen und den Rückfluss der Zellen entlang des Penetrationsweges [170, 237]. Zusätzlich konnten mehrere klinische Studien zeigen, dass bei einem Myokardinfarkt etwa 16 bis 21 % des gesamten linken Ventrikels betroffen sind [238-240]. Für eine effiziente Regeneration des betroffenen Gebiets und die Wiederherstellung der Funktionsfähigkeit ist daher eine starke räumliche Verteilung der injizierten Zellen notwendig. Die Injektion mit einer einzelnen Kanüle setzt daher Mehrfachinjektionen voraus. Für eine Studie in Makakenaffen wurden beispielsweise bis zu 15 Injektionen vorgenommen, um eine ausreichende Verteilung der Kardiomyozyten im Myokard zu erreichen [154, 235]. Eine alternative Injektionsvorrichtung, bestehend aus sechs 23 G Kanülen, mit jeweils zwei zusätzlichen seitlichen Bohrungen, wurde von Tabei und Kollegen entwickelt [241]. Bei der Injektion von aus hiPSC gewonnenen Kardiomyozyten-Sphäroiden in das Myokard von Schweinen konnte unter Verwendung der Injektionsvorrichtung im Vergleich zu einer einzelnen 23 G Kanüle die Retentionsrate von 17 % auf 48 % gesteigert werden.

In dieser Arbeit wurde eine 27 G Kanüle als Referenz verwendet, was im mittleren Bereich der in der Literatur eingesetzten Kanülen (23 bis 29 G) liegt [154, 234-236, 241]. Wie bereits bei Tabei und Kollegen [241], führte die Einzelinjektion mit einer 27 G Kanüle bei den ex vivo Versuchen in Schweineherzen auch in unserer Studie zu einer lokal begrenzten Verteilung der hiPSC-Kardiomyozyten. Im Gegensatz dazu konnte mit dem neuen Wasserstrahlsystem eine bessere Verteilung sowohl bei den mit Eisenoxid beschichteten Mikropartikeln im MRT als auch bei den fluoreszenzmarkierten Kardiomyozyten bei der Auswertung im IVIS (In vivo imaging system) detektiert werden. Auffällig war, dass mit der Einstellung E60 für den Penetrationsstrahl tendenziell eine etwas breitere Verteilung der Kardiomyozyten im Myokard beobachtet werden konnte, wogegen die Einstellung E80 zu einer Kanalbildung und einer eher weniger breiten Verteilung führte.

Ebenso auffällig war bei der Analyse der fluoreszenzmarkierten Kardiomyozyten, die mit der 27 G Kanüle injiziert wurden, die signifikant stärkere Verteilung über die Herzkranzgefäße im Vergleich zu der Injektion mit dem Wasserstrahlsystem. Ähnliche Ergebnisse konnten ebenfalls bei parallel zu dieser Studie laufenden in vivo Versuchen von Linzenbold und Kollegen nach der Injektion von MSCs in den Schließmuskel von Schweinen festgestellt werden [242]. Während die Wasserstrahl-basierte Injektion zu einer präzisen und weiträumigen Verteilung der Zellen führte, konnten bei drei von vier Schweinen, die mit einer Williams Nadel (~23 G) injiziert wurden, keine oder an unerwünschten Stellen Zellen gefunden werden.

Auf die Anwendung im Herzen bezogen, kann eine mechanische Verletzung der Blutgefäße bei der Applikation von Kardiomyozyten in vivo zur Verteilung von Kardiomyozyten über die Koronararterien führen [242]. Durch Bildung von Zellaggregaten kann es anschließend zum Verschluss der Gefäße und zu einer erneuten Ischämie im Herzen kommen. Zusätzlich geht durch die mechanische Verletzung des gesunden Herzmuskelgewebes die Gefahr einer Verstärkung der in Folge des Myokardinfarktes auftreten Entzündungsreaktionen aus, was zu einem erhöhten Risiko von Herzrhythmusstörungen führen kann [243].

Neben dem Verlust der Funktion können Zellen, die bei der Injektion beschädigt werden, ebenso Auslöser von Entzündungsreaktionen sein. Die Viabilität und Zellwiederfindung stellt somit ein kritisches Maß für die Beurteilung der Injektionsmethode dar. Verglichen mit der 27 G Kanüle mit einem Durchmesser von etwa 400 µm, besitzt die Düse des Wasserstrahl-Systems ausschließlich einen Durchmesser von 150 µm. Dadurch bewegen sich die Zellen im Wasserstrahlsystem schneller und reagieren demzufolge empfindlicher auf Scherspannung. Die Viabilität der Kardiomyozyten hängt somit bei dem Wasserstrahlsystem maßgeblich vom Injektionsdruck ab. Der in vitro Vergleich von drei verschiedenen Drücken (E5, E10 und E20) beim Injektionsstrahl zeigte, dass das Wasserstrahlsystem zunächst keinen bzw. nur einen geringen Einfluss auf die Viabilität der Zellen hat im Vergleich zur Injektion mit einer 27 G Kanüle hat. Bei der Zellwiederfindung konnte jedoch mit der Einstellung E20 vermutlich durch die bei der Injektion auftretenden Scherkräfte eine deutliche Abnahme der Zellwiederfindung detektiert werden.

Das Wasserstrahl-System eignet sich somit grundsätzlich zur gewebe- und blutgefäßschonenden Injektion von Zellen. Jedoch muss der Injektionsdruck auf die jeweiligen

Zellen und das Zielgewebe abgestimmt werden, um die initiale Schädigung der zu applizierenden Zellen sowie weitere Entzündungsreaktionen des Gewebes zu vermeiden. Ebenso sollten der Druck und das Volumen des Penetrationsstrahls auf das jeweilige Gewebe abgestimmt werden. Bei einem zu hohen Injektionsvolumen kann der Druck des umliegenden Gewebes zu groß werden, so dass die Zellsuspension nach der Injektion aus dem Myokard gedrückt wird. Weitere Untersuchungen mit höheren Fallzahlen sollten deshalb zur Ermittlung der idealen Einstellungen durchgeführt werden.

Die Verabreichung der hiPSC-Kardiomoyzyten wurden in dieser Arbeit sowohl bei der Verwendung des Wasserstrahl-Systems als auch bei der Injektion über die Kanüle am Epikard durchgeführt. In vivo wird die epikardiale Injektion in der Regel am offenen Herzen bei einer Thorakotomie während eines künstlich herbeigeführten Herzstillstands [244] oder bei einer seitlichen Minithorakotomie [245] durchgeführt. Da es sich hierbei um medizinisch aufwendige und invasive Eingriffe handelt, sind diese mit einem beträchtlichen Risiko und möglichen Komplikationen verbunden. Mit Katheter-gestützten Methoden, wie der endokardialen [246-248] oder der intrakoronaren [233, 249-251] Injektion, stehen auch weniger invasive Methoden für die Zellapplikation zur Verfügung. Das neuartige Wasserstrahl-basierte Zellinjektionssystem ist neben der in dieser Arbeit gezeigten epikardialen Verabreichung ebenso für eine endokardiale als auch eine intrakoronare Verabreichung geeignet und könnte damit die Zelltransplantation in Zukunft präziser, weniger invasiv und belastend für den Patienten machen.

4.4 Besiedelung und osteogene Differenzierung von JPCs auf β-TCP Scaffolds

Die Regenerative Medizin stellt mit der Reparatur von kleinen und großen Knochendefekten ein zentrales Forschungsgebiet im Bereich der Mund-, Kiefer- und Gesichtschirurgie dar. Durch den Einsatz von autologen MSCs wird versucht, biologische Prozesse, die während der Embryogenese ablaufen, zu imitieren und somit eine gesteigerte Knochenregeneration zu erreichen [252]. Die MSCs, die in der Knochenregeneration zur Anwendung kommen, stammen meist aus dem Knochenmark [253, 254] oder dem Zahn- und Kiefergewebe [28, 255]. Während die Isolierung von MSCs aus dem Knochenmark ein invasiver und schmerzhafter Eingriff für den Patienten ist und auf Grund der sehr geringen Menge an MSCs im Knochenmark (~0,001–0,01%) meist

nicht ausreichend genug Zellen für einen erkennbaren osteogenen Effekt gewonnen werden können [256, 257], sind JPCs im Kieferperiost leichter zugänglich und zeigen zudem ein sehr gutes osteogenes Differenzierungspotential [131, 132].

Bei Knochendefekten die eine kritische Größe überschreiten, reicht dagegen die Verabreichung von MSCs allein meist nicht aus. Um in Zukunft auch die Regeneration von größeren Knochendefekten zu ermöglichen, wurde in dieser Arbeit zunächst die Kultivierung von JPCs auf β-TCP-Gerüsten und die anschließende Differenzierung zu osteogenen Progenitorzellen untersucht. Mit β-TCP als Biomaterial kann die Knochenstruktur imitiert werden, um eine Umgebung zu schaffen, die der physiologischen Umgebung im Körper ähnelt und eine Ansiedlung von Knochenzellen und die Regeneration von gesundem Knochengewebe fördert. Zusätzlich konnte gezeigt werden, dass durch die physiologische Degradierung von β-TCP nach der Implantation anorganisches Material wie Kalzium- (Ca^{2+}) und Phosphationen (PO_4^{2-}) freigesetzt wird, die die Differenzierung in Osteoblasten ähnlichen Zellen und die Mineralisierung bei der Knochenregeneration nachweislich unterstützen [137]. Eine Beschichtung der Biomaterialien mit Polymeren wie PLGA kann zudem die mechanische Stabilität bei größeren Knochendefekten erhöhen und zu einer verstärkten Zelladhäsion beitragen [138]. Darüber hinaus kann durch Modifikation der PLGA-Beschichtung mit Wachstums- und/oder Differenzierungsfaktoren die Biofunktionalität sowie die Vaskulogenese und Angiogenese des Knochenersatzes verbessert werden [258, 259].

Die Beschichtung der β-TCP Gerüste führte in dieser Studie zu einer glatteren und weniger porösen Struktur im Vergleich zu den unbeschichteten β-TCP-Gerüsten. Da die Porengröße und die Makro- und Mikroporosität wichtig für die osteogene Differenzierung sind [253], kann die osteogene Differenzierung dadurch positiv oder negativ beeinflusst werden. Eine Analyse der Viabilität über den Zellmetabolismus zeigte geringe, aber dennoch signifikante Schwankungen zwischen PLGA beschichteten und unbeschichteten Gerüsten. Insbesondere bei der osteogenen Differenzierung konnten diese über die Differenzierungsdauer von 13 Tagen ausgeglichen werden. Ebenso zeigten die REM Aufnahmen sowohl bei den PLGA-beschichteten als auch bei den unbeschichteten β-TCP Gerüsten eine gleichmäßige und fast vollständige Zellbesiedelung der Gerüste an Tag 15. Um das osteogene Differenzierungspotential der JPCs auf den verschieden behandelten Gerüsten zu testen, wurden diese für 15 Tage ent-

weder im Standard JPC-Kulturmedium oder im osteogenen Induktionsmedium kultiviert. Bei dem osteogenen Differenzierungsmedium wurde hierbei auf die gängigen osteogenen Differenzierungstreiber Dexamethason-, Ascorbinsäure- und β-Glycerophosphat zurückgegriffen. Die signifikant erhöhte Expression und Aktivität von ALPL (Alkaline phosphatase L) sowie die erhöhten Hydroxylapatit-Ablagerungen (Mineralisierung) bestätigten hierbei die erfolgreiche osteogene Differenzierung. Die hier durchgeführten Analysen der ALP-Genexpression und ALP-Aktivität deuten darauf hin, dass die Kultivierung von JPCs auf der PLGA-Beschichtung zu einer verstärkten osteogenen Zelldifferenzierung führt.

4.4.1 Einfluss von zellbesiedelten Biomaterialien auf die Hämostase

Während der Transplantation der generierten Knochen-Gerüste kommt es beim Patienten durch den Eingriff zu Gewebeverletzungen und somit zu direktem Blutkontakt. Je nach Biomaterial und Oberflächeneigenschaften kann dies durch die Absorption von Proteinen und Zellen zur Aktivierung der Thrombozyten und Leukozyten sowie zur Einleitung der Gerinnung führen [260]. Durch diese primären Schritte bildet sich eine provisorische Matrix, die die späteren Reaktionen des Wirts auf die Implantate beeinflusst. Neben dem Gerüstmaterial können auch die auf den Gerüsten ausgesäten Zellen einen Einfluss auf die Hämokompatibilität bzw. die Hämostase haben.

Um mögliche Interaktionen bei einer zukünftigen klinischen Anwendung abschätzen zu können, wurde nach dem Nachweis der erfolgreichen Besiedelung und der osteogenen Differenzierung der JPCs auf den PLGA-beschichteten und unbeschichteten β-TCP-Gerüsten der Kontakt der zellbesiedelten Gerüste (nativ und osteogen induziert) mit humanem Vollblut nachgestellt und die Aktivierungsmarker analysiert. Die Versuchsplanung und -durchführung erfolgte hierbei gemäß ISO 10993-4 für die biologische Beurteilung von Medizinprodukten in Kontakt mit Blut.

Die Inkubation von PLGA-beschichteten oder unbeschichteten β-TCP-Scaffolds mit frischem Vollblut zeigte weder bei nativen noch bei osteogen induzierten JPCs eine Verringerung der Blutzellzahl im Vergleich zu den Kontrollproben ohne Scaffolds. Außerdem konnten weder Hinweise auf Entzündungsreaktionen (PMN-Elastase), noch eine Aktivierung des Komplementsystems (SC5b-9) oder eine Aktivierung von Throm-

bozyten (β-TG) festgestellt werden. Die Analyse der Aktivierung des Gerinnungssystems über den TAT-Komplex zeigte dagegen erhöhte Werte bei zellbesiedelten β-TCP-Gerüsten, unabhängig von der Behandlung. Die Aktivierung der Gerinnungskaskade führt zur Bildung von Thrombin und anschließend zur Bildung eines Fibrinnetzwerkes. REM-Analysen bestätigten die Aktivierung des Gerinnungssystems über die Bildung eines Fibrinnetzwerks mit eingeschlossenen Erythrozyten auf der Oberfläche der mit Zellen besiedelten β-TCP-Gerüsten. Im Gegensatz dazu waren bei den Gerüsten ohne Zellen keine Fibrinnetzwerke und zudem Erythrozyten-Ablagerungen ausschließlich in den Hohlräumen der Gerüste nachweisbar.

Das Gerinnungssystem kann über den intrinsischen Weg der Kontaktaktivierung oder den extrinsischen Weg über TF aktiviert werden [184]. In früheren Studien konnte bereits festgestellt werden, dass nach intravenöser Applikation bei Mäusen [261] und intramyokardialer Applikation bei Schweinen [262] aus menschlichem Knochenmark und parodontalem Ligament gewonnen MSCs zu thromboembolischen Ereignissen kommen kann. Eine intensive Untersuchung einer weiteren Studie ergab, dass die thromboembolischen Komplikationen mit der starken Expression von TF von MSCs zusammenhängen und somit eine Aktivierung des Gerinnungssystems über den extrinsischen Aktivierungsweg auslösen können [263].

Bei einer möglichen klinischen Anwendung kommt es beim Freipräparieren der Implantationsstelle zur Verletzung des vaskularisierten Gewebes und somit zum Blutkontakt des Knochen-Gerüsts. Durch die Aktivierung des Gerinnungssystems wird sofort eine provisorischen Matrix ausgebildet. Das darin enthaltene Plasmafibronektin kann dabei die Zelladhäsion über Integrin-Rezeptoren fördern. Dadurch werden die Migration und Adhäsion verschiedener Zelltypen, wie Fibroblasten und Endothelzellen, stimuliert. Zusätzlich fördert die gebildete Matrix die Adhäsion und Aktivierung von Thrombozyten. Aktivierte Thrombozyten, die in der provisorischen Matrix eingeschlossen sind, können verschiedene Wachstumsfaktoren freisetzen, wie PDGF (Platelet-derived growth factor), VEGF (Vascular endothelial growth factor), bFGF (Basic fibroblast growth factor)und TGF-β (Transforming growth factor-β), die zur Rekrutierung von Fibroblasten, Endothelzellen und Immunzellen führen [264]. Die rekrutierten Endothelzellen können durch Einwachsen in das Gerüst und durch auslösen angiogenetischer Prozesse zur Vaskularisierung des Gerüsts beitragen. Die zeitnahe Gefäßneu-

bildung, die die Versorgung der Knochen-Konstrukte mit Sauerstoff und anderen Nährstoffen sicherstellt, ist eine entscheidende Komponente für die Integration der Gerüste in das umliegende Gewebe und ein zentraler Punkt für die rasche Knochenheilung [265]. Die Aktivierung der Blutgerinnung durch JPC-besiedelte β-TCP Gerüste könnte somit im Vergleich zu JPC-freien Gerüsten die Neovaskularisierung und die Heilungsreaktionen weiter fördern, was zu einer beschleunigten Knochenregeneration führen kann.

5 Ausblick

In dieser Arbeit gelang es, mittels srRNA rückstandsfreie hiPSCs aus RECs herzustellen und diese zu funktionalen Kardiomyozyten zu differenzieren. Mit der Abwandlung des CAM-Assays konnte zudem eine Alternative in vivo Methode zur Teratombildung in Nagetieren zur Bestimmung der Pluripotenz von hiPSCs etabliert werden. Im Anschluss an die erfolgreiche Charakterisierung der hiPSC-Kardiomyozyten konnten mit den ex vivo Versuchen zur wasserstrahlbasierten Applikation der hiPSC-Kardiomyozyten vielversprechende Daten zu dem Injektionssystem gesammelt werden. Damit konnte die Grundlage für eine gewebe- und blutgefäßschonende Injektion von Kardiomyozyten zur Regeneration des Herzmuskels nach einem Myokardinfarkt gelegt werden. Darüber hinaus konnte gezeigt werden, dass neben Biomaterialien, die häufig im Knochen Tissue Engineering eingesetzt werden, auch Zellen wie MSCs bzw. JPCs beim Kontakt mit Blut die Hämostase und somit möglicherweise die Knochenheilung beeinflussen können.

Bevor eine therapeutische Anwendung von Stammzellen bzw. aus Stammzellen generierter Zellen am Patienten stattfinden kann, muss die Sicherheit und Wirksamkeit dieser Zellen in vivo untersucht werden. Insbesondere die Reprogrammierung von somatischen Zellen zu hiPSCs ist mit einer ausführlichen in vitro und in vivo Charakterisierung verbunden. Mit der Abwandlung des CAM-Assays als in vivo Nachweis für die Pluripotenz von PSCs, steht zukünftig eine kostengünstige und schnelle in vivo Methode zur Verfügung, die den Anforderungen der 3R-Regel (Replacement, Reduction und Refinement) zur Reduktion von Tierversuchen und Tierleid gerecht wird.

Um die Sicherheit, der aus den Stammzellen differenzierten Zellen zu erhöhen, kann eine Separierung nach Oberflächenmolekülen durchgeführt werden. Hierbei können durch FACS- oder MACS-gestützte Systeme oder durch die Kombination verschiedener Verfahren die generierten Zellen weiter angereichert werden. Zudem kann durch das Einbauen von Selektionsverfahren in den Differenzierungsprozess die Wahrscheinlichkeit von Rückständen und somit die Wahrscheinlichkeit einer Teratombildung nach der Transplantation deutlich verringert werden. Durch weitere Fortschritte in der Erforschung molekularer Mechanismen der Embryonalentwicklung kann die Funktionalität der generierten Zellen weiter spezialisiert werden, wie beispielsweise durch eine Subdifferenzierung der hiPSC-Kardiomyozyten zu nodalen, atrialen oder

ventrikulären Kardiomyozyten. Somit kann die Differenzierung auf den jeweiligen Einsatzort abgestimmt und Risiken können minimiert werden.

Weiterhin ist für den erfolgreichen Einsatz von Stammzellen in der Regenerativen Medizin die Art der Applikation von großer Bedeutung, um die Zellen effektiv und schonend an den gewünschten Ort im Körper einzubringen. Für die Applikation von Zellen im Herzen kann die wasserstrahlbasierte Methode mit ihrer großflächigen und gewebe- und blutgefäßschonenden Zellinjektion entscheidende Vorteile gegenüber der Injektion mit Kanülen aufweisen. Jedoch sollten die Ergebnisse mit weiteren Versuchen und der Evaluation der Injektionsparameter im in vivo Großtier-Modell bestätigt werden. Eine Alternative zu zellbasierten Ansätzen zur Myokardregeneration stellt die Applikation von kleinen biologisch aktiven Molekülen, von Wachstumsfaktoren und bzw. oder verschiedenen RNAs dar. Hierbei könnte die wasserstrahlbasierte Injektion mit ihrer weiträumigen Verteilung ebenfalls deutliche Vorteile gegenüber herkömmlichen Methoden bieten. Zusätzlich könnte durch einen minimalinvasiven Katheter-gestützten Zugang des Wasserstrahl-Systems die Applikation von Zellen oder biologisch aktiver Moleküle über die Koronararterien oder über das Endokard ermöglicht werden. Dadurch könnte die Applikation vereinfacht und die Belastung für den Patient deutlich verringert werden.

Stammzellbasierte Anwendungen stellen somit einen vielversprechenden Ansatz für die Regenerative Medizin dar. Je nach Anwendungsgebiet stehen hierzu auch heute schon unterschiedliche Applikationswege (Zellsuspensionen oder Biomaterialien) zur Verfügung. Mit dem weiteren Fortschritt der Technologien, wie beispielsweise dem 3D-Bioprinting, könnte in der Zukunft mit autologen Zellen eine auf den Patienten abgestimmte Regeneration von geschädigtem Gewebe bis hin zum Ersatz von Teilen oder ganzen Organen stattfinden und die Heilung von bisher nicht behandelbaren Erkrankungen ermöglichen.

6 Literaturverzeichnis

1. Spallanzani, L., M. Maty, and Pre-1801 Imprint Collection (Library of Congress), *An essay on animal reproductions*. 1769, London: T. Becket and P.A. de Hondt. iv, 86 p.
2. Roensch, K., et al., *Progressive specification rather than intercalation of segments during limb regeneration.* Science, 2013. **342**(6164): p. 1375-9.
3. Debuque, R.J. and J.W. Godwin, *Research into the Cellular and Molecular Mechanisms of Regeneration in Salamanders: Then and Now.* Innovations in Molecular Mechanisms and Tissue Engineering, 2016: p. 1-21.
4. Godwin, J.W. and N. Rosenthal, *Scar-free wound healing and regeneration in amphibians: immunological influences on regenerative success.* Differentiation, 2014. **87**(1-2): p. 66-75.
5. Frobisch, N.B., C. Bickelmann, and F. Witzmann, *Early evolution of limb regeneration in tetrapods: evidence from a 300-million-year-old amphibian.* Proc Biol Sci, 2014. **281**(1794): p. 20141550.
6. Cuenca-Lopez, M.D., et al., *Adult stem cells applied to tissue engineering and regenerative medicine.* Cell Mol Biol (Noisy-le-grand), 2008. **54**(1): p. 40-51.
7. Bajaj, P., et al., *3D biofabrication strategies for tissue engineering and regenerative medicine.* Annu Rev Biomed Eng, 2014. **16**: p. 247-76.
8. Kami, D. and S. Gojo, *Tuning cell fate: from insights to vertebrate regeneration.* Organogenesis, 2014. **10**(2): p. 231-40.
9. Kusumi, K. and J. Wilson-Rawls, *Innovations in Molecular Mechanisms and Tissue Engineering*, in *Stem Cell Biology and Regenerative Medicine,*. 2016, Springer International Publishing : Imprint: Humana,: Cham. p. 1 online resource (X, 182 pages 22 illustrations, 19 illustrations in color.
10. Kusama, K., W.L. Donegan, and T.G. Samter, *An investigation of colon cancer associated with urinary diversion.* Dis Colon Rectum, 1989. **32**(8): p. 694-7.
11. Redd, M.J., et al., *Wound healing and inflammation: embryos reveal the way to perfect repair.* Philos Trans R Soc Lond B Biol Sci, 2004. **359**(1445): p. 777-84.
12. Langer, R. and J.P. Vacanti, *Tissue engineering.* Science, 1993. **260**(5110): p. 920-6.
13. Murphy, C.M., et al., *Cell-scaffold interactions in the bone tissue engineering triad.* Eur Cell Mater, 2013. **26**: p. 120-32.
14. Atala, A., *Tissue engineering of reproductive tissues and organs.* Fertil Steril, 2012. **98**(1): p. 21-9.
15. Selden, C. and B. Fuller, *Role of Bioreactor Technology in Tissue Engineering for Clinical Use and Therapeutic Target Design.* Bioengineering (Basel), 2018. **5**(2).
16. Chan, B.P. and K.W. Leong, *Scaffolding in tissue engineering: general approaches and tissue-specific considerations.* Eur Spine J, 2008. **17 Suppl 4**: p. 467-79.
17. Lu, T., Y. Li, and T. Chen, *Techniques for fabrication and construction of three-dimensional scaffolds for tissue engineering.* Int J Nanomedicine, 2013. **8**: p. 337-50.
18. Zakrzewski, W., et al., *Stem cells: past, present, and future.* Stem Cell Res Ther, 2019. **10**(1): p. 68.
19. Aly, R.M., *Current state of stem cell-based therapies: an overview.* Stem Cell Investig, 2020. **7**: p. 8.
20. Prentice, D.A., *Adult Stem Cells.* Circ Res, 2019. **124**(6): p. 837-839.

21. Lukomska, B., et al., *Challenges and Controversies in Human Mesenchymal Stem Cell Therapy.* Stem Cells Int, 2019. **2019**: p. 9628536.
22. Friedenstein, A.J., R.K. Chailakhjan, and K.S. Lalykina, *The development of fibroblast colonies in monolayer cultures of guinea-pig bone marrow and spleen cells.* Cell Tissue Kinet, 1970. **3**(4): p. 393-403.
23. Friedenstein, A.J., R.K. Chailakhyan, and U.V. Gerasimov, *Bone marrow osteogenic stem cells: in vitro cultivation and transplantation in diffusion chambers.* Cell Tissue Kinet, 1987. **20**(3): p. 263-72.
24. Friedenstein, A.J., S. Piatetzky, II, and K.V. Petrakova, *Osteogenesis in transplants of bone marrow cells.* J Embryol Exp Morphol, 1966. **16**(3): p. 381-90.
25. Young, H.E., et al., *Human reserve pluripotent mesenchymal stem cells are present in the connective tissues of skeletal muscle and dermis derived from fetal, adult, and geriatric donors.* Anat Rec, 2001. **264**(1): p. 51-62.
26. Heidari, B., et al., *Comparison of proliferative and multilineage differentiation potential of sheep mesenchymal stem cells derived from bone marrow, liver, and adipose tissue.* Avicenna J Med Biotechnol, 2013. **5**(2): p. 104-17.
27. Gullo, F. and C. De Bari, *Prospective purification of a subpopulation of human synovial mesenchymal stem cells with enhanced chondro-osteogenic potency.* Rheumatology (Oxford), 2013. **52**(10): p. 1758-68.
28. Olbrich, M., et al., *Isolation of osteoprogenitors from human jaw periosteal cells: a comparison of two magnetic separation methods.* PLoS One, 2012. **7**(10): p. e47176.
29. Romanov, Y.A., V.A. Svintsitskaya, and V.N. Smirnov, *Searching for alternative sources of postnatal human mesenchymal stem cells: candidate MSC-like cells from umbilical cord.* Stem Cells, 2003. **21**(1): p. 105-10.
30. Erices, A., P. Conget, and J.J. Minguell, *Mesenchymal progenitor cells in human umbilical cord blood.* Br J Haematol, 2000. **109**(1): p. 235-42.
31. Gong, X., et al., *Isolation and characterization of lung resident mesenchymal stem cells capable of differentiating into alveolar epithelial type II cells.* Cell Biol Int, 2014. **38**(4): p. 405-11.
32. Hoffmann, A., et al., *Neotendon formation induced by manipulation of the Smad8 signalling pathway in mesenchymal stem cells.* J Clin Invest, 2006. **116**(4): p. 940-52.
33. De Bari, C., et al., *Skeletal muscle repair by adult human mesenchymal stem cells from synovial membrane.* J Cell Biol, 2003. **160**(6): p. 909-18.
34. Lee, C.H., E.K. Moioli, and J.J. Mao, *Fibroblastic differentiation of human mesenchymal stem cells using connective tissue growth factor.* Conf Proc IEEE Eng Med Biol Soc, 2006. **2006**: p. 775-8.
35. Cortes-Medina, L.V., et al., *Neuronal Transdifferentiation Potential of Human Mesenchymal Stem Cells from Neonatal and Adult Sources by a Small Molecule Cocktail.* Stem Cells Int, 2019. **2019**: p. 7627148.
36. Christ, B. and M.M. Dollinger, *The generation of hepatocytes from mesenchymal stem cells and engraftment into the liver.* Curr Opin Organ Transplant, 2011. **16**(1): p. 69-75.
37. Chen, L.B., X.B. Jiang, and L. Yang, *Differentiation of rat marrow mesenchymal stem cells into pancreatic islet beta-cells.* World J Gastroenterol, 2004. **10**(20): p. 3016-20.
38. Wynn, R.F., et al., *A small proportion of mesenchymal stem cells strongly expresses functionally active CXCR4 receptor capable of promoting migration to bone marrow.* Blood, 2004. **104**(9): p. 2643-5.

39. Linero, I. and O. Chaparro, *Paracrine effect of mesenchymal stem cells derived from human adipose tissue in bone regeneration.* PLoS One, 2014. **9**(9): p. e107001.
40. Le Blanc, K. and D. Mougiakakos, *Multipotent mesenchymal stromal cells and the innate immune system.* Nat Rev Immunol, 2012. **12**(5): p. 383-96.
41. Squillaro, T., G. Peluso, and U. Galderisi, *Clinical Trials With Mesenchymal Stem Cells: An Update.* Cell Transplant, 2016. **25**(5): p. 829-48.
42. Turinetto, V., E. Vitale, and C. Giachino, *Senescence in Human Mesenchymal Stem Cells: Functional Changes and Implications in Stem Cell-Based Therapy.* Int J Mol Sci, 2016. **17**(7).
43. Wobus, A.M. and K.R. Boheler, *Embryonic stem cells: prospects for developmental biology and cell therapy.* Physiol Rev, 2005. **85**(2): p. 635-78.
44. Kiskinis, E. and K. Eggan, *Progress toward the clinical application of patient-specific pluripotent stem cells.* J Clin Invest, 2010. **120**(1): p. 51-9.
45. Thomson, J.A., et al., *Embryonic stem cell lines derived from human blastocysts.* Science, 1998. **282**(5391): p. 1145-7.
46. Damschen, G., et al., *Der moralische Status menschlicher Embryonen : pro und contra Spezies-, Kontinuums-, Identitäts- und Potentialitätsargument*. De Gruyter Studienbuch. 2003, Berlin ; New York: De Gruyter. viii, 331 p.
47. Group, T.H. *World Stem Cell Policies*. 2006 [cited 2021 07/15/21]; Available from: http://www.hinxtongroup.org/wp.html.
48. Gurdon, J.B., T.R. Elsdale, and M. Fischberg, *Sexually mature individuals of Xenopus laevis from the transplantation of single somatic nuclei.* Nature, 1958. **182**(4627): p. 64-5.
49. Takahashi, K. and S. Yamanaka, *Induction of pluripotent stem cells from mouse embryonic and adult fibroblast cultures by defined factors.* Cell, 2006. **126**(4): p. 663-76.
50. Takahashi, K., et al., *Induction of pluripotent stem cells from adult human fibroblasts by defined factors.* Cell, 2007. **131**(5): p. 861-72.
51. Young, R.A., *Control of the embryonic stem cell state.* Cell, 2011. **144**(6): p. 940-54.
52. Pauklin, S., R.A. Pedersen, and L. Vallier, *Mouse pluripotent stem cells at a glance.* J Cell Sci, 2011. **124**(Pt 22): p. 3727-32.
53. Yu, J., et al., *Induced pluripotent stem cell lines derived from human somatic cells.* Science, 2007. **318**(5858): p. 1917-20.
54. Jiang, J., et al., *A core Klf circuitry regulates self-renewal of embryonic stem cells.* Nat Cell Biol, 2008. **10**(3): p. 353-60.
55. Meissner, A., *Epigenetic modifications in pluripotent and differentiated cells.* Nat Biotechnol, 2010. **28**(10): p. 1079-88.
56. Atkinson, S. and L. Armstrong, *Epigenetics in embryonic stem cells: regulation of pluripotency and differentiation.* Cell Tissue Res, 2008. **331**(1): p. 23-9.
57. Lister, R., et al., *Hotspots of aberrant epigenomic reprogramming in human induced pluripotent stem cells.* Nature, 2011. **471**(7336): p. 68-73.
58. Nelakanti, R.V., N.G. Kooreman, and J.C. Wu, *Teratoma formation: a tool for monitoring pluripotency in stem cell research.* Curr Protoc Stem Cell Biol, 2015. **32**: p. 4A 8 1-4A 8 17.
59. Ye, L., et al., *Blood cell-derived induced pluripotent stem cells free of reprogramming factors generated by Sendai viral vectors.* Stem Cells Transl Med, 2013. **2**(8): p. 558-66.
60. Aasen, T., et al., *Efficient and rapid generation of induced pluripotent stem cells from human keratinocytes.* Nat Biotechnol, 2008. **26**(11): p. 1276-84.

61. Zhou, T., et al., *Generation of induced pluripotent stem cells from urine.* J Am Soc Nephrol, 2011. **22**(7): p. 1221-8.
62. Ingelfinger, J.R., *Nephrogenic adenomas as renal tubular outposts.* N Engl J Med, 2002. **347**(9): p. 684-6.
63. Zhao, T., et al., *Immunogenicity of induced pluripotent stem cells.* Nature, 2011. **474**(7350): p. 212-5.
64. Pera, M.F., *Stem cells: The dark side of induced pluripotency.* Nature, 2011. **471**(7336): p. 46-7.
65. Wernig, M., et al., *c-Myc is dispensable for direct reprogramming of mouse fibroblasts.* Cell Stem Cell, 2008. **2**(1): p. 10-2.
66. Okita, K., T. Ichisaka, and S. Yamanaka, *Generation of germline-competent induced pluripotent stem cells.* Nature, 2007. **448**(7151): p. 313-7.
67. Soldner, F., et al., *Parkinson's disease patient-derived induced pluripotent stem cells free of viral reprogramming factors.* Cell, 2009. **136**(5): p. 964-77.
68. Fusaki, N., et al., *Efficient induction of transgene-free human pluripotent stem cells using a vector based on Sendai virus, an RNA virus that does not integrate into the host genome.* Proc Jpn Acad Ser B Phys Biol Sci, 2009. **85**(8): p. 348-62.
69. Stadtfeld, M., et al., *Induced pluripotent stem cells generated without viral integration.* Science, 2008. **322**(5903): p. 945-9.
70. Kim, D., et al., *Generation of human induced pluripotent stem cells by direct delivery of reprogramming proteins.* Cell Stem Cell, 2009. **4**(6): p. 472-6.
71. Okita, K., et al., *Generation of mouse-induced pluripotent stem cells with plasmid vectors.* Nat Protoc, 2010. **5**(3): p. 418-28.
72. Hou, P., et al., *Pluripotent stem cells induced from mouse somatic cells by small-molecule compounds.* Science, 2013. **341**(6146): p. 651-4.
73. Warren, L., et al., *Highly efficient reprogramming to pluripotency and directed differentiation of human cells with synthetic modified mRNA.* Cell Stem Cell, 2010. **7**(5): p. 618-30.
74. Steinle, H., et al., *Concise Review: Application of In Vitro Transcribed Messenger RNA for Cellular Engineering and Reprogramming: Progress and Challenges.* Stem Cells, 2017. **35**(1): p. 68-79.
75. Steinle, H., et al., *Generation of iPSCs by Nonintegrative RNA-Based Reprogramming Techniques: Benefits of Self-Replicating RNA versus Synthetic mRNA.* Stem Cells Int, 2019. **2019**: p. 7641767.
76. Yakubov, E., et al., *Reprogramming of human fibroblasts to pluripotent stem cells using mRNA of four transcription factors.* Biochem Biophys Res Commun, 2010. **394**(1): p. 189-93.
77. Sahin, U., K. Kariko, and O. Tureci, *mRNA-based therapeutics--developing a new class of drugs.* Nat Rev Drug Discov, 2014. **13**(10): p. 759-80.
78. Rettig, L., et al., *Particle size and activation threshold: a new dimension of danger signaling.* Blood, 2010. **115**(22): p. 4533-41.
79. Zou, S., et al., *Lipid-mediated delivery of RNA is more efficient than delivery of DNA in non-dividing cells.* Int J Pharm, 2010. **389**(1-2): p. 232-43.
80. Rejman, J., et al., *mRNA transfection of cervical carcinoma and mesenchymal stem cells mediated by cationic carriers.* J Control Release, 2010. **147**(3): p. 385-91.
81. Angel, M. and M.F. Yanik, *Innate immune suppression enables frequent transfection with RNA encoding reprogramming proteins.* PLoS One, 2010. **5**(7): p. e11756.

82. Drews, K., et al., *The cytotoxic and immunogenic hurdles associated with non-viral mRNA-mediated reprogramming of human fibroblasts.* Biomaterials, 2012. **33**(16): p. 4059-68.
83. Kariko, K., et al., *Suppression of RNA recognition by Toll-like receptors: the impact of nucleoside modification and the evolutionary origin of RNA.* Immunity, 2005. **23**(2): p. 165-75.
84. Colamonici, O.R., et al., *Vaccinia virus B18R gene encodes a type I interferon-binding protein that blocks interferon alpha transmembrane signaling.* J Biol Chem, 1995. **270**(27): p. 15974-8.
85. Michel, T., et al., *Efficient reduction of synthetic mRNA induced immune activation by simultaneous delivery of B18R encoding mRNA.* J Biol Eng, 2019. **13**: p. 40.
86. Yoshioka, N., et al., *Efficient generation of human iPSCs by a synthetic self-replicative RNA.* Cell Stem Cell, 2013. **13**(2): p. 246-54.
87. Petrakova, O., et al., *Noncytopathic replication of Venezuelan equine encephalitis virus and eastern equine encephalitis virus replicons in Mammalian cells.* J Virol, 2005. **79**(12): p. 7597-608.
88. Jose, J., J.E. Snyder, and R.J. Kuhn, *A structural and functional perspective of alphavirus replication and assembly.* Future Microbiol, 2009. **4**(7): p. 837-56.
89. Foo, S.S., et al., *The genetics of alphaviruses.* Future Virology, 2011. **6**(12): p. 1407-1422.
90. Rupp, J.C., et al., *Alphavirus RNA synthesis and non-structural protein functions.* J Gen Virol, 2015. **96**(9): p. 2483-2500.
91. Aviner, R., *The science of puromycin: From studies of ribosome function to applications in biotechnology.* Comput Struct Biotechnol J, 2020. **18**: p. 1074-1083.
92. Bruns, A.M., et al., *The innate immune sensor LGP2 activates antiviral signaling by regulating MDA5-RNA interaction and filament assembly.* Mol Cell, 2014. **55**(5): p. 771-81.
93. Rehwinkel, J. and M.U. Gack, *RIG-I-like receptors: their regulation and roles in RNA sensing.* Nature Reviews Immunology, 2020. **20**(9): p. 537-551.
94. Takeuchi, O. and S. Akira, *Recognition of viruses by innate immunity.* Immunol Rev, 2007. **220**: p. 214-24.
95. Alexopoulou, L., et al., *Recognition of double-stranded RNA and activation of NF-kappaB by Toll-like receptor 3.* Nature, 2001. **413**(6857): p. 732-8.
96. Diebold, S.S., et al., *Innate antiviral responses by means of TLR7-mediated recognition of single-stranded RNA.* Science, 2004. **303**(5663): p. 1529-31.
97. Heil, F., et al., *Species-specific recognition of single-stranded RNA via toll-like receptor 7 and 8.* Science, 2004. **303**(5663): p. 1526-9.
98. Yamamoto, M., et al., *Cutting edge: a novel Toll/IL-1 receptor domain-containing adapter that preferentially activates the IFN-beta promoter in the Toll-like receptor signaling.* J Immunol, 2002. **169**(12): p. 6668-72.
99. Burns, K., et al., *MyD88, an adapter protein involved in interleukin-1 signaling.* J Biol Chem, 1998. **273**(20): p. 12203-9.
100. Tatematsu, M., et al., *Extracellular RNA Sensing by Pattern Recognition Receptors.* J Innate Immun, 2018. **10**(5-6): p. 398-406.
101. Loo, Y.M. and M. Gale, Jr., *Immune signaling by RIG-I-like receptors.* Immunity, 2011. **34**(5): p. 680-92.
102. Rodriguez, K.R., A.M. Bruns, and C.M. Horvath, *MDA5 and LGP2: accomplices and antagonists of antiviral signal transduction.* J Virol, 2014. **88**(15): p. 8194-200.

103. Kawai, T., et al., *IPS-1, an adaptor triggering RIG-I- and Mda5-mediated type I interferon induction.* Nat Immunol, 2005. **6**(10): p. 981-8.
104. Seth, R.B., et al., *Identification and characterization of MAVS, a mitochondrial antiviral signaling protein that activates NF-kappaB and IRF 3.* Cell, 2005. **122**(5): p. 669-82.
105. Kawai, T. and S. Akira, *The roles of TLRs, RLRs and NLRs in pathogen recognition.* Int Immunol, 2009. **21**(4): p. 317-37.
106. Sabbah, A., et al., *Activation of innate immune antiviral responses by Nod2.* Nat Immunol, 2009. **10**(10): p. 1073-80.
107. Kanneganti, T.D., et al., *Critical role for Cryopyrin/Nalp3 in activation of caspase-1 in response to viral infection and double-stranded RNA.* J Biol Chem, 2006. **281**(48): p. 36560-8.
108. Schneider, W.M., M.D. Chevillotte, and C.M. Rice, *Interferon-stimulated genes: a complex web of host defenses.* Annu Rev Immunol, 2014. **32**: p. 513-45.
109. Chambers, S.M., et al., *Highly efficient neural conversion of human ES and iPS cells by dual inhibition of SMAD signaling.* Nat Biotechnol, 2009. **27**(3): p. 275-80.
110. Kunisada, Y., et al., *Small molecules induce efficient differentiation into insulin-producing cells from human induced pluripotent stem cells.* Stem Cell Res, 2012. **8**(2): p. 274-84.
111. Borchin, B., J. Chen, and T. Barberi, *Derivation and FACS-mediated purification of PAX3+/PAX7+ skeletal muscle precursors from human pluripotent stem cells.* Stem Cell Reports, 2013. **1**(6): p. 620-31.
112. Buikema, J.W., et al., *Wnt Activation and Reduced Cell-Cell Contact Synergistically Induce Massive Expansion of Functional Human iPSC-Derived Cardiomyocytes.* Cell Stem Cell, 2020. **27**(1): p. 50-63 e5.
113. Bilousova, G., et al., *Osteoblasts derived from induced pluripotent stem cells form calcified structures in scaffolds both in vitro and in vivo.* Stem Cells, 2011. **29**(2): p. 206-16.
114. Afshari, A., et al., *Different approaches for transformation of mesenchymal stem cells into hepatocyte-like cells.* Stem Cell Res Ther, 2020. **11**(1): p. 54.
115. Gao, X., et al., *Hepatocyte-like cells derived from human induced pluripotent stem cells using small molecules: implications of a transcriptomic study.* Stem Cell Res Ther, 2020. **11**(1): p. 393.
116. Oh, Y. and J. Jang, *Directed Differentiation of Pluripotent Stem Cells by Transcription Factors.* Mol Cells, 2019. **42**(3): p. 200-209.
117. Baxter, D.J. and M.M. Shroff, *Developmental maxillofacial anomalies.* Semin Ultrasound CT MR, 2011. **32**(6): p. 555-68.
118. Foster, B.L., et al., *Rare bone diseases and their dental, oral, and craniofacial manifestations.* J Dent Res, 2014. **93**(7 Suppl): p. 7S-19S.
119. Terashima, A. and H. Takayanagi, *The role of bone cells in immune regulation during the course of infection.* Semin Immunopathol, 2019. **41**(5): p. 619-626.
120. Chukwulebe, S. and C. Hogrefe, *The Diagnosis and Management of Facial Bone Fractures.* Emerg Med Clin North Am, 2019. **37**(1): p. 137-151.
121. Araujo, M.G. and J. Lindhe, *Dimensional ridge alterations following tooth extraction. An experimental study in the dog.* J Clin Periodontol, 2005. **32**(2): p. 212-8.
122. Rolski, D., et al., *The Management of Patients after Surgical Treatment of Maxillofacial Tumors.* Biomed Res Int, 2016. **2016**: p. 4045329.

123. Schmitz, J.P. and J.O. Hollinger, *The critical size defect as an experimental model for craniomandibulofacial nonunions.* Clin Orthop Relat Res, 1986(205): p. 299-308.
124. Fernandez de Grado, G., et al., *Bone substitutes: a review of their characteristics, clinical use, and perspectives for large bone defects management.* Journal of tissue engineering, 2018. **9**: p. 2041731418776819-2041731418776819.
125. Meloni, S.M., et al., *Horizontal ridge augmentation using GBR with a native collagen membrane and 1:1 ratio of particulate xenograft and autologous bone: A 3-year after final loading prospective clinical study.* Clin Implant Dent Relat Res, 2019. **21**(4): p. 669-677.
126. Urban, I.A., et al., *Horizontal ridge augmentation with a collagen membrane and a combination of particulated autogenous bone and anorganic bovine bone-derived mineral: a prospective case series in 25 patients.* Int J Periodontics Restorative Dent, 2013. **33**(3): p. 299-307.
127. Kinoshita, Y. and H. Maeda, *Recent developments of functional scaffolds for craniomaxillofacial bone tissue engineering applications.* ScientificWorldJournal, 2013. **2013**: p. 863157.
128. Kon, T., et al., *Expression of osteoprotegerin, receptor activator of NF-kappaB ligand (osteoprotegerin ligand) and related proinflammatory cytokines during fracture healing.* J Bone Miner Res, 2001. **16**(6): p. 1004-14.
129. Langenbach, F. and J. Handschel, *Effects of dexamethasone, ascorbic acid and beta-glycerophosphate on the osteogenic differentiation of stem cells in vitro.* Stem Cell Res Ther, 2013. **4**(5): p. 117.
130. Janicki, P. and G. Schmidmaier, *What should be the characteristics of the ideal bone graft substitute? Combining scaffolds with growth factors and/or stem cells.* Injury, 2011. **42**: p. S77-S81.
131. De Bari, C., et al., *Mesenchymal multipotency of adult human periosteal cells demonstrated by single-cell lineage analysis.* Arthritis Rheum, 2006. **54**(4): p. 1209-21.
132. Bruder, S.P., N. Jaiswal, and S.E. Haynesworth, *Growth kinetics, self-renewal, and the osteogenic potential of purified human mesenchymal stem cells during extensive subcultivation and following cryopreservation.* J Cell Biochem, 1997. **64**(2): p. 278-94.
133. Przekora, A., et al., *Do novel cement-type biomaterials reveal ion reactivity that affects cell viability in vitro?* Open Life Sciences, 2014. **9**(3): p. 277-289.
134. Maquet, V., et al., *Preparation, characterization, and in vitro degradation of bioresorbable and bioactive composites based on Bioglass-filled polylactide foams.* J Biomed Mater Res A, 2003. **66**(2): p. 335-46.
135. Fairag, R., et al., *Three-Dimensional Printed Polylactic Acid Scaffolds Promote Bone-like Matrix Deposition in Vitro.* ACS Appl Mater Interfaces, 2019. **11**(17): p. 15306-15315.
136. Putri, T.S., K. Hayashi, and K. Ishikawa, *Bone regeneration using β-tricalcium phosphate (β-TCP) block with interconnected pores made by setting reaction of β-TCP granules.* J Biomed Mater Res A, 2020. **108**(3): p. 625-632.
137. Chang, Y.L., C.M. Stanford, and J.C. Keller, *Calcium and phosphate supplementation promotes bone cell mineralization: implications for hydroxyapatite (HA)-enhanced bone formation.* J Biomed Mater Res, 2000. **52**(2): p. 270-8.

138. Ardjomandi, N., et al., *Coating of ß-tricalcium phosphate scaffolds-a comparison between graphene oxide and poly-lactic-co-glycolic acid.* Biomed Mater, 2015. **10**(4): p. 045018.
139. Wong, N.D., *Epidemiological studies of CHD and the evolution of preventive cardiology.* Nat Rev Cardiol, 2014. **11**(5): p. 276-89.
140. Thomas, H., et al., *Global Atlas of Cardiovascular Disease 2000-2016: The Path to Prevention and Control.* Glob Heart, 2018. **13**(3): p. 143-163.
141. Laslett, L.J., et al., *The worldwide environment of cardiovascular disease: prevalence, diagnosis, therapy, and policy issues: a report from the American College of Cardiology.* J Am Coll Cardiol, 2012. **60**(25 Suppl): p. S1-49.
142. Lazar, E., H.A. Sadek, and O. Bergmann, *Cardiomyocyte renewal in the human heart: insights from the fall-out.* Eur Heart J, 2017. **38**(30): p. 2333-2342.
143. Talman, V. and H. Ruskoaho, *Cardiac fibrosis in myocardial infarction-from repair and remodeling to regeneration.* Cell Tissue Res, 2016. **365**(3): p. 563-81.
144. Konstam, M.A., et al., *Evaluation and Management of Right-Sided Heart Failure: A Scientific Statement From the American Heart Association.* Circulation, 2018. **137**(20): p. e578-e622.
145. Samanta, A., et al., *Bone marrow cells for heart repair: clinical evidence and perspectives.* Minerva Cardioangiol, 2017. **65**(3): p. 299-313.
146. Xu, W., et al., *Mesenchymal stem cells from adult human bone marrow differentiate into a cardiomyocyte phenotype in vitro.* Exp Biol Med (Maywood), 2004. **229**(7): p. 623-31.
147. Amini, H., et al., *Cardiac progenitor cells application in cardiovascular disease.* J Cardiovasc Thorac Res, 2017. **9**(3): p. 127-132.
148. Sebastiao, M.J., et al., *Human cardiac progenitor cell activation and regeneration mechanisms: exploring a novel myocardial ischemia/reperfusion in vitro model.* Stem Cell Res Ther, 2019. **10**(1): p. 77.
149. Zuba-Surma, E.K., et al., *Very small embryonic-like stem cells: biology and therapeutic potential for heart repair.* Antioxidants & redox signaling, 2011. **15**(7): p. 1821-1834.
150. Csobonyeiova, M., S. Polak, and L. Danisovic, *Perspectives of induced pluripotent stem cells for cardiovascular system regeneration.* Exp Biol Med (Maywood), 2015. **240**(5): p. 549-56.
151. Lian, X., et al., *Robust cardiomyocyte differentiation from human pluripotent stem cells via temporal modulation of canonical Wnt signaling.* Proc Natl Acad Sci U S A, 2012. **109**(27): p. E1848-57.
152. Lian, X., et al., *Directed cardiomyocyte differentiation from human pluripotent stem cells by modulating Wnt/beta-catenin signaling under fully defined conditions.* Nat Protoc, 2013. **8**(1): p. 162-75.
153. Watanabe, E., et al., *Cardiomyocyte transplantation in a porcine myocardial infarction model.* Cell Transplant, 1998. **7**(3): p. 239-46.
154. Shiba, Y., et al., *Allogeneic transplantation of iPS cell-derived cardiomyocytes regenerates primate hearts.* Nature, 2016. **538**(7625): p. 388-391.
155. Ishida, M., et al., *Transplantation of Human-induced Pluripotent Stem Cell-derived Cardiomyocytes Is Superior to Somatic Stem Cell Therapy for Restoring Cardiac Function and Oxygen Consumption in a Porcine Model of Myocardial Infarction.* Transplantation, 2019. **103**(2): p. 291-298.
156. Ye, L., et al., *Cardiac repair in a porcine model of acute myocardial infarction with human induced pluripotent stem cell-derived cardiovascular cells.* Cell Stem Cell, 2014. **15**(6): p. 750-61.

157. Yanamandala, M., et al., *Overcoming the Roadblocks to Cardiac Cell Therapy Using Tissue Engineering.* J Am Coll Cardiol, 2017. **70**(6): p. 766-775.
158. He, L. and X. Chen, *Cardiomyocyte Induction and Regeneration for Myocardial Infarction Treatment: Cell Sources and Administration Strategies.* Adv Healthc Mater, 2020. **9**(22): p. e2001175.
159. Gao, L., et al., *Large Cardiac Muscle Patches Engineered From Human Induced-Pluripotent Stem Cell-Derived Cardiac Cells Improve Recovery From Myocardial Infarction in Swine.* Circulation, 2018. **137**(16): p. 1712-1730.
160. Jang, J., et al., *3D printed complex tissue construct using stem cell-laden decellularized extracellular matrix bioinks for cardiac repair.* Biomaterials, 2017. **112**: p. 264-274.
161. Hao, T., et al., *Injectable Fullerenol/Alginate Hydrogel for Suppression of Oxidative Stress Damage in Brown Adipose-Derived Stem Cells and Cardiac Repair.* ACS Nano, 2017. **11**(6): p. 5474-5488.
162. Castilho, M., et al., *Melt Electrowriting Allows Tailored Microstructural and Mechanical Design of Scaffolds to Advance Functional Human Myocardial Tissue Formation.* Advanced Functional Materials, 2018. **28**(40): p. 1803151.
163. Shin, S.R., et al., *Carbon-nanotube-embedded hydrogel sheets for engineering cardiac constructs and bioactuators.* ACS Nano, 2013. **7**(3): p. 2369-80.
164. Gao, L., et al., *Myocardial Tissue Engineering With Cells Derived From Human-Induced Pluripotent Stem Cells and a Native-Like, High-Resolution, 3-Dimensionally Printed Scaffold.* Circ Res, 2017. **120**(8): p. 1318-1325.
165. Hasenfuss, G., *Heart rate as a determinant of cardiac function - Basic mechanisms and clinical significance - Introduction.* Basic Research in Cardiology, 1998. **93**: p. Iii-Iii.
166. Patra, C. and F.B. Engel, *Silk for cardiac tissue engineering.* Silk Biomaterials for Tissue Engineering and Regenerative Medicine, 2014. **74**: p. 429-455.
167. Gerbin, K.A., et al., *Enhanced Electrical Integration of Engineered Human Myocardium via Intramyocardial versus Epicardial Delivery in Infarcted Rat Hearts.* PLoS One, 2015. **10**(7): p. e0131446.
168. Cui, H., et al., *4D physiologically adaptable cardiac patch: A 4-month in vivo study for the treatment of myocardial infarction.* Sci Adv, 2020. **6**(26): p. eabb5067.
169. Halbach, M., et al., *Electrophysiological integration and action potential properties of transplanted cardiomyocytes derived from induced pluripotent stem cells.* Cardiovasc Res, 2013. **100**(3): p. 432-40.
170. O'Cearbhaill, E.D., K.S. Ng, and J.M. Karp, *Emerging medical devices for minimally invasive cell therapy.* Mayo Clin Proc, 2014. **89**(2): p. 259-73.
171. Krishnan, A., et al., *Scaled interfacial activity of proteins at the liquid-vapor interface.* J Biomed Mater Res A, 2004. **68**(3): p. 544-57.
172. Anderson, J.M., A. Rodriguez, and D.T. Chang, *Foreign body reaction to biomaterials.* Semin Immunol, 2008. **20**(2): p. 86-100.
173. Jaffer, I.H., et al., *Medical device-induced thrombosis: what causes it and how can we prevent it?* J Thromb Haemost, 2015. **13 Suppl 1**: p. S72-81.
174. Vogler, E.A. and C.A. Siedlecki, *Contact activation of blood-plasma coagulation.* Biomaterials, 2009. **30**(10): p. 1857-69.
175. Grunkemeier, J.M., et al., *The effect of adsorbed fibrinogen, fibronectin, von Willebrand factor and vitronectin on the procoagulant state of adherent platelets.* Biomaterials, 2000. **21**(22): p. 2243-52.
176. Long, A.T., et al., *Contact system revisited: an interface between inflammation, coagulation, and innate immunity.* J Thromb Haemost, 2016. **14**(3): p. 427-37.

177. Rossaint, J., A. Margraf, and A. Zarbock, *Role of Platelets in Leukocyte Recruitment and Resolution of Inflammation.* Front Immunol, 2018. **9**: p. 2712.
178. Johne, J., et al., *Platelets promote coagulation factor XII-mediated proteolytic cascade systems in plasma.* Biol Chem, 2006. **387**(2): p. 173-8.
179. Franz, S., et al., *Immune responses to implants - a review of the implications for the design of immunomodulatory biomaterials.* Biomaterials, 2011. **32**(28): p. 6692-709.
180. Andersson, J., et al., *Binding of C3 fragments on top of adsorbed plasma proteins during complement activation on a model biomaterial surface.* Biomaterials, 2005. **26**(13): p. 1477-85.
181. Andersson, J., et al., *C3 adsorbed to a polymer surface can form an initiating alternative pathway convertase.* J Immunol, 2002. **168**(11): p. 5786-91.
182. Ritis, K., et al., *A novel C5a receptor-tissue factor cross-talk in neutrophils links innate immunity to coagulation pathways.* J Immunol, 2006. **177**(7): p. 4794-802.
183. Kappelmayer, J., et al., *Tissue factor is expressed on monocytes during simulated extracorporeal circulation.* Circ Res, 1993. **72**(5): p. 1075-81.
184. Weber, M., et al., *Blood-Contacting Biomaterials: In Vitro Evaluation of the Hemocompatibility.* Front Bioeng Biotechnol, 2018. **6**: p. 99.
185. Mohan, C.C., K.P. Chennazhi, and D. Menon, *In vitro hemocompatibility and vascular endothelial cell functionality on titania nanostructures under static and dynamic conditions for improved coronary stenting applications.* Acta Biomater, 2013. **9**(12): p. 9568-77.
186. Streller, U., et al., *Design and evaluation of novel blood incubation systems for in vitro hemocompatibility assessment of planar solid surfaces.* J Biomed Mater Res B Appl Biomater, 2003. **66**(1): p. 379-90.
187. Gerling, K., et al., *A Novel C1-Esterase Inhibitor Oxygenator Coating Prevents FXII Activation in Human Blood.* Biomolecules, 2020. **10**(7).
188. Van Kruchten, R., J.M. Cosemans, and J.W. Heemskerk, *Measurement of whole blood thrombus formation using parallel-plate flow chambers - a practical guide.* Platelets, 2012. **23**(3): p. 229-42.
189. Lackner, J.M., et al., *Hemocompatibility of Inorganic Physical Vapor Deposition (PVD) Coatings on Thermoplastic Polyurethane Polymers.* J Funct Biomater, 2012. **3**(2): p. 283-97.
190. Stang, K., et al., *Hemocompatibility testing according to ISO 10993-4: discrimination between pyrogen- and device-induced hemostatic activation.* Mater Sci Eng C Mater Biol Appl, 2014. **42**: p. 422-8.
191. Wang, D.A., et al., *Surface coating of stearyl poly(ethylene oxide) coupling-polymer on polyurethane guiding catheters with poly(ether urethane) film-building additive for biomedical applications.* Biomaterials, 2001. **22**(12): p. 1549-62.
192. Standardization, I.O.f., *Biological Evaluation of Medical Devices Part 4: Selection of tests for interactions with blood*. 2017.
193. Raab, S., et al., *A Comparative View on Human Somatic Cell Sources for iPSC Generation.* Stem Cells Int, 2014. **2014**: p. 768391.
194. Kim, Y., et al., *The Generation of Human Induced Pluripotent Stem Cells from Blood Cells: An Efficient Protocol Using Serial Plating of Reprogrammed Cells by Centrifugation.* Stem Cells Int, 2016. **2016**: p. 1329459.
195. Tan, H.K., et al., *Human finger-prick induced pluripotent stem cells facilitate the development of stem cell banking.* Stem Cells Transl Med, 2014. **3**(5): p. 586-98.

196. Loh, Y.H., et al., *Generation of induced pluripotent stem cells from human blood.* Blood, 2009. **113**(22): p. 5476-9.
197. Ringsrud, K.M., *Cells in the Urine Sediment.* Laboratory Medicine, 2001. **32**(3): p. 153-155.
198. Schumann, G.B., *Urine sediment examination / G. Berry Schumann*. 1980, Baltimore: Williams & Wilkins.
199. Zhou, H., et al., *Generation of induced pluripotent stem cells using recombinant proteins.* Cell Stem Cell, 2009. **4**(5): p. 381-4.
200. Ban, H., et al., *Efficient generation of transgene-free human induced pluripotent stem cells (iPSCs) by temperature-sensitive Sendai virus vectors.* Proc Natl Acad Sci U S A, 2011. **108**(34): p. 14234-9.
201. Yoshioka, N. and S.F. Dowdy, *Enhanced generation of iPSCs from older adult human cells by a synthetic five-factor self-replicative RNA.* PLoS One, 2017. **12**(7): p. e0182018.
202. Kim, Y.G., et al., *Recombinant Vaccinia virus-coded interferon inhibitor B18R: Expression, refolding and a use in a mammalian expression system with a RNA-vector.* PLoS One, 2017. **12**(12): p. e0189308.
203. Umrath, F., et al., *Generation of iPSCs from Jaw Periosteal Cells Using Self-Replicating RNA.* Int J Mol Sci, 2019. **20**(7).
204. Laurent, L.C., et al., *Dynamic changes in the copy number of pluripotency and cell proliferation genes in human ESCs and iPSCs during reprogramming and time in culture.* Cell Stem Cell, 2011. **8**(1): p. 106-18.
205. Marti, M., et al., *Characterization of pluripotent stem cells.* Nat Protoc, 2013. **8**(2): p. 223-53.
206. Izutani, R., H. Ohyanagi, and R.P. MacDermott, *Quantitative PCR for detection of femtogram quantities of interleukin-8 mRNA expression.* Microbiol Immunol, 1994. **38**(3): p. 233-7.
207. Yu, F., et al., *Kruppel-like factor 4 (KLF4) is required for maintenance of breast cancer stem cells and for cell migration and invasion.* Oncogene, 2011. **30**(18): p. 2161-72.
208. Foster, K.W., et al., *Oncogene expression cloning by retroviral transduction of adenovirus E1A-immortalized rat kidney RK3E cells: transformation of a host with epithelial features by c-MYC and the zinc finger protein GKLF.* Cell Growth Differ, 1999. **10**(6): p. 423-34.
209. Foster, K.W., et al., *Increase of GKLF messenger RNA and protein expression during progression of breast cancer.* Cancer Res, 2000. **60**(22): p. 6488-95.
210. Aldahmash, A., et al., *Teratoma formation in immunocompetent mice after syngeneic and allogeneic implantation of germline capable mouse embryonic stem cells.* Asian Pac J Cancer Prev, 2013. **14**(10): p. 5705-11.
211. Cao, F., et al., *Spatial and temporal kinetics of teratoma formation from murine embryonic stem cell transplantation.* Stem Cells Dev, 2007. **16**(6): p. 883-91.
212. Lee, A.S., et al., *Effects of cell number on teratoma formation by human embryonic stem cells.* Cell Cycle, 2009. **8**(16): p. 2608-12.
213. Zhang, W.Y., P.E. de Almeida, and J.C. Wu, *Teratoma formation: A tool for monitoring pluripotency in stem cell research*, in *StemBook*. 2008: Cambridge (MA).
214. Kunz, P., et al., *Optimization of the chicken chorioallantoic membrane assay as reliable in vivo model for the analysis of osteosarcoma.* PLoS One, 2019. **14**(4): p. e0215312.
215. Dohle, D.S., et al., *Chick ex ovo culture and ex ovo CAM assay: how it really works.* J Vis Exp, 2009(33).

216. Deryugina, E.I. and J.P. Quigley, *Chick embryo chorioallantoic membrane model systems to study and visualize human tumor cell metastasis.* Histochem Cell Biol, 2008. **130**(6): p. 1119-30.
217. Petrovova, E., et al., *Preclinical alternative model for analysis of porous scaffold biocompatibility in bone tissue engineering.* ALTEX, 2019. **36**(1): p. 121-130.
218. Itzhaki, I., et al., *Calcium handling in human induced pluripotent stem cell derived cardiomyocytes.* PLoS One, 2011. **6**(4): p. e18037.
219. Mehta, A., et al., *A systemic evaluation of cardiac differentiation from mRNA reprogrammed human induced pluripotent stem cells.* PLoS One, 2014. **9**(7): p. e103485.
220. Khan, K.M., J. Patel, and T.J. Schaefer, *Nifedipine*, in *StatPearls*. 2021, StatPearls Publishing

221. Szymanski, M.W. and D.P. Singh, *Isoproterenol*, in *StatPearls*. 2021: Treasure Island (FL).
222. Desimine, V.L., et al., *Biased Agonism/Antagonism of Cardiovascular GPCRs for Heart Failure Therapy.* Int Rev Cell Mol Biol, 2018. **339**: p. 41-61.
223. Dubois, N.C., et al., *SIRPA is a specific cell-surface marker for isolating cardiomyocytes derived from human pluripotent stem cells.* Nat Biotechnol, 2011. **29**(11): p. 1011-8.
224. Davis, J., et al., *In vitro model of ischemic heart failure using human induced pluripotent stem cell-derived cardiomyocytes.* JCI Insight, 2021. **6**(10).
225. Lopaschuk, G.D. and J.S. Jaswal, *Energy metabolic phenotype of the cardiomyocyte during development, differentiation, and postnatal maturation.* J Cardiovasc Pharmacol, 2010. **56**(2): p. 130-40.
226. Tohyama, S., et al., *Distinct metabolic flow enables large-scale purification of mouse and human pluripotent stem cell-derived cardiomyocytes.* Cell Stem Cell, 2013. **12**(1): p. 127-37.
227. Kadari, A., et al., *Robust Generation of Cardiomyocytes from Human iPS Cells Requires Precise Modulation of BMP and WNT Signaling.* Stem Cell Rev Rep, 2015. **11**(4): p. 560-9.
228. Maas, R.G.C., et al., *Massive expansion and cryopreservation of functional human induced pluripotent stem cell-derived cardiomyocytes.* STAR Protoc, 2021. **2**(1): p. 100334.
229. Cyganek, L., et al., *Deep phenotyping of human induced pluripotent stem cell-derived atrial and ventricular cardiomyocytes.* JCI Insight, 2018. **3**(12).
230. Schweizer, P.A., et al., *Subtype-specific differentiation of cardiac pacemaker cell clusters from human induced pluripotent stem cells.* Stem Cell Res Ther, 2017. **8**(1): p. 229.
231. Jager, L., et al., *A novel waterjet technology for transurethral cystoscopic injection of viable cells in the urethral sphincter complex.* Neurourol Urodyn, 2020. **39**(2): p. 594-602.
232. Nagaya, N., et al., *Intravenous administration of mesenchymal stem cells improves cardiac function in rats with acute myocardial infarction through angiogenesis and myogenesis.* Am J Physiol Heart Circ Physiol, 2004. **287**(6): p. H2670-6.
233. Chen, S.L., et al., *Effect on left ventricular function of intracoronary transplantation of autologous bone marrow mesenchymal stem cell in patients with acute myocardial infarction.* Am J Cardiol, 2004. **94**(1): p. 92-5.

234. Chow, A., et al., *Human Induced Pluripotent Stem Cell-Derived Cardiomyocyte Encapsulating Bioactive Hydrogels Improve Rat Heart Function Post Myocardial Infarction.* Stem Cell Reports, 2017. **9**(5): p. 1415-1422.
235. Chong, J.J., et al., *Human embryonic-stem-cell-derived cardiomyocytes regenerate non-human primate hearts.* Nature, 2014. **510**(7504): p. 273-7.
236. Zhao, X., et al., *Comparison of Non-human Primate versus Human Induced Pluripotent Stem Cell-Derived Cardiomyocytes for Treatment of Myocardial Infarction.* Stem Cell Reports, 2018. **10**(2): p. 422-435.
237. Amer, M.H., et al., *Translational considerations in injectable cell-based therapeutics for neurological applications: concepts, progress and challenges.* NPJ Regen Med, 2017. **2**: p. 23.
238. Pokorney, S.D., et al., *Infarct healing is a dynamic process following acute myocardial infarction.* J Cardiovasc Magn Reson, 2012. **14**: p. 62.
239. Ingkanisorn, W.P., et al., *Gadolinium delayed enhancement cardiovascular magnetic resonance correlates with clinical measures of myocardial infarction.* J Am Coll Cardiol, 2004. **43**(12): p. 2253-9.
240. Lund, G.K., et al., *Prediction of left ventricular remodeling and analysis of infarct resorption in patients with reperfused myocardial infarcts by using contrast-enhanced MR imaging.* Radiology, 2007. **245**(1): p. 95-102.
241. Tabei, R., et al., *Development of a transplant injection device for optimal distribution and retention of human induced pluripotent stem cellderived cardiomyocytes.* J Heart Lung Transplant, 2019. **38**(2): p. 203-214.
242. Linzenbold, W., et al., *Rapid and precise delivery of cells in the urethral sphincter complex by a novel needle-free waterjet technology.* BJU Int, 2021. **127**(4): p. 463-472.
243. Fukushima, S., et al., *Direct intramyocardial but not intracoronary injection of bone marrow cells induces ventricular arrhythmias in a rat chronic ischemic heart failure model.* Circulation, 2007. **115**(17): p. 2254-61.
244. Patel, A.N., et al., *Surgical treatment for congestive heart failure with autologous adult stem cell transplantation: a prospective randomized study.* J Thorac Cardiovasc Surg, 2005. **130**(6): p. 1631-8.
245. Pompilio, G., et al., *Direct minimally invasive intramyocardial injection of bone marrow-derived AC133+ stem cells in patients with refractory ischemia: preliminary results.* Thorac Cardiovasc Surg, 2008. **56**(2): p. 71-6.
246. Perin, E.C., et al., *Transendocardial, autologous bone marrow cell transplantation for severe, chronic ischemic heart failure.* Circulation, 2003. **107**(18): p. 2294-302.
247. Fuchs, S., et al., *Safety and feasibility of transendocardial autologous bone marrow cell transplantation in patients with advanced heart disease.* Am J Cardiol, 2006. **97**(6): p. 823-9.
248. Tse, H.F., et al., *Prospective randomized trial of direct endomyocardial implantation of bone marrow cells for treatment of severe coronary artery diseases (PROTECT-CAD trial).* Eur Heart J, 2007. **28**(24): p. 2998-3005.
249. Strauer, B.E., et al., *Regeneration of human infarcted heart muscle by intracoronary autologous bone marrow cell transplantation in chronic coronary artery disease: the IACT Study.* J Am Coll Cardiol, 2005. **46**(9): p. 1651-8.
250. Katritsis, D.G., et al., *Transcoronary transplantation of autologous mesenchymal stem cells and endothelial progenitors into infarcted human myocardium.* Catheter Cardiovasc Interv, 2005. **65**(3): p. 321-9.

251. Plewka, M., et al., *Effect of intracoronary injection of mononuclear bone marrow stem cells on left ventricular function in patients with acute myocardial infarction.* Am J Cardiol, 2009. **104**(10): p. 1336-42.
252. Perez, J.R., et al., *Tissue Engineering and Cell-Based Therapies for Fractures and Bone Defects.* Front Bioeng Biotechnol, 2018. **6**: p. 105.
253. Akita, S., et al., *Cranial bone defect healing is accelerated by mesenchymal stem cells induced by coadministration of bone morphogenetic protein-2 and basic fibroblast growth factor.* Wound Repair Regen, 2004. **12**(2): p. 252-9.
254. Yoon, E., et al., *In vivo osteogenic potential of human adipose-derived stem cells/poly lactide-co-glycolic acid constructs for bone regeneration in a rat critical-sized calvarial defect model.* Tissue Eng, 2007. **13**(3): p. 619-27.
255. Gronthos, S., et al., *Postnatal human dental pulp stem cells (DPSCs) in vitro and in vivo.* Proc Natl Acad Sci U S A, 2000. **97**(25): p. 13625-30.
256. Pittenger, M.F., et al., *Multilineage potential of adult human mesenchymal stem cells.* Science, 1999. **284**(5411): p. 143-7.
257. Hernigou, P., et al., *Percutaneous autologous bone-marrow grafting for nonunions. Influence of the number and concentration of progenitor cells.* J Bone Joint Surg Am, 2005. **87**(7): p. 1430-7.
258. Kim, S.E., et al., *Enhancement of ectopic bone formation by bone morphogenetic protein-2 delivery using heparin-conjugated PLGA nanoparticles with transplantation of bone marrow-derived mesenchymal stem cells.* J Biomed Sci, 2008. **15**(6): p. 771-7.
259. Jeon, O., et al., *Long-term delivery enhances in vivo osteogenic efficacy of bone morphogenetic protein-2 compared to short-term delivery.* Biochem Biophys Res Commun, 2008. **369**(2): p. 774-80.
260. Liu, X., et al., *Blood compatible materials: state of the art.* J Mater Chem B, 2014. **2**(35): p. 5718-5738.
261. Tatsumi, K., et al., *Tissue factor triggers procoagulation in transplanted mesenchymal stem cells leading to thromboembolism.* Biochem Biophys Res Commun, 2013. **431**(2): p. 203-9.
262. Gleeson, B.M., et al., *Bone Marrow-Derived Mesenchymal Stem Cells Have Innate Procoagulant Activity and Cause Microvascular Obstruction Following Intracoronary Delivery: Amelioration by Antithrombin Therapy.* Stem Cells, 2015. **33**(9): p. 2726-37.
263. Coppin, L., E. Sokal, and X. Stephenne, *Thrombogenic Risk Induced by Intravascular Mesenchymal Stem Cell Therapy: Current Status and Future Perspectives.* Cells, 2019. **8**(10).
264. Olczyk, P., L. Mencner, and K. Komosinska-Vassev, *The role of the extracellular matrix components in cutaneous wound healing.* Biomed Res Int, 2014. **2014**: p. 747584.
265. Stegen, S., N. van Gastel, and G. Carmeliet, *Bringing new life to damaged bone: the importance of angiogenesis in bone repair and regeneration.* Bone, 2015. **70**: p. 19-27.

7 Anhang

7.1 Eigenanteil der wissenschaftlichen Veröffentlichungen

7.1.1 Publikation I

Reprogramming of urine-derived renal epithelial cells into iPSCs using srRNA and consecutive differentiation into beating cardiomyocytes

Heidrun Steinle*:	Studien Design und Konzept, Methodenetablierung, Durchführung von Experimenten, Auswertung und Evaluierung von Daten, Schreiben des Manuskripts
Marbod Weber*:	Methodenetablierung, Durchführung von Experimenten, Auswertung und Evaluierung von Daten, Schreiben des Manuskripts
Sonia Golombek:	Korrekturlesen des Manuskripts
Andreas Behring:	Methodenetablierung
Ulrike Mau-Holzmann:	Supervision und Interpretation von Karyogrammanalysen, Korrekturlesen des Manuskripts
Christiane von Ohle:	Supervision von CSLM Experimenten
Christian Schlensak:	Korrekturlesen des Manuskripts
Hans Peter Wendel:	Supervision der Studie, Korrekturlesen des Manuskripts
Meltem Avci-Adali:	Konzeption und Supervision der Studie, Daten Evaluierung, Korrekturlesen des Manuskripts

* gleichermaßen beigetragen

7.1.2 Publikation II:

An Alternative In Vivo Model to Evaluate Pluripotency of Patient-Specific hiPSCs

Josefin Weber*:	Studien Design und Konzept, Methodenetablierung, Durchführung von Experimenten, Auswertung und Evaluierung von Daten, Schreiben des Manuskripts
Marbod Weber*:	Studien Design und Konzept, Methodenetablierung, Durchführung von Experimenten, Auswertung und Evaluierung von Daten, Schreiben des Manuskripts
Heidrun Steinle:	Methodenetablierung
Christian Schlensak:	Korrekturlesen des Manuskripts
Hans Peter Wendel:	Supervision der Studie, Korrekturlesen des Manuskripts
Meltem Avci-Adali:	Konzeption und Supervision der Studie, Daten Evaluierung, Korrekturlesen des Manuskripts

* gleichermaßen beigetragen

7.1.3 Publikation III:

Hydrojet-based delivery of footprint-free iPSC-derived cardiomyocytes into porcine myocardium

Marbod Weber:	Studien Design und Konzept, Methodenetablierung, Durchführung von Experimenten, Auswertung und Evaluierung von Daten, Schreiben des Manuskripts
Andreas Fech:	Methodenetablierung
Luise Jäger:	Studien Design und Konzept, Methodenetablierung, Durchführung von Experimenten, Korrekturlesen des Manuskripts
Heidrun Steinle:	Durchführung von Experimenten, Methodenetablierung
Louisa Bühler:	Durchführung von Experimenten
Regine Mariette Perl:	Durchführung von Experimenten
Petros Martirosian:	Durchführung von Experimenten, Methodenetablierung, Schreiben und Korrekturlesen des Manuskripts
Roman Mehling:	Durchführung von Experimenten
Dominik Sonanini:	Durchführung von Experimenten
Wilhelm K. Aicher:	Studien Design und Konzept, Korrekturlesen des Manuskripts
Konstantin Nikolaou:	Studien Design und Konzept, Korrekturlesen des Manuskripts
Christian Schlensak:	Korrekturlesen des Manuskripts
Markus D. Enderle:	Supervision der Studie, Korrekturlesen des Manuskripts
Hans-Peter Wendel:	Supervision der Studie, Korrekturlesen des Manuskripts
Walter Linzenbold:	Konzeption und Supervision der Studie, Daten Evaluierung, Korrekturlesen des Manuskripts
Meltem Avci-Adali:	Konzeption und Supervision der Studie, Daten Evaluierung, Schreiben und Korrekturlesen des Manuskripts

7.1.4 Publikation IV:

Influence of human jaw periosteal cells seed-ed β-tricalcium phosphate scaffolds on blood coagulation

Marbod Weber:	Studien Design und Konzept, Methodenetablierung, Durchführung von Experimenten, Auswertung und Evaluierung von Daten, Schreiben des Manuskripts
Felix Umrath:	Studien Design und Konzept, Methodenetablierung, Durchführung von Experimenten, Korrekturlesen des Manuskripts
Heidrun Steinle:	Methodenetablierung
Lukas-Frank Schmitt:	Durchführung von Experimenten
Lin Tzu Yu:	Durchführung von Experimenten
Christian Schlensak:	Korrekturlesen des Manuskripts
Hans Peter Wendel:	Supervision der Studie, Korrekturlesen des Manuskripts
Siegmar Reinert:	Supervision der Studie, Korrekturlesen des Manuskripts
Dorothea Alexander*:	Konzeption und Supervision der Studie, Daten Evaluierung, Korrekturlesen des Manuskripts
Meltem Avci-Adali*:	Konzeption und Supervision der Studie, Daten Evaluierung, Korrekturlesen des Manuskripts

* gleichermaßen beigetragen

7.2 Liste aller wissenschaftlichen Veröffentlichungen

Steinle H, Weber J, Stoppelkamp S, Große-Berkenbusch K, Golombek S, **Weber M**, Canak-Ipek T, Trenz SM, Schlensak C, Avci-Adali M. Delivery of synthetic mRNAs for tissue regeneration. Adv Drug Deliv Rev. 2021 Dec;179:114007.

Weber J.*, **Weber M.***, Steinle H., Schlensak C., Wendel H.P., Avci-Adali M. “An alternative in vivo model to evaluate pluripotency of patient-specific iPSCs”. ALTEX. 2021;38(3):442-450.

Weber M., Fech A., Jäger L., Steinle H., Bühler L., Perl R.M., Martirosian P., Mehling R., Sonanini D., Aicher W.K., Nikolaou K., Schlensak C., Enderle M.D., Wendel H.P., Linzenbold W., Avci-Adali M. “Hydrojet-based delivery of footprint-free iPSC-derived cardiomyocytes into porcine myocardium”. Sci Rep. 2020 Oct 8;10(1):16787.

Umrath F., **Weber M.**, Reinert S., Wendel H.P., Avci-Adali M., Alexander D. “iPSC-Derived MSCs Versus Originating Jaw Periosteal Cells: Comparison of Resulting Phenotype and Stem Cell Potential”. Int J Mol Sci. 2020 Jan 16;21(2):587.

Steinle H.*, **Weber M.***, Behring A., Mau-Holzmann U., von Ohle C., Popov A.F., Schlensak C., Wendel H.P., Avci-Adali M. “Reprogramming of Urine-Derived Renal Epithelial Cells into iPSCs Using srRNA and Consecutive Differentiation into Beating Cardiomyocytes”. Mol Ther Nucleic Acids. 2019 Sep 6;17:907-921.

Umrath F., Steinle H., **Weber M.**, Wendel H.P., Reinert S., Alexander D., Avci-Adali M. “Generation of iPSCs from Jaw Periosteal Cells Using Self-Replicating RNA”. Int J Mol Sci. 2019 Apr 3;20(7):1648.

Steinle H., **Weber M.**, Behring A., Mau-Holzmann U., Schlensak C., Wendel H.P., Avci-Adali M. “Generation of iPSCs by Nonintegrative RNA-Based Reprogramming Techniques: Benefits of Self-Replicating RNA versus Synthetic mRNA”. Stem Cells Int. 2019 Jun 19;2019:7641767.

Weber M., Steinle H., Golombek S., Hann L., Schlensak C., Wendel H.P., Avci-Adali M. “Blood-Contacting Biomaterials: In Vitro Evaluation of the Hemocompatibility”. Front Bioeng Biotechnol. 2018 Jul 16;6:99.

* gleichermaßen beigetragen

7.3 Wissenschaftliche Veröffentlichungen im Original

7.3.1 Publikation I:

Reprogramming of Urine-Derived Renal Epithelial Cells into iPSCs Using srRNA and Consecutive Differentiation into Beating Cardiomyocytes

Molecular Therapy
Nucleic Acids
Original Article

Reprogramming of Urine-Derived Renal Epithelial Cells into iPSCs Using srRNA and Consecutive Differentiation into Beating Cardiomyocytes

Heidrun Steinle,[1,4] Marbod Weber,[1,4] Andreas Behring,[1] Ulrike Mau-Holzmann,[2] Christiane von Ohle,[3] Aron-Frederik Popov,[1] Christian Schlensak,[1] Hans Peter Wendel,[1] and Meltem Avci-Adali[1]

[1]Department of Thoracic and Cardiovascular Surgery, University Hospital Tübingen, Calwerstraße 7/1, 72076 Tübingen, Germany; [2]Institute of Medical Genetics and Applied Genomics, University Hospital Tübingen, Calwerstraße 7, 72076 Tübingen, Germany; [3]Department of Conservative Dentistry and Periodontology, Centre of Dentistry, Oral Medicine and Maxillofacial Surgery, University Hospital Tübingen, Osianderstraße 2-8, 72076 Tübingen, Germany

The generation of induced pluripotent stem cells (iPSCs) from patient's somatic cells and the subsequent differentiation into desired cell types opens up numerous possibilities in regenerative medicine and tissue engineering. Adult cardiomyocytes have limited self-renewal capacity; thus, the efficient, safe, and clinically applicable generation of autologous cardiomyocytes is of great interest for the treatment of damaged myocardium. In this study, footprint-free iPSCs were successfully generated from urine-derived renal epithelial cells through a single application of self-replicating RNA (srRNA). The expression of pluripotency markers and the *in vitro* as well as *in vivo* trilineage differentiation were demonstrated. Furthermore, the resulting iPSCs contained no residual srRNA, and the karyotyping analysis demonstrated no detectable anomalies. The cardiac differentiation of these iPSCs resulted in autologous contracting cardiomyocytes after 10 days. We anticipate that the use of urine as a non-invasive cell source to obtain patient cells and the use of srRNA for reprogramming into iPSCs will greatly improve the future production of clinically applicable cardiomyocytes and other cell types. This could allow the regeneration of tissues by generating sufficient quantities of autologous cells without the risk of immune rejection.

INTRODUCTION

Heart failure is currently one of the leading causes of death and affects 23 million people worldwide.[1] In addition to atrial fibrillation and arterial hypertension, myocardial infarction is a common cause of heart failure. The destruction of cardiomyocytes is associated with a reduced pumping capacity of the heart. Because of the extremely low self-renewal capacity of cardiomyocytes with less than 1% per year in adult hearts, a physiologically sufficient regeneration of the myocardium is not feasible.[2] In end-stage heart failure, solely organ transplantation can ensure the survival of patients. To overcome the lack of donor organs for transplantation, there is an explicit need for regenerative therapeutic strategies to treat advanced heart failure.

Previous *in vivo* studies with different species demonstrated that the transplantation of cardiomyocytes can improve the performance of the heart after myocardial infarction.[3,4] However, human implementation is currently failing due to the lack of reliable sources of human cardiomyocytes. To overcome this limitation, various approaches have been developed to generate cardiomyocytes from different cell sources, including bone-marrow-derived stem cells,[5] embryonic stem cells (ESCs),[6,7] and induced pluripotent stem cells (iPSCs).[8,9] In particular, iPSCs are a promising cell source to obtain autologous cells. Since iPSCs are produced from a patient's somatic cells, their generation and application avoid ethical concerns associated with ESCs. Furthermore, rejection reactions are prevented, because the generated cells are autologous. In addition to the application of iPSCs in the field of regenerative medicine, cardiomyocytes derived from iPSCs allow the screening and discovery of drugs, the prediction of cardiotoxicity,[10] and the study of cardiovascular diseases.[11]

Reprogramming of somatic cells into iPSCs was first achieved in murine fibroblasts by Yamanaka and colleagues[12,13] and shortly thereafter in human fibroblasts using retroviral vectors encoding four transcription factors: KLF4, c-MYC, OCT4, and SOX2. Hitherto, human fibroblasts have been the most commonly used cell source for reprogramming studies.[14] Fibroblasts are usually obtained from skin biopsies, which represent an invasive procedure and lead to an injury of healthy tissue. This is associated with pain and additional burden for the patient. Naturally, due to physiological self-renewal of the epithelial tissue in the urinary tract, approximately 2,000 to 7,000 human renal proximal tubule epithelial cells are detached daily and excreted with urine.[15] Thus, the collection and reprogramming of these urine-derived cells represent a promising simple and non-invasive strategy for obtaining patient's own somatic cells.

Received 25 February 2019; accepted 22 July 2019;
https://doi.org/10.1016/j.omtn.2019.07.016.

[4]These authors contributed equally to this work.

Correspondence: Meltem Avci-Adali, PhD, Department of Thoracic and Cardiovascular Surgery, University Hospital Tübingen, Calwerstraße 7/1, 72076 Tübingen, Germany.
E-mail: meltem.avci-adali@uni-tuebingen.de

The genome-integrating viral vectors originally used by Yamanaka et al.[12,13] are carrying a certain risk. The random insertion of retroviral vectors into the genome can lead to mutations and, thereby, to the development of tumors. Furthermore, the retroviral introduction of c-MYC in the cells can lead to increased tumorigenesis in mice.[16,17] Thus, these iPSCs generated by retroviral vectors cannot be clinically used. Meanwhile, several non-integrating approaches have been developed that reduce concerns regarding genetic alterations in iPSCs.[18–22] In particular, synthetic mRNA-based approaches are promising.[23] Thereby, the exogenous delivery of synthetic mRNAs into somatic cells leads to transient expression of desired proteins under physiological conditions by cells' translational machinery. In contrast to plasmid DNA, synthetic mRNAs do not need to enter the cell nucleus. This results in an immediate translation of delivered mRNA in the cytosol and eliminates the risk of genomic integration and insertional mutagenesis.[24] The incorporation of modified nucleotides during the *in vitro* transcription (IVT) or codon optimization[25] can significantly improve the stability of synthetic mRNAs, drastically reduce immune responses triggered by recognition of foreign RNAs, and increase the recruitment and recycling of ribosomes and, thereby, result in enhanced translation efficiency.[26–29]

Due to the transient nature, synthetic mRNAs can be used to express reprogramming factors to obtain footprint-free iPSCs.[22] However, the transient presence of the exogenously delivered mRNAs also necessitates the daily transfection of cells with the synthetic mRNAs during the reprogramming process, which is cost intensive, time consuming, and associated with increased cellular stress. To overcome these hurdles, self-replicating RNAs (srRNAs) can be used to express the reprogramming factors for an extended period of time,[30] without the need for repeated transfections. The srRNA contains the coding sequences of four transcription factors-OCT4, KLF4, SOX2, and c-MYC-and four non-structural proteins (nsP1–nsP4), which encode the RNA replication complex of Venezuelan equine encephalitis (VEE) virus.[30,31]

In this study, using srRNA, footprint-free iPSCs were generated from adult human urine-derived epithelial cells, and the successful generation of beating autologous cardiomyocytes from these iPSCs was demonstrated.

RESULTS

Reprogramming of Urine-Derived RECs into iPSCs Using OCT4, KLF4, SOX2, IRES-cMyc (OKSiM)-GFP srRNA

Cells were collected from urine of 4 different donors. The renal epithelial origin of the isolated and expanded cells at passage 2 or 3 was confirmed using flow cytometry. The analysis showed that 95.8% ± 1.3% of the cells positively express epithelial marker β-catenin and that 99.8% ± 0.2% of the cells express the renal proximal tubular marker CD13 (Figure 1A).

To control the transfection and translation of the srRNA in cells, an IRES-GFP encoding sequence was cloned into the T7-VEE-OKSiM plasmid for the synthesis of OKSiM-GFP srRNA (Figure 1B). For reprogramming, 5×10^4 renal epithelial cells (RECs) were seeded on gelatin-coated wells. Using the established reprogramming protocol (Figure 1C), 21 to 30 days post-transfection, 3 to 25 primary iPSC colonies were obtained per well. After 24 h and reaching approximately 50% confluency (Figure 1D), a single transfection with 0.5 μg OKSiM-GFP srRNA was performed for 4 h. Subsequently, cells were cultivated in B18R-containing medium. Using flow cytometry, a strong GFP reporter protein expression was detected in 7.2% ± 2.8% of the cells 2 days post-transfection (n = 4). On the third day after transfection, 0.8 μg/mL puromycin was added to the medium to select srRNA-transfected cells. After 24 h, only a partial antibiotic-mediated, selective cell death was detected. On day 7 after transfection, a significant reduction in cell numbers was observed, and GFP^+ cells carrying the reprogramming srRNAs survived and grew in colonies. On day 7, the cells underwent severe morphological changes, and small round cells with large nuclei appeared (Figure 1D). Afterward, the medium was changed to E8 stem cell medium containing B18R. In the following days, when the cells reached 90% confluency during the reprogramming process, the cells were split at a 1:2 or 1:4 ratio onto vitronectin-coated plates. On day 13, an increase in colony size was detected. After 26 days, iPSC colonies were identified using live-cell staining (antibody against SSEA-4). Thereafter, B18R was withdrawn from the medium to eliminate the reprogramming srRNA from the cells, and iPSCs were either immediately picked or further cultivated for about 4–7 days until primary iPSC colonies increased in size (D33). Manually picked iPSC colonies were transferred onto the vitronectin-coated wells of a 12-well plate.

Characterization of iPSCs Derived from RECs

Expression of Pluripotency Markers

After the reprogramming of adult somatic RECs into iPSCs, the expression of pluripotency markers was analyzed in iPSCs at passage 4 by immunostaining with specific antibodies. Fluorescence microscopy analyses revealed a strong expression of NANOG, OCT4, SOX2, SSEA-4, TRA-1-60, and LIN28 within the entire iPSC colonies (Figure 2A). Furthermore, flow cytometry analyses demonstrated that 85% ± 6% of iPSCs (passages 5–7) were expressing NANOG and that 91% ± 4% of cells were positive for TRA-1-60 (Figure 2B). Further cultivation and expansion of iPSCs until passage 25, corresponding to 4–5 months in culture, had no effect on TRA-1-60 and NANOG expression (Figure S1). Additionally, gene expression of SOX2, OCT4, LIN28, NANOG, and E-cadherin was quantified using qRT-PCR. The obtained REC-iPSCs (passages 3–6) showed—like the commercially available positive control iPSC cell line WT02, which was generated using a Sendai virus vector from dermal fibroblasts—a significantly high expression of SOX2 (1,510-fold), OCT4 (173-fold), LIN28 (4,376-fold), NANOG (733-fold), and E-cadherin (4,230-fold), compared to the initial RECs (Figure 2C).

Trilineage Differentiation of iPSCs

The differentiation potential of the obtained iPSCs (passages 3–7) into all three germ layers was evaluated *in vitro* using a directed 7-day differentiation protocol (StemMACS Trilineage Differentiation Kit from Miltenyi Biotec) followed by specific antibody staining and

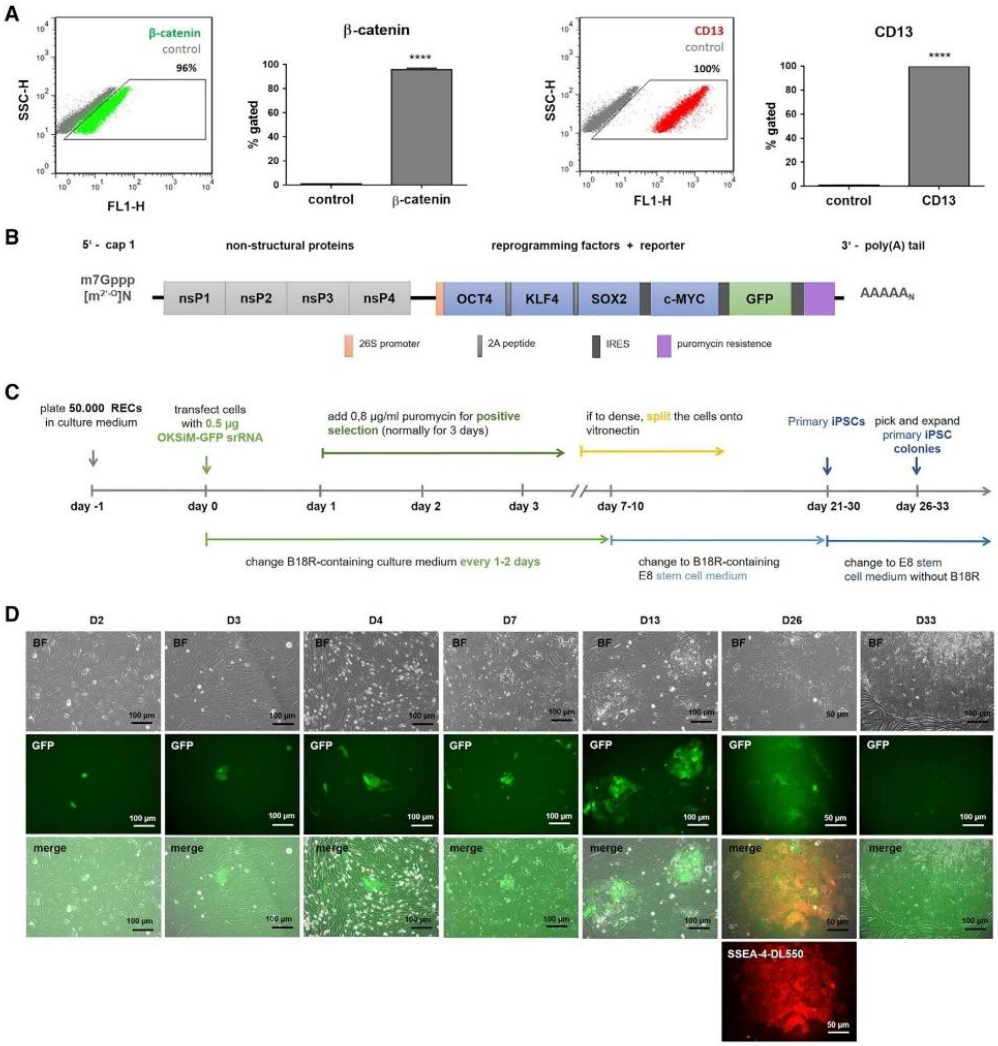

Figure 1. Reprogramming of Urine-Derived RECs into iPSCs Using OKSiM-GFP srRNA

(A) Flow cytometry analysis of RECs after staining with antibodies against epithelial marker β-catenin and renal epithelial marker CD13. Results are shown as mean + SD (n = 4). Statistical differences were determined using paired t test (****p < 0.0001). (B) Schematic overview of srRNA construct. The synthetized srRNA contains the coding sequences for the non-structural proteins (nsP1–nsP4) of VEE to allow self-replication of srRNA, the reprogramming factors (OCT4, KLF4, SOX2, and c-MYC), and the reporter protein GFP. The internal ribosome entry sites (IRES) sequences (linked to c-MYC and GFP) control ribosome entry and, therefore, protein production. The 5′ end was modified with a cap1 structure, and a poly(A) tail was added at the 3′ end. For positive selection, the srRNA also encodes a puromycin resistance. (C) Timeline for the generation of iPSCs from RECs using srRNA. (D) Microscopic images of RECs after the transfection with 0.5 µg srRNA. A few cells expressing the reporter protein GFP were detected 2 days after the transfection (D2). At day 3, puromycin was added for 3 days to eliminate cells, which are not transfected (D3). In the following days, GFP-positive cells proliferated and generated colonies (D4). At day 7, mainly GFP-positive cells had survived, and non-transfected cells were dying (D7). At day 13, an increased size of colonies was observed (D13). After 26 days, iPSC colonies were stained with DL550-labeled live antibody against SSEA-4 (D26). Depending on the colony size, primary iPSCs were picked the next day or further cultivated up to 7 days (D33) until colonies increased in size. The detached iPSCs were transferred into vitronectin-coated wells.

quantification using flow cytometry. The mesoderm induction resulted in the generation of elongated endothelial-like cells as well as multilayer accumulations of smooth muscle-like cells (Figure 3). The endoderm induction led to the detection of a dense cell layer similar to that of early hepatocyte-like cells. The ectoderm induction resulted in cells arranged in neural rosettes. The successful

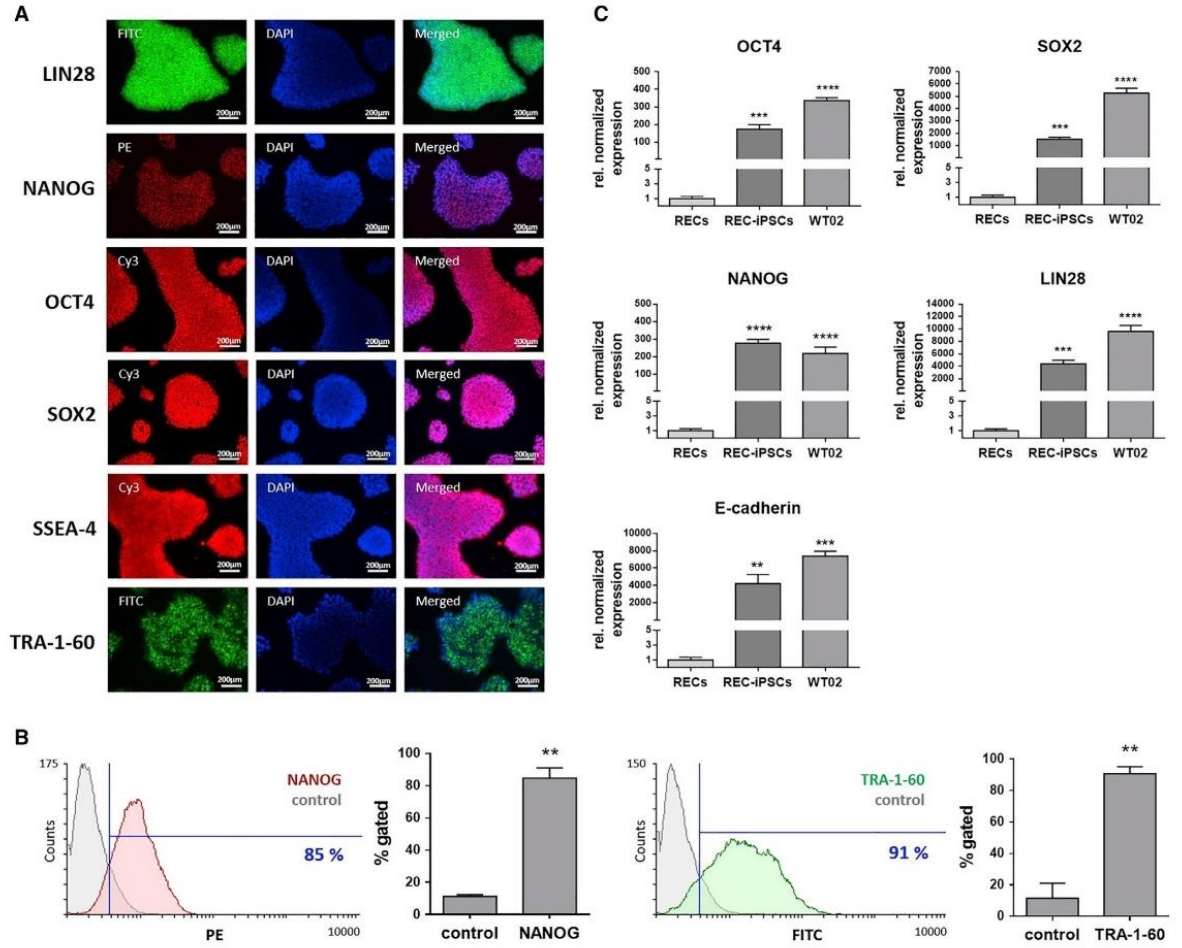

Figure 2. Analysis of Pluripotency Marker Expression in iPSCs Generated from RECs

(A) Representative immunofluorescence microscopy images of iPSCs (passage 4) stained with LIN28-, NANOG-, OCT4-, SOX2-, SSEA-4-, and TRA-1-60-specific antibodies. (B) Flow cytometry analysis of iPSCs (passages 5–7) stained with antibodies specific for NANOG and TRA-1-60. Results are shown as mean + SD (n = 3). (C) Expression analysis of SOX2, OCT4, LIN28, NANOG, and E-cadherin transcripts using qRT-PCR. mRNA levels were normalized to GAPDH mRNA levels, and the results are presented relative to the expression levels in RECs. Results are shown as mean + SEM (n = 4). Statistical differences were determined using paired t test (**p < 0.01; ***p < 0.001, ****p<0.0001).

mesodermal commitment was shown by detecting 48% ± 17% CD31-positive and 74% ± 17% SMA-positive cells. The endoderm differentiation resulted in 95% ± 3% AFP-positive and 97% ± 4% CXCR4-positive cells. The ectodermal distinction was demonstrated by the detection of 96% ± 2% paired box gene 6 (PAX6)-positive and 98% ± 1% class III β-tubulin (TUBB3)-positive cells.

Teratoma Formation of iPSCs

The *in vivo* differentiation capacity of the generated iPSCs into tissue types of all three germ layers was assessed using chorioallantoic membrane (CAM) assay. Therefore, 2 × 10^6 iPSCs (passages 8–11) were suspended in Matrigel and applied onto the CAM. After 10 days of incubation, the formed cell mass was excised together with the CAM (Figure 4A). Histological analysis revealed mesodermal, endodermal, and ectodermal differentiation of applied iPSCs within the teratoma tissue mass (Figure 4B). The differentiation into mesodermal tissue was demonstrated by the presence of bone-like and connective tissue structures in teratoma sections. The differentiation toward endodermal tissue was shown by the detection of gland- and gut-like epithelial tissues, and the generation of ectodermal tissue was demonstrated by the presence of squamous epithelial tissue and neural epithelium starting to form rosette-like structures.

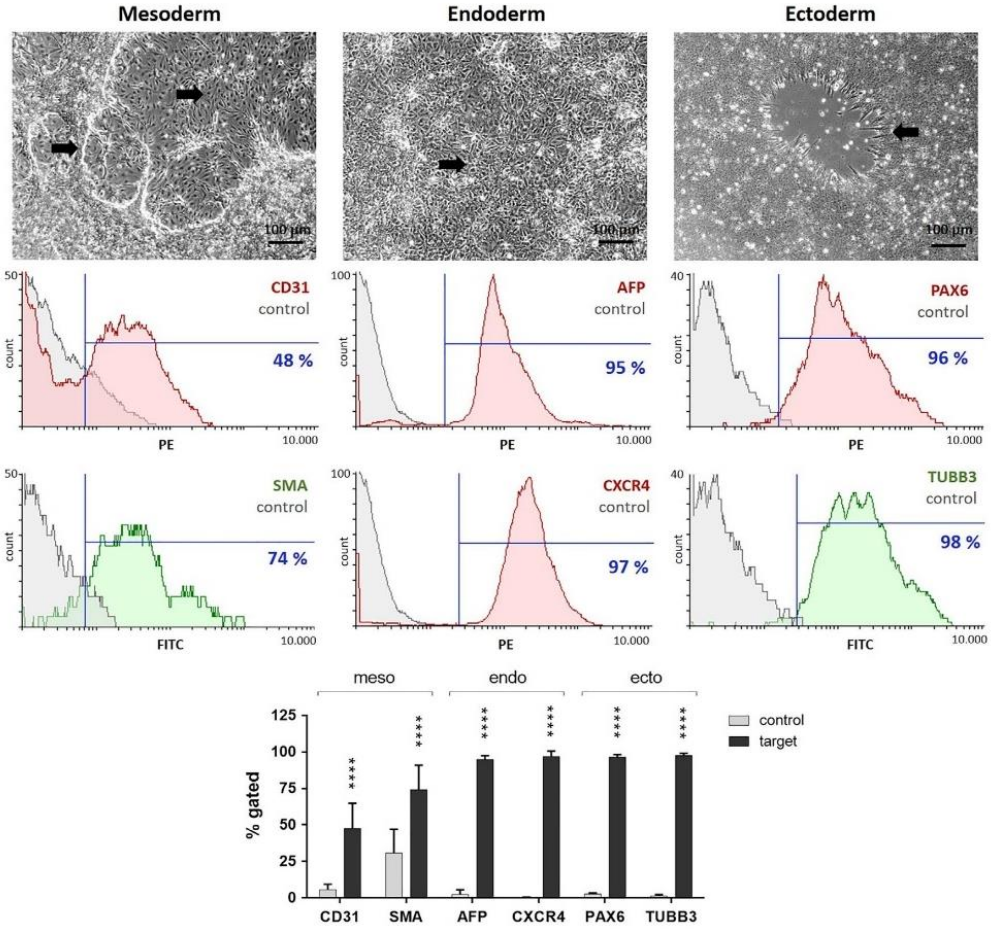

Figure 3. *In Vitro* Differentiation Potential of iPSCs Derived from RECs into the Three Germ Layers: Mesoderm, Endoderm, and Ectoderm

After 7 days of trilineage differentiation, cells with changed phenotypes (indicated with arrows) were observed. Flow cytometry analysis confirmed the differentiation of iPSCs (passages 3–7) into all three germ layers by detection of mesodermal (CD31 and SMA), definitive-endodermal (AFP and CXCR4), and neuroectodermal (PAX6 and TUBB3) cells. Compared to controls, differentiated cells showed significantly increased expression of mesodermal, endodermal, and ectodermal markers. Scale bars of phase contrast microscopic pictures represent 100 µm. Results are shown as mean + SD (n = 4). Statistical differences were determined using one-way ANOVA followed by Bonferroni's multiple comparison test (****$p < 0.0001$).

Downregulation of Oncogenic Transcription Factors and Elimination of srRNA after the Reprogramming of RECs into iPSCs and Analysis of Genomic Stability

Since a permanently elevated expression of KLF4 and c-MYC is associated with an increased tumorigenesis,[16] the expression levels of these transcription factors were determined in obtained iPSCs (passage 3) using qRT-PCR. The analyses revealed that the expression of KLF4 and c-MYC in iPSCs was not significantly different from the expression levels of the initial RECs (Figure 5A). To eliminate the exogenously delivered srRNA in the reprogrammed cells, B18R protein treatment was discontinued between day 21 and day 30 of reprogramming. The elimination of srRNA was analyzed in iPSCs at passage 3 using qRT-PCR. Thereby, the srRNA-specific nsP2 and nsP4 coding regions were detected. RECs transfected with srRNA (RECs+) and cultivated for 2 days demonstrated approximately 2×10^6-fold higher numbers of srRNA transcripts compared to untransfected RECs (Figure 5B). In contrast, no residual srRNA expression was detected in iPSCs. Subsequently, the obtained amplicons were analyzed using agarose gel electrophoresis. As shown in Figure 5C, solely RECs+ showed transcripts with the expected product length of 192 bp for nsP2 and 238 bp for nsP4. To analyze the genomic stability of iPSCs, karyotyping of chromosomes was performed with the initial urine-derived RECs as well as with the generated iPSCs (at passages 4–6). The results revealed no changes

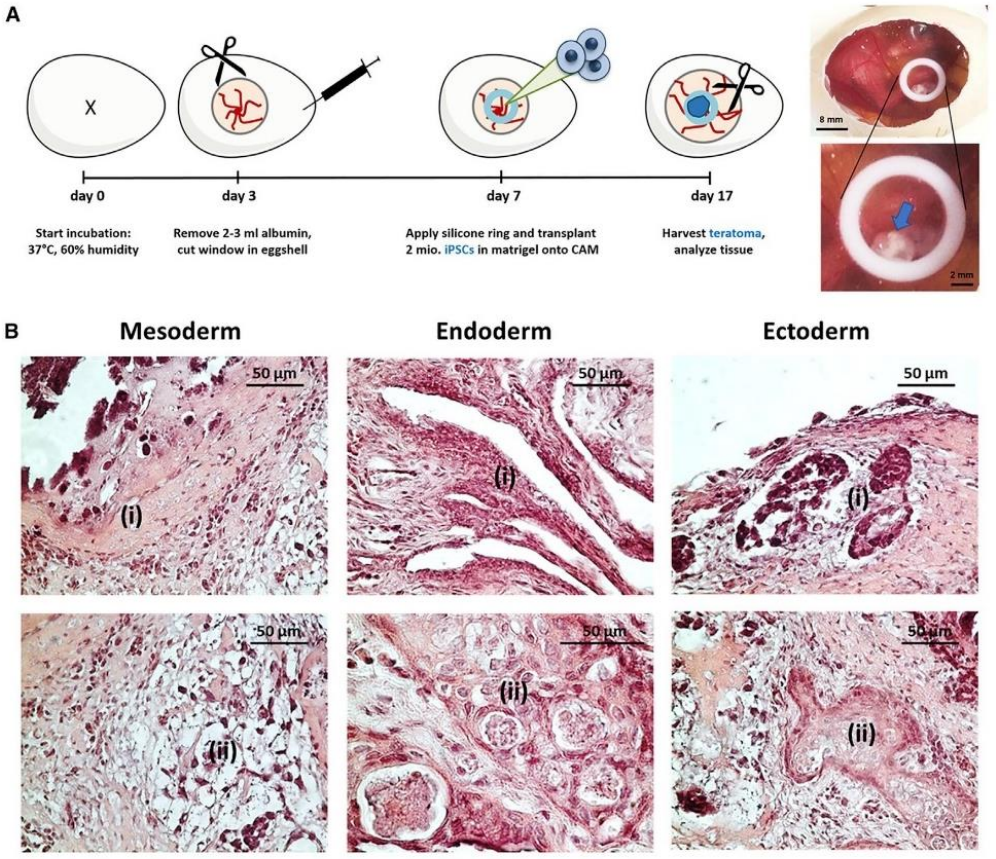

Figure 4. *In Vivo* Analysis of Teratoma Formation by Application of iPSCs onto CAM

(A) Schematic representation of the implementation of CAM assay for the analysis of teratoma formation. 2×10^6 iPSCs (passages 8–11) were applied into the inner area of a silicone ring (Ø 8 mm), which was placed onto the CAM on day 7 of incubation. After 10 days of incubation, teratomas (indicated with an arrow) were excised, and histological analyses were performed. (B) A representative microscopic image of H&E-stained teratoma sections showing iPSC-derived tissues of all three germ layers: mesoderm (i, bone-like tissue; ii, connective tissue), endoderm (i, gut-like epithelium; ii, gland-like epithelium), and ectoderm (i, primitive neural rosettes; ii, squamous epithelium).

in number and appearance of chromosomes, including their length, banding pattern, and centromere position after the reprogramming procedure (Figure 5D).

Characterization of Generated Cardiomyocytes from iPSCs

iPSCs (passages 4–12) generated from 4 different donors were differentiated within 10–14 days into beating cardiomyocytes (passage 0). Using flow cytometry, the yield of cardiac troponin T (cTNT)-positive cardiomyocytes was determined after the enrichment procedure and resulted in 89.2% ± 1.7% cTNT-positive cells (Figure 6A). The fluorescence microscopic overview of cTNT and α-actinin (ACTN2) double-stained cells confirmed the high amount of cardiac cells compared to a few solely DAPI-stained nuclei (Figure 6B). The differentiated cells also showed the typical elongated rod-like shape of cardiomyocytes. More detailed confocal laser scanning micrographs of the cells in passage 1 demonstrated the structural arrangement of the expressed cardiomyocyte-specific proteins, cTNT, cardiac myosin heavy chain (MYH6), or the muscle-specific marker alpha smooth muscle actin (ACTA2) (Figure 6C). The staining of cells with cTNT-specific antibody revealed the cardiomyocyte-specific sarcomeric structures within the cells. Moreover, using qRT-PCR, the expression of cardiomyocyte-specific markers, atrial natriuretic peptide (ANP), cTNT, α-actin cardiac muscle 1 (ACTC1), and MYH6 was analyzed. The obtained cells (passage 0) expressed 5.4×10^4-fold increased levels of ANP, 2.9×10^4-fold higher cTNT levels, 5.5×10^3-fold higher ACTC1 levels, and 2.2×10^4-fold higher MYH6 levels compared to those in the initial RECs (Figure 6D). Furthermore, the presence of cardiac troponin I (TNNI3) was analyzed in cell culture supernatants 13 to 16 days after starting the iPSC differentiation into cardiomyocytes (Figure 6E). A significantly higher concentration of TNNI3 (0.26 ± 0.11 µg/L) was detected in cardiomyocyte cell culture supernatants compared to iPSC culture

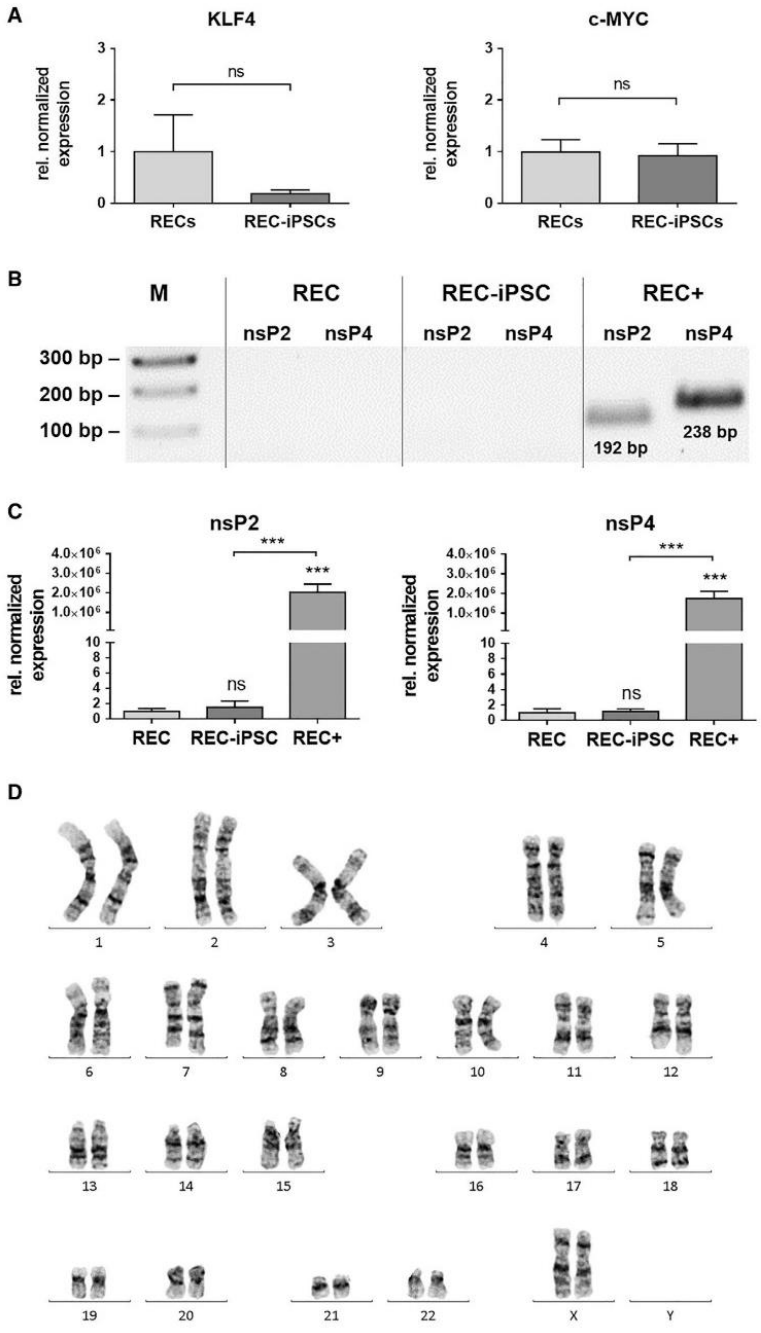

Figure 5. Detection of Oncogenic Transcription Factors and srRNA after the Reprogramming of RECs into iPSCs and Analysis of the Genomic Stability of REC-Derived iPSCs

(A) Analysis of KLF4 and c-MYC expression in iPSCs (passage 3) generated by a single transfection with srRNA. The qRT-PCR results are presented relative to the expression levels in the initial RECs. Results are shown as mean + SEM (n = 4). (B) Quantification of srRNA in RECs 2 days after the srRNA transfection (REC+) and in iPSCs (passage 3) using qRT-PCR. Thereby, nsP2- and nsP4-encoding regions of the srRNA were detected using specific primers. The results are presented relative to the expression levels of initial RECs without srRNA transfection. Results are shown as mean + SEM (n = 4). Statistical differences were determined using paired t test (***$p < 0.001$). (C) Detection of nsP2 and nsP4 specific amplicons in qRT-PCR products using 1% agarose gel electrophoresis. (D) Representative karyotype image of REC-iPSCs (passage 4) obtained from a female subject showing a normal 46XX karyotype by G-banding (n = 3).

medium supernatants (<0.03 μg/L, which represents the lower TNNI3 detection limit). Thereby, the successful differentiation of iPSCs into cardiomyocytes was demonstrated.

Characterization of Contracting Cardiomyocytes

The rhythmic beating is a typical characteristic of fetal and immature stem-cell-derived cardiomyocytes.[32] Thus, to show and analyze the contraction of obtained cardiomyocytes (passage 0), short video recordings were made for 30 s, with 7 pictures per second. Using MATLAB application Motion GUI, the motion directions were calculated and indicated by arrows in Figure 7A (Video S1). Thereby, wide ranges of motion and directional synchronous contractions were detected. Furthermore, the areas with the highest movement rate are shown in the heatmap (Figure 7B). Beating rates were calculated by the time shift between contractions. Cardiomyocytes produced from the iPSCs of 4 different REC donors showed uniform motion patterns during the recording time, with a mean beating rate of 25.24 ± 3.44 beats per minute, which corresponds to a beating frequency of 0.42 Hz ± 0.06 Hz (Figure 7C). Fluorescence microscopic recordings of Ca^{2+} transients in the cardiomyocyte cultures showed Ca^{2+} oscillations (Figure 7D; Video S2), which proved the electromechanical coupling of obtained cardiomyocytes. These findings revealed that the generated cardiomyocytes were functional in regulating intracellular Ca^{2+} signaling. In addition, the beating rate was determined in the presence of Ca^{2+} antagonist nifedipine or β-adrenoceptor agonist isoproterenol (Figure 7E). The treatment of cardiomyocytes with 0.1, 1, or 10 μM nifedipine led to the complete inhibition of cardiomyocyte

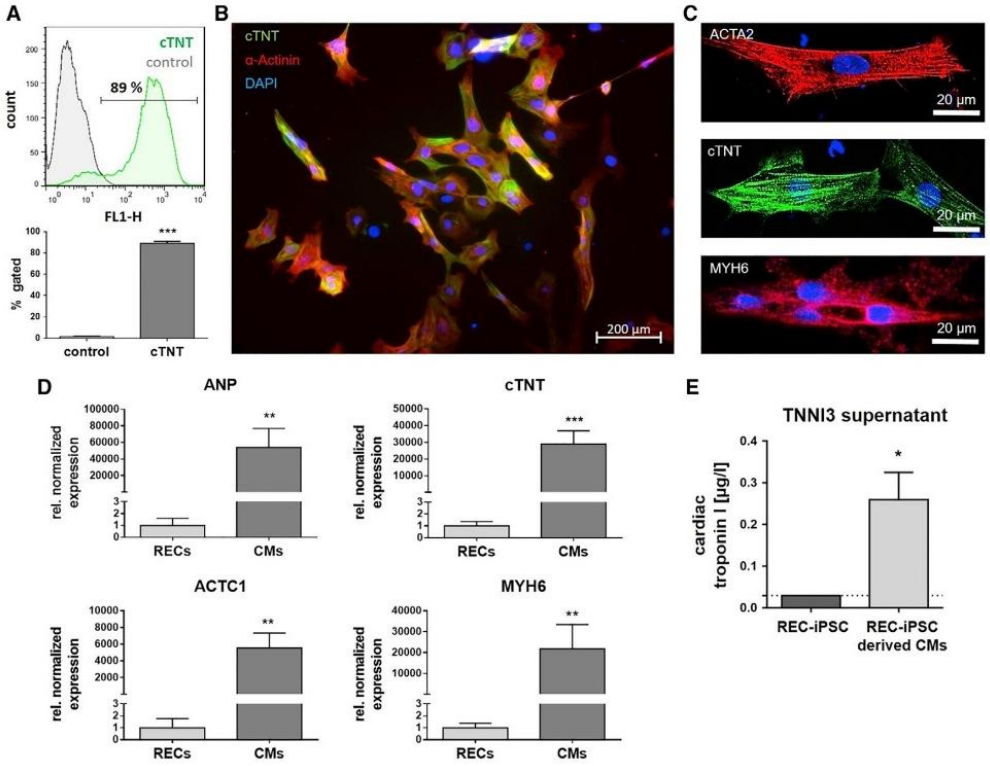

Figure 6. Analysis of Cells Obtained after Cardiac Differentiation of REC-Derived iPSCs

(A) Flow cytometry analysis of cTNT-expressing cells after cardiac differentiation and enrichment. (B) Fluorescence microscopic overview of cTNT- and α-actinin (ACTN2)-positive cells in passage 1 after the cardiac differentiation. Counterstaining of nuclei was performed with DAPI. (C) Confocal-laser-scanning microscopic analysis of cardiomyocyte-specific ACTA2, cTNT, and MYH6 expression. Nuclei were stained with SYTO9. (D) qRT-PCR gene expression analysis of cardiac-specific proteins ANP, cTNT, ACTC1, and MYH6 in passage 1 after the differentiation. (E) Detection of TNNI3 concentration in cardiomyocyte culture supernatants and in iPSC culture supernatants as control. Results are shown as mean + SEM (n = 3). Statistical differences were determined using paired t test (*$p < 0.05$; **$p < 0.01$; ***$p < 0.001$).

contractions. In contrast, the treatment of cardiomyocytes with 0.01 µM isoproterenol increased the beating rate from 32.42 ± 2.09 beats per minute to 40.09 ± 7.71 beats per minute. At an isoproterenol concentration of 0.1 µM, the beating rate reached 50.61 ± 6.52 beats per minute. After the removal of nifedipine and isoproterenol and cultivation of cells for a few hours in cardiomyocyte maintenance medium (CMM), the cells recovered and displayed initial beat rates.

DISCUSSION

In recent years, the ability to generate iPSCs from somatic cells has led to considerable progress in regenerative medicine, and the reprogramming has become a powerful tool in the field of tissue engineering. In this study, we established a method to generate footprint-free cardiomyocytes by using the autologous cell material from the patient's urine and srRNA. First, urine-derived human RECs were reprogrammed using srRNA into iPSCs and then differentiated into beating autologous cardiomyocytes. The obtained iPSCs showed self-renewability and the expression of pluripotency-specific markers, while no residual srRNA and genomic abnormalities were detected. The trilineage differentiation potential of REC-derived iPSCs was demonstrated *in vitro* as well as *in vivo*. Moreover, the cardiac differentiation of these cells resulted in the generation of contractile cardiomyocytes. Thus, the results clearly demonstrated that autologous footprint-free iPSCs as well as cardiomyocytes can be obtained by using the patient's urine as a source for somatic cells. Thereby, invasive biopsies for isolation of somatic cells is not required. Since the obtained cells are footprint-free and autologous, they might have a high potential to be used for the regeneration of injured myocardium.

Urine is a naturally excreted material; therefore, the sampling of patients' urine offers an easy, non-invasive, low-cost, and pain-free method for the collection of sufficient numbers of human somatic cells for reprogramming. Due to natural physiological self-renewal of the epithelial tissue in the urinary tract, approximately 2,000 to 7,000 cells are daily detached and excreted with the urine.[15] In urine,

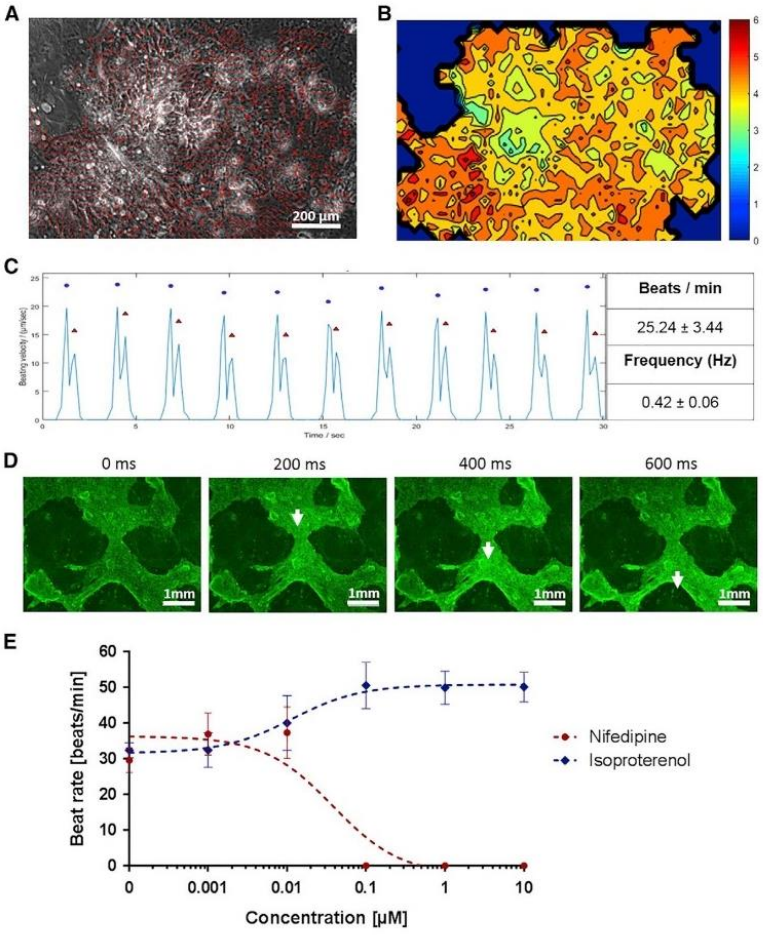

Figure 7. Characterization of Contracting Cardiomyocytes

(A) Arrow-based display of the directed contractions of cardiomyocytes (passage 0). (B) Heatmap depicting the time-averaged magnitude of motion in the x and y directions. An increase of movement is indicated by colors from blue to red. (C) Representative display of beating velocity (micrometers per second) during the recorded time of 30 s. Blue dots indicate contraction, and red triangles indicate the relaxation. Beat rate and frequency (mean ± SD) of iPSC-derived cardiomyocytes were calculated via motion tracking (n = 4). (D) Ca^{2+} imaging of cardiomyocytes. Representative images of every 200 ms are shown. White arrows indicate the position of Ca^{2+} transients. (E) Dose-response curves of isoproterenol- and nifedipine-treated cardiomyocytes (mean ± SD; n = 3).

3 types of epithelial cells can be found: renal, transitional, and squamous.[33] RECs line the nephron as a single layer. An increased number of these cells in the urine can indicate an infection or kidney disease. Transitional epithelial cells are a multilayer of epithelial cells that line the urinary bladder. A few transitional cells are present in the urine of healthy persons, and increased numbers are associated with infection or transitional cell carcinoma. Most often, these cells are also found in the urine after urethral or ureteral catheterization. Squamous epithelial cells line the urethra and vagina, and this type of epithelial cells is most often found in female urine. Large numbers of squamous cells in female urine generally indicates vaginal contamination. However, during a culturing time of 3 to 5 days in renal epithelial proliferation medium, the squamous epithelial cells do not adhere to the cell culture plate and are removed after the medium change. Typically, 3 to 6 small colonies of RECs appear and grow steadily.

In our study, 100–200 mL urine was enough to obtain a sufficient amount of cells for the reprogramming procedure. However, by using an increased amount of urine, more cells could be obtained; thereby, the expansion time of the cells could be reduced. Furthermore, the proliferation rate of the cells can vary between different donors and ages and might influence the reprogramming efficiency. In this study, the isolated cells from urine samples were positive for the epithelial marker β-catenin and the renal proximal tubular marker CD13. In contrast to urine sampling, the commonly used somatic cells are obtained from skin samples (fibroblasts)[14] or blood cells[34] by invasive procedures. Cutting out healthy skin pieces is, of course, a painful procedure and is associated with the risk of infection. Furthermore, the reprogramming of blood cells is difficult, and the efficiency is known to be relatively low.[35] It has also been shown that iPSCs derived from different cell sources maintain a distinct molecular pattern of epigenetic markers, which is linked to the donor tissue.[36] This might result in the improved differentiation potential of iPSCs into the initial somatic cell type. In this study, the successful differentiation of urine-derived REC-iPSCs into cells of all three germline directions was demonstrated.

The reprogramming was performed by a single transfection of RECs with a synthetic srRNA that encodes four reprogramming factors—OCT4, KLF4, SOX2, and c-MYC—as well as the fluorescent reporter protein GFP and contains an open reading frame for puromycin resistance. The puromycin resistance enables the positive selection of srRNA-containing cells, which improves the reprogramming efficiency. In comparison to viral-vector-based methods, the use of srRNA prevents random integration of reprogramming factors into the genome and enables the generation of footprint-free iPSCs. Furthermore, compared to the application of synthetic mRNA for the generation of iPSCs,[22] which requires a daily transfection of 5 different mRNAs into the same target cell, a single transfection of

cells with srRNA is sufficient for the complete reprogramming period.

The addition of B18R protein into the reprogramming medium suppresses the type-I-interferon-associated immune responses[37] to the srRNA; thereby, the premature degradation of the srRNA in the cells can be prevented. After the reprogramming, the termination of B18R addition leads to the degradation of srRNA.[30] Furthermore, the incorporation of IRES-GFP into the srRNA allowed the control of successful transfection and translation of srRNA during the reprogramming process. Additionally, in the absence of the immunosuppressive protein B18R, the decrease of the fluorescence intensity indicated the degradation of the srRNA in the cells. Moreover, the implementation of qRT-PCR using specific primers for the nsP2 and nsP4 regions of the srRNA provided the evidence for the srRNA degradation, since, in obtained iPSCs (passage 3), no srRNA could be detected. The proto-oncogenes c-MYC and KLF4 are expressed in different types of cancer,[38,39] and the permanent overexpression of these genes is associated with an increased tumorigenesis.[16,40] Thus, although the expression of these proteins is required during the reprogramming, after the reprogramming, they should be downregulated. This was also demonstrated in our obtained iPSCs; the expression of c-MYC and KLF4 was not significantly different from the expression in precursor RECs. Furthermore, the decrease of c-MYC and KLF4 expression also indicates the degradation of the srRNA construct in the iPSCs.

In addition to expressing certain proteins responsible for maintaining the pluripotency and the self-renewal capacity of iPSCs, another key feature of iPSCs is the ability to differentiate into each of the three germ layers: mesoderm, endoderm, and ectoderm. We successfully demonstrated the ability of the obtained iPSCs to form each of the germ layers after directed differentiation *in vitro* as well as *in vivo* after the application of iPSCs on CAM. Compared to the teratoma formation in mice, which is incubated for about 4 weeks, the application of 2×10^6 iPSCs on CAM and the incubation time of 10 days were sufficient to form all three germ layers. The cardiac differentiation of renal-epithelial-cell-derived iPSCs resulted already after 7 days in beating cardiomyocytes with a beating rate of approximately 25 beats per minute. The treatment of these cells with 0.1 μM nifidipine resulted in complete inhibition of beating. In contrast, the pharmacological modulation of REC-iPSC-derived cardiomyocytes with isoproterenol led to an increased beating rate.

The future application of these cells for the repair of damaged heart tissues requires the production of pure cardiomyocyte cultures in a large-scale format and the selection of the appropriate subtype-specific cardiomyocytes—nodal, atrial, or ventricular cardiomyocytes.[41–43] Furthermore, the complete differentiation of iPSCs into mature cardiomyocytes should be ensured.[44,45] Dubois et al.[46] demonstrated by using an anti-SIRPA antibody and fluorescence-activated cell sorting (FACS) that cardiomyocytes can be enriched from human pluripotent stem cells. In our study, we used the lactate-based method to enrich cardiomyocytes.[47] Due to differences in energy substrate metabolism, compared to other mammalian cells, cardiomyocytes are able to produce energy also from lactate or fatty acids instead of glucose.[48] Thus, the cultivation of cells in glucose-depleted and lactate-supplemented medium leads to the survival of cardiomyocytes and the elimination of undifferentiated cells. Using this method, 89.2% ± 1.7% cTNT-positive cells were obtained.

Heart failure and myocardial infarction mainly affect the ventricles of the heart; thus, to prevent arrhythmias after transplantation of the cells into cardiac ventricles, the ventricular subtype of cardiomyocytes should be applied. Therefore, cell sorting can be performed to obtain pure cardiomyocyte subtypes for different applications. The commonly used marker specific for ventricular cardiomyocytes is the myosin light chain 2v (MLC-2v), and the myosin light chain 2a (MLC-2a) is considered as a specific marker for atrial cardiomyocytes.

Conclusions

The non-invasive collection of somatic cells from urine and the one-off application of srRNA could allow the easy and efficient generation of sufficient and unlimited numbers of patient-specific iPSCs, which can then be differentiated besides cardiomyocytes also into other desired cell types without any genomic integration. Thereby, personalized cell therapy of different diseases can be enabled, which prevents rejection reactions and the use of immunosuppressive drugs with their long-term complications. Thereby, the outcome of various cell therapy approaches can be greatly improved, and the generated cells can also serve as cell models for studying specific genetic diseases and treatment methods.

MATERIALS AND METHODS

Production of Synthetic srRNA

The T7-VEE-OKSiM plasmid[30] containing the VEE non-structural protein coding sequences (nsP1 to nsP4) to enable the RNA replication and the coding sequences of OCT4, KLF4, SOX2, and c-MYC was purchased from Addgene (LGC Standards, Teddington, UK). To monitor the transfection and reprogramming efficiency, an additional sequence encoding an IRES (internal ribosome entry site) and the reporter protein GFP were cloned by Aldevron (Fargo, ND, USA) into the plasmid, which is then called OKSiM-GFP plasmid.

To amplify the OKSiM-GFP plasmid, *E. coli* competent cells (α-Select Chemically Competent Cells, Bioline, Luckenwalde, Germany) were transformed with 100 ng plasmid and cultivated in lysogeny broth (LB) medium containing 50 μg/mL ampicillin. Plasmid isolation was performed using the QIAprep Spin Miniprep Kit (QIAGEN, Hilden, Germany). Afterward, 36 μg OKSiM-GFP plasmid was linearized using 5 μL FastDigest MluI restriction enzyme (Thermo Fisher Scientific, Waltham, MA, USA) and 20 μL 1× reaction buffer in a total volume of 200 μL for 3 h at 37°C. The linearized DNA was purified using the Isolate II PCR and Gel Kit (Bioline) and analyzed using 1% agarose gel electrophoresis.

For the synthesis of srRNA, IVT was performed for 2 h at 37°C using the RiboMAX Large Scale Production System—T7 Kit (Promega, Madison, WI, USA) according to the manufacturer's instructions. The IVT reaction mixture contained 10 μg linearized OKSiM-GFP

plasmid DNA and 40 U RiboLock RNase Inhibitor (Thermo Fisher Scientific) in 100 μL. Afterward, DNA templates were removed by adding 1 μL TURBO DNase for 15 min at 37°C. Next, 5′-end capping was performed using the ScriptCap Cap1 Capping System followed by 3′-end polyadenylation with the A-Plus Poly(A) Polymerase Tailing Kit (both from Cellscript, Madison, WI, USA) according to manufacturer's instructions. Following each reaction step, the srRNA was purified using the RNeasy Kit (QIAGEN) and eluted in nuclease-free water. The purity and specific length of generated srRNA products were analyzed using 1% agarose gel containing 2.2 M formaldehyde and 1× GelRed (Biotium, Fremont, CA, USA) in 1× MOPS (3-(N-morpholino)propanesulfonic acid) buffer. Electrophoresis was performed at 100 V for 60 min in 1× MOPS buffer.

Isolation and Cultivation of RECs from Urine

RECs were isolated from 100–200 mL urine from healthy donors (men and women between 25 and 35 years of age) by centrifugation at 400 × *g* for 10 min. Afterward, cells were washed with 50 μg/mL gentamicin and 250 μg/mL amphotericin B (Sigma-Aldrich) containing Dulbecco's PBS (DPBS; Thermo Fisher Scientific) and centrifuged at 200 × *g* for 10 min. Then, cells were suspended in 1 mL primary medium consisting of DMEM/F12 high glucose supplemented with 10% fetal bovine serum (FBS), REGM Renal Epithelial Growth Medium SingleQuots Kit (Lonza, Basel, Switzerland), 50 μg/mL gentamicin, and 250 μg/mL amphotericin B and plated in one well of a 0.1% gelatin-coated 12-well plate. For the next 3 days, 1 mL primary medium was added each day. The obtained cells were then cultivated in proliferation medium (REMC) consisting of 50% renal epithelial (RE) basal medium with REGM Bullet Kit supplements (Lonza, Basel, Switzerland) and 50% mesenchymal cell (MC) proliferation medium (DMEM high glucose supplemented with 10% FBS, 1× GlutaMax, 1× MEM (minimum essential medium) non-essential amino acids (NEAA), 50 μg/mL gentamicin, and 250 μg/mL amphotericin B, 5 ng/mL basic fibroblast growth factor (bFGF), 5 ng/mL platelet-derived growth factor (PDGF)-AB, and 5 ng/mL epidermal growth factor (EGF). Cell culture reagents were obtained from Thermo Fisher Scientific and recombinant human growth factors were obtained from Peprotech (Hamburg, Germany). Cells were cultivated at 37°C with 5% CO_2, and the medium was changed every 2–3 days. After reaching 80% confluency, RECs were detached using 0.04% trypsin/0.03% EDTA, and the reaction was stopped using trypsin-neutralizing solution (TNS; 0.05% trypsin inhibitor in 0.1% BSA, PromoCell, Heidelberg, Germany). Afterward, cells were centrifuged for 5 min at 300 × *g* and seeded on 0.1% gelatin (Sigma-Aldrich Chemie, Steinheim, Germany)-coated cell culture plates. The characterization of RECs was performed by flow cytometry using antibodies specific for epithelial marker β-catenin and renal proximal tubular marker CD13 (Miltenyi Biotec, Bergisch Gladbach, Germany).

Reprogramming of RECs into iPSCs Using srRNA

To perform reprogramming, 5×10^4 RECs (from 4 different donors, passages 2–3) were seeded per well of a 12-well plate coated with 0.1% gelatin and incubated overnight at 37°C in proliferation medium. Next day, the cells were incubated for 45–60 min with proliferation medium containing 200 ng/mL B18R interferon inhibitor (Thermo Fisher Scientific) at hypoxia (37°C, 5% CO_2, 5% O_2). For the transfection, lipoplexes were generated by the incubation of 0.5 μg OKSiM-GFP srRNA and 1.5 μL Lipofectamine Messenger Max (Thermo Fisher Scientific) in 0.5 mL Opti-MEM I reduced serum medium (Opti-MEM, Thermo Fisher Scientific) for 15 min at room temperature (RT). RECs were washed with DPBS, and lipoplexes were added. After 4 h of incubation, lipoplexes were discarded, and 1 mL fresh proliferation medium containing 200 ng/mL B18R was added for further incubation at 37°C with 5% CO_2 and 5% O_2 for 24h. Until day 3, the medium was replaced daily, and at day 3, 0.8 μg/mL puromycin (Sigma-Aldrich) was added to the proliferation medium to select srRNA-containing transfected cells. After 2–3 days of incubation, untransfected cells were eliminated. Thereafter, B18R-containing proliferation medium was changed every day. At day 7 of reprogramming, medium was changed to E8 stem cell medium (Essential 8, Thermo Fisher Scientific) supplemented with 200 ng/mL B18R. After the first appearance of iPSC colonies (beginning on day 21), B18R was withdrawn from the medium. iPSC colonies, which were positively stained with DyLight 550-labeled mouse anti-human StainAlive SSEA-4 antibody (Stemgent) were picked manually and seeded on 0.5 μg/cm^2 vitronectin (Thermo Fisher Scientific)-coated tissue culture plates and expanded in E8 medium.

Cultivation of iPSCs Derived from RECs

After reaching confluence, iPSCs were washed once with DPBS and incubated for 5–10 min at RT with DPBS containing 0.5 mM EDTA (Sigma-Aldrich). After the detachment, cells were suspended in E8 medium containing 10 μg/mL ROCK inhibitor Y-27632 (Enzo Life Sciences, Lausen, Switzerland) and passaged at a split ratio of 1:10 or 5×10^5 cells per vitronectin-coated well of a 6-well plate or in T25 culture flasks. iPSCs were cultivated at 37°C and 5% CO_2, and E8 medium was changed daily.

Flow Cytometry

Cells were washed with 1 mL DPBS and detached using 0.04% trypsin/0.03% EDTA, and the reaction was stopped by adding TNS (PromoCell). The cells were then centrifuged (5 min at 400 × *g*), washed with DPBS, and fixed for 10 min at RT in 0.5 mL fixation solution (R&D Systems). After washing with DPBS, cells were suspended in washing buffer (Permeabilization/Wash Buffer I, R&D Systems), and 5 μL fluorescently labeled antibody was added and incubated for 45 min at RT. Afterward, cells were washed with 0.5 mL washing buffer, suspended in 200 μL 1× BD CellFIX solution (Becton Dickinson, Heidelberg, Germany), and measured using a BD FACScan flow cytometer (Becton Dickinson) and Flowing Software (Turku Centre for Biotechnology, Turku, Finland).

qRT-PCR

To perform qRT-PCR analysis, 300 ng RNA was reverse transcribed into complementa DNA (cDNA) using the iScript Kit (Bio-Rad). The primers used for the specific amplification of transcripts are listed in Table S1, and they were ordered from Ella Biotech (Martinsried, Germany) and used at a final concentration of 300 nM. Real-time qRT-PCR reactions were performed in a CFX Connect Real-Time PCR

Detection System (Bio-Rad) using IQ SYBR Green Supermix (Bio-Rad). Expression of constitutively expressed gene GAPDH (glyceraldehyde 3-phosphate dehydrogenase) was used as an internal control for the amount of RNA input. Primers were designed by using the Primer-Blast tool from NCBI.[49] Melting temperatures and self-complementarities were checked using the Oligonucleotide Properties Calculator from Northwestern University Medical School.[50]

The qRT-PCR amplification of cDNA was performed under the following conditions: 3 min at 95°C for one cycle, followed by 40 cycles of 95°C for 15 s, 60°C for 30 s, and 72°C for 10 s. After 40 cycles, melt curve analysis was performed to ensure the specificity of the products. The qRT-PCR reactions were run in triplicate with a total volume of 15 μL per well. Levels of mRNA for each gene were normalized to GAPDH, and the results are shown relative to control mRNA levels.

Characterization of iPSCs Derived from RECs

Detection of Pluripotency Markers

Immunocytochemistry of iPSCs. 5×10^5 iPSCs (passages 4–5) were seeded on vitronectin-coated glass slides in 12-well plates and cultured for 2–3 days in cell culture medium until reaching 50%–70% confluency. Cells were washed 2× with 1 mL DPBS and fixed for 10 min at RT with 0.5 mL fixation solution (R&D Systems, Minneapolis, MN, USA). After washing with 0.5 mL washing buffer, the cells were incubated for 1.5 h at RT in washing buffer containing 5% BSA. Then, cells were incubated 3 h at RT with fluorescently labeled antibodies in washing buffer containing 1% BSA or overnight at 4°C with primary antibodies. After washing 3× with 0.5 mL washing buffer, the staining of the cells with fluorescently labeled secondary antibodies was performed for 1 h at RT in washing buffer containing 1% BSA. Afterward, the cells were washed 3× with washing buffer, DPBS, and then water. Subsequently, the coverslips were mounted using Fluoroshield mounting medium with DAPI (Abcam, Cambridge, UK). Rabbit anti-human POU5F1 (OCT4) (Sigma-Aldrich Chemie), rabbit anti-human SOX2 (Stemgent, Cambridge, MA, USA), and mouse anti-human LIN28A (6D1F9) (Thermo Fisher Scientific) antibodies were used as primary antibodies. Fluorescein isothiocyanate (FITC)-labeled sheep anti-mouse immunoglobulin G (IgG) (whole molecule; Sigma-Aldrich) and Cy3-labeled goat anti-rabbit IgG cross-adsorbed secondary antibody (Thermo Fisher Scientific) were used according to the manufacturer's instructions. Furthermore, phycoerythrin (PE)-labeled mouse anti-human NANOG antibody (BD, Franklin Lakes, NJ, USA), DyLight 488-labeled mouse anti-human StainAlive TRA-1-60 antibody (Stemgent), and DyLight 550-labeled mouse anti-human StainAlive SSEA-4 antibody (Stemgent) were used. Fluorescence images were taken using an Axiovert 135 microscope and AxioVision 4.8.2 software (Carl Zeiss, Oberkochen, Germany).

Gene Expression Analysis of iPSCs. RNA from 1×10^6 iPSCs (passages 3–6) was isolated using the Aurum Total RNA Mini Kit (Bio-Rad, Munich, Germany) according to manufacturer's instructions, and qRT-PCR analysis was performed to detect the expression of OCT4, SOX2, NANOG, LIN28, E-cadherin, KLF4, and c-MYC. Levels of mRNA for each gene were normalized to that of GAPDH, and the results are shown relative to control mRNA levels in RECs. The commercially available iPSC line WTSli020-A (referred to as WT02 and generated from dermal fibroblasts using Sendai virus vector by the delivery of OCT4, SOX2, KLF4, and c-MYC; European Bank for induced pluripotent Stem Cells; Babraham, UK]) was used as iPSC control.

Trilineage Differentiation of iPSCs

To analyze the ability of the obtained iPSCs to differentiate into the three embryonal germ layers the directed differentiation of iPSCs (at passages 3–7) into meso-, endo-, and ectoderm was tested using the human StemMACS Trilineage Differentiation Kit (Miltenyi Biotec, Bergisch Gladbach, Germany) according the manufacturer's instructions. Therefore, optimized cell numbers were seeded per well of a vitronectin-coated 12-well plate: mesoderm differentiation (1×10^5 iPSCs), endoderm differentiation (2×10^5 iPSCs), and ectoderm differentiation (1.5×10^5 iPSCs). At day 7, the differentiated cells were analyzed using flow cytometry.

The mesodermal differentiation capacity was analyzed by the formation of endothelial cells, using PE-labeled mouse anti-human CD31 antibody (BD Biosciences, Franklin Lakes, NJ, USA), and the formation of smooth muscle cells, using Alexa Fluor 488-labeled anti-human α-smooth muscle actin (SMA) antibody (R&D Systems). The endodermal differentiation capacity is characterized by the presence of definitive endoderm cells using PE-labeled anti-human α-fetoprotein (AFP) antibody (R&D Systems) and PE-labeled anti-human C-X-C chemokine receptor type 4 (CXCR4) antibody (R&D Systems). Ectodermal differentiation potential was assessed through the presence of neuroectoderm cells using PE-labeled anti-PAX6 antibody (Miltenyi Biotec) and Alexa Fluor 488-labeled anti-human neuron-specific TUBB3 antibody (BD Biosciences).

Teratoma Formation of iPSCs Using Chicken Embryo CAM Assay

To confirm the trilineage differentiation potential of iPSCs, the *in vivo* formation of teratomas was analyzed using CAM assay. Fresh fertilized chicken eggs of the Lohmann White × White Rock breed chicken variety were obtained from the breeding facility Matthias Sittig (Buchholz, Germany). The eggs were incubated for 3 days at 37°C and 60% relative humidity in an egg incubator (Heka-Brutgeräte, Rietberg-Varensell, Germany) and completely rotated twice a day. At day 3 of incubation, 2–3 mL albumin was aspirated by inserting an 18G needle at the tip of the egg without harming the yolk. Subsequently, a semi-permeable adhesive tape, Suprasorb F (Lohmann & Rauscher, Rengsdorf, Germany), was stuck to the eggshell. A circular window (Ø 1–1.5 cm) was cut into the shell. Unfertilized eggs showing no vasculature or heart beating were removed. Then, using the adhesive tape, the window was sealed to prevent dehydration and to minimize the risk of infection. Afterward, the eggs were incubated without rotation. At day 7, 2×10^6 iPSCs (passages 8–11) were suspended in 50 μL cell culture medium and mixed with 50 μL

Matrigel (hECS qualified, Corning). A silicone ring with an inner diameter of 0.8 cm (neoLab, Leonberg, Germany) was carefully placed onto the CAM, and 100 μL Matrigel-containing cells was applied into the inner circle of the ring. The eggs were then sealed and further incubated. At day 17, the CAMs were excised around the application area and fixed overnight at 4°C with 4% paraformaldehyde (Merck, Darmstadt, Germany). After washing with DPBS, the specimens were dehydrated using ascending ethanol series and embedded in paraffin for sectioning. Sections were cut at 8-μm thickness and stained with H&E (Morphisto, Frankfurt, Germany).

Genomic Stability of iPSCs

The genomic stability of iPSCs was analyzed by karyotyping at the Institute of Medical Genetics and Applied Genomics, University of Tübingen, Tübingen, Germany. Therefore, RECs and RE-derived iPSCs (at passages 4–7) were treated for 1 h with Colcemid (Biochrom), incubated with 0.075 M KCl for 30 min at 37°C, and fixed with 1:3 acidic acid:methanol. Karyotyping was performed on G-banded metaphase chromosomes (banding quality of 400–500 bp) using standard cytogenetic procedures. An intact genome was demonstrated by karyotyping (numerical analysis of 15 mitoses and structural analysis of at least 5 mitoses).

Detection of srRNA Elimination after the Reprogramming of Cells

RNA from 1×10^6 iPSCs (passage 3) was isolated using the Aurum Total RNA Mini Kit according to manufacturer's instructions. Using nsP2- and nsP4-specific primers (Table S1) and qRT-PCR, the presence of srRNA in generated iPSCs was analyzed. RNA levels were normalized to GAPDH, and the results are shown relative to control RNA levels in RECs. In addition, to obtain a positive control, cells were transfected with 1 μg srRNA, and the RNA was isolated after 2 days of cultivation.

Differentiation of iPSCs into Cardiomyocytes

The differentiation of iPSCs from 4 different donors into cardiomyocytes was performed using the PSC Cardiomyocyte Differentiation Kit (Thermo Fisher Scientific) according to the manufacturer's instructions. Therefore, 2×10^5 iPSCs (passages 4–12) were seeded on Geltrex LDEV-Free hESC-Qualified Reduced Growth Factor Basement Membrane Matrix (Thermo Fisher Scientific) (1:100 diluted in CMM) or on 0.5 μg/cm^2 vitronectin-coated wells of a 6-well plate. After 3–4 days cultivation in E8 medium, the differentiation protocol started. The cells were incubated for 2 days with cardiomyocyte differentiation medium A and then for 2 days with cardiomyocyte differentiation medium B. On the fifth day of differentiation, CMM was added to the cells for the following days of differentiation.

After 7–12 days, when contracting cardiomyocytes were observed (passage 0), the medium was changed to cardiomyocyte enrichment medium (CEM): RPMI 1640 medium without glucose (Thermo Fisher) containing 0.25% BSA (Fraction V, Sigma-Aldrich), 4 mM sodium lactate (Fisher Chemicals), 4 mM HEPES (Thermo Fisher), and 6.5 μM ascorbic acid (Acros Organics, Geel, Belgium). After 4–6 days, cardiomyocytes were passaged using 1 mL TrypLE solution (Thermo Fisher), and the reaction was stopped by adding an equal volume of TNS (PromoCell). Cell suspension was filtered through a 100-μm cell strainer (Greiner Bio-One, Frickenhausen, Germany) and centrifuged at 200 × *g* for 5 min. The cells were suspended in CMM, seeded onto Geltrex- or vitronectin-coated cell culture plates with a density of 1×10^5 cells per square centimeter (passage 1), and cultivated in a humidified atmosphere at 37°C and 5% CO_2. After 4–6 days of enrichment procedure, the yield of differentiated cardiomyocytes was determined by flow cytometry using FITC-labeled mouse anti-human cTNT antibody from Miltenyi Biotec.

Detection of Cardiomyocyte Markers

Immunocytochemistry of Cardiomyocytes Derived from iPSCs

1×10^6 iPSC-derived cardiomyocytes (passage 1) were plated on Geltrex-coated glass slides in 12-well plates and cultivated for 2 days in CMM. Rabbit anti-human cTNT antibody, mouse anti-human ACTA2 (both from R&D Systems), and mouse anti-human MYH6 antibody (GeneTex, Irvine, CA, USA) were used as cardiomyocyte-specific primary antibodies. NL637-conjugated donkey anti-mouse IgG (R&D Systems) and Cy3-labeled goat anti-rabbit IgG (Thermo Fisher Scientific) were used as secondary antibodies. Primary and secondary antibodies were applied as recommended by the manufacturer. Nuclei were stained using a final concentration of 5 μM SYTO 9 Green Fluorescent Nucleic Acid Stain (Thermo Fisher Scientific) in DPBS. Fluorescence images were taken after washing with DBPS using a Leica TCS SP5 confocal laser scanning microscope and the Leica Application Suite Advanced Fluorescence (2.7.3.9723) software (Leica, Wetzlar, Germany). To obtain fluorescence microscopic overview images of cardiomyocytes derived from iPSCs, cells were stained using FITC-labeled anti-human cTNT and PE-labeled anti-human (sarcomeric) α-actinin (ACTN2) antibodies from Miltenyi Biotech and Fluoroshield Mounting Medium with DAPI (Abcam). Fluorescence images were taken using an Axiovert 135 microscope and AxioVision 4.8.2 software (Carl Zeiss).

Gene Expression Analysis of Cardiomyocytes Derived from iPSCs

RNA from 1×10^6 iPSC-derived cardiomyocytes (12–16 days after starting the differentiation; passage 0) was isolated using the Aurum Total RNA Mini Kit according to manufacturer's instructions, and qRT-PCR analysis was performed to detect the expression of ANP, cTNT, MYH6, and α-actinin, cardiac muscle 1 (ACTC1). Levels of mRNA for each gene were normalized to GAPDH, and the results are shown relative to control mRNA levels in RECs.

Detection of Cardiac Troponin I

1×10^6 iPSCs (passages 4–8) were seeded per well on Geltrex-coated 6-well plates and differentiated for 12–16 days into cardiomyocytes. The supernatants (CMM) of beating cardiomyocyte cultures (passage 0) were analyzed to measure the TNNI3 content using ADVIA Centaur XPT (TnI-Ultra chemiluminescent immunoassay, Siemens Healthcare Diagnostics, Eschborn, Germany) according to the manufacturer's instructions. Additionally, the TNNI3 concentration was

measured in cell culture supernatants of RECs (REMC medium) and REC-derived iPSCs (E8 medium) as well as in fresh CMM.

Characterization of Contracting Cardiomyocytes

Video Microscopy

Video recordings of beating cells were performed to analyze the mechanical beating behavior of obtained cardiomyocytes from 4 different donors. Therefore, 7 images per second were taken for 30 s using an Axiovert 135 microscope and AxioVision 4.8.2 software (Carl Zeiss). The beating center(s) and the beat rate of obtained cardiomyocytes were determined using the MATLAB application Motion GUI.[51]

Analysis of Electromechanical Coupling Using Ca^{2+} Imaging

To analyze the electromechanical coupling of the obtained cardiomyocytes, calcium imaging was performed. Ca^{2+} oscillations are an indication of a fully differentiated cardiac phenotype and key regulator in controlling cardiomyocyte relaxation and contraction. To evaluate the intracellular Ca^{2+} behavior, Ca^{2+} transients were measured from spontaneously contracting cardiomyocytes (passage 0, 4 donors) using the Fluo-4 Direct Calcium Assay Kit (Thermo Fisher Scientific) according to the manufacturer's instructions. Beating cardiomyocytes were obtained 12 days after the differentiation of iPSCs on Geltrex-coated wells of a 6-well plate. The obtained cells were incubated for 30 min at 37°C with 1 mL 1× Fluo-4 Direct Calcium Assay Reagent Solution and 1 mL CMM. Using a fluorescence microscope (Axiovert 135), Ca^{2+} transients were recorded within the next 30 min at RT with 5 pictures per second and a 30 ms exposure time at 494 nm excitation wavelength.

Response of Cardiomyocytes to Pharmacological Modulation

To analyze the reaction of the generated REC-iPSC derived cardiomyocytes on pharmaceutical drugs, the cells were treated with 0.0001, 0.001, 0.01, 0.1, 1.0, or 10 μM Ca^{2+} channel blocker nifedipine or β-adrenoceptor agonist isoproterenol. Stock solutions of 100 mM nifedipine or 100 mM isoproterenol (both from Sigma Aldrich) were prepared in DMSO and diluted in CMM. Cardiomyocyte culture medium was replaced 11 or 13 days after starting the differentiation process (passage 0) by preheated (37°C) drug dilutions in CMM and incubated for 5 min at 37°C. Video recordings of 20 s each were performed using AxioCam and an Axiovert 135 microscope, and the beat rate was analyzed using Motion GUI. After recordings, the medium was changed to CMM.

Statistical Analysis

Data are shown as mean ± SD or SEM. Paired t test or one-way ANOVA for repeated measurements followed by Bonferroni's multiple comparison test was performed to compare the means. Two-tailed statistical analyses were performed using GraphPad Prism 6.01 (GraphPad Software, La Jolla, CA, USA). Differences of $p < 0.05$ were considered significant.

SUPPLEMENTAL INFORMATION

Supplemental Information can be found online at https://doi.org/10.1016/j.omtn.2019.07.016.

AUTHOR CONTRIBUTIONS

H.S. and M.A.-A. conceived and designed the experiments. H.S. and M.W. performed the experiments with support from A.B., A.-F.P., H.P.W., and M.A.-A., and analyzed the data. U.M.-H. performed karytotyping analysis and interpretation. C.v.O. performed CLSM investigations. H.P.W. and C.S. contributed reagents, materials, and analysis tools. H.S., M.W., and M.A.-A. wrote the paper. M.A.-A. supervised the project.

CONFLICTS OF INTEREST

The authors declare no competing interests.

ACKNOWLEDGMENTS

For TNNI3 detection in supernatants, the authors would like to thank Dr. Ingo Rettig at the Division of Endocrinology, Diabetology, Vascular Medicine, Nephrology and Clinical Chemistry, Department of Internal Medicine IV, University of Tübingen, Germany. We would also like to thank Jeannette Schöne and Elisa Kächele for excellent cytogenetic technical assistance and Annika Hechler for assistance with the collection of CLSM data. This study was funded by the German Research Foundation (Deutsche Forschungsgemeinschaft; DFG) through AV 133/7-1.

REFERENCES

1. Roger, V.L. (2013). Epidemiology of heart failure. Circ. Res. *113*, 646–659.
2. Bergmann, O., Zdunek, S., Felker, A., Salehpour, M., Alkass, K., Bernard, S., Sjostrom, S.L., Szewczykowska, M., Jackowska, T., Dos Remedios, C., et al. (2015). Dynamics of cell generation and turnover in the human heart. Cell *161*, 1566–1575.
3. Li, R.K., Jia, Z.Q., Weisel, R.D., Mickle, D.A.G., Zhang, J., Mohabeer, M.K., Rao, V., and Ivanov, J. (1996). Cardiomyocyte transplantation improves heart function. Ann. Thorac. Surg. *62*, 654–660.
4. Watanabe, E., Smith, D.M., Jr., Delcarpio, J.B., Sun, J., Smart, F.W., Van Meter, C.H., Jr., and Claycomb, W.C. (1998). Cardiomyocyte transplantation in a porcine myocardial infarction model. Cell Transplant. *7*, 239–246.
5. Valarmathi, M.T., Fuseler, J.W., Goodwin, R.L., Davis, J.M., and Potts, J.D. (2011). The mechanical coupling of adult marrow stromal stem cells during cardiac regeneration assessed in a 2-D co-culture model. Biomaterials *32*, 2834–2850.
6. Caspi, O., Itzhaki, I., Kehat, I., Gepstein, A., Arbel, G., Huber, I., Satin, J., and Gepstein, L. (2009). In vitro electrophysiological drug testing using human embryonic stem cell derived cardiomyocytes. Stem Cells Dev. *18*, 161–172.
7. Mummery, C., Ward-van Oostwaard, D., Doevendans, P., Spijker, R., van den Brink, S., Hassink, R., van der Heyden, M., Opthof, T., Pera, M., de la Riviere, A.B., et al. (2003). Differentiation of human embryonic stem cells to cardiomyocytes: role of coculture with visceral endoderm-like cells. Circulation *107*, 2733–2740.
8. Zhang, J., Wilson, G.F., Soerens, A.G., Koonce, C.H., Yu, J., Palecek, S.P., Thomson, J.A., and Kamp, T.J. (2009). Functional cardiomyocytes derived from human induced pluripotent stem cells. Circ. Res. *104*, e30–e41.
9. Burridge, P.W., and Zambidis, E.T. (2013). Highly efficient directed differentiation of human induced pluripotent stem cells into cardiomyocytes. Methods Mol. Biol. *997*, 149–161.
10. Mathur, A., Loskill, P., Shao, K., Huebsch, N., Hong, S., Marcus, S.G., Marks, N., Mandegar, M., Conklin, B.R., Lee, L.P., and Healy, K.E. (2015). Human iPSC-based cardiac microphysiological system for drug screening applications. Sci. Rep. *5*, 8883.
11. Moretti, A., Bellin, M., Welling, A., Jung, C.B., Lam, J.T., Bott-Flügel, L., Dorn, T., Goedel, A., Höhnke, C., Hofmann, F., et al. (2010). Patient-specific induced pluripotent stem-cell models for long-QT syndrome. N. Engl. J. Med. *363*, 1397–1409.
12. Takahashi, K., and Yamanaka, S. (2006). Induction of pluripotent stem cells from mouse embryonic and adult fibroblast cultures by defined factors. Cell *126*, 663–676.

13. Takahashi, K., Tanabe, K., Ohnuki, M., Narita, M., Ichisaka, T., Tomoda, K., and Yamanaka, S. (2007). Induction of pluripotent stem cells from adult human fibroblasts by defined factors. Cell *131*, 861–872.

14. Raab, S., Klingenstein, M., Liebau, S., and Linta, L. (2014). A comparative view on human somatic cell sources for iPSC generation. Stem Cells Int. *2014*, 768391.

15. Ingelfinger, J.R. (2002). Nephrogenic adenomas as renal tubular outposts. N. Engl. J. Med. *347*, 684–686.

16. Okita, K., Ichisaka, T., and Yamanaka, S. (2007). Generation of germline-competent induced pluripotent stem cells. Nature *448*, 313–317.

17. Wernig, M., Meissner, A., Cassady, J.P., and Jaenisch, R. (2008). c-Myc is dispensable for direct reprogramming of mouse fibroblasts. Cell Stem Cell *2*, 10–12.

18. Stadtfeld, M., Nagaya, M., Utikal, J., Weir, G., and Hochedlinger, K. (2008). Induced pluripotent stem cells generated without viral integration. Science *322*, 945–949.

19. Kaji, K., Norrby, K., Paca, A., Mileikovsky, M., Mohseni, P., and Woltjen, K. (2009). Virus-free induction of pluripotency and subsequent excision of reprogramming factors. Nature *458*, 771–775.

20. Yu, J., Hu, K., Smuga-Otto, K., Tian, S., Stewart, R., Slukvin, I.I., and Thomson, J.A. (2009). Human induced pluripotent stem cells free of vector and transgene sequences. Science *324*, 797–801.

21. Zhou, H., Wu, S., Joo, J.Y., Zhu, S., Han, D.W., Lin, T., Trauger, S., Bien, G., Yao, S., Zhu, Y., et al. (2009). Generation of induced pluripotent stem cells using recombinant proteins. Cell Stem Cell *4*, 381–384.

22. Warren, L., Manos, P.D., Ahfeldt, T., Loh, Y.H., Li, H., Lau, F., Ebina, W., Mandal, P.K., Smith, Z.D., Meissner, A., et al. (2010). Highly efficient reprogramming to pluripotency and directed differentiation of human cells with synthetic modified mRNA. Cell Stem Cell *7*, 618–630.

23. Steinle, H., Behring, A., Schlensak, C., Wendel, H.P., and Avci-Adali, M. (2017). Concise review: application of in vitro transcribed messenger RNA for cellular engineering and reprogramming: progress and challenges. Stem Cells *35*, 68–79.

24. Rabinovich, P.M., and Weissman, S.M. (2013). Cell engineering with synthetic messenger RNA. Methods Mol. Biol. *969*, 3–28.

25. Thess, A., Grund, S., Mui, B.L., Hope, M.J., Baumhof, P., Fotin-Mleczek, M., and Schlake, T. (2015). Sequence-engineered mRNA without chemical nucleoside modifications enables an effective protein therapy in large animals. Mol. Ther. *23*, 1456–1464.

26. Anderson, B.R., Muramatsu, H., Nallagatla, S.R., Bevilacqua, P.C., Sansing, L.H., Weissman, D., and Karikó, K. (2010). Incorporation of pseudouridine into mRNA enhances translation by diminishing PKR activation. Nucleic Acids Res. *38*, 5884–5892.

27. Karikó, K., Buckstein, M., Ni, H., and Weissman, D. (2005). Suppression of RNA recognition by Toll-like receptors: the impact of nucleoside modification and the evolutionary origin of RNA. Immunity *23*, 165–175.

28. Karikó, K., Muramatsu, H., Welsh, F.A., Ludwig, J., Kato, H., Akira, S., and Weissman, D. (2008). Incorporation of pseudouridine into mRNA yields superior nonimmunogenic vector with increased translational capacity and biological stability. Mol. Ther. *16*, 1833–1840.

29. Svitkin, Y.V., Cheng, Y.M., Chakraborty, T., Presnyak, V., John, M., and Sonenberg, N. (2017). N1-methyl-pseudouridine in mRNA enhances translation through eIF2α-dependent and independent mechanisms by increasing ribosome density. Nucleic Acids Res. *45*, 6023–6036.

30. Yoshioka, N., Gros, E., Li, H.R., Kumar, S., Deacon, D.C., Maron, C., Muotri, A.R., Chi, N.C., Fu, X.D., Yu, B.D., and Dowdy, S.F. (2013). Efficient generation of human iPSCs by a synthetic self-replicative RNA. Cell Stem Cell *13*, 246–254.

31. Petrakova, O., Volkova, E., Gorchakov, R., Paessler, S., Kinney, R.M., and Frolov, I. (2005). Noncytopathic replication of Venezuelan equine encephalitis virus and eastern equine encephalitis virus replicons in Mammalian cells. J. Virol. *79*, 7597–7608.

32. Mummery, C.L., Zhang, J., Ng, E.S., Elliott, D.A., Elefanty, A.G., and Kamp, T.J. (2012). Differentiation of human embryonic stem cells and induced pluripotent stem cells to cardiomyocytes: a methods overview. Circ. Res. *111*, 344–358.

33. Ringsrud, K.M. (2001). Cells in the urine sediment. Lab. Med. *32*, 153–155.

34. Loh, Y.H., Agarwal, S., Park, I.H., Urbach, A., Huo, H., Heffner, G.C., Kim, K., Miller, J.D., Ng, K., and Daley, G.Q. (2009). Generation of induced pluripotent stem cells from human blood. Blood *113*, 5476–5479.

35. Kim, Y., Rim, Y.A., Yi, H., Park, N., Park, S.H., and Ju, J.H. (2016). The generation of human induced pluripotent stem cells from blood cells: an efficient protocol using serial plating of reprogrammed cells by centrifugation. Stem Cells Int. *2016*, 1329459.

36. Kim, K., Doi, A., Wen, B., Ng, K., Zhao, R., Cahan, P., Kim, J., Aryee, M.J., Ji, H., Ehrlich, L.I., et al. (2010). Epigenetic memory in induced pluripotent stem cells. Nature *467*, 285–290.

37. Kim, Y.G., Baltabekova, A.Z., Zhiyenbay, E.E., Aksambayeva, A.S., Shagyrova, Z.S., Khannanov, R., Ramanculov, E.M., and Shustov, A.V. (2017). Recombinant Vaccinia virus-coded interferon inhibitor B18R: Expression, refolding and a use in a mammalian expression system with a RNA-vector. PLoS ONE *12*, e0189308.

38. Foster, K.W., Ren, S., Louro, I.D., Lobo-Ruppert, S.M., McKie-Bell, P., Grizzle, W., Hayes, M.R., Broker, T.R., Chow, L.T., and Ruppert, J.M. (1999). Oncogene expression cloning by retroviral transduction of adenovirus E1A-immortalized rat kidney RK3E cells: transformation of a host with epithelial features by c-MYC and the zinc finger protein GKLF. Cell Growth Differ. *10*, 423–434.

39. Foster, K.W., Frost, A.R., McKie-Bell, P., Lin, C.Y., Engler, J.A., Grizzle, W.E., and Ruppert, J.M. (2000). Increase of GKLF messenger RNA and protein expression during progression of breast cancer. Cancer Res. *60*, 6488–6495.

40. Yu, F., Li, J., Chen, H., Fu, J., Ray, S., Huang, S., Zheng, H., and Ai, W. (2011). Kruppel-like factor 4 (KLF4) is required for maintenance of breast cancer stem cells and for cell migration and invasion. Oncogene *30*, 2161–2172.

41. Später, D., Hansson, E.M., Zangi, L., and Chien, K.R. (2014). How to make a cardiomyocyte. Development *141*, 4418–4431.

42. Cyganek, L., Tiburcy, M., Sekeres, K., Gerstenberg, K., Bohnenberger, H., Lenz, C., Henze, S., Stauske, M., Salinas, G., Zimmermann, W.H., et al. (2018). Deep phenotyping of human induced pluripotent stem cell-derived atrial and ventricular cardiomyocytes. JCI Insight *3*, 99941.

43. Schweizer, P.A., Darche, F.F., Ullrich, N.D., Geschwill, P., Greber, B., Rivinius, R., Seyler, C., Müller-Decker, K., Draguhn, A., Utikal, J., et al. (2017). Subtype-specific differentiation of cardiac pacemaker cell clusters from human induced pluripotent stem cells. Stem Cell Res. Ther. *8*, 229.

44. Besser, R.R., Ishahak, M., Mayo, V., Carbonero, D., Claure, I., and Agarwal, A. (2018). Engineered microenvironments for maturation of stem cell derived cardiac myocytes. Theranostics *8*, 124–140.

45. Di Baldassarre, A., Cimetta, E., Bollini, S., Gaggi, G., and Ghinassi, B. (2018). Human-induced pluripotent stem cell technology and cardiomyocyte generation: progress and clinical applications. Cells *7*, E48.

46. Dubois, N.C., Craft, A.M., Sharma, P., Elliott, D.A., Stanley, E.G., Elefanty, A.G., Gramolini, A., and Keller, G. (2011). SIRPA is a specific cell-surface marker for isolating cardiomyocytes derived from human pluripotent stem cells. Nat. Biotechnol. *29*, 1011–1018.

47. Tohyama, S., Hattori, F., Sano, M., Hishiki, T., Nagahata, Y., Matsuura, T., Hashimoto, H., Suzuki, T., Yamashita, H., Satoh, Y., et al. (2013). Distinct metabolic flow enables large-scale purification of mouse and human pluripotent stem cell-derived cardiomyocytes. Cell Stem Cell *12*, 127–137.

48. Lopaschuk, G.D., and Jaswal, J.S. (2010). Energy metabolic phenotype of the cardiomyocyte during development, differentiation, and postnatal maturation. J. Cardiovasc. Pharmacol. *56*, 130–140.

49. Ye, J., Coulouris, G., Zaretskaya, I., Cutcutache, I., Rozen, S., and Madden, T.L. (2012). Primer-BLAST: a tool to design target-specific primers for polymerase chain reaction. BMC Bioinformatics *13*, 134.

50. Kibbe, W.A. (2007). OligoCalc: an online oligonucleotide properties calculator. Nucleic Acids Res. *35*, W43–W46.

51. Huebsch, N., Loskill, P., Mandegar, M.A., Marks, N.C., Sheehan, A.S., Ma, Z., Mathur, A., Nguyen, T.N., Yoo, J.C., Judge, L.M., et al. (2015). Automated video-based analysis of contractility and calcium flux in human-induced pluripotent stem cell-derived cardiomyocytes cultured over different spatial scales. Tissue Eng. Part C Methods *21*, 467–479.

7.3.2 Publikation II:

An Alternative In Vivo Model to Evaluate Pluripotency of Patient-Specific hiPSCs

ALTEX preprint
published January 25, 2021
doi:10.14573/altex.2005221

Research Article

An Alternative *In Vivo* Model to Evaluate Pluripotency of Patient-Specific hiPSCs

Josefin Weber[#], Marbod Weber[#], Heidrun Steinle, Christian Schlensak, Hans-Peter Wendel and Meltem Avci-Adali
University Hospital Tuebingen, Department of Thoracic and Cardiovascular Surgery, Tuebingen, Germany

Abstract
The generation of autologous human induced pluripotent stem cells (hiPSCs) from patient's somatic cells and the subsequent differentiation of these cells into desired cell types offer innovative treatment options for tissue regeneration. The hiPSCs obtained are usually implanted in immunodeficient mice and teratoma formation is analyzed after 4 to 6 weeks to assess the pluripotency of these cells. In this study, an alternative *in vivo* model based on chicken egg chorioallantoic membrane (CAM) was established to analyze the pluripotency of newly created hiPSCs. Therefore, 0.5, 1, 2, 4 x 10^6 hiPSCs generated from urine-derived renal epithelial cells were seeded on CAM and incubated for 9 days. Teratoma formation was detected in 70% of eggs inoculated with 2 x 10^6 hiPSCs and in 100% of eggs after the application of 4 x 10^6 hiPSCs. All teratomas exhibited vascular structures. The robustness of the CAM model was further confirmed using two additional hiPSC lines derived from human fibroblasts (NuFFs) or jaw periosteal cells. The presence of all three germ layers within the teratomas was successfully verified by histochemical and immunofluorescence staining and gene expression analysis of germ layer-specific markers. Urine-derived renal epithelial cells were used as negative control and showed no teratoma formation. The CAM-based *in vivo* model provides an optimal *in vivo* test environment for the pluripotency evaluation of newly generated hiPSC lines. Furthermore, this simple, fast, inexpensive, and reproducible method reduces the suffering of animals and thus implements the principles of the 3Rs (replacement, reduction, and refinement).

1 Introduction

The groundbreaking discovery of the reprogrammability of somatic cells into human induced pluripotent stem cells (hiPSCs) opened up new opportunities in the field of tissue engineering and the development of personalized cell therapies. Since hiPSCs are derived from patient´s somatic cells, their generation and use avoid ethical concerns related to embryonic stem cells. Thus, hiPSCs are a promising cell source to generate patient-specific cell types. Yamanaka and colleagues first reprogramed murine fibroblasts into iPSCs (Takahashi and Yamanaka, 2006), and shortly thereafter reprogramming was also demonstrated in human fibroblasts using retroviral vectors encoding four transcription factors, Klf4, c-Myc, Oct4, and Sox2 (Takahashi et al., 2007). However, retroviral vectors are inserted into the host genome and this is associated with a significant risk of insertional mutagenesis, incomplete transgene silencing or reactivation, and residual expression of reprogramming factors, which can lead to tumor development (Cieślar-Pobuda et al., 2017). Therefore, to prevent genetic alterations in hiPSCs for later clinical applications, several non-genome integrating approaches have been developed (Kaji et al., 2009; Yu et al., 2009; Warren et al., 2010). Especially, synthetic messenger RNA-based reprogramming methods using synthetic messenger RNA (mRNA) or self-replicating RNA (srRNA) are promising (Steinle et al., 2017, 2019a). After the exogenous delivery of reprogramming factor encoding RNAs into somatic cells, desired reprogramming factors are expressed under physiological conditions by cells' translational machinery until the cells are reprogrammed. In comparison to plasmid DNA, synthetic mRNAs or srRNAs do not need to enter the cell nucleus. This allows the expression of desired proteins in dividing and non-dividing cells and results in an immediate translation of delivered mRNA or srRNA in the cytosol. Since these RNAs are not integrated into the genome, the risk of insertional mutagenesis can be eliminated (Rabinovich and Weissman, 2013).

After the successful generation of hiPSC lines, a detailed characterization of the cells is inevitable. In addition to the exclusion of genetic abnormalities and the expression of proteins associated with stem cell properties, the confirmation of pluripotency is required. To confirm the pluripotency of newly generated hiPSC lines, the differentiation into three germ layers is analyzed by subcutaneous or intramuscular injection of hiPSCs in immunodeficient mice (DeBord et al., 2018;

[#] equally contributed

Received May 22, 2020; Accepted January 20, 2021;
Epub January 25, 2021; © The Authors, 2021.

ALTEX 38(#), ###-###. doi:10.14573/altex.2005221

Correspondence: Meltem Avci-Adali, Ph.D.,
Department of Thoracic and Cardiovascular Surgery, University Hospital Tuebingen,
Calwerstr. 7/1, 72076 Tuebingen, Germany
(meltem.avci-adali@uni-tuebingen.de)

ALTEX preprint
published January 25, 2021
doi:10.14573/altex.2005221

Nelakanti et al., 2015). Animals are monitored for 6–8 weeks and sacrificed to explant the teratoma before it is larger than 1 cm^3. Because of its tumor-like growth, it can cause pain and suffering of the animals and raises ethical concerns (Buta et al., 2013). In addition, keeping immunodeficient mice is time-consuming and expensive. In recent years, the chorioallantoic membrane (CAM) assay was applied to investigate angiogenesis (Steinle et al., 2018; Naik et al., 2018), tumorigenesis (Li et al., 2015; Dexter et al., 1983; Durupt et al., 2012; Rovithi et al., 2017), bone and cartilage generation (Moreno-Jimenez et al., 2016), and irritant potential of chemicals (Gilleron et al., 1996; Ying et al., 2010). CAM is formed by the fusion of the mesodermal layer of the allantois with the mesodermal layer of the chorion until the third day of development of the chicken embryo (Kunz et al., 2019; Dohle et al., 2009). The highly vascularized CAM mimics a perfect environment for cell transplantation and it can maintain engrafted cells (Deryugina and Quigley, 2008). Furthermore, CAM assay provides a highly reproducible, cost-effective, immunodeficient, and noninnervated extra-embryonic test environment (Kunz et al., 2019; Kunzi-Rapp et al., 2001), and implements the 3R principles (reduction, replacement, and refinement) (Petrovova et al., 2019). An ethical advantage of the CAM assay is that the CAM itself is not innervated, allowing the growth of xenografts without pain or impairment of the embryo (Kunz et al., 2019). Furthermore, the lack of nociception in chicken embryos due to incomplete neuronal differentiation until 14 days of its gestation period makes the model a favorable alternative to rodent models (Buhr et al., 2020). Therefore, in some countries, ethical approval is not required for CAM assays with chicken embryos until 14 days of development. However, there are other countries, where the chicken embryo is not considered as an independent living animal until day 17 or hatching (Winter et al., 2020), so ethical approval for animal experiments is not required. Thus, depending on the country, the legal requirements should be followed and, if necessary, the approval of the ethics committee for animal experiments should be obtained.

In this study, we describe the applicability of a CAM assay-based *in vivo* model as an alternative to conventional rodent models for analyzing the pluripotency of patient-specific hiPSCs by spontaneous teratoma formation.

2 Material and methods

Cultivation of hiPSCs

Footprint-free hiPSCs were generated by reprogramming of human renal epithelial cells (RECs) isolated from 100-200 ml urine of healthy human donors using VEE-OKSiM-GFP srRNA encoding OCT4, KLF4, SOX2, cMYC, and GFP. The transfection and reprogramming were performed according to our recent study (Steinle et al., 2019b). The obtained hiPSCs were cultivated on T25 culture flasks coated with 0.5 mg/cm^2 vitronectin (Thermo Fisher Scientific, Waltham, MA, USA) in E8 stem cell medium (Essential 8, Thermo Fisher Scientific) at 37°C and 5 % CO_2. After reaching 70 % confluence, hiPSCs were washed once with Dulbecco's Phosphate-Buffered Saline (DPBS) (Thermo Fisher Scientific) and incubated for 5 min at 37 °C with DPBS containing 0.5 mM EDTA (Sigma-Aldrich, Steinheim, Germany). After detachment, cells were suspended in E8 medium containing 10 µM ROCK inhibitor Y-27632 (Enzo Life Sciences, Lausen, Switzerland) and passaged at a 1:10 split ratio into a new vitronectin-coated T25 culture flask. hiPSCs were cultivated at 37 °C and 5 % CO_2 (normoxia). After 24 h, the medium was changed to E8 medium without ROCK inhibitor Y-27632 and daily medium changes were performed.

Cultivation of RECs

RECs were isolated as described in our previously published study (Steinle et al., 2019b) and cultivated at 37 °C with 5 % CO_2 in 0.1 % gelatin-coated 12-well plates with proliferation medium consisting of 50 % renal epithelial (RE) basal medium with REGM Bullet Kit supplements (Lonza, Basel, Switzerland) and 50 % mesenchymal cell proliferation medium (DMEM high glucose supplemented with 10 % FBS, 1x GlutaMax, 1x MEM (minimum essential medium) non-essential amino acids (NEAA), 50 mg/mL gentamicin, and 250 mg/mL amphotericin B, 5 ng/mL basic fibroblast growth factor (bFGF), 5 ng/mL platelet-derived growth factor (PDGF)-AB, and 5 ng/mL epidermal growth factor (EGF). Cell culture reagents were obtained from Thermo Fisher Scientific and recombinant human growth factors were acquired from Peprotech (Hamburg, Germany). The medium was changed every three days. When reaching 80 % confluency, RECs were passaged using 0.04 % trypsin/0.03 % EDTA. The reaction was stopped using trypsin-neutralizing solution (TNS; 0.05 % trypsin inhibitor in 0.1 % BSA, PromoCell, Heidelberg, Germany). Afterwards, cells were centrifuged for 5 min at 300 x g and seeded on 0.1 % gelatin (Sigma-Aldrich)-coated T75 cell culture flasks.

Chorioallantoic membrane (CAM) assay

Fertilized chicken eggs of the Lohmann White x White Rock breed chicken were obtained from a breeding facility (Matthias Sittig, Buchholz, Germany). Feathers, dirt, and excrement from the eggshells were removed by wiping with a wet tissue. Then, the eggs were placed in the egg incubator (Heka-Brutgeräte, Rietberg-Varensell, Germany) and incubated at 37 °C and 60 % relative humidity (Day 0). The eggs were completely rotated twice a day. At day 3 after fertilization, an 18G needle was inserted at the tip of the egg without harming the yolk and 2-3 ml albumen was removed to lower the level of the CAM. In the following, a semi-permeable adhesive tape, Suprasorb F (Lohmann & Rauscher, Rengsdorf, Germany) was fixed on the eggshell. Then, under a sterile bench, using sterile surgical scissors a circular opening (Ø 1–1.5 cm) was cut into the eggshell without destroying the CAM. Unfertilized eggs without heart beating or any vasculature were discarded. Afterwards, the window of the eggshell of viable eggs was closed again with the adhesive tape to prevent dehydration and to minimize the risk of contamination. Subsequently, eggs were incubated without rotation at 37 °C and 75 % relative humidity. On day 7, the semi-permeable adhesive tape covering the circular opening was carefully opened with sterile scissors. Then, the development of the eggs was analyzed. Insufficiently developed or contaminated eggs without clearly visible vasculature and movement of the embryo were removed. Sterile silicone sealing rings of cryovials with an inner diameter of 0.85 cm (neoLab, Leonberg, Germany) were carefully placed onto the CAM. To apply the hiPSCs into the silicone ring, 0.5, 1, 2, or 4 x 10^6 hiPSCs (passage 11) were suspended in 50 µl cell culture medium and mixed with 50 µl Matrigel (hECS qualified,

ALTEX preprint
published January 25, 2021
doi:10.14573/altex.2005221

Corning, NY, USA). As a control, 1 x 10^6 RECs were also applied onto CAM. After the application, the opening in the eggshell was sealed with the adhesive tape again and further incubated at 38 °C and 80 % relative humidity. On day 16, the CAMs including the generated teratoma were excised around the silicone ring and fixed overnight at 4 °C with 4 % paraformaldehyde (PFA, Merck, Darmstadt, Germany) for further analysis.

To verify the robustness of the CAM model, 2x10^6 hiPSCs, which were generated from newborn human foreskin fibroblasts (NuFFs, Amsbio, Milton Park, UK) or human jaw periosteal cells (JPCs) using srRNA were also applied onto CAM and the teratomas generated were analyzed.

Paraffin embedding and histochemical evaluation of teratomas

The PFA-fixed teratomas and CAMs seeded with RECs as negative controls were washed with DPBS, dehydrated using ascending ethanol series from 50 %, 70 %, 80 %, 90 % to 99 %, and embedded in paraffin for sectioning. Using a microtome (MICROM GmbH, Walldorf, Germany), 5 µm thick sections were obtained from paraffin-embedded tissues. Sections were placed on SuperFrost microscope slides (R. Langenbrinck GmbH, Emmendingen). The sections were then deparaffinized and rehydrated by xylene, a descending ethanol series from 100 %, 80 %, 70 % to 60 %, and deionized water. Afterwards, the sections were stained with hematoxylin and eosin (H&E) (Morphisto, Frankfurt, Germany). In the next step, sections were dehydrated using an ascending ethanol series from 60 %, 70 %, 80 % to 100 %, and xylene. Finally, the sections were covered with glass coverslips. The teratoma structures were microscopically analyzed regarding the presence of tissue-specific structures.

To prove the presence of the cells from all three germ layers, immunohistochemical stainings were performed using an automated immunostainer (Ventana Medical Systems, Inc., Arizona, USA) and specific antibodies against early cell types of three germ layers according to the company's protocols with slight modifications. Monoclonal mouse anti-human CD34 antibody (Dako, Agilent Technologies, Santa Clara, USA) was used to show the presence of mesoderm tissue. CD34 is a marker for hematopoietic stem cells and endothelial progenitor cells. Monoclonal mouse anti-human SALL4 antibody (M03), clone 6E3, (Abnova, Taipeh, Taiwan) was used to detect endoderm tissue. The presence of ectodermal tissue was validated using the monoclonal mouse anti-human vimentin (V9) (ROCHE, Basel, Switzerland) antibody, which is a neural and pancreatic progenitor cell marker. CAMs with the generated teratomas and RECs as negative controls were stained to confirm specific antibody staining. All antibodies were visualized by the automated immunostainer using DAB (deaminobenzidine). Counterstaining was performed using hematoxylin. Images were taken using Axiovert135 microscope (Carl Zeiss, Oberkochen, Germany) and EOS Utility software (Canon, Tokyo, Japan).

Cryosectioning and immunofluorescence staining of teratomas

The PFA-fixed teratomas were washed in DPBS and then dehydrated at RT by sucrose (Saccharose, Sigma-Aldrich) solutions of increasing concentrations of 10%, 15%, and 20%. Each incubation was performed for 15 minutes. Teratomas were then transferred into Tissue-Tek Cryomolds (Sakura Finetek Germany GmbH, Staufen im Breisgau, Germany), embedded in Tissue-Tek (Sakura Finetek Germany GmbH), and stored at -80 °C. The frozen block was sectioned at 18 µm using the cryomicrotome (Leica Biosystems Nussloch GmbH, Nußloch, Germany). After overnight drying at RT, the immunostaining of sections was performed.

To perform immunofluorescence staining, the teratoma sections were washed with DPBS and blocked with 4% BSA in DPBS for 1 h at RT. Sections were then incubated for 1 h at RT with fluorescently labeled antibodies in DPBS with 2% BSA or in DPBS with 2% BSA and Triton X-100 (Sigma-Aldrich) for intracellular staining. After washing, the coverslips were mounted using Fluoroshield mounting medium with DAPI (Abcam, Cambridge, UK). To detect the three different germ layers Alexa Fluor® 488-mouse anti-human β-tubulin (BD Biosciences, Franklin Lakes, USA), PE-mouse anti-human CD31, and PE-mouse anti-human CXCR4 (both from Miltenyi Biotec, Bergisch Gladbach, Germany) antibodies were used. Stainings with the respective isotypes were performed as controls.

qRT-PCR analysis

RNA was isolated from the explanted teratomas generated from 2 x 10^6 hiPSCs or hiPSCs cultivated in cell culture plates (control) using the Aurum™ Total RNA Mini Kit (Bio-Rad, Munich, Germany). 300 ng RNA was reverse transcribed into complementary DNA (cDNA) using the iScript kit (Bio-Rad). The primers used for the specific amplification of transcripts ordered from Eurofins (Luxembourg, Luxembourg) or ELLA Biotech (Martinsried, Germany) and listed in Table 1. They were used at a final concentration of 300 nM. Real-time qRT-PCR reactions were performed in a CFX Connect Real-Time PCR Detection System (Bio-Rad) using IQ SYBR Green Supermix (Bio-Rad). Expression of constitutively expressed gene GAPDH (glyceraldehyde 3-phosphate dehydrogenase) was used as an internal control for the amount of RNA input. Primers were designed by using the Primer-Blast tool from NCBI (Ye et al., 2012). Melting temperatures and self-complementarities were checked using the Oligonucleotide Properties Calculator from Northwestern University Medical School (Kibbe, 2007).

The qRT-PCR amplification of cDNA was performed under the following conditions: 3 min at 95 °C for one cycle, followed by 40 cycles of 95 °C for 15 s, 60 °C for 30 s, and 72 °C for 10 s. After 40 cycles, melt curve analyses were performed to detect the specific amplification of transcripts. The qRT-PCR reactions were run in triplicates with a total volume of 15 µL per well. Levels of mRNA for each gene were normalized to GAPDH. The results are shown relative to control mRNA levels.

ALTEX preprint
published January 25, 2021
doi:10.14573/altex.2005221

Table 1: List of primer sequences used for qRT-PCR analysis

Gene	Germ layer	Forward primer 5' - 3'	Reverse primer 5' - 3'
GAPDH	-	TCAACAGCGACACCCACTCC	TGAGGTCCACCACCCTGTTG
CD31	Mesoderm	GAACGGAAGGCTCCCTTGA	AGGGCAGGTTCATAAATAAGTGC
CD34		GATTGCACTGGTCACCTCGG	TCCGTGTAATAAGGGTCTTCGC
αSMA		GAGGGAAGGTCCTAACAGCC	TAGTCCCGGGGATAGGCAAA
FOXA2	Endoderm	TGCACTCGGCTTCCAGTATG	CGTGTTCATGCCGTTCATCC
AFP		AAATGCGTTTCTCGTTGCTT	GAGTTGGCAACAAGTGGCTG
Pax6	Ectoderm	CTGAGGAATCAGAGAAGACAGGC	ATGGAGCCAGATGTGAAGGAGG
Sox1		AATACTGGAGACGAACGCCG	AACCCAAGTCTGGTGTCAGC

GAPDH: Glyceraldehyde-3-phosphate dehydrogenase; αSMA: alpha-smooth muscle actin; FOXA2: Forkhead box protein A2; AFP: Alpha-fetoprotein; Pax6: Paired box gene 6; Sox1: Sex determining region Y-box 1.

3 Results

3.1 Analysis of teratoma formation by application of hiPSCs onto CAM

To analyze the teratoma formation of newly generated hiPSCs, a CAM-based assay was established (Fig. 1A). The viability of embryos was evaluated with 176 viable eggs. After the opening of eggs on day 3 and incubating the eggs until day 7, only 15 embryos died, which corresponds to a survival rate of 91.14%. After 16 days, 63.31 % of the initial embryos were still viable (Fig. 1B). Using a total of 33 eggs, the formation of teratomas was analyzed by seeding different numbers of hiPSCs on CAM. Teratoma formation was analyzed 9 days after the inoculation of CAM with 0.5, 1, 2, or 4 x 10^6 hiPSCs (Fig. 1C). Teratomas were formed in 30.33 % (3/10) of the eggs after the application of 0.5 x 10^6 hiPSCs and the efficiency increased to 50 % (5/10) after the application of 1 x 10^6 hiPSCs. Above all, the inoculation of CAM with 2 x 10^6 hiPSCs increased the generation of teratoma formation to 70 % (7/10). The application of 4 x 10^6 hiPSCs resulted in the formation of teratomas in 100 % of the eggs (Fig. S1[1]).

3.2 Analysis of the teratoma size, tissue structures, and vascularization

To analyze the effect of the initial cell number on the resulting size of the teratoma, 0.5, 1, or 2 x 10^6 hiPSCs were seeded on the CAM (Fig. 2A). Additionally, teratoma formation was analyzed after the application of 4 x 10^6 hiPSCs in three eggs (Fig. S1[1]). On the 16th day of incubation, the hiPSC-derived teratomas were explanted. The H&E staining of CAMs seeded with 0.5, 1, 2 x 10^6 hiPSCs (Fig. 2B), or 4 x 10^6 hiPSCs (Fig. 1D) showed that the teratomas formed contain different types of tissues. The seeding of 1 x 10^6 RECs onto the CAM showed no teratoma formation (Fig. 2B, control). Furthermore, the size of the teratomas was measured (Fig. 2A, 2C). Especially, the seeding of 2 x 10^6 hiPSCs on CAM led to an increased teratoma size (24.47 ± 11.71 mm²) compared to the seeding of 1 x 10^6 (12.79 ± 1.91 mm²) or 0.5 x 10^6 hiPSCs (12.5 ± 0.69 mm²) (Fig. 2C). Furthermore, the histological examinations showed the formation of vascular structures within the teratomas, which enable the blood supply to the cells within the teratoma (Fig. 2D).

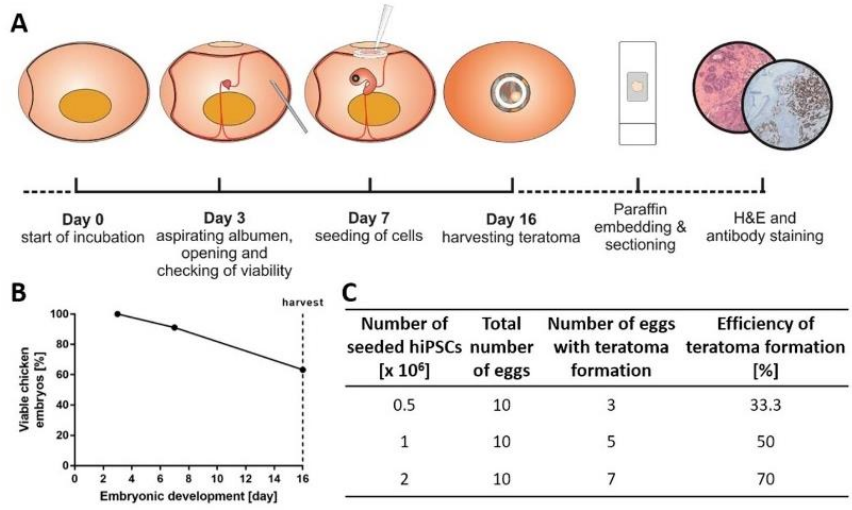

Number of seeded hiPSCs [x 10^6]	Total number of eggs	Number of eggs with teratoma formation	Efficiency of teratoma formation [%]
0.5	10	3	33.3
1	10	5	50
2	10	7	70

Fig. 1: Evaluation of teratoma formation after the seeding of hiPSCs on CAM
A) Schematic representation of the CAM-based assay to evaluate teratoma formation. The teratoma formation assay was completed within 16 days after the start of the incubation of the eggs. Subsequently, teratomas were embedded, sectioned, and histologically analyzed. **B)** The survival rate of chicken embryos in CAM assay (n = 176). **C)** Efficiency of teratoma formation depending on the inoculated hiPSC numbers on CAM.

[1] doi:10.14573/altex.2005221s

ALTEX preprint
published January 25, 2021
doi:10.14573/altex.2005221

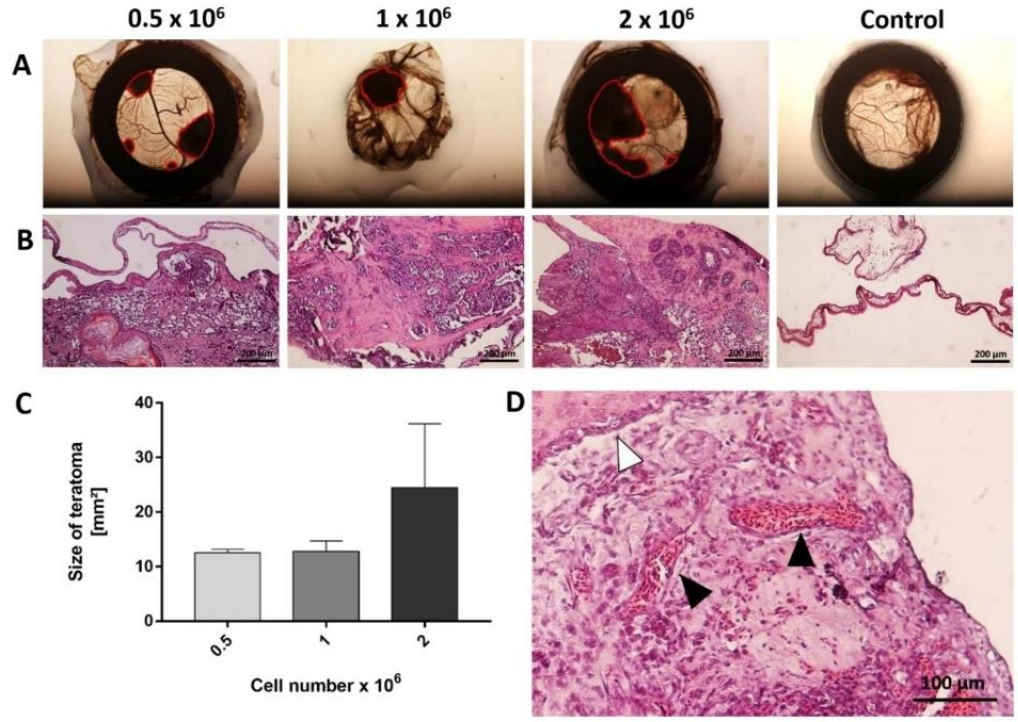

Fig. 2: Analysis of teratoma size, tissue structures, and vascularization
A) Pictures of excised CAM with formed teratomas after the seeding of 0.5, 1, or 2 x 10^6 hiPSCs on CAM. As a control, 1 x 10^6 RECs were seeded. Teratomas are encircled in red. **B)** H&E-stained sections of the teratomas or CAM. **C)** The size of the generated teratomas was determined by area calculation (red encircled area in **A**). **D)** H&E staining of a teratoma section showing vascular structures (black arrows) inside a teratoma generated from 2 x 10^6 hiPSCs. The white arrow shows the CAM.

3.3 Analysis of the tri-lineage differentiation of the hiPSCs

The H&E staining of the explanted teratomas, which were generated from 2 x 10^6 hiPSCs, revealed the tri-lineage differentiation of hiPSCs seeded on CAM (Fig. 3). The differentiation into mesodermal tissue was demonstrated by the presence of bone-like (Fig. 3A I) and into endodermal tissue was shown by the detection of the primitive gut-like epithelium (Fig. 3A II). Furthermore, the presence of squamous epithelial tissue (Fig. 3A III) showed the differentiation of hiPSCs into ectoderm tissue. In addition, the immunohistochemical analyses demonstrated the expression of the mesoderm marker CD34 (Fig. 3B I), endoderm marker SALL4 (Fig. 3B II), and the ectoderm marker vimentin (Fig. 3B III) associated with the respective morphological structures. The antibodies showed no binding to tissue sections of CAMs that were seeded with RECs (Fig. S2A[1]).

The immunofluorescence analyses of cryosections with specific antibodies revealed a strong expression of CD31 within the mesodermal tissue structures (Fig. 3C I), CXCR4 within endodermal tissue (Fig. 3C II), and β-tubulin within ectodermal structures (Fig. 3C III). As a control, teratoma tissue sections were also stained with isotype controls, which showed no binding (Fig. S2B[1]). Furthermore, the immunofluorescence analyses of CAMs seeded with RECs showed no binding to CAM (Fig. S2C[1]).

Moreover, using qRT-PCR, increased expression of mesoderm (CD31, CD34, and SMA), endoderm (FOXA2 and AFP), and ectoderm (SOX1 and PAX6) markers was detected on CAMs seeded with 2 x 10^6 hiPSCs and incubated for 16 days compared to hiPSCs cultivated in cell culture flasks with E8 medium (Fig. 3D).

To further prove the functionality of the CAM model, the teratoma formation potential of two other hiPSC lines, which were generated in our laboratory by reprogramming of human fibroblasts (NuFFs) or JPCs, was assessed by seeding of 2 x 10^6 cells on CAM. The H&E staining of the explanted teratomas, which were generated from NuFFs-derived (Fig. 4A) or JPCs-derived (Fig. 4B) hiPSCs, demonstrated the tri-lineage differentiation potential as the RECs-derived hiPSCs (Fig. 3). The differentiation into mesodermal tissue was demonstrated by the presence of bone-like structures (Fig. 4A I) and adipose tissue (Fig. 4B I). Furthermore, gut-like epithelium showing endodermal differentiation (Fig. 4A II and Fig. 4B II) and squamous epithelium showing ectodermal differentiation (Fig. 4A III and Fig. 4B III) were detected.

4 Discussion

Patient-specific hiPSCs offer the possibility to regenerate destroyed cell types and tissues for personalized treatment. After the generation of hiPSCs and the differentiation, an extensive characterization of the cells including the pluripotency is required. Typically, cells are implanted in immunodeficient mice to demonstrate the ability of newly created hiPSCs to

ALTEX preprint
published January 25, 2021
doi:10.14573/altex.2005221

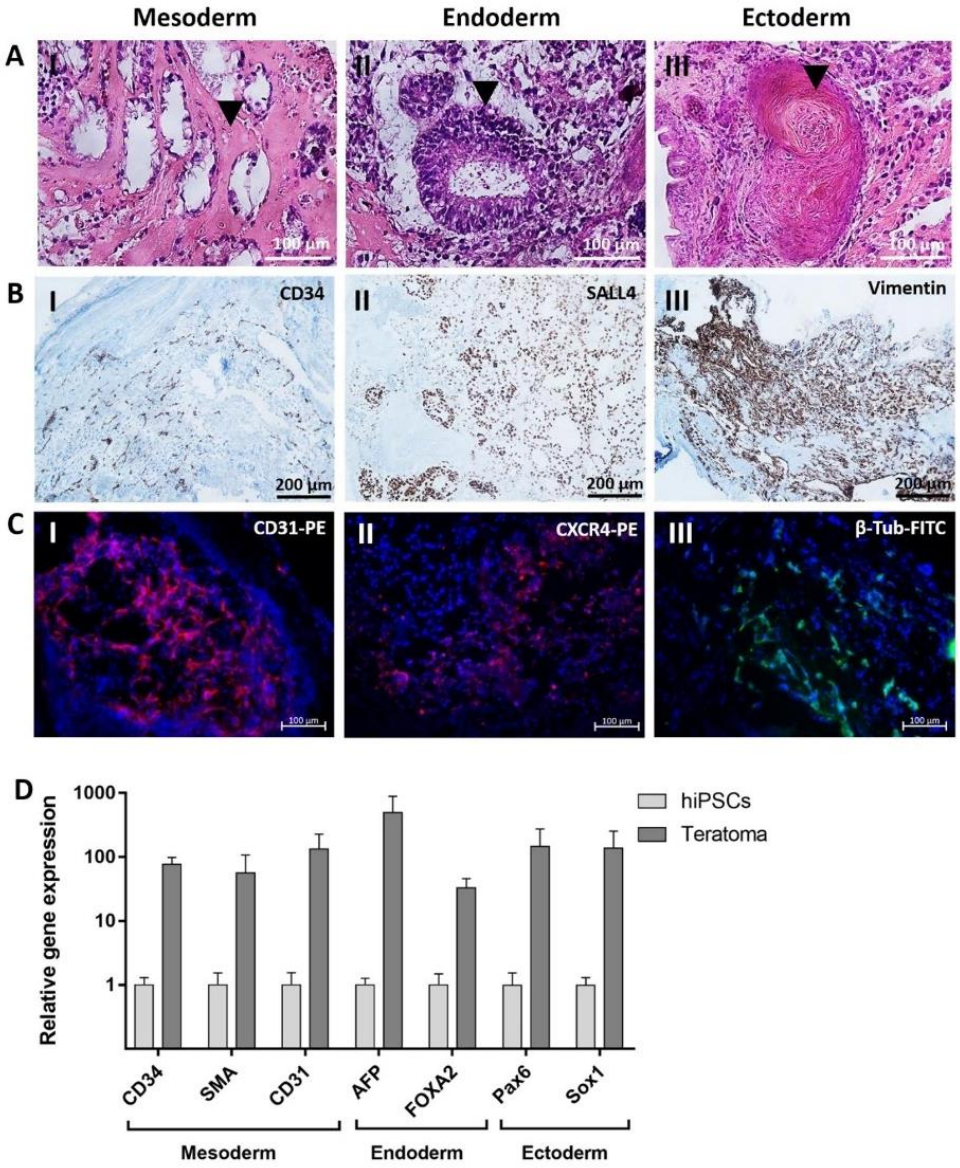

Fig. 3: Detection of three germ layer-specific tissue types in teratoma sections
Teratomas were generated by seeding of 2 x 10^6 hiPSCs on CAMs. **A)** Representative microscopic images of teratoma sections stained with H&E showing hiPSC-derived tissues of all three germ layers. Mesoderm: **(I)** bone-like tissue, Endoderm: **(II)** primitive gut-like epithelium, Ectoderm: **(III)** squamous epithelium. The arrows indicate the described germ layer-specific structures. **B)** Representative microscopic images of immunohistochemical stainings using antibodies against **(I)** CD34, **(II)** SALL4, and **(III)** vimentin. Antibody-stained tissue structures are brown and the sections were counterstained with hematoxylin. **C)** Representative immunofluorescence images of teratoma sections stained with **(I)** PE-mouse anti-human-CD31, **(II)** PE-mouse anti-human CXCR4, or **(III)** Alexa Fluor® 488-mouse anti-human β-tubulin antibodies. **D)** qRT-PCR expression analysis of CD34, SMA, CD31, AFP, FOXA2, Pax6, and Sox1 transcripts in teratomas generated from 2 x 10^6 hiPSCs. mRNA levels were normalized to GAPDH mRNA levels. Results are shown relative to hiPSCs cultivated in cell culture flask as mean + SEM (n=3)

differentiate into all cell types of three germ layers, mesoderm, endoderm, and ectoderm (Nelakanti et al., 2015). In this study, we tested the applicability of the CAM assay as a new *in vivo* model for the evaluation of the pluripotency of hiPSCs to reduce animal suffering.

Commonly, subcutaneous (Cao et al., 2007), intramuscular (Lee et al., 2009), intramyocardial (Cao et al., 2006), or sub-renal capsule implantation of hiPSCs is performed into 15 to 20 immunodeficient mice aged 6 to 10 weeks. The animals are maintained for a period of approximately 4 to 6 weeks to allow the growth of the implanted cells and teratoma formation (Nelakanti et al., 2015; Aldahmash et al., 2013). If the cells are transplanted subcutaneously or intraperitoneally, very palpable teratomas are often formed 4 to 6 weeks post-injection (Zhang et al., 2008). The teratomas can be measured using the traditional caliper method and visually (Hentze et al., 2009). Mice should be sacrificed before the teratoma is larger than 1

ALTEX preprint
published January 25, 2021
doi:10.14573/altex.2005221

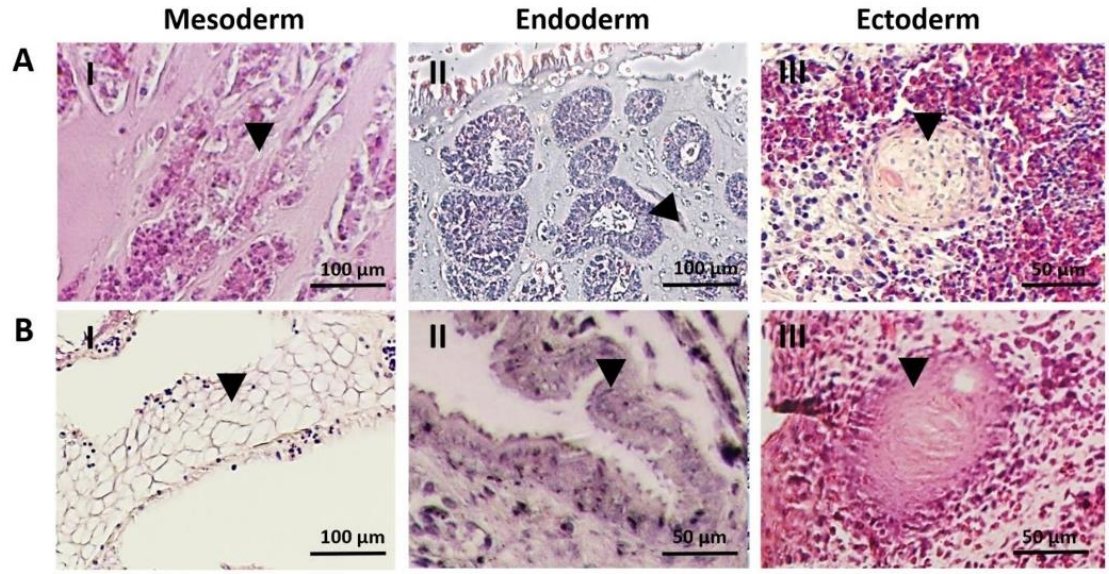

Fig. 4: Detection of the three germ layer-specific tissue types in teratoma sections generated from NuFFs- or JPCs-derived hiPSCs
Representative microscopic images of H&E stained teratoma sections of **A)** NuFFs-derived hiPSCs: Mesoderm: **(I)** bone-like tissue, Endoderm: **(II)** primitive gut-like epithelium, and Ectoderm: **(III)** squamous epithelium, and **B)** JPCs-derived hiPSCs: Mesoderm: **(I)** adipose tissue, Endoderm: **(II)** primitive gut-like epithelium, and Ectoderm: **(III)** squamous epithelium. The arrows indicate the described germ layer-specific structures.

cm^3 or earlier if the dimension reached impairs animals' behavior, motility, food and water intake due to pain or distress (Nelakanti et al., 2015). The composition of the explanted teratomas is then analyzed using histological and immunohistochemical stainings. Using the established CAM assay, the incubation of implanted hiPSCs for 9 days was sufficient to form characteristic tissue structures of all three germ layers. Thus, the established CAM model is cost-effective and less time-consuming. Moreover, since the CAM is not innervated, it allows the growth of xenografts without pain or impairment of the embryo (Kunz et al., 2019). The highly vascularized CAM efficiently supports the growth of the teratoma. Furthermore, the immaturity of the chicken embryo´s immune system enables the applicability of cells from different species (Deryugina and Quigley, 2008) without rejecting the seeded cells.

Although the established CAM assay-based method has several advantages over the *in vivo* mouse teratoma assay, it also has some limitations. Teratoma formation on CAM can only be performed for 9-10 days after the application of hiPSCs, as the chick hatches 21 days after incubation. In contrast, teratoma formation in mice is performed for approximately 4 to 6 weeks (Nelakanti et al., 2015) and the incubation period can be extended to increase the size or tissue maturation of the teratoma if the animal´s behavior is not negatively affected by the size of the teratoma. In a recent study, kinetic trajectories showed that approximately 37 days are required to see and measure the size of the teratoma externally (McDonald et al., 2020). Thus, we assume that the tissue structures formed in teratomas on CAM are less mature than those in mice, since the teratoma formation in mice lasts about 6 weeks and on CAM for 9-10 days. However, the established CAM assay is clearly appropriate to demonstrate the tri-lineage differentiation capability of the generated hiPSCs. The robustness of the established CAM assay has been demonstrated by the successful generation of teratomas after the application of hiPSC lines generated from NuFFs or JPCs in addition to hiPSCs derived from RECs. The tri-lineage differentiation was successfully demonstrated with all three hiPSC lines. RECs seeded on CAM did not cause any teratoma formation.

The Matrigel used to apply the hiPSCs to CAM is obtained from the murine Engelbreth-Holm-Swarm (EHS) tumor. Therefore, replacing Matrigel by synthetic hydrogels, such as polymers and scaffolds based on polyacrylamide and polyethylene glycol (PEG) (Aisenbrey and Murphy, 2020), will further reduce and prevent pain and suffering of animals in the future.

To test the influence of inoculated cell numbers on teratoma formation, different numbers of hiPSCs were seeded on CAM. The increase of the cell number from 0.5 x 10^6 to 2 x 10^6 hiPSCs led to a higher teratoma formation efficiency (33.3% versus 70%). The further increase of hiPSC number to 4 x 10^6 cells resulted in teratoma formation on all CAMs. However, our results showed that 2 x 10^6 hiPSCs are sufficient to obtain teratomas containing cells of all three germ layers. Thus, we recommend using 2x10^6 or more hiPSCs for the teratoma analysis. In immunodeficient mice, usually, 1 x 10^6 cells are used per injection, and it has also been shown that injections of 2 or 4 x 10^6 hiPSCs can increase the chances of successful teratoma formation in mice (Nelakanti et al., 2015).

Cells of all three germ layers were detected within the formed teratoma from 2 x 10^6 hiPSCs. The presence of endoderm, mesoderm, and ectoderm tissue cell types was detected using specific antibodies as well as by detection of the expression using qRT-PCR. In addition to using the established CAM model to analyze the pluripotency of hiPSCs, it can also be applied to determine whether unwanted hiPSCs remain in the differentiated cells. The implantation of remaining not fully differentiated hiPSCs can lead to the formation of teratomas and has to be avoided for clinical use. Thus, this CAM

ALTEX preprint
published January 25, 2021
doi:10.14573/altex.2005221

assay can be also applied to analyze the safety of the hiPSC-derived cell types and the complete differentiation of hiPSCs into somatic cells.

5 Conclusion

In this study, an alternative *in vivo* model was established and tested to evaluate the pluripotency of newly generated hiPSC lines within 9 days. The CAM model is a valuable method to bridge the gap between *in vitro* cell culture and *in vivo* animal experiments. In contrast to the immunodeficient mouse model, it is simple, inexpensive, and time-saving. The application of this CAM assay will reduce the number of required animals and suffering to respect the 3Rs principles. Besides the pluripotency evaluation of the reprogrammed cells, CAM assay can be also applied to test the safety of differentiated cells from hiPSCs.

References

Aisenbrey, E. A. and Murphy, W. L. (2020). Synthetic alternatives to matrigel. *Nat Rev Mater 5*, 539-551. doi:10.1038/s41578-020-0199-8

Aldahmash, A., Atteya, M., Elsafadi, M. et al. (2013). Teratoma formation in immunocompetent mice after syngeneic and allogeneic implantation of germline capable mouse embryonic stem cells. *Asian Pac J Cancer Prev 14*, 5705-5711. doi:10.7314/apjcp.2013.14.10.5705

Buhr, C. R., Wiesmann, N., Tanner, R. C. et al. (2020). The chorioallantoic membrane assay in nanotoxicological research-an alternative for *in vivo* experimentation. *Nanomaterials (Basel) 10*, 2328. doi:10.3390/nano10122328

Buta, C., David, R., Dressel, R. et al. (2013). Reconsidering pluripotency tests: Do we still need teratoma assays? *Stem Cell Res 11*, 552-562. doi:10.1016/j.scr.2013.03.001

Cao, F., Lin, S., Xie, X. et al. (2006). *In vivo* visualization of embryonic stem cell survival, proliferation, and migration after cardiac delivery. *Circulation 113*, 1005-1014. doi:10.1161/CIRCULATIONAHA.105.588954

Cao, F., van der Bogt, K. E., Sadrzadeh, A. et al. (2007). Spatial and temporal kinetics of teratoma formation from murine embryonic stem cell transplantation. *Stem Cells Dev 16*, 883-891. doi:10.1089/scd.2007.0160

Cieślar-Pobuda, A., Knoflach, V., Ringh, M. V. et al. (2017). Transdifferentiation and reprogramming: Overview of the processes, their similarities and differences. *Biochimica et Biophysica Acta (BBA)-Molecular Cell Research 1864*, 1359-1369. doi:10.1016/j.bbamcr.2017.04.017

DeBord, L. C., Pathak, R. R., Villaneuva, M. et al. (2018). The chick chorioallantoic membrane (cam) as a versatile patient-derived xenograft (pdx) platform for precision medicine and preclinical research. *Am J Cancer Res 8*, 1642-1660.

Deryugina, E. I. and Quigley, J. P. (2008). Chick embryo chorioallantoic membrane model systems to study and visualize human tumor cell metastasis. *Histochem Cell Biol 130*, 1119-1130. doi:10.1007/s00418-008-0536-2

Dexter, D. L., Lee, E. S., DeFusco, D. J. et al. (1983). Selection of metastatic variants from heterogeneous tumor cell lines using the chicken chorioallantoic membrane and nude mouse. *Cancer Res 43*, 1733-1740.

Dohle, D. S., Pasa, S. D., Gustmann, S. et al. (2009). Chick ex ovo culture and ex ovo cam assay: How it really works. *J Vis Exp* doi:10.3791/1620

Durupt, F., Koppers-Lalic, D., Balme, B. et al. (2012). The chicken chorioallantoic membrane tumor assay as model for qualitative testing of oncolytic adenoviruses. *Cancer Gene Ther 19*, 58-68. doi:10.1038/cgt.2011.68

Gilleron, L., Coecke, S., Sysmans, M. et al. (1996). Evaluation of a modified het-cam assay as a screening test for eye irritancy. *Toxicol In Vitro 10*, 431-446. doi:10.1016/0887-2333(96)00021-5

Hentze, H., Soong, P. L., Wang, S. T. et al. (2009). Teratoma formation by human embryonic stem cells: Evaluation of essential parameters for future safety studies. *Stem Cell Res 2*, 198-210. doi:10.1016/j.scr.2009.02.002

Kaji, K., Norrby, K., Paca, A. et al. (2009). Virus-free induction of pluripotency and subsequent excision of reprogramming factors. *Nature 458*, 771-775. doi:10.1038/nature07864

Kibbe, W. A. (2007). Oligocalc: An online oligonucleotide properties calculator. *Nucleic Acids Res 35*, W43-46. doi:10.1093/nar/gkm234

Kunz, P., Schenker, A., Sahr, H. et al. (2019). Optimization of the chicken chorioallantoic membrane assay as reliable *in vivo* model for the analysis of osteosarcoma. *PLoS One 14*, e0215312. doi:10.1371/journal.pone.0215312

Kunzi-Rapp, K., Genze, F., Kufer, R. et al. (2001). Chorioallantoic membrane assay: Vascularized 3-dimensional cell culture system for human prostate cancer cells as an animal substitute model. *J Urol 166*, 1502-1507. doi:10.1016/s0022-5347(05)65820-x

Lee, A. S., Tang, C., Cao, F. et al. (2009). Effects of cell number on teratoma formation by human embryonic stem cells. *Cell Cycle 8*, 2608-2612. doi:10.4161/cc.8.16.9353

Li, M., Pathak, R. R., Lopez-Rivera, E. et al. (2015). The in ovo chick chorioallantoic membrane (cam) assay as an efficient xenograft model of hepatocellular carcinoma. *J Vis Exp* doi:10.3791/52411

McDonald, D., Wu, Y., Dailamy, A. et al. (2020). Defining the teratoma as a model for multi-lineage human development. *Cell 183*, 1402-1419 e1418. doi:10.1016/j.cell.2020.10.018

Moreno-Jimenez, I., Hulsart-Billstrom, G., Lanham, S. A. et al. (2016). The chorioallantoic membrane (cam) assay for the study of human bone regeneration: A refinement animal model for tissue engineering. *Sci Rep 6*, 32168. doi:10.1038/srep32168

Naik, M., Brahma, P. and Dixit, M. (2018). A cost-effective and efficient chick ex-ovo cam assay protocol to assess angiogenesis. *Methods Protoc 1*, doi:10.3390/mps1020019

ALTEX preprint
published January 25, 2021
doi:10.14573/altex.2005221

Nelakanti, R. V., Kooreman, N. G. and Wu, J. C. (2015). Teratoma formation: A tool for monitoring pluripotency in stem cell research. *Curr Protoc Stem Cell Biol 32*, 4A 8 1-17. doi:10.1002/9780470151808.sc04a08s32

Petrovova, E., Giretova, M., Kvasilova, A. et al. (2019). Preclinical alternative model for analysis of porous scaffold biocompatibility in bone tissue engineering. *ALTEX 36*, 121-130. doi:10.14573/altex.1807241

Rabinovich, P. M. and Weissman, S. M. (2013). Cell engineering with synthetic messenger rna. *Methods Mol Biol 969*, 3-28. doi:10.1007/978-1-62703-260-5_1

Rovithi, M., Avan, A., Funel, N. et al. (2017). Development of bioluminescent chick chorioallantoic membrane (cam) models for primary pancreatic cancer cells: A platform for drug testing. *Sci Rep 7*, 44686. doi:10.1038/srep44686

Steinle, H., Behring, A., Schlensak, C. et al. (2017). Concise review: Application of *in vitro* transcribed messenger rna for cellular engineering and reprogramming: Progress and challenges. *Stem Cells 35*, 68-79. doi:10.1002/stem.2402

Steinle, H., Golombek, S., Behring, A. et al. (2018). Improving the angiogenic potential of epcs via engineering with synthetic modified mrnas. *Mol Ther Nucleic Acids 13*, 387-398. doi:10.1016/j.omtn.2018.09.005

Steinle, H., Weber, M., Behring, A. et al. (2019a). Generation of ipscs by nonintegrative rna-based reprogramming techniques: Benefits of self-replicating rna versus synthetic mrna. *Stem Cells Int 2019*, 7641767. doi:10.1155/2019/7641767

Steinle, H., Weber, M., Behring, A. et al. (2019b). Reprogramming of urine-derived renal epithelial cells into ipscs using srrna and consecutive differentiation into beating cardiomyocytes. *Mol Ther Nucleic Acids 17*, 907-921. doi:10.1016/j.omtn.2019.07.016

Takahashi, K. and Yamanaka, S. (2006). Induction of pluripotent stem cells from mouse embryonic and adult fibroblast cultures by defined factors. *Cell 126*, 663-676. doi:10.1016/j.cell.2006.07.024

Takahashi, K., Tanabe, K., Ohnuki, M. et al. (2007). Induction of pluripotent stem cells from adult human fibroblasts by defined factors. *Cell 131*, 861-872. doi:10.1016/j.cell.2007.11.019

Warren, L., Manos, P. D., Ahfeldt, T. et al. (2010). Highly efficient reprogramming to pluripotency and directed differentiation of human cells with synthetic modified mrna. *Cell Stem Cell 7*, 618-630. doi:10.1016/j.stem.2010.08.012

Winter, G., Koch, A. B. F., Loffler, J. et al. (2020). Multi-modal pet and mr imaging in the hen's egg test-chorioallantoic membrane (het-cam) model for initial *in vivo* testing of target-specific radioligands. *Cancers (Basel) 12*, doi:10.3390/cancers12051248

Ye, J., Coulouris, G., Zaretskaya, I. et al. (2012). Primer-blast: A tool to design target-specific primers for polymerase chain reaction. *BMC Bioinformatics 13*, 134. doi:10.1186/1471-2105-13-134

Ying, Y., Xingfen, Y., Wengai, Z. et al. (2010). Combined *in vitro* tests as an alternative to *in vivo* eye irritation tests. *Altern Lab Anim 38*, 303-314. doi:10.1177/026119291003800413

Yu, J., Hu, K., Smuga-Otto, K. et al. (2009). Human induced pluripotent stem cells free of vector and transgene sequences. *Science 324*, 797-801. doi:10.1126/science.1172482

Zhang, W. Y., de Almeida, P. E. and Wu, J. C. (2008). Teratoma formation: A tool for monitoring pluripotency in stem cell research. In (eds.), *Stembook*. Cambridge (MA): doi:10.3824/stembook.1.53.1

Conflict of interest

All authors declare no competing financial interests relevant to the submitted work.

Acknowledgements

For antibody staining, the authors would like to thank Dr. Irene Gonzalez Menendez and Prof. Dr. Leticia Quintanilla de Fend at the Institute of Pathology, University Hospital & Comprehensive Cancer Center, University of Tübingen. JPCs were obtained from Prof. Dr. Dorothea Alexander-Friedrich, Department of Oral and Maxillofacial Surgery, University Hospital Tübingen.

We acknowledge support by the German Research Foundation (Deutsche Forschungsgemeinschaft; DFG) through AV 133/7-1 and the Open Access Publishing Fund of University of Tübingen.

7.3.3 Publikation III:

Hydrojet-based delivery of footprint-free iPSC-derived cardiomyocytes into porcine myocardium

www.nature.com/scientificreports

SCIENTIFIC REPORTS
nature research

OPEN

Hydrojet-based delivery of footprint-free iPSC-derived cardiomyocytes into porcine myocardium

Marbod Weber[1], Andreas Fech[2], Luise Jäger[2], Heidrun Steinle[1], Louisa Bühler[2], Regine Mariette Perl[3], Petros Martirosian[3], Roman Mehling[4], Dominik Sonanini[4], Wilhelm K. Aicher[5], Konstantin Nikolaou[3], Christian Schlensak[1], Markus D. Enderle[2], Hans Peter Wendel[1], Walter Linzenbold[2] & Meltem Avci-Adali[1]✉

The reprogramming of patient´s somatic cells into induced pluripotent stem cells (iPSCs) and the consecutive differentiation into cardiomyocytes enables new options for the treatment of infarcted myocardium. In this study, the applicability of a hydrojet-based method to deliver footprint-free iPSC-derived cardiomyocytes into the myocardium was analyzed. A new hydrojet system enabling a rapid and accurate change between high tissue penetration pressures and low cell injection pressures was developed. Iron oxide-coated microparticles were ex vivo injected into porcine hearts to establish the application parameters and the distribution was analyzed using magnetic resonance imaging. The influence of different hydrojet pressure settings on the viability of cardiomyocytes was analyzed. Subsequently, cardiomyocytes were delivered into the porcine myocardium and analyzed by an in vivo imaging system. The delivery of microparticles or cardiomyocytes into porcine myocardium resulted in a widespread three-dimensional distribution. In vitro, 7 days post-injection, only cardiomyocytes applied with a hydrojet pressure setting of E20 (79.57 ± 1.44%) showed a significantly reduced cell viability in comparison to the cells applied with 27G needle (98.35 ± 5.15%). Furthermore, significantly less undesired distribution of the cells via blood vessels was detected compared to 27G needle injection. This study demonstrated the applicability of the hydrojet-based method for the intramyocardial delivery of iPSC-derived cardiomyocytes. The efficient delivery of cardiomyocytes into infarcted myocardium could significantly improve the regeneration.

Cardiovascular diseases (CVDs) are the main cause of death with over 17 million deaths globally per year, which represents 30% of all deaths, and it is expected to reach 23.6 million by 2030[1]. CVDs include disorders that can affect the heart and the blood vessels, such as angina, myocardial infarction, and peripheral artery disease. The death of cardiomyocytes following myocardial infarction induces a reaction cascade leading to cell death within hours after coronary artery occlusion[2] and ending with collagen matrix production and scar formation[3].

Unfortunately, cardiomyocytes have an extremely low renewal capacity with approximately 1% per year at the age of 20, declining to less than 0.5% per year in elderly individuals[4]. Due to this very limited regeneration capacity of the adult human hearts, lost contractile cells are replaced by a fibrotic scar produced by fibroblasts and myofibroblasts. This leads to the remodeling of the myocardium including thickening (hypertrophy) and stiffening (fibrosis) of the left ventricular wall[5] and ultimately results in impaired cardiac function.

[1]Department of Thoracic and Cardiovascular Surgery, University Hospital Tuebingen, Calwerstraße 7/1, 72076 Tuebingen, Germany. [2]Erbe Elektromedizin Tuebingen, Waldhoernlestr. 17, 72072 Tuebingen, Germany. [3]Diagnostic and Interventional Radiology, University Hospital Tuebingen, Hoppe-Seyler-Strasse 3, 72076 Tuebingen, Germany. [4]Department of Preclinical Imaging and Radiopharmacy, Werner Siemens Imaging Center, Eberhard Karls University, Roentgenweg 13, 72076 Tuebingen, Germany. [5]Department of Urology, ZMF, University Hospital Tuebingen, Waldhoernlestr. 22, 72072 Tuebingen, Germany. ✉email: meltem.avci-adali@uni-tuebingen.de

To date, various cell-based approaches[6] were clinically tested to promote cardiac regeneration by integration, differentiation, and proliferation of implanted cells, such as the application of mesenchymal stromal cells (MSCs) isolated from bone marrow[7] or adipose tissue-derived stem cells[8], skeletal myoblasts[9], circulating progenitor cells[10], and cardiac stem cells[11]. However, recent data suggest that the clinically observed benefit associated with the injection of bone marrow-derived cells is primarily due to the release of paracrine factors[12,13]. But there is a certain risk for spontaneous osteogenic differentiation of such cells after the in vivo application. For instance, intramyocardial calcification was reported after transplantation of unpurified bone marrow cells into the infarcted myocardium of rats[14]. In another study, encapsulated calcified or ossified structures were also found after the injection of MSCs into infarcted mice hearts[15].

The discovery of the reprogrammability of somatic cells in induced pluripotent stem cells (iPSCs)[16,17] opened up new possibilities for regenerative therapies in general. These cells have the potential to differentiate into a variety of cell types of the body and the unlimited proliferation capacity of iPSCs could particularly allow the generation of large numbers of autologous cardiomyocytes for the repair of infarcted myocardium. Since the first generation of iPSCs from fibroblasts by using retroviral vectors[16,17], other integrative vectors such as lentiviral vectors[18], plasmids[19], or piggyBac transposon-based delivery systems[20] were also used to reprogram somatic cells. New strategies are focusing on non-integrative methods, such as the use of adenoviral[21], Sendai[22], and episomal vectors[23], mRNA[24], or proteins[25] to obtain clinically applicable terminally differentiated cells from iPSCs. In a recent study, we have shown that by using self-replicating RNA, iPSCs could be generated from human urine-derived renal epithelial cells and beating cardiomyocytes were obtained from these iPSCs[26]. This method allows the non-invasive and simple collection of patient´s somatic cells for reprogramming and the footprint-free generation of iPSCs for subsequent differentiation into cardiomyocytes, which can be used to repair infarcted myocardium.

Regarding cell delivery strategy and functional outcome, an inconclusive view arises from the literature. For example, the incorporation of endothelial and smooth muscle cells into patches increased the resistance of cardiomyocytes to hypoxic injury as well as the engraftment of transplanted cardiomyocytes[27] and the implantation of such fibrin patches enhanced left ventricular function in a porcine myocardial infarction model[28]. However, Gerbin and colleagues reported the formation of scar tissue that physically separated the epicardial patch from the host myocardium[29]. In contrast, the injection of cardiomyocytes directly into the myocardium resulted in electrical integration of implanted cells[29,30]. However, covering a large area of myocardial infarction may require multiple injections, leading to procedural damage to the myocardium[31] and should, therefore, be avoided. Recently, Jäger et al.[32] described a hydrojet-based method for the delivery of MSCs into urethral tissue. They demonstrated a better yield of viable cells compared to needle injections with a fast and precise injection of viable next to or into the sphincter muscle. Here, we aimed to evaluate this new hydrojet concept for the delivery of cardiomyocytes derived from footprint-free generated iPSCs into porcine myocardium. The application was compared to the needle-based application of iPSC-derived cardiomyocytes.

Material and methods

Ethics statement. Renal epithelial cells were isolated from the urine of healthy donors, which gave written informed consent to participate. The study was approved by the Ethics Committee of the Medical Faculty of the University of Tuebingen (911/2018BO2). All experiments were performed in accordance with relevant guidelines and regulations. Since no living animals were used in this study, ethical approval for animal testing was not required. Hearts of German Landrace pigs were purchased from a regional butcher´s shop (Faerber, Balingen, Germany).

Cultivation of footprint-free iPSCs from urine-derived renal epithelial cells. Footprint-free iPSCs were generated as previously described in our recent study[26] by seeding of 5×10^4 renal epithelial cells obtained from 100–200 ml urine of healthy donors per well of a 12-well plate coated with 0.1% gelatin. The reprogramming was performed by transfection with 0.5 µg self-replicating RNA (VEE-OKSiM-GFP RNA). The generated iPSC colonies were detached and seeded onto 0.5 µg/cm^2 vitronectin-coated (Thermo Fisher Scientific, Waltham, USA) tissue culture flasks. The cells were cultivated in Essential 8 (E8) medium (Thermo Fisher Scientific) at 37 °C and 5% CO_2 with daily medium changes and passaged every 4–6 days. After reaching confluence, iPSCs were washed with Dulbecco's phosphate-buffered saline (DPBS, Thermo Fisher Scientific) and detached by 5 min incubation with DPBS containing 0.5 mM ethylenediaminetetraacetic acid (EDTA, Sigma-Aldrich, St. Louis, USA). After detachment, the EDTA solution was aspirated and the cells were rinsed with E8 medium. 2×10^5 cells were seeded per well of vitronectin-coated 6-well plates in E8 medium containing 10 µg/ml ROCK inhibitor Y-27632 (Enzo Life Sciences, Lausen, Switzerland).

Generation of iPSC-derived cardiomyocytes. To generate cardiomyocytes, 2×10^5 iPSCs were resuspended in E8 medium containing 10 µg Y-27632 and seeded per well of vitronectin-coated six-well plates. For the differentiation, PSC cardiomyocyte differentiation kit (Thermo Fisher Scientific) was used according to manufacturer's instructions with small modifications. On day 0, the medium was changed to cardiomyocyte differentiation medium A. On day 2, the medium was changed to cardiomyocyte differentiation medium B. On day 4, cardiomyocyte maintenance medium (CMM) was added to the cells and further cultivated until day 10 to 12 with medium changes every other day. The differentiation of iPSCs into cardiomyocytes was determined by flow cytometry and immunofluorescence microscopy using PE-labeled mouse anti-human α-actinin and FITC-labeled anti-human cardiac troponin T antibodies (both from Miltenyi Biotec, Bergisch Gladbach, Germany). A more detailed characterization of the cardiomyocytes generated from footprint-free iPSCs was performed in our recent study[26].

Modified ERBEJET®2. A modified ERBEJET®2 from Erbe Elektromedizin GmbH (Tuebingen, Germany) was used to apply cells and microparticles into the porcine heart muscle. The new hydrojet system[32] allowed the generation of pressures (E = effects) ranging from E5 to E80 while enabling a rapid and accurate change between tissue penetration pressures and cell injection pressures. First, using a "tissue penetration jet", 1 ml 0.9% NaCl solution was applied with high pressures E60 or E80 to penetrate the heart tissue. Afterwards, 100 µl cell or microparticle suspension was delivered using an "injection jet" with low pressures (E5, E10, or E20) to distribute the cells or particles within the penetrated myocardium.

Application of magnetic polystyrene microparticles into porcine hearts. To simulate and predict the distribution of cardiomyocytes after the injection into the myocardium using a 27G needle or the new hydrojet system, magnetic polystyrene microparticles (Sigma-Aldrich; 6.8×10^6 particles/ml) with a similar diameter as cardiomyocytes (10 ± 0.5 µm) were chosen and injected into porcine hearts. Therefore, porcine hearts were rinsed with 0.9% NaCl solution, sealed in plastic bags and warmed in a water bath to 37 °C to simulate physiological body temperature. Afterwards, using the hydrojet system, the microparticles were injected in the transversal plane 2 cm above the apex from two sites at a 90° angle to the left lateral and dorsal side. Tissue penetration pressures of E60 or E80 were applied combined with an injection pressure of E10—expressed as E60/E10 and E80/E10, respectively. Based on a preliminary phantom study (data not shown), two different quantities of microparticles (85,000 or 42,500) were selected for the assessment of the optimal particle concentration in terms of magnetic resonance imaging (MRI) detection of the artifact signal.

For each hydrojet injection, 100 µl 0.9% NaCl with 85,000 or 42,500 microparticles was used. As a reference, microparticles were also injected into heart muscles using a 27G needle. Therefore, the needle was inserted 2 cm above the apex at a 90° angle from two sites 0.5 cm deep into the myocardium. The hearts were positioned in beakers filled with 0.9% NaCl and MRI was performed.

MRI of porcine hearts. The microparticle injected hearts were scanned on a 3 T MRI system (MAGNETOM Prisma^{fit}, Siemens Healthineers, Erlangen, Germany). The body coil was used for homogeneous radio frequency transmission and a 20-channel head coil was utilized for signal receiving. Morphology and other structures of the hearts were assessed by using a proton-density weighted fast spin-echo sequence with TR/TE = 3000/11 ms, echo train length of 10, acquisition bandwidth of 240 Hz/pixel, field-of-view of 128×128 mm^2, slice thickness of 2 mm, 21 slices, 384×384 matrix, two acquisitions, and scan time of 3:50 min. To identify depositions of injected microparticles, series of images were acquired using gradient-echo (GRE) sequence with multiple echo times (TEs). The GRE sequence was used as an MRI technique sensitive to the distribution of the Larmor frequency in the immediate vicinity of the magnetic microparticles. Higher amounts of magnetic microparticles result in a reduced effective transversal relaxation time and can be localized as negative contrasted signal voids in the magnitude images. In addition, the magnetic microparticles produce field inhomogeneities, which can be seen as a characteristical dipole field pattern in the GRE phase images. An identifier for the magnetic microparticles in contrast to the tissue with low signal intensity is the enlargement of the size of the signal voids with increasing TE. The orientation, position, thickness, and number of slices in measurements with the GRE sequence were identical to those in the fast spin-echo (FSE) sequence. The imaging parameters were: TR = 42 ms; TEs = 2.65, 6.71, 10.77, 14.83, 18.89, and 22.95 ms; acquisition bandwidth = 650 Hz/Pixel; flip angle = 25°; field-of-view = 128×128 mm^2; matrix = 256×256; acquisition = 2; and a scan time of 5:06 min.

Analysis of microparticle distribution in porcine hearts. To compare the distribution of microparticles applied into myocardial tissue using hydrojet or 27G needle, DICOM (Digital Imaging and Communications in Medicine) data received from MRI were analyzed using 3D Slicer software (3D Slicer software, version 4.10.2). All sections were retraced with the segmentation function, reconstructed to a three-dimensional (3D) shape considering the layer thickness (2 mm) and layer distance (0.2 mm), and displayed with a smoothing factor of 0.5. Subsequently, the dark particle spots were reconstructed in the same way and the volumes were determined using the segmentation statistics function.

Analysis of the viability of cardiomyocytes after the application with the hydrojet system. Cardiomyocytes obtained 10–12 days after the differentiation of iPSCs were washed with 1 ml DPBS per well and detached using 1 ml TrypLE (Thermo Fisher Scientific) for 10 min. Afterwards, 1 ml trypsin neutralization solution (TNS, PromoCell, Heidelberg, Germany) was added per well of the six-well plate. Cells were centrifuged at $200 \times g$ for 5 min and washed once with 5 ml DPBS. Afterwards, cardiomyocytes were resuspended in CMM with a final concentration of 1×10^7 cells/ml. To analyze the impact of the injection jet pressure on the viability of cardiomyocytes, 100 µl cell suspension containing 1×10^6 cardiomyocytes was injected and collected in 15 ml tubes filled with 2 ml prewarmed CMM. Injection pressures of E5, E10, and E20 were investigated. The same procedure was also performed by manual injection of 100 µl cell suspension with a 27G needle syringe. Cells were counted in a Neubauer chamber and the viability was determined using trypan blue (Thermo Fisher Scientific). In an additional experiment, the same injection procedures were repeated and the cardiomyocytes were centrifuged at $200 \times g$ for 5 min, resuspended, and seeded into vitronectin coated 48-well plates in CMM. The cell viability was measured after 24 h and 7 days using PrestoBlue assay. Therefore, the medium was replaced by 1 ml PrestoBlue solution (Thermo Fisher Scientific), diluted 1:10 in CMM, and cells were incubated for 90 min. The metabolized solution was then analyzed in triplicates using a fluorescence microplate reader (Mithras LB 940, Berthold Technologies, Bad Wildbad, Germany). Additionally, the cells were stained using calcein AM (Thermo Fisher Scientific) and analyzed using Axiovert135 microscope and AxioVision 4.8.2 software (Carl Zeiss).

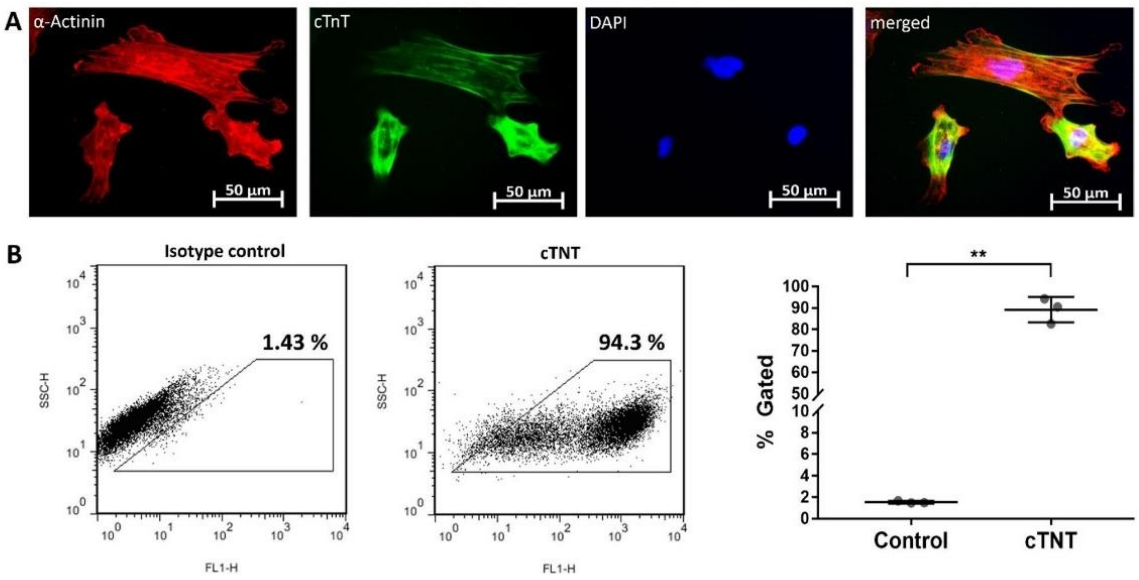

Figure 1. Analysis of cells obtained after cardiac differentiation of iPSCs. **(A)** Fluorescence microscopic images of cTNT and α-actinin positive cells after cardiomyocyte differentiation. Nuclei were stained with DAPI. **(B)** Detection of cTNT positive cells after the cardiac differentiation by flow cytometry. Results are shown as mean ± SD (n = 3). Statistical differences were determined using paired t-test (**p < 0.01).

Labeling of the cardiomyocytes with near-infrared fluorescent dye and application into porcine hearts. For the staining, 1×10^7 cardiomyocytes were resuspended in 1 ml DPBS and incubated for 20 min with 300 µM XenoLight DiR fluorescent dye (PerkinElmer, Waltham, MA, USA) dissolved in DMSO. Afterwards, cells were centrifuged at 200 × g for 5 min, washed twice with 5 ml DPBS and resuspended in 1 ml prewarmed CMM medium.

Porcine hearts were rinsed with 0.9% NaCl solution, sealed in plastic bags and warmed up to 37 °C in a water bath to simulate physiological body temperature. Before injection, hearts were cut 5 cm horizontally above the apex and the upper part was removed. This allowed better positioning and observation of the hearts by an vivo imaging system (IVIS Spectrum, Perkin Elmer). Then, 1×10^6 XenoLight DiR fluorescent dye-labeled cardiomyocytes resuspended in 100 µl CMM or 100 µl CMM without cells were injected at a 90° angle 2 cm above the apex into the myocardium either using the new hydrojet system (E60/E10, E80/E10) or a 27 G needle.

Detection of injected cardiomyocytes using IVIS in porcine heart. After the injection of cardiomyocytes, near-infrared imaging was performed using IVIS. The imaging was performed by placing the apex upwards. Subsequently, the apex was cut sagittally at the injection site into two parts and imaging was performed again. Fluorescence intensity and distribution areas were analyzed with Living Image® software (PerkinElmer). In order to measure the distribution of cells only in the tissue (myocardium), the detected fluorescence of cells distributed via blood vessels was analyzed separately. The fluorescence emission was normalized to photons per second per square centimeter per steradian and expressed as average radiant efficiency [p/s/cm²/sr]/[µW/cm²].

Statistical analysis. Data are shown as mean ± standard deviation (SD) or standard error of the mean (SEM). The comparison of the means of normally distributed data was performed by paired t-test or one-way analysis of variance (ANOVA) for repeated measurements followed by Bonferroni's multiple comparison test. The means of non-normally distributed data were compared using Kruskal–Wallis test followed by Dunn's multiple comparison test. Statistical analyses were performed double-tailed using GraphPad Prism 6.01 (GraphPad Software, La Jolla, CA, USA). Differences of $p < 0.05$ were considered significant.

Results

Analysis of differentiated cardiomyocytes from iPSCs. Using the PSC cardiomyocyte differentiation kit, iPSCs were differentiated within 10–12 days into beating cardiomyocytes. The obtained cells showed the typical elongated rod-like shape of cardiomyocytes and the fluorescence microscopic analyses demonstrated the expression of cTNT as well as α-actinin (Fig. 1A). Flow cytometry analysis revealed that 89.17 ± 5.9% of obtained cells were cTNT positive (Fig. 1B) ($p^{**} = 0.0016$).

Particle distribution in porcine hearts. After the application of 85,000 or 42,500 magnetic polystyrene microparticles into porcine hearts using the new hydrojet system and the E80/E10 pressure setting, MRI was

performed. The application of 85,000 microparticles led to a stronger artifact signal than 42,500 microparticles (Fig. 2A). Therefore, 85,000 microparticles were applied in further experiments. To compare the distribution of microparticles after the needle- and hydrojet system-based application, microparticles were injected from two sites 2 cm above the apex at a 90° angle to each other and the sagittal plane. After the needle injection, two small localized but strong artifacts were detected in the MRI images near the sites of injection. In contrast, the application of microparticles using the hydrojet system with penetration pressures of E60/E10 and an injection pressure of E10 resulted in a wider distribution of the microparticles in the myocardium (Fig. 2B). However, the higher tissue penetration pressure E80 led to a channel formation, which was clearly visible after the reconstruction of the 3D structure of the heart using 3D Slicer software (Fig. 2C). Compared to the 27G needle injection, both applications with the hydrojet system showed significantly larger distribution volumes [Fig. 2D; E60/E10: $2377 \pm 270\ mm^3$ ($p^{**} = 0.0038$); E80/E10: $1811 \pm 386\ mm^3$ ($p^* = 0.0439$); 27G needle: $975 \pm 228\ mm^3$].

Viability and recovery of cardiomyocytes after the application with hydrojet system. To analyze the recovery and viability of cardiomyocytes, 1×10^6 cells were injected with different pressures, E5, E10, and E20, respectively, as well as 27G needle into CMM. The cell viability and recovery rate were determined using trypan blue staining. No differences in cell viability were detected between the application with 27G needle and hydrojet system (Fig. 3A). The use of 27G needle and hydrojet with a pressure setting of E5 and E10 resulted in an initial cell number loss of 23.3% (27G needle), 25.1% (E5) and 30.1% (E10). However, an injection pressure of E20 led to significantly reduced cell recovery ($43.1 \pm 9.0\%$) compared to 27G needle application [$76.7 \pm 9.6\%$, ($^*p = 0.0121$)] and the use of injection pressure E5 [$74.9 \pm 9.6\%$, ($^*p = 0.0261$)]. These results were also confirmed by performing calcein AM staining 24 h after seeding of recovered cells (Fig. 3B).

Additionally, PrestoBlue assay was performed after 24 h and 7 days of cultivation of cardiomyocytes injected by 27G needle or the hydrojet system with different injection pressure settings (E5, E10, or E20) (Fig. 4). The cells applied by hydrojet technique showed only a slightly reduced cell viability at injection pressure settings of E5 [$86.8 \pm 0.5\%$ ($^{****}p < 0.0001$)], E10 [$87.82 \pm 0.83\%$ ($^{***}p = 0.0002$)], and at E20 [$84.69 \pm 0.72\%$ ($^{****}p < 0.0001$)] compared to the 27G needle injected cardiomyocytes ($95.64 \pm 1.6\%$). However, 7 days after the injection, only the cells applied with a pressure setting of E20 showed a significantly reduced cell viability versus the cells applied by 27G needle (27G needle: $98.35 \pm 5.15\%$ versus E20: $79.57 \pm 1.44\%$, $^*p = 0.0102$).

Distribution of applied cardiomyocytes in porcine hearts. To determine the distribution of cardiomyocytes in porcine hearts, 1×10^6 XenoLight DiR fluorescent dye-labeled cardiomyocytes were injected into the myocardium using a 27G needle or the hydrojet system with E60/E10 or E80/E10 setting. The NIR-labeled cardiomyocytes were detected using IVIS in the apex region of the hearts before and after the cutting of the injection site in two halves for detection of the cells inside the myocardium (Fig. 5A). Inside the myocardium, the needle injection showed the smallest distribution area ($2.3 \pm 0.6\ cm^2$) as well as the lowest radiant efficiency ($33.2 \pm 9.0 \times 10^7$) compared to the application of cardiomyocytes using the hydrojet system (E60/10: distribution area of $4.2 \pm 1.5\ cm^2$, radiant efficiency of $56.2 \times 10^7 \pm 27.6 \times 10^7$; E80/10: distribution area of $3.8 \pm 1.0\ cm^2$, radiant efficiency of $47.8 \times 10^7 \pm 12.2 \times 10^7$) (Fig. 5B). Interestingly, the needle injection resulted in a significantly more pronounced distribution of cardiomyocytes via blood vessels to undesired regions of the heart (Fig. 5A) compared to the hydrojet injections [27G: $3.6 \pm 1.1\ cm^2$, E60/10: $0.8 \pm 0.8\ cm^2$ ($p^* = 0.0174$), E80/10: $0.7 \pm 0.4\ cm^2$ ($p^* = 0.0149$)] (Fig. 5C).

Discussion

Over the past decade, the ability to generate patient-specific iPSCs from somatic cells has led to significant advances in regenerative medicine and tissue engineering, which raise the hope for healing infarcted myocardium. In this study, we evaluated the deliverability of patient-specific cardiomyocytes derived from footprint-free iPSCs using a new hydrojet system into the myocardium and analyzed the distribution of the delivered cells in comparison to standard needle injection. The MRI and IVIS analyses demonstrated that the hydrojet system can be used to transfer cardiomyocytes into the myocardium with an improved distribution and significantly less injury of cardiac blood vessels compared to the single needle injection. The in vitro analyses showed that the transfer of cardiomyocytes by hydrojet with appropriate settings does not impair the recovery rate. The new hydrojet system allowed the precise application of two different jet pressures. The first jet enabled the penetration of the tissue (here epicardium and partly the myocardium) while the second jet gently transferred the cells into the target region (here the myocardium).

The transfer of cardiomyocytes by hydrojet injection pressures of E5 and E10 had no significant influence on the recovery rate when compared to the injection with a 27G needle. In contrast, the transfer of cells at higher pressures, i.e. E20, led to a significant loss of the initial cell numbers. These results were not unexpected, as higher pressures correlate positively with velocity and, accordingly, increased shear stress which facilitates cell disruption[33]. Similar results have recently been shown for the injection of MSCs into the urinary sphincter complex[32].

Immediately after the injection of cardiomyocytes by 27G needle or hydrojet, no influence on cell viability was detected using trypan blue staining. However, 24 h after the cultivation of these cells, a slightly decreased cell viability was detected in cardiomyocytes injected with hydrojet compared to 27G needle injection. After 7 days of cultivation, the viability of cells applied with E20 pressure setting remained still significantly lower than the needle injection. The viability of cells applied with E5 and E10 pressure settings was not significantly different but lower than the needle application.

Even though single-needle injection is a widespread cell delivery technique[34–37], needle injections generally bear multifactorial disadvantages that may influence the viability, placement, retention rate, or distribution of

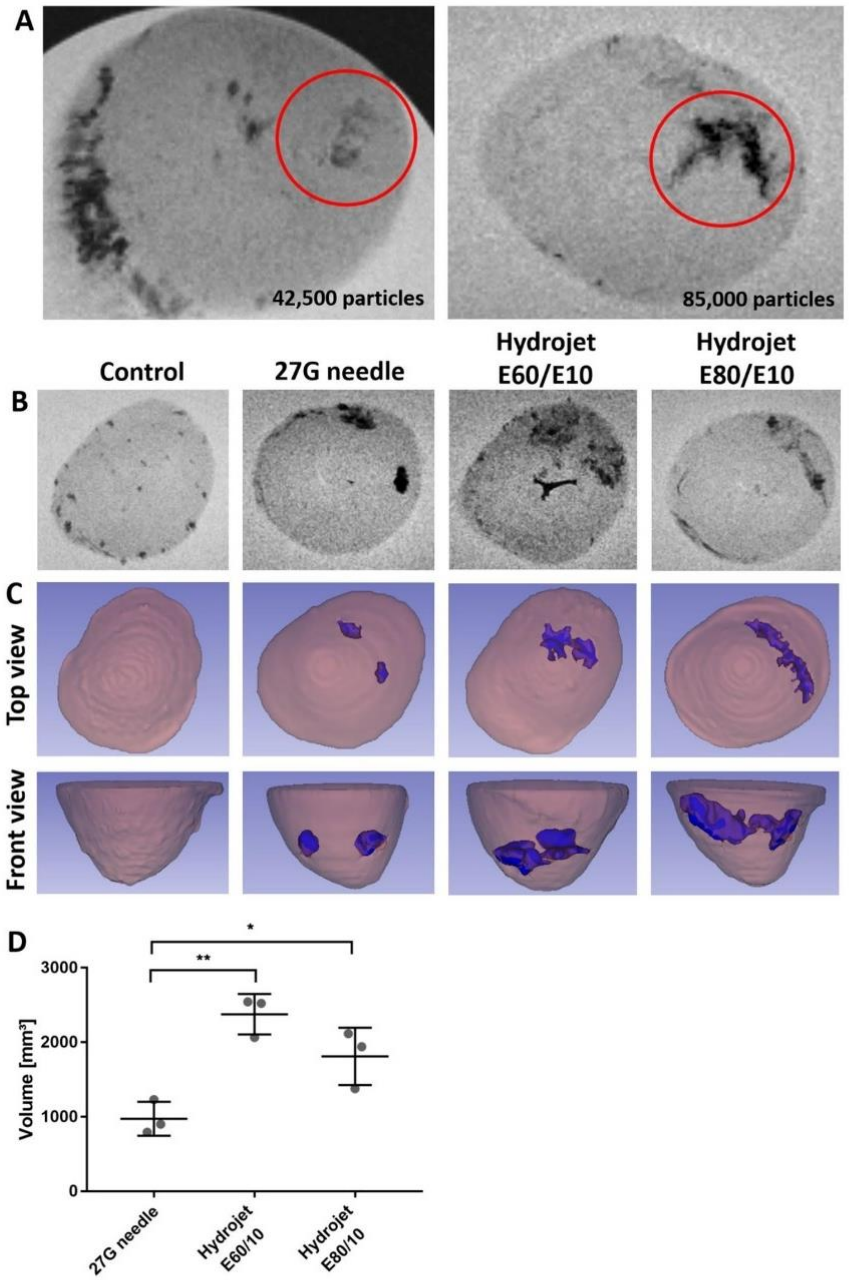

Figure 2. Detection of microparticle distribution in the porcine hearts using magnetic resonance imaging (MRI). **(A)** Determination of detectable microparticle amount in porcine hearts using 45,000 or 85,000 microparticles. A single injection of particles was performed using the new hydrojet system with tissue penetration pressure of E80 and injection pressure of E10 (E80/E10). The microparticles in the heart are highlighted by a red encircled region. **(B)** MRI of microparticles after the application of 85,000 microparticles (two injections) using 27G needle or the hydrojet system with tissue penetration pressures of E80 or E60 and an injection pressure of E10 (E80/E10 or E60/E10). **(C)** 3D reconstruction of particle distribution in porcine hearts using 3D Slicer software. **(D)** Comparison of microparticle distribution volume in porcine hearts. Results are shown as mean ± SD (n = 3). Statistical differences were determined using one-way ANOVA followed by Bonferroni's multiple comparison test (*$p < 0.05$; **$p < 0.01$).

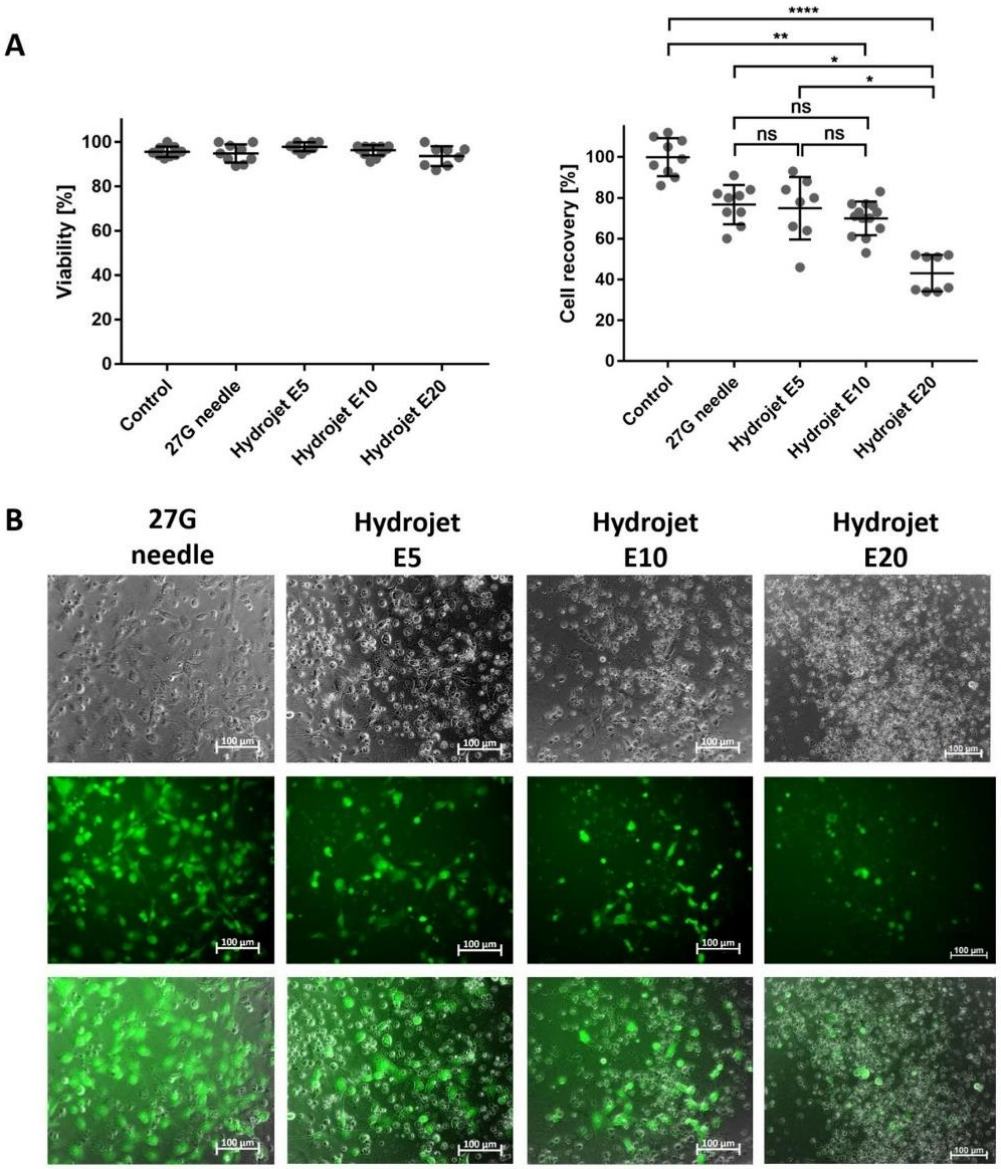

Figure 3. Analysis of the viability and recovery rates of cardiomyocytes immediately after the injection using hydrojet or 27G needle and calcein AM staining of injected cells 24 h after cultivation. **(A)** Determination of cell viability and cell recovery by trypan blue staining and counting of cells immediately after the injection of 1×10^6 cardiomyocytes in CMM using a 27G needle or the hydrojet system with different injection pressure settings (E5, E10, or E20). Results are shown as mean ± SD (control, 27G needle (n = 9), E5 and E20 (n = 8), E10 (n = 15). Statistical differences were determined using one-way ANOVA followed by Bonferroni's multiple comparison test or Kruskal–Wallis test followed by Dunn's multiple comparison test (*$p < 0.05$; **$p < 0.01$; ****$p < 0.0001$, ns: non-significant). **(B)** Representative images of calcein AM stained cardiomyocytes 24 h after the cultivation of injected cells in cell culture plates for 24 h.

cells[31]. In our study, a 27G needle was used as reference, which represents a common needle size since previous cardiomyocyte injection experiments report varying needle sizes from 23 to 29G[34–38]. While small needle sizes can lead to increased damage of the cardiomyocytes due to higher shear stress and pressures generated during the injection, needles with a larger diameter have an increased risk of tissue and blood vessel injury or facilitate the reflux of the cells along the penetration tract[31,39]. Concerning the specific application here, needle injection methods can cause a mechanical injury of healthy myocardial tissue and lead to inflammation of the myocardium, which in turn can increase the risk of cardiac arrhythmia[40]. Moreover, needle injection leads to the injury

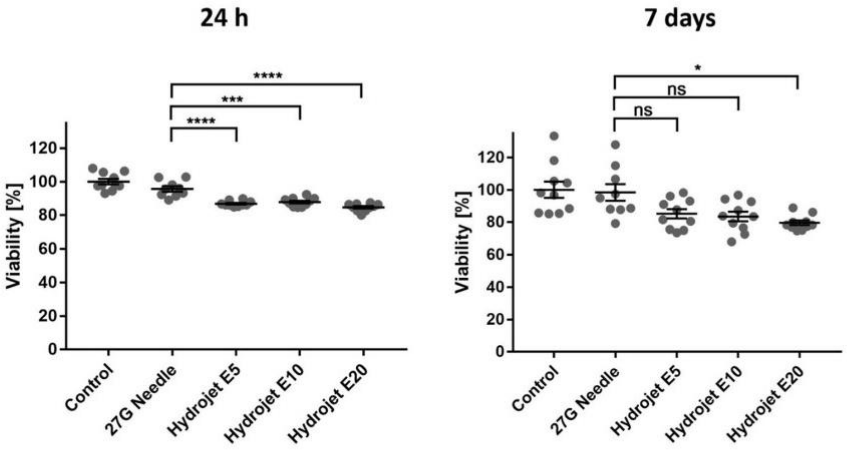

Figure 4. Analysis of the viability of cardiomyocytes 24 h and 7 days after the application of cells. Determination of cell viability using PrestoBlue assay 24 h and 7 days after the seeding of injected cardiomyocytes into cell culture plates. The viability of cardiomyocytes without injection (control) was set to 100% and the viability of cardiomyocytes injected by 27G needle or hydrojet was expressed relative to these cells. Results are shown as mean ± SEM [control, E5, E10, and E20 (n = 10), and 27G needle (n = 9)]. Statistical differences were determined using one-way ANOVA followed by Bonferroni's multiple comparison test (*$p < 0.05$, ***$p < 0.001$, ****$p < 0.0001$).

of cardiac blood vessels and thereby to an undesired spread of cardiomyocytes via blood vessels to untargeted regions in the heart. In vivo, the aggregation of cardiomyocytes in the coronary arteries could result in blockage of vessels and induce ischemia.

Different approaches were applied to deliver cells into the myocardium such as intravenous infusion[41,42], perfusion via the cardiac arteries[43–47] or multiple injections into the myocardium[37,48]. In a recent study, Tabei et al. applied a newly developed injection device with six needles to deliver human iPSC-derived cardiomyocyte spheroids into the myocardium[38]. Thereby, a retention rate of approximately 48% was achieved compared to the retention rate of around 17% using a single 23G needle. Multiple injections not only affect the retention rate, but also increase the size of the myocardial area in which the cells are distributed. For example, up to 15 injections were applied to deliver cardiomyocytes into the heart of Macaque monkeys[34, 35]. Several clinical studies have shown that about 16% to 21% of the total mass of the left ventricle was affected immediately after the myocardial infarction[49–51]. Thus, to efficiently regenerate the affected myocardium and to restore the functionality, a wide distribution of the injected cells is essential.

In our study, the 27G needle injection resulted in a limited distribution of cells, which was also shown in studies performed by Tabei et al.[38]. In contrast, the sequential application of two differently pressured fluid jets by the new hydrojet system allowed an improved distribution of iron oxide coated microparticles and cardiomyocytes compared to the single-needle injection, without injury of adjacent blood vessels. Thus, the entire infarct area could be covered without major tissue injury by only 2 to 3 repeated injections with the hydrojet. However, further in vivo studies with larger cohort sizes are necessary to establish the exact settings for hydrojet injection into the myocardium. In this study, a trend towards a somewhat more widespread distribution of cardiomyocytes was observed with E60 setting for penetration jet, however, due to the limited sample size, a clear difference between E60 or E80 setting for tissue penetration and cell deposition was not observed.

Both hydrojet application and needle injection were performed epicardially, which is the method applied most frequently for targeted and precise delivery of cells into the infarcted myocardium[52]. This is typically performed under cardiac arrest by open heart thoracotomies[53] or without cardiac arrest via lateral minithoracotomies[54]. These invasive procedures are associated with a considerable risk of complications. Thus, less invasive catheter-based intramyocardial[55–59] or intracoronary delivery methods[43–47] have been already investigated. Injection studies by Grossmann et al. showed an equal or improved distribution when using endocardial applications compared to epicardial administration[60]. Both endocardial and intracoronary administrations are suitable for the new hydrojet system and could make hydrojet-based cell transplantation more precise, less invasive and less traumatic for the patients in the future.

Conclusion

The novel hydrojet-based cell transfer technology enabled the efficient ex vivo administration of cardiomyocytes into the porcine myocardium using a novel sequential fluid application. Compared to standard needle injections, the hydrojet-based application resulted in significantly less displacement of cells via coronary vessels. Thereby, potential risks due to occlusion of the vessels by aggregated cardiomyocytes and ischemia can be prevented. In

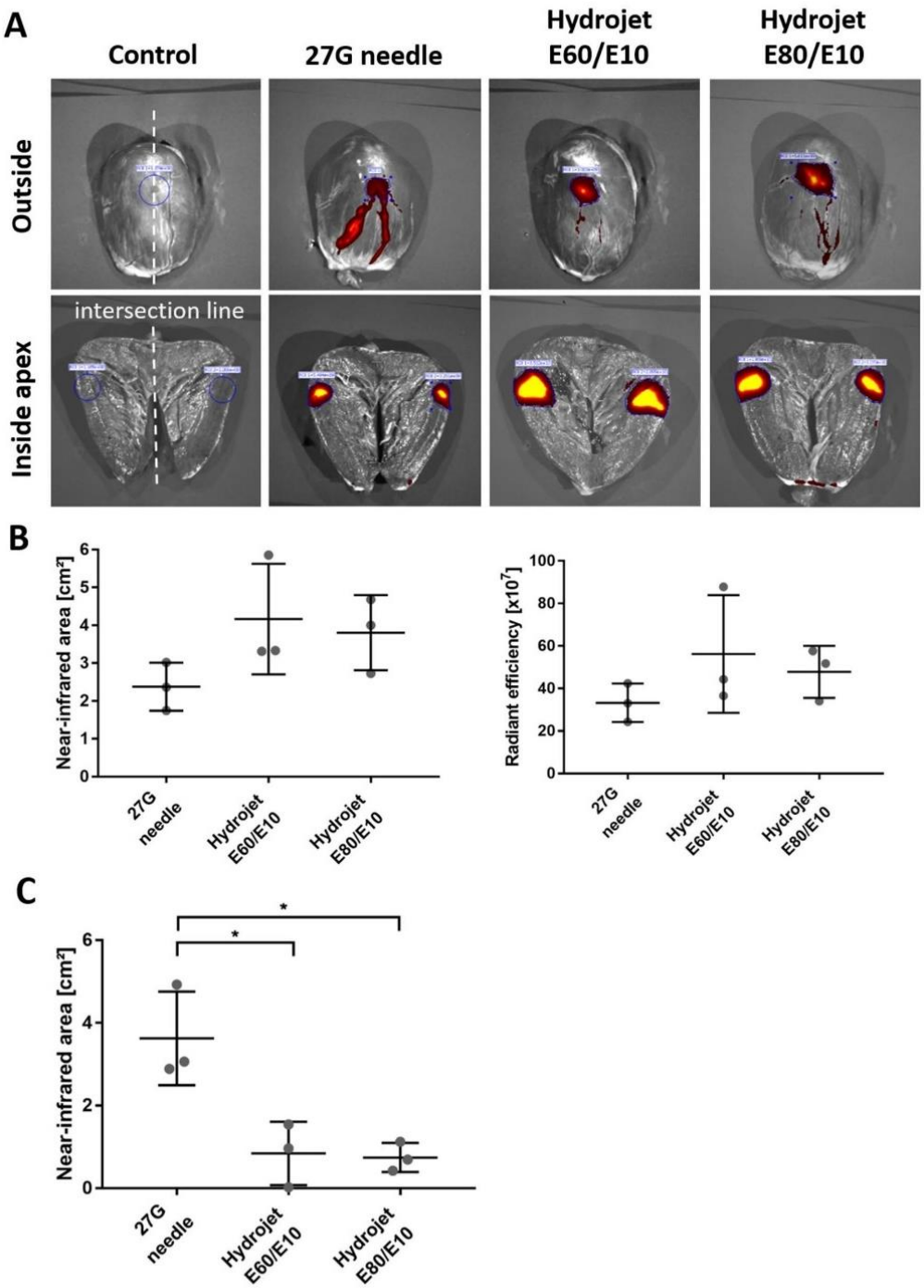

Figure 5. Distribution of cardiomyocytes in porcine hearts after the application with hydrojet system. 100 µl CMM without or with XenoLight DiR fluorescent dye-labeled 1×10^6 cardiomyocytes was applied using 27G needle or hydrojet system with tissue penetration pressures of E80 or E60 and injection pressure of E10 (E80/E10 or E60/E10) into porcine hearts. (**A**) IVIS images of the apex region of the hearts from outside and inside of the myocardium. The intersection of the apex is schematically indicated as a white line. (**B**) Comparison of the radiant efficiency and near-infrared area after the application of cardiomyocytes into the myocardium. (**C**) Detection of the NIR-labeled area of blood vessels containing cardiomyocytes. Results are shown as mean ± SD (n = 3). Statistical differences were determined using one-way ANOVA followed by Bonferroni's multiple comparison test (*$p < 0.05$).

the future, this novel cell delivery technique may simplify the treatment of myocardial infarction with patient-specific iPSC-derived cells and increase treatment efficiency.

Received: 20 April 2020; Accepted: 14 September 2020
Published online: 08 October 2020

References

1. Wong, N. D. Epidemiological studies of CHD and the evolution of preventive cardiology. *Nat. Rev. Cardiol.* **11**(5), 276 (2014).
2. Cahill, T. J., Choudhury, R. P. & Riley, P. R. Heart regeneration and repair after myocardial infarction: Translational opportunities for novel therapeutics. *Nat. Rev. Drug Discov.* **16**(10), 699 (2017).
3. Li, Z. & Guan, J. Hydrogels for cardiac tissue engineering. *Polymers* **3**(2), 740–761 (2011).
4. Lázár, E., Sadek, H. A. & Bergmann, O. Cardiomyocyte renewal in the human heart: Insights from the fall-out. *Eur. Heart J.* **38**(30), 2333–2342 (2017).
5. Talman, V. & Ruskoaho, H. Cardiac fibrosis in myocardial infarction—From repair and remodeling to regeneration. *Cell Tissue Res.* **365**(3), 563–581 (2016).
6. Ptaszek, L. M. *et al.* Towards regenerative therapy for cardiac disease. *Lancet* **379**(9819), 933–942 (2012).
7. Karantalis, V. *et al.* Autologous mesenchymal stem cells produce concordant improvements in regional function, tissue perfusion, and fibrotic burden when administered to patients undergoing coronary artery bypass grafting. *Circ. Res.* **114**(8), 1302–1310 (2014).
8. Houtgraaf, J. H. *et al.* First experience in humans using adipose tissue-derived regenerative cells in the treatment of patients with ST-segment elevation myocardial infarction. *J. Am. Coll. Cardiol.* **59**(5), 539–540 (2012).
9. Menasche, P. *et al.* The myoblast autologous grafting in ischemic cardiomyopathy (MAGIC) trial—First randomized placebo-controlled study of myoblast transplantation. *Circulation* **117**(9), 1189–1200 (2008).
10. Assmus, B. *et al.* Transplantation of progenitor cells and regeneration enhancement in acute myocardial infarction (TOPCARE-AMI). *Circulation* **106**(24), 3009–3017 (2002).
11. Makkar, R. R. *et al.* Intracoronary cardiosphere-derived cells for heart regeneration after myocardial infarction (CADUCEUS): A prospective, randomised phase 1 trial. *Lancet* **379**(9819), 895–904 (2012).
12. Beer, L. *et al.* Peripheral blood mononuclear cell secretome for tissue repair. *Apoptosis* **21**(12), 1336–1353 (2016).
13. Gnecchi, M. *et al.* Paracrine mechanisms in adult stem cell signaling and therapy. *Circ. Res.* **103**(11), 1204–1219 (2008).
14. Yoon, Y.-S. *et al.* Unexpected severe calcification after transplantation of bone marrow cells in acute myocardial infarction. *Circulation* **109**(25), 3154–3157 (2004).
15. Breitbach, M. *et al.* Potential risks of bone marrow cell transplantation into infarcted hearts. *Blood* **110**(4), 1362–1369 (2007).
16. Takahashi, K. & Yamanaka, S. Induction of pluripotent stem cells from mouse embryonic and adult fibroblast cultures by defined factors. *Cell* **126**(4), 663–676 (2006).
17. Takahashi, K. *et al.* Induction of pluripotent stem cells from adult human fibroblasts by defined factors. *Cell* **131**(5), 861–872 (2007).
18. Yu, J., *et al*. Induced pluripotent stem cell lines derived from human somatic cells. *Science***318**(5858), 1917–1920 (2007).
19. Kaji, K. *et al.* Virus-free induction of pluripotency and subsequent excision of reprogramming factors. *Nature* **458**(7239), 771 (2009).
20. Woltjen, K. *et al.* piggyBac transposition reprograms fibroblasts to induced pluripotent stem cells. *Nature* **458**(7239), 766 (2009).
21. Zhou, W. & Freed, C. R. Adenoviral gene delivery can reprogram human fibroblasts to induced pluripotent stem cells. *Stem cells* **27**(11), 2667–2674 (2009).
22. Seki, T. *et al.* Generation of induced pluripotent stem cells from human terminally differentiated circulating T cells. *Cell Stem Cell* **7**(1), 11–14 (2010).
23. Narsinh, K.H., *et al*. Generation of adult human induced pluripotent stem cells using nonviral minicircle DNA vectors.*Nat. Protocols***6**(1), 78 (2011).
24. Warren, L. *et al.* Highly efficient reprogramming to pluripotency and directed differentiation of human cells with synthetic modified mRNA. *Cell Stem Cell* **7**(5), 618–630 (2010).
25. Kim, D. *et al.* Generation of human induced pluripotent stem cells by direct delivery of reprogramming proteins. *Cell Stem Cell* **4**(6), 472 (2009).
26. Steinle, H. *et al.* Reprogramming of urine-derived renal epithelial cells into iPSCs using srRNA and consecutive differentiation into beating cardiomyocytes. *Mol. Ther. Nucleic Acids* **17**, 907–921 (2019).
27. Ye, L. *et al.* Cardiac repair in a porcine model of acute myocardial infarction with human induced pluripotent stem cell-derived cardiovascular cells. *Cell Stem Cell* **15**(6), 750–761 (2014).
28. Gao, L. *et al.* Large cardiac muscle patches engineered from human induced-pluripotent stem cell-derived cardiac cells improve recovery from myocardial infarction in swine. *Circulation* **137**(16), 1712–1730 (2018).
29. Gerbin, K. A. *et al.* Enhanced electrical integration of engineered human myocardium via intramyocardial versus epicardial delivery in infarcted rat hearts. *PLoS ONE* **10**(7), e0131446 (2015).
30. Halbach, M. *et al.* Electrophysiological integration and action potential properties of transplanted cardiomyocytes derived from induced pluripotent stem cells. *Cardiovasc. Res.* **100**(3), 432–440 (2013).
31. O'Cearbhaill, E.D., Ng, K.S., Karp, J.M. Emerging medical devices for minimally invasive cell therapy. in *Mayo Clinic Proceedings*. (Elsevier, London, 2014).
32. Jager, L. *et al.* A novel waterjet technology for transurethral cystoscopic injection of viable cells in the urethral sphincter complex. *Neurourol. Urodyn.* **39**(2), 594–602 (2020).
33. Aguado, B. A. *et al.* Improving viability of stem cells during syringe needle flow through the design of hydrogel cell carriers. *Tissue Eng. Part A* **18**(7–8), 806–815 (2012).
34. Shiba, Y. *et al.* Allogeneic transplantation of iPS cell-derived cardiomyocytes regenerates primate hearts. *Nature* **538**(7625), 388–391 (2016).
35. Chong, J. J. *et al.* Human embryonic-stem-cell-derived cardiomyocytes regenerate non-human primate hearts. *Nature* **510**(7504), 273–277 (2014).
36. Zhao, X. *et al.* Comparison of non-human primate versus human induced pluripotent stem cell-derived cardiomyocytes for treatment of myocardial infarction. *Stem Cell Rep.* **10**(2), 422–435 (2018).
37. Chow, A. *et al.* Human induced pluripotent stem cell-derived cardiomyocyte encapsulating bioactive hydrogels improve rat heart function post myocardial infarction. *Stem Cell Rep.* **9**(5), 1415–1422 (2017).
38. Tabei, R. *et al.* Development of a transplant injection device for optimal distribution and retention of human induced pluripotent stem cellderived cardiomyocytes. *J. Heart Lung Transplant* **38**(2), 203–214 (2019).
39. Amer, M. H. *et al.* Translational considerations in injectable cell-based therapeutics for neurological applications: Concepts, progress and challenges. *NPJ Regen. Med.* **2**, 23 (2017).
40. Fukushima, S. *et al.* Direct intramyocardial but not intracoronary injection of bone marrow cells induces ventricular arrhythmias in a rat chronic ischemic heart failure model. *Circulation* **115**(17), 2254–2261 (2007).

41. Nagaya, N. *et al.* Intravenous administration of mesenchymal stem cells improves cardiac function in rats with acute myocardial infarction through angiogenesis and myogenesis. *Am. J. Physiol. Heart Circ. Physiol.* **287**(6), H2670–H2676 (2004).
42. Luger, D. *et al.* Intravenously delivered mesenchymal stem cells: Systemic anti-inflammatory effects improve left ventricular dysfunction in acute myocardial infarction and ischemic cardiomyopathy. *Circ. Res.* **120**(10), 1598–1613 (2017).
43. Chen, S. L. *et al.* Effect on left ventricular function of intracoronary transplantation of autologous bone marrow mesenchymal stem cell in patients with acute myocardial infarction. *Am. J. Cardiol.* **94**(1), 92–95 (2004).
44. Strauer, B. E. *et al.* Regeneration of human infarcted heart muscle by intracoronary autologous bone marrow cell transplantation in chronic coronary artery disease: The IACT Study. *J. Am. Coll. Cardiol.* **46**(9), 1651–1658 (2005).
45. Bartunek, J. *et al.* Intracoronary injection of CD133-positive enriched bone marrow progenitor cells promotes cardiac recovery after recent myocardial infarction: Feasibility and safety. *Circulation* **112**(9 Suppl), I178–I183 (2005).
46. Katritsis, D. G. *et al.* Transcoronary transplantation of autologous mesenchymal stem cells and endothelial progenitors into infarcted human myocardium. *Catheter Cardiovasc. Interv.* **65**(3), 321–329 (2005).
47. Plewka, M. *et al.* Effect of intracoronary injection of mononuclear bone marrow stem cells on left ventricular function in patients with acute myocardial infarction. *Am. J. Cardiol.* **104**(10), 1336–1342 (2009).
48. Otto Beitnes, J. *et al.* Intramyocardial injections of human mesenchymal stem cells following acute myocardial infarction modulate scar formation and improve left ventricular function. *Cell Transplant* **21**(8), 1697–1709 (2012).
49. Pokorney, S. D. *et al.* Infarct healing is a dynamic process following acute myocardial infarction. *J. Cardiovasc. Magn. Reson.* **14**(1), 62 (2012).
50. Ingkanisorn, W. P. *et al.* Gadolinium delayed enhancement cardiovascular magnetic resonance correlates with clinical measures of myocardial infarction. *J. Am. Coll. Cardiol.* **43**(12), 2253–2259 (2004).
51. Lund, G. K. *et al.* Prediction of left ventricular remodeling and analysis of infarct resorption in patients with reperfused myocardial infarcts by using contrast-enhanced MR imaging. *Radiology* **245**(1), 95–102 (2007).
52. Sheng, C. C., Zhou, L. & Hao, J. Current stem cell delivery methods for myocardial repair. *Biomed. Res. Int.* **2013**, 547902 (2013).
53. Patel, A. N. *et al.* Surgical treatment for congestive heart failure with autologous adult stem cell transplantation: a prospective randomized study. *J. Thorac. Cardiovasc. Surg.* **130**(6), 1631–1638 (2005).
54. Pompilio, G. *et al.* Direct minimally invasive intramyocardial injection of bone marrow-derived AC133+ stem cells in patients with refractory ischemia: Preliminary results. *Thorac. Cardiovasc. Surg.* **56**(2), 71–76 (2008).
55. Perin, E. C. *et al.* Transendocardial, autologous bone marrow cell transplantation for severe, chronic ischemic heart failure. *Circulation* **107**(18), 2294–2302 (2003).
56. Fuchs, S. *et al.* Safety and feasibility of transendocardial autologous bone marrow cell transplantation in patients with advanced heart disease. *Am. J. Cardiol.* **97**(6), 823–829 (2006).
57. Dohmann, H. F. *et al.* Transendocardial autologous bone marrow mononuclear cell injection in ischemic heart failure: postmortem anatomicopathologic and immunohistochemical findings. *Circulation* **112**(4), 521–526 (2005).
58. Tse, H. F. *et al.* Prospective randomized trial of direct endomyocardial implantation of bone marrow cells for treatment of severe coronary artery diseases (PROTECT-CAD trial). *Eur. Heart J.* **28**(24), 2998–3005 (2007).
59. Trachtenberg, B. *et al.* Rationale and design of the transendocardial injection of autologous human cells (bone marrow or mesenchymal) in chronic ischemic left ventricular dysfunction and heart failure secondary to myocardial infarction (TAC-HFT) trial: A randomized, double-blind, placebo-controlled study of safety and efficacy. *Am. Heart J.* **161**(3), 487–493 (2011).
60. Grossman, P. M. *et al.* Incomplete retention after direct myocardial injection. *Catheter Cardiovasc. Interv.* **55**(3), 392–397 (2002).

Acknowledgements
The authors would like to express their gratitude to Stefanie Elser for the phantom study and Jonas Winter for assistance in validation of the hydrojet device. This work was in part supported by grants from DFG, BMBF and EU to WKA. We acknowledge support by Open Access Publishing Fund of University of Tuebingen.

Author contributions
M.A.A., W.L., L.J., M.W., and K.N. conceived and designed the experiments. M.W. and L.J. performed the experiments with support from L.B., H.S., M.D.E., and W.K.A., R.M.P., and P.M. performed MRI investigations. R.M. and D.S. performed IVIS analysis. A.F., W.L., M.D.E., and L.J. were mainly involved in the development of the hydrojet device. H.P.W., M.A.A., C.S., and M.D.E. contributed reagents, materials, and analysis tools. M.W. and M.A.A. wrote the paper. M.A.A. and W.L. supervised the project.

Funding
Open Access funding enabled and organized by Projekt DEAL.

Competing interests
LJ, WL, AF, LB, MDE are employees of Erbe Elektromedizin GmbH, Tuebingen. All other authors declare no competing financial and non-financial interests relevant to the submitted work.

Additional information
Correspondence and requests for materials should be addressed to M.A.-A.

Reprints and permissions information is available at www.nature.com/reprints.

Publisher's note Springer Nature remains neutral with regard to jurisdictional claims in published maps and institutional affiliations.

7.3.4 Publikation IV:

Influence of human jaw periosteal cells seeded β-tricalcium phosphate scaffolds on blood coagulation

International Journal of *Molecular Sciences*

MDPI

Article

Influence of Human Jaw Periosteal Cells Seeded β-Tricalcium Phosphate Scaffolds on Blood Coagulation

Marbod Weber [1], Felix Umrath [2], Heidrun Steinle [1], Lukas-Frank Schmitt [2], Lin Tzu Yu [2], Christian Schlensak [1], Hans-Peter Wendel [1], Siegmar Reinert [2], Dorothea Alexander [2,†] and Meltem Avci-Adali [1,*,†]

[1] Department of Thoracic and Cardiovascular Surgery, University Hospital Tuebingen, Calwerstraße 7/1, 72076 Tuebingen, Germany; marbod.weber@uni-tuebingen.de (M.W.); heidrun.steinle@uni-tuebingen.de (H.S.); christian.schlensak@med.uni-tuebingen.de (C.S.); hans-peter.wendel@med.uni-tuebingen.de (H.-P.W.)

[2] Department of Oral and Maxillofacial Surgery, University Hospital Tübingen, Osianderstr. 2–8, 72076 Tübingen, Germany; Felix.Umrath@med.uni-tuebingen.de (F.U.); Lukas-frank.schmitt@student.uni-tuebingen.de (L.-F.S.); lgmolly24@gmail.com (L.T.Y.); siegmar.reinert@med.uni-tuebingen.de (S.R.); dorothea.alexander@med.uni-tuebingen.de (D.A.)

* Correspondence: meltem.avci-adali@uni-tuebingen.de; Tel.: +49-707-1298-6605; Fax: +49-707-129-5369

† These authors contributed equally to this work.

Abstract: Tissue engineering offers auspicious opportunities in oral and maxillofacial surgery to heal bone defects. For this purpose, the combination of cells with stability-providing scaffolds is required. Jaw periosteal cells (JPCs) are well suited for regenerative therapies, as they are easily accessible and show strong osteogenic potential. In this study, we analyzed the influence of uncoated and polylactic-co-glycolic acid (PLGA)-coated β-tricalcium phosphate (β-TCP) scaffolds on JPC colonization and subsequent osteogenic differentiation. Furthermore, interaction with the human blood was investigated. This study demonstrated that PLGA-coated and uncoated β-TCP scaffolds can be colonized with JPCs and further differentiated into osteogenic cells. On day 15, after cell seeding, JPCs with and without osteogenic differentiation were incubated with fresh human whole blood under dynamic conditions. The activation of coagulation, complement system, inflammation, and blood cells were analyzed using ELISA and scanning electron microscopy (SEM). JPC-seeded scaffolds showed a dense cell layer and osteogenic differentiation capacity on both PLGA-coated and uncoated β-TCP scaffolds. SEM analyses showed no relevant blood cell attachment and ELISA results revealed no significant increase in most of the analyzed cell activation markers (β-thromboglobulin, Sc5B-9, polymorphonuclear (PMN)-elastase). However, a notable increase in thrombin-antithrombin III (TAT) complex levels, as well as fibrin fiber accumulation on JPC-seeded β-TCP scaffolds, was detected compared to the scaffolds without JPCs. Thus, this study demonstrated that besides the scaffold material the cells colonizing the scaffolds can also influence hemostasis, which can influence the regeneration of bone tissue.

Keywords: jaw periosteal cells; bone tissue engineering; biomaterial; β-tricalcium phosphate; hemocompatibility

Citation: Weber, M.; Umrath, F.; Steinle, H.; Schmitt, L.-F.; Yu, L.T.; Schlensak, C.; Wendel, H.-P.; Reinert, S.; Alexander, D.; Avci-Adali, M. Influence of Human Jaw Periosteal Cells Seeded β-Tricalcium Phosphate Scaffolds on Blood Coagulation. *Int. J. Mol. Sci.* **2021**, *22*, 9942. https://doi.org/10.3390/ijms22189942

Academic Editor: Silvia Panseri

Received: 18 August 2021
Accepted: 10 September 2021
Published: 14 September 2021

Publisher's Note: MDPI stays neutral with regard to jurisdictional claims in published maps and institutional affiliations.

1. Introduction

The repair of small and large bone defects is of key interest in oral and maxillofacial surgery. Thus, molecular, as well as cell-based therapies are applied for the engineering of new bone tissue. In most studies, mesenchymal stromal cells (MSCs) derived from bone marrow have been used for regenerative bone formation [1,2]. These cells have a multipotential differentiation capacity into osteoblasts, adipocytes, and chondrocytes [3,4]. MSCs derived from the periosteal tissue are well accessible during routine maxillofacial surgeries [5]. Jaw periosteal cells (JPCs) show strong multipotency [6] and

higher proliferation and self-renewal rates compared to bone marrow-derived MSCs [7,8]. In addition, JPCs exhibit reliable osteogenic differentiation while showing a lower chondrogenic and adipogenic differentiation capacity compared to bone marrow-derived MSCs. [8]. Consequently, JPCs represent an optimal alternative for bone tissue engineering [9–12].

Besides cellular components, biomaterials used as scaffolds for cells play a decisive role in bone repair [13]. The scaffolds should be biocompatible, support cell attachment, provide stability, and have osteoconductive and osteoinductive properties. For this purpose, different scaffold materials were used, such as hydroxyapatite [14], low-temperature calcium phosphate cement [15], bioactive glass [16], polylactide acid [17], and β-TCP [18]. Calcium phosphate bioceramics have been reported to possess osteoconductive and osteoinductive characteristics due to their structural and chemical similarity to bone tissue, and they can facilitate the osteogenic differentiation of mesenchymal stem cells [19]. β-TCP also offers good structural stability during biodegradation and new bone formation [20]. Moreover, during degradation, large quantities of calcium (Ca^{2+}) and phosphate ions (PO_4^{2-}) are released, which are essential inorganic salts for new bone formation [21]. Due to these advantages, β-TCP scaffolds are frequently used in the field of oral and maxillofacial surgery [22,23]. Furthermore, these materials for bone regeneration can be functionalized with cell-binding ligands to improve cell adhesion on their surface [24,25]. It has been demonstrated that a thin coating with poly-lactic-co-glycolic acid (PLGA) can improve the mechanical stability and biocompatibility of β-TCP scaffolds and increase the adhesion and proliferation of JPCs [26].

Immediately after implantation into the bone defects, scaffolds/implants come into close contact with blood, which can lead to the adsorption of plasma proteins on their surface. Plasma proteins can trigger coagulation via the intrinsic pathway, activation of leukocytes, adhesion and activation of platelets [27]. This blood–biomaterial interaction leads to the provisional matrix formation and influences subsequent host reactions to the implants. In the case that scaffolds are colonized with cells, resident cells also come into close contact with blood after the implantation. As a complex biological system, interactions between blood components and JPCs cultivated three-dimensionally on the scaffolds cannot be excluded and also need to be examined in detail. Thus, in this study, we evaluated the interaction of fresh human blood with PLGA-coated and uncoated β-TCP scaffolds seeded with undifferentiated or osteogenically induced JPCs. Hemocompatibility tests were performed according to ISO 10993-4 guidelines.

2. Results

2.1. Detection of JPCs on Uncoated and PLGA-Coated β-TCP Scaffolds

Uncoated β-TCP scaffolds showed a rough porous surface, while the PLGA-coated scaffolds showed a smooth and less porous structure (Supplementary Figure S1). The β-TCP scaffolds with and without PLGA coating were seeded with 5×10^4 JPCs and cultured either in hPL10 maintenance medium or osteogenic induction medium and after 15 days, histological sections were generated. Using toluidine blue staining, cells were detected in sections of PLGA-coated as well as uncoated β-TCP scaffolds (Figure 1A) with more intense staining in PLGA-coated β-TCP scaffolds. The presence of cells in the scaffolds was also confirmed by SEM (Figure 1B). Depending on the surface structure of the scaffolds, a confluent layer of cells was detected on smooth scaffold surfaces, but also porous surfaces with cavities contained incorporated cells. JPCs cultivated on PLGA-coated β-TCP scaffolds without osteogenic induction at days 6 and 13 showed a slightly lower cell viability compared to the JPCs on uncoated scaffolds (Figure 1C). However, no significant differences in cell viability were detected with osteogenically induced JPCs at days 6 and 13. The osteogenic induction of JPCs seeded on PLGA-coated β-TCP scaffolds

led to improved cell viability in contrast to JPCs without osteogenic induction at days 6 and 13.

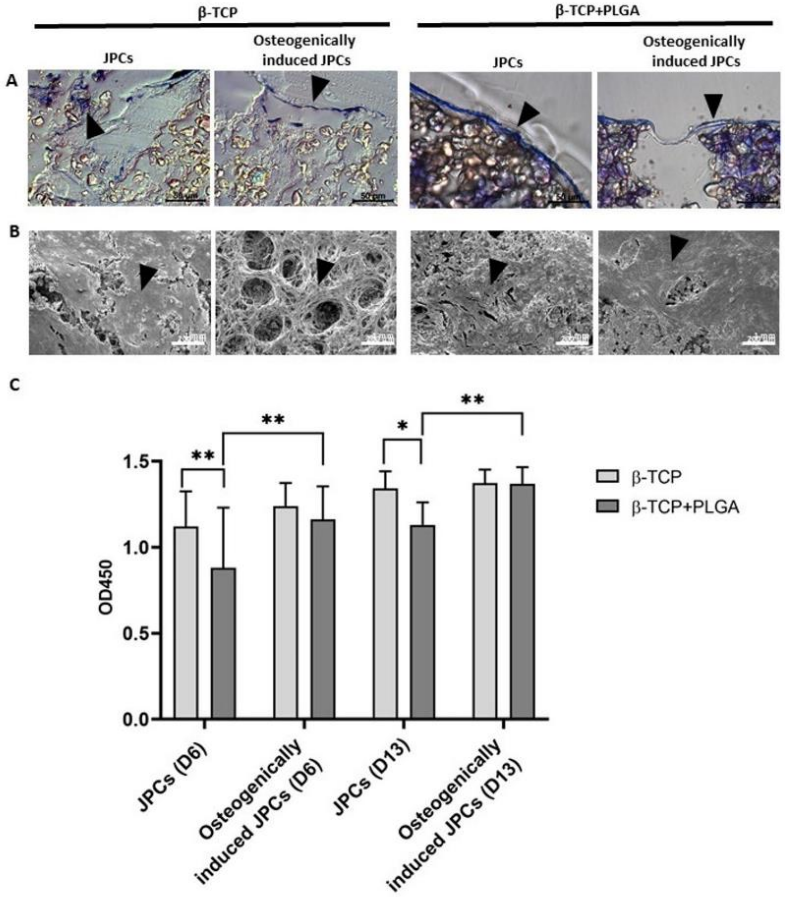

Figure 1. Detection of JPCs on uncoated or PLGA-coated β-TCP scaffolds with and without osteogenic induction and analysis of cell viability. 5×10^4 JPCs were seeded and cultivated for 15 days with or without osteogenic induction medium. (**A**) Histological sections of β-TCP scaffolds with or without PLGA coating were stained with toluidine blue. Arrows indicate toluidine blue-stained cells in histological sections. (**B**) Overview and magnified SEM images of JPCs and osteogenically induced JPCs on β-TCP scaffolds with or without PLGA coating. Black arrows indicate cells on the scaffolds. (**C**) Cell viability was determined by measuring metabolic activity using the colorimetric EZ4U assay. The conversion of tetrazolium salts to formazan derivatives by living cells was measured photometrically at 450 nm. Results are shown as the mean + SD ($n = 3$). Statistical differences were determined using two-way ANOVA (* $p < 0.05$, ** $p < 0.01$).

2.2. Osteogenic Differentiation of JPCs and Cell Mineralization on β-TCP Scaffolds

JPCs were seeded onto β-TCP scaffolds with and without PLGA coating and cultivated with or without osteogenic induction medium. After 6 and 13 days of cultivation, osteogenic differentiation of JPCs was assessed by investigating ALP expression using real-time qRT-PCR, ALP activity, and hydroxyapatite formation (Figure 2).

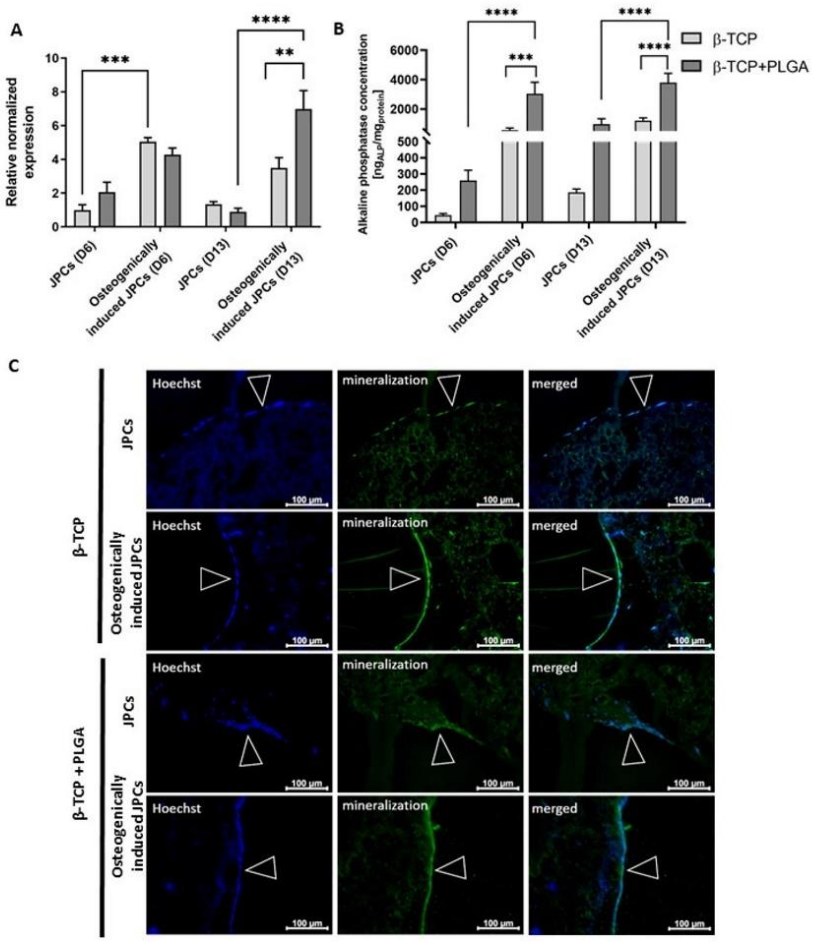

Figure 2. Osteogenic differentiation of JPCs seeded on uncoated and PLGA-coated β-TCP scaffolds. (**A**) Detection of ALP gene expression in JPCs cultivated for 6 and 13 days on uncoated or PLGA-coated β-TCP scaffolds with or without osteogenic induction using qRT-PCR. The mRNA levels were normalized to GAPDH and the results are presented relative to JPCs without osteogenic induction on day 6. Results are shown as the mean + SEM (n = 3). (**B**) Detection of alkaline phosphatase activity of JPCs cultivated on uncoated or PLGA-coated scaffolds with or without osteogenic induction medium using the Sensolyte pNPP Alkaline Phosphatase Colorimetric Assay kit. ALP concentrations were normalized to total protein concentrations, which were determined using a BCA assay. Results are shown as the mean + SEM (n = 3). Statistical differences were determined using two-way ANOVA (** $p < 0.01$, *** $p < 0.001$, **** $p < 0.0001$). (**C**) Detection of mineralization on day 15 in uncoated or PLGA-coated β-TCP scaffolds with and without osteogenic induction using OsteoImaging mineralization assay. Nuclei were stained blue using Hoechst dye. The green fluorescent staining showed cell mineralization. Arrows indicate confluent cell layers on β-TCP scaffolds.

After 6 days of osteogenic induction, significantly increased expression of ALP transcript levels was detected in JPCs cultivated on uncoated β-TCP scaffolds compared to JPCs without osteogenic induction (Figure 2A). After 13 days of cultivation on PLGA-coated β-TCP scaffolds, significantly higher ALP transcript levels were detected in JPCs with osteogenic induction compared to the JPCs without osteogenic induction. The osteogenically induced JPCs on PLGA-coated scaffolds also showed significantly higher ALP transcript levels compared to the JPCs on uncoated β-TCP scaffolds. The osteogenic

stimulation of JPCs on PLGA-coated β-TCP scaffolds resulted in significantly increased ALP activity (Figure 2B). Furthermore, a significantly increased ALP activity was detected at day 6 and 13 in osteogenically stimulated JPCs seeded on PLGA-coated scaffolds compared to those seeded on uncoated scaffolds.

Furthermore, the hydroxyapatite produced by the cells was detected after 15 days of cultivation using the OsteoImage mineralization assay (Figure 2C). An enhanced and continuous mineralization layer was detected in scaffolds cultivated in osteogenic induction medium compared to the scaffolds cultivated in the standard hPL10 maintenance medium, which showed only sporadic mineralization. Thereby, the successful osteogenic differentiation of JPCs was demonstrated in PLGA coated and uncoated β-TCP scaffolds.

2.3. Interaction of β-TCP Scaffolds with Human Blood

β-TCP scaffolds with or without cells were incubated for 90 min at 37 °C with human whole blood to analyze the impact of β-TCP scaffolds and seeded cells on different stages of the hemostatic system.

Analysis of Blood Cell Counts

The interaction of whole blood with biomaterial surfaces can lead to the activation of platelets and leukocytes as well as to the adhesion of these cells to the surface of scaffolds. These interactions can lead to decreased cell numbers in the analyzed blood samples. Therefore, the cell counts were measured before and after the incubation of scaffolds with blood. Performed analyses showed no significant differences in the numbers of platelets, erythrocytes, and leukocytes of the control blood without scaffolds compared to the scaffolds with or without cells and with or without osteogenic induction (Figure 3).

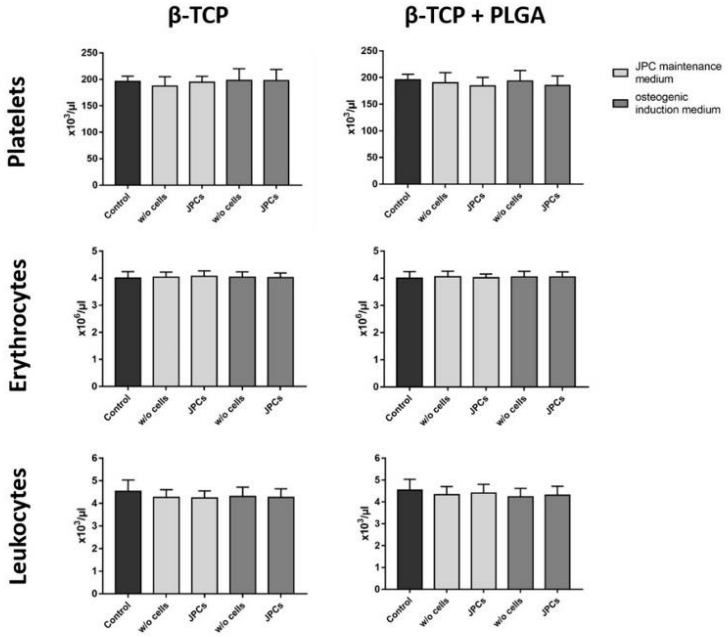

Figure 3. Analysis of blood cell counts after the incubation of blood with β-TCP scaffolds seeded with and without JPCs. PLGA-coated or uncoated β-TCP scaffolds with or without JPCs and with or without osteogenic induction were incubated for 90 min at 37 °C with fresh human blood and the numbers of platelets, erythrocytes, and leukocytes were analyzed. Whole human blood without scaffolds served as a control. Results are shown as the mean + SD (n = 3). Statistical differences were

determined using one-way ANOVA for repeated measurements followed by Bonferroni's multiple comparison test.

2.4. Analysis of Activation Markers

2.4.1. Activation of Leukocytes

The contact of blood with artificial surfaces can trigger inflammatory processes, which can lead to the activation of leukocytes, such as polymorphonuclear (PMN) leukocytes. This can result in the release of the proteolytic enzyme PMN elastase. In this study, incubation of blood with scaffolds alone or with scaffolds colonized with cells did not significantly alter the PMN elastase concentration compared to the control group (Figure 4). Thus, the tested scaffolds and cells did not activate an inflammatory reaction in the analyzed blood samples.

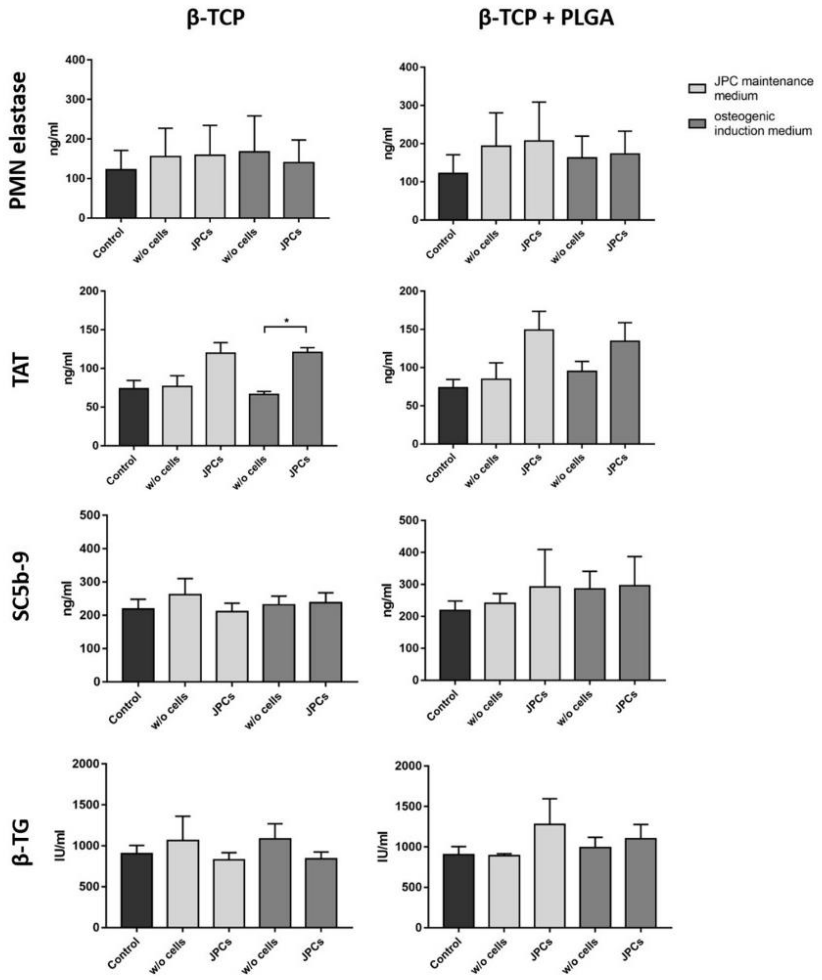

Figure 4. Analysis of hemocompatibility after the incubation of β-TCP scaffolds with and without cells. Analysis of PMN elastase, TAT, SC5b-9, and β-TG concentrations in plasma after the incubation of PLGA-coated or uncoated β-TCP scaffolds with or without JPCs and with or without osteogenic induction for 90 min at 37 °C with fresh human blood. Blood samples without scaffolds served as controls. Results are shown as the mean + SD (n = 3). Statistical differences were determined using Kruskal–Wallis tests followed by Dunn's multiple comparison tests (PMN elastase) or one-way ANOVA followed by Bonferroni's multiple comparison tests.

2.4.2. Activation of the Coagulation System

The interaction of plasma proteins with artificial surfaces can lead to the activation of the intrinsic coagulation pathway. This results in the conversion of prothrombin into thrombin, which in turn leads to the formation of a dense fibrin network. Excessive fibrin formation is counteracted by the coagulation inhibitor antithrombin III, which neutralizes thrombin by forming TAT. Thus, TAT concentration in plasma serves as a marker for the detection of coagulation activation. Scaffolds seeded with JPCs resulted in an increased TAT plasma concentration compared to the scaffolds without cells (Figure 4). In particular, the β-TCP scaffolds seeded with JPCs and cultivated in an osteogenic induction medium led to significantly higher TAT levels. The scaffolds without cells showed similar TAT values as the control.

2.4.3. Activation of the Complement System

The complement system, which consists of more than 30 proteins, is part of the innate immune system. The contact of foreign surfaces with blood can activate the complement cascade and leads to the generation of the terminal complement complex SC5b9 complex. As a final complex, SC5b-9 is well suited as an indicator of complement activation. The incubation of scaffolds with and without cells in human blood did not induce complement activation (Figure 4).

2.4.4. Activation of Platelets

The activation of platelets leads to the release of β-TG, which is stored in alpha granules of platelets. The incubation of uncoated or PLGA coated β-TCP scaffolds with and without cells for 90 min in whole blood did not lead to an increased β-TG concentration (Figure 4). Furthermore, the cultivation of JPCs in osteogenic or maintenance medium did not influence measured β-TG levels in plasma.

2.5. SEM Analyses of the β-TCP Scaffolds after Blood Contact

SEM was performed to visualize potential fibrin deposits and the attachment of platelets to the scaffolds. The overview images of uncoated β-TCP scaffolds without cells showed an intense red coloration (Figure 5). In contrast, PLGA-coated scaffolds without cells showed reduced red accumulations in the cavities of the scaffold and cell-seeded scaffolds were shown to be largely white with only a few red accumulations. SEM images of the scaffolds without cells also showed accumulations of erythrocytes in the cavities of the scaffold. Thus, the visible red color could be caused by the entrapped erythrocytes in the cavities of the scaffolds. JPC seeded scaffolds showed small accumulations of fibrin networks. Below those fibrin fibers, dense JPC layers were visible, which partly covered the cavities and might be responsible for the reduced entrapment of erythrocytes and red coloration of the scaffolds. A confluent cell layer was detected on the surface of PLGA-coated and uncoated scaffolds cultivated in osteogenic induction medium and reduced fibrin networks.

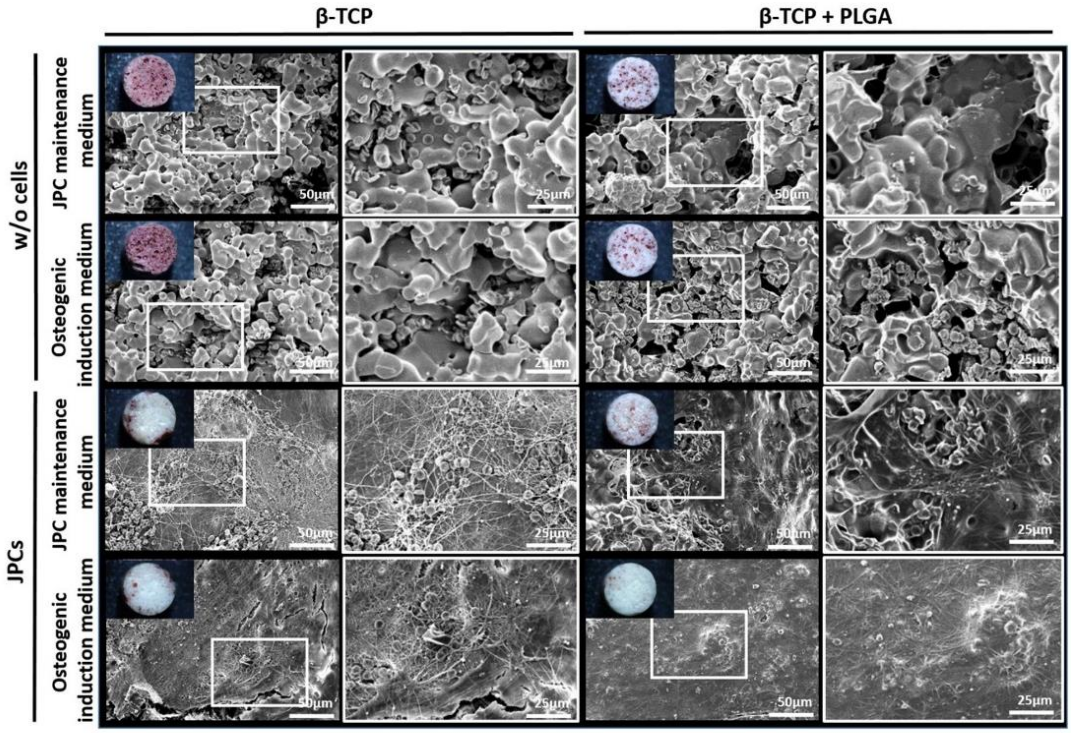

Figure 5. Overview and representative SEM images of β-TCP scaffolds seeded with osteogenically induced and untreated JPCs after the incubation with human blood. SEM images of uncoated and PLGA-coated scaffolds after 90 min of incubation with human whole blood in the rotation model. White frames are showing regions with increased magnification.

3. Discussion

The insertion of implants results in tissue injury and direct contact with blood, which can lead to the activation of platelets, leukocytes, and coagulation [27]. A provisional matrix is formed that influences the subsequent host responses to implants. In addition to the scaffold material, the cells seeded on the scaffolds may also have an impact on hemocompatibility. In this study, we used human fresh blood to analyze the impact of PLGA-coated or uncoated β-TCP scaffolds seeded with untreated or osteogenically induced JPCs on hemocompatibility according to ISO 10993-4 for the biological evaluation of medical devices.

JPCs represent an excellent stem cell type for the repair of small and large bone defects in oral and maxillofacial surgery. The combination of stability-providing scaffolds with cells showing osteogenic potential can be suitable for bone regenerative therapies. Furthermore, the use of PLGA-coated β-TCP scaffolds in combination with JPCs can increase the structural stability of used scaffolds. In addition, the degradation of β-TCP leads to the release of inorganic material such as calcium (Ca^{2+}) and phosphate ions (PO_4^{2-}), which have been shown to support mineralization in osteoblast-like cells [21]. In previous studies, PLGA coating resulted in increased JPC proliferation rates [26]. Furthermore, PLGA can be used for biofunctionalization with growth and/or differentiation factors to improve the biofunctionality of the scaffold [28,29].

In this study, coating of β-TCP scaffolds with PLGA resulted in scaffolds with a smoother and less porous structure than uncoated β-TCP scaffolds. However, both scaffold types proved to be suitable substrates for cell adhesion and supported periosteal cell growth. SEM images showed that uncoated and PLGA-coated β-TCP scaffolds were

uniformly covered with cells. Successful osteogenic differentiation of JPCs on β-TCP scaffolds was confirmed by significantly increased ALP gene expression levels and activity as well as an increased hydroxyapatite deposition (mineralization) compared with constructs seeded with JPCs cultivated in standard hPL10 medium. The herein performed ALP gene expression and ALP activity analyses indicate that the cultivation of JPCs on PLGA coating led to increased osteogenic cell differentiation.

The incubation of PLGA-coated or uncoated β-TCP scaffolds seeded with JPCs or osteogenically induced JPCs with whole fresh blood showed no reduction in blood cell counts compared to the control samples without scaffolds. Furthermore, no inflammatory reactions (PMN elastase), activation of the complement system (SC5b-9), or activation of thrombocytes (β-TG) were detected. Although statistically significant only with osteogenically induced JPCs on uncoated β-TCP scaffolds, increased TAT levels, indicative of coagulation activation, were detected when scaffolds were seeded with periosteal cells. The activation of the coagulation cascade can lead to the generation of thrombin and subsequently to the formation of a fibrin network. SEM analyses also confirmed the formation of a fibrin network with entrapped erythrocytes on the surface of the cell-seeded β-TCP scaffolds. In contrast, erythrocytes without the formation of a fibrin network were detected mainly in the cavities of scaffolds without seeded cells.

The coagulation system can be activated via the contact activation (intrinsic) or the tissue factor (extrinsic) pathway [30]. Previous studies reported that human bone marrow- and periodontal ligament-derived MSCs can lead to thromboembolism after intravenous infusion in mice [31] and intracoronary application in pigs [32]. Intensive investigations revealed that the thromboembolic complications were triggered by the strong expression of the tissue factor on the surface of MSCs and the activation of blood coagulation via the extrinsic pathway [33].

During implantation, injury of the vascularized tissue leads to an immediate development of a provisional matrix at the implant site. The generated fibrin network provides a provisional scaffold for wound healing [34]. This matrix also contains plasma fibronectin, which enhances cell adhesion via integrin receptors. Thereby, the migration and adhesion of various cell types, such as fibroblasts and endothelial cells, are stimulated. The formed matrix can also increase the adhesion and activation of platelets. Activated platelets entrapped in the provisional matrix can release various growth factors, such as PDGF, VEGF, bFGF, and TGF-β, which can further enhance the recruitment of fibroblasts, endothelial cells, and immune cells [35]. Attracted endothelial cells improve angiogenesis and fibroblasts produce extracellular matrix proteins, especially collagen. The formation of new blood vessels plays an important role in supplying oxygen and nutrients to the cells of tissue-engineered constructs, and their timely generation is a critical component for the engraftment of constructs and bone healing [36]. Thus, activation of blood coagulation by JPC-populated β-TCP scaffolds compared to JPCs-free scaffolds could further facilitate neovascularization and healing responses resulting in an improved bone healing process.

4. Materials and Methods

4.1. Coating of β-TCP Scaffolds with PLGA

The TCP scaffolds were coated with PURASORB PLGA (Corbion Purac, Gorinchem, The Netherlands). Briefly, the polymer (ester terminated, inherent viscosity in $CHCl_3$ of 0.4 dL/g) was dissolved in ethyl acetate to obtain a 20% PLGA solution. To perform the PLGA coating, the cylindrical β-TCP scaffolds (Cerasorb M®, Curasan, Kleinostheim, Germany) were immersed in the PLGA solution for 15 min and dried in a desiccator. The polymer uptake was measured by weighing and calculating an average of 20 samples.

4.2. Cultivation of JPCs

JPCs were isolated from the periosteal tissue of three healthy donors after receiving written informed consent. Periosteal tissue was obtained during interventions at the Department of Oral and Maxillofacial Surgery after approval by the local ethical committee (6182017BO2).

The cultivation of JPCs was performed in hPL5 medium consisting of DMEM/F12 (Thermo Fisher Scientific Inc., Waltham, MA, USA) supplemented with 5% human platelet lysate (hPL, ZKT Tübingen GmbH, Germany), 100 U/mL penicillin-streptomycin (Lonza, Basel, Switzerland), and 2.5 µg/mL amphotericin B (Biological Industries, Kibbutz Beit Haemek, Israel) in T75 cell culture flasks at 37 °C and 5% CO_2. The medium was changed every 2–3 days. After reaching 80% confluency, JPCs were detached using TrypleExpress (Thermo Fisher Scientific Inc., Waltham, MA, USA) and the reaction was stopped using hPL5-medium. Afterwards, cells were centrifuged for 5 min at 350× *g* and seeded 1:10 diluted in T75 cell culture flasks.

4.3. Seeding of β-TCP Scaffolds with JPCs and Osteogenic Induction

Uncoated or PLGA-coated β-TCP tricalcium phosphate scaffolds were placed in each well of a 96-well plate and preconditioned with 200 µL hPL5-medium at 37 °C. After 1 h, the medium was aspirated and each scaffold was seeded with 5×10^4 JPCs in 50 µL hPL5 medium. The cells were incubated for 2 h at 37 °C to allow cell adherence and then 150 µL medium was added. After 24 h, scaffolds seeded with cells were transferred into a new 96-well plate and 200 µL hPL10 medium (DMEM/F12 containing 10% hPL, 100 U/mL penicillin-streptomycin (Lonza, Basel, Switzerland), 2.5 µg/mL amphotericin B) or osteogenic induction medium (hPL10 containing 0.1 mM L-ascorbic acid 2-phosphate (Sigma-Aldrich, Taufkirchen, Germany), β-glycerophosphate (AppliChem, Darmstadt, Germany), and 4 µM dexamethasone (Sigma-Aldrich)) were added to each scaffold. Cells seeded onto β-TCP scaffolds were cultivated at 37 °C for 15 days with medium changes every 2–3 days.

4.4. Analysis of Cell Viability of JPCs on β-TCP Scaffolds

The EZ4U kit (Biomedica, Vienna, Austria) was used to compare the mitochondrial activity of JPCs cultured on uncoated or PLGA-coated scaffolds. This analysis was performed on day 6 and day 13 of osteogenic differentiation.

The medium was aspirated from the scaffolds and 200 µL of fresh control JPC standard maintenance (hPL5 medium) or osteogenic induction medium and 20 µL of tetrazolium salt substrate was added to each well. After 3 h of incubation at 37 °C and 5% CO_2, 150 µL were pipetted into a new 96-well plate and absorbance was measured at a wavelength of 450/620 nm using an ELx800 microplate reader (Bio-Tek, Winooski, VT, USA). KC4 software was used for analysis.

4.5. RNA Isolation from JPCs Cultured on β-TCP Scaffolds

Cell-seeded scaffolds were transferred to LysingMatrix D Tubes (MP Biomedicals, Santa Ana, CA, USA) containing 600 µL RA1 buffer + TCEP (NucleoSpin RNA Mini Kit, Macherey Nagel, Düren, Germany). Thereafter, samples were homogenized using the FastPrep-24 instrument (MP BiomedicalsSanta Ana, CA, USA). After centrifugation, 500 µL supernatant was transferred into a microcentrifuge tube and total RNA was isolated using the NucleoSpin RNA Mini Kit (Macherey Nagel, Düren, Germany) according to the manufacturer's instructions.

4.6. qRT-PCR Analysis

Total RNA was isolated from JPC seeded β-TCP scaffolds 6 and 13 days after starting the osteogenic induction). As a control, the RNA was isolated from JPC seeded β-TCP

scaffolds cultured without osteogenic activators. Complementary DNA (cDNA) was obtained by reverse transcription of 25 ng RNA using the iScript kit (Bio-Rad, Munich, Germany). For the specific amplification of osteogenic markers, the following primers were ordered from Eurofins (Luxemburg, Luxemburg): Alkaline phosphatase (ALP) (forward primer: 5′TGTTCCTGGGAGATGGGTCAG-3′ and reverse primer: 5′CTTGGAGAGGGCCACGAAG-3′). Primers were designed by using the Primer-Blast tool from NCBI [37]. Melting temperatures and self-complementarities were checked using the oligonucleotide properties calculator from Northwestern University Medical School [38]. Real-time qRT-PCR was performed using 300 nM primers, IQ™ SYBR®Green Supermix (Bio-Rad), and CFX Connect Real-Time PCR Detection System (Bio-Rad). The amplification of cDNA was performed under the following conditions: 3 min at 95 °C for one cycle, followed by 40 cycles of 95 °C for 15 s, 60 °C for 30 s, and 72 °C for 10 s. Melting curve analysis was performed to ensure the specificity of the PCR products. The samples were run in triplicate with a total volume of 15 µL per well. Levels of mRNA for each gene were normalized to the constitutively expressed internal standard gene glyceraldehyde-3-phosphate dehydrogenase (GAPDH). The results were shown relative to the mRNA levels of JPCs cultivated in a standard maintenance medium (hPL10).

4.7. Analysis of Alkaline Phosphatase (ALP) Activity of JPCs in β-TCP Scaffolds.

The ALP activity of JPCs on uncoated and coated β-TCP scaffolds was analyzed on day 6 and day 13 of osteogenic differentiation. Four scaffolds were used for each sample. Four scaffolds incubated with the standard JPC maintenance medium during the same time served as controls.

Analysis was performed using the Sensolyte pNPP alkaline phosphatase colorimetric assay kit (AnaSpec, Fremont, CA, USA). For extraction of cell lysates, scaffolds were crushed using MagNA Lyser Green Beads tubes (Roche Diagnostics, Rotkreuz, Switzerland) and a FastPrep®-24 device (MP Biomedicals, Santa Ana, CA, USA). For this purpose, MagNA Lyser Green Beads tubes (Roche Diagnostics, Germany) were first filled with 600 µL lysis buffer and placed on ice. The scaffolds were washed twice with 200 µL assay buffer and four scaffolds of the same condition were transferred into one tube. Subsequently, the scaffolds were disrupted using the FastPrep®-24 device (MP Biomedicals, Santa Ana, CA, USA) and the cells were lysed during this process. After cooling on ice, the tubes were centrifuged (10,000× *g* at 4 °C, 10 min) and 400 µL of the supernatant was pipetted into a fresh 2 mL tube. Then, the sample was centrifuged again (2500× *g*, 4 °C, 10 min) and 350 µL of the clear cell lysate was transferred to a fresh 2 mL tube. Samples were diluted 1:5 and 1:10 with assay buffer and standards with a known ALP concentration were prepared. 50 µL of the diluted cell suspensions and standards were pipetted into a 96-well plate and 50 µL of pNPP substrate solution was added. After 30 min of incubation at room temperature, 50 µL of stop solution was added to terminate the reaction. Subsequently, absorbance was measured at a wavelength of 405 nm using an ELx800 plate reader (Bio-Tek, Winooski, VT, USA).

To account for possible differences in cell numbers on the scaffolds, the determined ALP concentration was normalized to the total protein concentration. This was determined using the Pierce BCA Protein Assay Kit (Thermo Fisher Scientific Inc., Waltham, MA, USA) according to the manufacturer's instructions. Using an ELx800 plate reader (Bio-Tek, Winooski, VT, USA), the absorbance at a wavelength of 550 nm was measured. KC4 software was used for analysis. Based on the ALP concentration and the total protein concentration, the ALP fraction in the total protein concentration (ng AP/mg protein) was calculated.

4.8. Embedding and Generation of thin Polished Sections of β-TCP Scaffolds Seeded with JPCs

After 15 days of cultivation, the scaffolds seeded with JPCs were washed twice in phosphate-buffered saline (PBS) without Mg^{2+} und Ca^{2+}, fixed in 4% paraformaldehyde (PFA), and washed again twice in PBS. Ascending alcohol series (70%, 80%, 96%, 2 × 100%

EtOH, 15 min each) and xylene (2 x 100%, 30 min each) were used for dehydration and degreasing. To facilitate polymethyl methacrylate (PMMA) infiltration, the samples were incubated twice for 1 h in absolute acetone. Subsequently, the scaffolds were transferred into 2 mL microcentrifuge tubes and treated overnight at 4 °C with 300 µL of solution A (500 mL destabilized base solution, 25 g PMMA powder, 3 g hardener 1, Technovit 9100 (Kulzer, Wehrheim, Germany)). The next day, samples were embedded in 2 mL embedding solution (9 parts solution A with 1 part solution B (44 mL base solution, 4 mL hardener, and 2.2 mL regulator), Technovit 9100). The embedding solution was cured overnight at −18 °C in the absence of oxygen, and then for 24 h at 4 °C. Subsequently, the samples were transferred for 1 h into a 37 °C water bath for complete polymerization of the embedding solution.

Embedded scaffolds were cut to sections of 5 µm using an electronic rotary microtome (pfm Rotary 3006 EM; pfm medical AG, Cologne, Germany) with a hard-cutting blade (SH35W Feather microtome blade HP TC; Feather Safety Razor Co., LTD., Osaka, Japan). To stabilize the samples, sections were collected on transparent adhesive tape (tesafilm, Beiersdorf AG, Norderstedt, Germany) and transferred to microscope slides.

4.9. Toluidine Blue Staining

First, the sections were acidified with 10% acetic acid for 5 min, washed with distilled water, and dried. In the next step, a drop of the toluidine staining solution (0.1% (*w*/*v*) toluidine blue O (Sigma-Aldrich) in distilled water) was added and incubated for 15 min. The sections were then rinsed with distilled water and dried overnight and mounted using DePeX (Serva, Heidelberg, Germany) and coverslips.

4.10. Analysis of Mineralization

After 15 days of JPC cultivation and osteogenic stimulation on β-TCP scaffolds, constructs were analyzed via OsteoImage™ mineralization assay kit (Lonza, Basel, Switzerland). Briefly, microtome sections of PMMA (Technovit 9100) embedded scaffolds were first deacrylated and then stained with the OsteoImage Mineralization Assay Kit (Lonza, Walkersville, MD, USA) for the detection of hydroxyapatite. Hoechst 33,342 (PromoKine, Heidelberg, Germany) was used as a nuclear counterstain.

For deacrylation, microtome sections were placed in a cuvette with 100% xylene for one min and then dried in a drying cabinet at 37 °C for at least 30 min. Next, the staining solution (Staining Reagent diluted 1:100 in Staining Reagent Dilution Buffer, OsteoImage Mineralization Assay)) was added to the samples and incubated for 30 min in the dark. After the washing with OsteoImage Wash Buffer, Hoechst 33,342 nuclear staining solution (1:1000 dilution of stock solution in PBS) was added to the samples for 10 min. After washing and drying, the sections were mounted with glycerol.

4.11. Analysis of Hemocompatibility

4.11.1. Collection of Human Blood

Human whole blood was collected from the antecubital vein of non-medicated healthy volunteers (n = 3) via venipuncture in monovettes preloaded with 1 IU/mL sodium heparin (LEO Pharma Inc., Neu-Isenburg, Germany). The blood sampling procedure was approved by the Ethics Committee of the medical faculty at the University of Tuebingen (287/2020BO2) and all subjects gave written informed consent.

4.11.2. Incubation of Scaffolds with Whole Human Blood

β-TCP scaffolds seeded with JPCs were cultivated in vitro for 15 days. The scaffolds were then transferred into 12 mL polypropylene round-bottom tubes (Becton Dickinson, Franklin Lakes, NJ, USA) containing 11 mL blood. Control tubes contained the same amount of fresh blood without scaffolds. The incubation with blood was performed at 37 °C for 90 min using a tube rotator (neoLab, Heidelberg, Germany) with 10 rpm. After 90

min, blood was transferred into monovettes containing ethylenediaminetetraacetic acid (EDTA) (Sarstedt Inc., Nümbrecht, Germany) for the analysis of complement activation and detection of cell numbers. Blood cell numbers were determined using a Micros 60 cell counter (ABX Diagnostics, Montpellier, France). A citrate solution containing monovettes (Sarstedt Inc.) was used to analyze PMN-elastase and TAT. To analyze β-TG concentrations, blood was transferred to citrate-theophylline-adenosine-dipyridamole (CTAD) containing monovettes (BD Biosciences Inc.) and stored for 15 min on ice. EDTA and CTAD monovettes were centrifuged at 2500× *g* for 20 min at 4 °C. Citrate blood monovettes were centrifuged at 1800× *g* for 18 min at RT. The plasma of each sample was shock frozen in liquid nitrogen and stored at −20 °C (EDTA and citrate plasma) or −80 °C (CTAD plasma) until further investigations.

4.11.3. Detection of Activation Markers

Commercially available enzyme-linked immunosorbent assays (ELISA) were used to investigate the hemocompatibility. The PMN-elastase ELISA (Demeditec, Kiel, Germany) was used to detect the activation of leukocytes. The activation of coagulation was detected using TAT ELISA (Enzygnost Micro Assay, Siemens Healthcare, Erlangen, Germany). Furthermore, SC5b-9 ELISA (Osteomedical GmbH, Bünde, Germany) was used to detect the complement activation and platelet activation was determined using β-TG ELISA (ASSERA-CHROM®, Diagnostica Stago, Asnieres, France). The ELISAs were performed according to the manufacturer's instructions.

4.11.4. Scanning Electron Microscopy (SEM)

After the incubation with blood, the β-TCP scaffolds were fixed overnight at 4 °C in 2% glutaraldehyde (Serva, Heidelberg, Germany). Overview images were taken with a Canon reflex camera EOS 450D (Canon, Tokyo, Japan) and a NOVEX RZB-SF stereo microscope (Euromex, Arnhem, The Netherlands). Afterwards, the samples were washed with PBS for 10 min and dehydrated with an ascending ethanol series (40% to 100% ethanol; Merk, Darmstadt, Germany) in 10 min steps. The scaffolds were dried in a critical point drier (Polaron E3100, GaLa Instruments, Bad Schwalbach, Germany). Subsequently, the scaffolds were sputtered with gold-palladium particles (Emitech K550X, GaLa Instruments, Bad Schwalbach, Germany) and analyzed by SEM (Zeiss LEO1430, Zeiss, Oberkochen, Germany).

4.12. Statistical Analysis

Data are shown as the mean + standard deviation (SD) or standard error of the mean (SEM). Means were compared using one or two-way analysis of variance (ANOVA) for repeated measurements followed by Bonferroni's multiple comparison test or using the Kruskal–Wallis test followed by Dunn's multiple comparisons test, depending on the distribution of the data. Statistical analyses were performed double-tailed using GraphPad Prism 6.01 (GraphPad Software, La Jolla, CA, USA). Differences of $p < 0.05$ were considered significant.

5. Conclusions

In this study, we demonstrated that uncoated and PLGA-coated β-TCP scaffolds are highly suitable for the colonization with JPCs and their further osteogenic differentiation. The osteogenic induction resulted in mineralization and increased expression of and ALP. Cell-free β-TCP scaffolds with and without PLGA coating showed no effect on blood cells, complement, and coagulation activation. In contrast, scaffolds seeded with JPCs led to increased levels of TAT and accumulation of fibrin fibers on the surface of the constructs, presumably through activation of the extrinsic coagulation pathway. These results demonstrated that hemocompatibility can not only be influenced by the scaffold material

alone but also by seeded cells inside the scaffolds, which can have an impact on tissue compatibility and the healing process within the bone defect.

Supplementary Materials: The following are available online at www.mdpi.com/article/10.3390/ijms22189942/s1.

Author Contributions: Conceptualization, D.A. and M.A.-A.; data curation, M.W.; formal analysis, M.W.; funding acquisition, D.A. and M.A.-A.; investigation, M.W., F.U., H.S., L.-F.S., and L.T.Y.; methodology, F.U., and H.S.; project administration, C.S., H.-P.W., S.R., and M.A.-A.; resources, D.A.; supervision, C.S., H.-P.W., S.R., D.A., and M.A.-A.; visualization, M.W.; writing—original draft, M.W.; writing—review and editing, F.U., D.A., and M.A.-A. All authors have read and agreed to the published version of the manuscript.

Funding: This study was funded by the German Research Foundation (Deutsche Forschungsgemeinschaft, DFG) through AV 133/7-3/AL 1486/6-3.

Institutional Review Board Statement: The study was conducted according to the guidelines of the Declaration of Helsinki, and approved by the Ethics Committee of the Medical Faculty of the University of Tuebingen (6182017BO2)/(287/2020BO2).

Informed Consent Statement: Informed consent was obtained from all subjects involved in the study.

Data Availability Statement: The analyzed data sets generated during the study are available from the corresponding author on reasonable request.

Acknowledgments: The authors gratefully acknowledge the support by Deutsche Forschungsgemeinschaft and the Open Access Publishing Fund of the University of Tübingen.

Conflicts of Interest: All authors declare no competing financial interests relevant to the submitted work.

References

1. Guan, M.; Yao, W.; Liu, R.; Lam, K.S.; Nolta, J.; Jia, J.; Panganiban, B.; Meng, L.; Zhou, P.; Shahnazari, M.; et al. Directing mesenchymal stem cells to bone to augment bone formation and increase bone mass. *Nat. Med.* **2012**, *18*, 456–462.
2. Vertenten, G.; Lippens, E.; Gironès, J.; Gorski, T.; Declercq, H.; Saunders, J.; Van den Broeck, W.; Chiers, K.; Duchateau, L.; Schacht, E.; et al. Evaluation of an injectable, photopolymerizable, and three-dimensional scaffold based on methacrylate-endcapped poly(D,L-lactide-co-epsilon-caprolactone) combined with autologous mesenchymal stem cells in a goat tibial unicortical defect model. *Tissue Eng Part A* **2009**, *15*, 1501–1511.
3. Caplan, A.I. Mesenchymal stem cells. *J. Orthop. Res.* **1991**, *9*, 641–650.
4. Halleux, C.; Sottile, V.; A Gasser, J.; Seuwen, K. Multi-lineage potential of human mesenchymal stem cells following clonal expansion. *J. Musculoskelet Neuronal Interact* **2001**, *2*, 71–76.
5. Olbrich, M.; Rieger, M.; Reinert, S.; Alexander, D. Isolation of osteoprogenitors from human jaw periosteal cells: A comparison of two magnetic separation methods. *PLoS ONE* **2012**, *7*, e47176.
6. De Bari, C.; Dell'Accio, F.; Vanlauwe, J.; Eyckmans, J.; Khan, I.; Archer, C.W.; Jones, E.A.; McGonagle, D.; Mitsiadis, T.; Pitzalis, C.; et al. Mesenchymal multipotency of adult human periosteal cells demonstrated by single-cell lineage analysis. *Arthritis Rheum.* **2006**, *54*, 1209–1221.
7. Bruder, S.P.; Jaiswal, N.; Haynesworth, S.E. Growth kinetics, self-renewal, and the osteogenic potential of purified human mesenchymal stem cells during extensive subcultivation and following cryopreservation. *J. Cell Biochem.* **1997**, *64*, 278–294.
8. Akintoye, S.O.; Lam, T.; Shi, S.; Brahim, J.; Collins, M.T.; Robey, P. Skeletal site-specific characterization of orofacial and iliac crest human bone marrow stromal cells in same individuals. *Bone* **2006**, *38*, 758–768.
9. Alexander, D.; Hoffmann, J.; Munz, A.; Friedrich, B.; Geis-Gerstorfer, J.; Reinert, S. Analysis of OPLA scaffolds for bone engineering constructs using human jaw periosteal cells. *J. Mater. Sci. Mater Med.* **2008**, *19*, 965–974.
10. Roberts, S.J.; van Gastel, N.; Carmeliet, G.; Luyten, F.P. Uncovering the periosteum for skeletal regeneration: The stem cell that lies beneath. *Bone* **2015**, *70*, 10–18.
11. Ferretti, C.; Mattioli-Belmonte, M. Periosteum derived stem cells for regenerative medicine proposals: Boosting current knowledge. *World J. Stem Cells* **2014**, *6*, 266–277.
12. Nakahara, H.; Bruder, S.P.; Goldberg, V.M.; I Caplan, A. In vivo osteochondrogenic potential of cultured cells derived from the periosteum. *Clin. Orthop. Relat. Res.* **1990**, *259*, 223–232.
13. Ghassemi, T.; Shahroodi, A.; Ebrahimzadeh, M.H.; Mousavian, A.; Movaffagh, J.; Moradi, A. Current Concepts in Scaffolding for Bone Tissue Engineering. *Arch. Bone Jt Surg.* **2018**, *6*, 90–99.

14. Przekora, A.; Vandrovcova, M.; Travnickova, M.; Pajorova, J.; Molitor, M.; Ginalska, G.; Bacakova, L. Evaluation of the potential of chitosan/beta-1,3-glucan/hydroxyapatite material as a scaffold for living bone graft production in vitro by comparison of ADSC and BMDSC behaviour on its surface. *Biomed Mater.* **2017**, *12*, 015030.
15. Przekora, A.; Czechowska, J.; Pijocha, D.; Ślósarczyk, A.; Ginalska, G. Do novel cement-type biomaterials reveal ion reactivity that affects cell viability in vitro? *Cent. Eur. J. Biol.* **2014**, *9*, 277–289.
16. Maquet, V.; Boccaccini, A.R.; Pravata, L.; Notingher, I.; Jérôme, R. Preparation, characterization, and in vitro degradation of bioresorbable and bioactive composites based on Bioglass-filled polylactide foams. *J. Biomed Mater. Res. A* **2003**, *66*, 335–346.
17. Fairag, R.; Rosenzweig, D.H.; Garcialuna, J.L.R.; Weber, M.H.; Haglund, L. Three-Dimensional Printed Polylactic Acid Scaffolds Promote Bone-like Matrix Deposition in Vitro. *ACS Appl. Mater. Interfaces* **2019**, *11*, 15306–15315.
18. Putri, T.S.; Hayashi, K.; Ishikawa, K. Bone regeneration using β-tricalcium phosphate (β-TCP) block with interconnected pores made by setting reaction of β-TCP granules. *J. Biomed. Mater. Res. Part A* **2020**, *108*, 625–632.
19. Müller, P.; Bulnheim, U.; Diener, A.; Lüthen, F.; Teller, M.; Klinkenberg, E.-D.; Neumann, H.-G.; Nebe, B.; Liebold, A.; Steinhoff, G.; et al. Calcium phosphate surfaces promote osteogenic differentiation of mesenchymal stem cells. *J. Cell Mol. Med.* **2008**, *12*, 281–291.
20. Wang, J.; Chen, W.; Li, Y.; Fan, S.; Weng, J.; Zhang, X. Biological evaluation of biphasic calcium phosphate ceramic vertebral laminae. *Biomaterials* **1998**, *19*, 1387–1392.
21. Chang, Y.L.; Stanford, C.M.; Keller, J.C. Calcium and phosphate supplementation promotes bone cell mineralization: Implications for hydroxyapatite (HA)-enhanced bone formation. *J. Biomed Mater. Res.* **2000**, *52*, 270–278.
22. Dorozhkin, S.V. Calcium Orthophosphate-Based Bioceramics. *Materials* **2013**, *6*, 3840–3942.
23. Baino, F. Biomaterials and implants for orbital floor repair. *Acta Biomater* **2011**, *7*, 3248–3266.
24. Wang, G.; Li, Y.; Sun, T.; Wang, C.; Qiao, L.; Wang, Y.; Dong, K.; Yuan, T.; Chen, J.; Chen, G.; et al. BMSC affinity peptide-functionalized beta-tricalcium phosphate scaffolds promoting repair of osteonecrosis of the femoral head. *J. Orthop. Surg. Res.* **2019**, *14*, 204.
25. Yang, D.-J.; Jeon, J.-H.; Lee, S.-Y.; An, H.-W.; Park, K.O.; Park, K.-B.; Kim, S. Effects of Collagen Grafting on Cell Behaviors in BCP Scaffold with Interconnected Pore Structure. *Biomater Res.* **2016**, *20*, 3.
26. Ardjomandi, N.; Henrich, A.; Huth, J.; Klein, C.P.A.T.; Schweizer, E.; Scheideler, L.; Rupp, F.; Reinert, S.; Alexander, D. Coating of ss-tricalcium phosphate scaffolds-a comparison between graphene oxide and poly-lactic-co-glycolic acid. *Biomed Mater* **2015**, *10*, 045018.
27. Liu, X.; Yuan, L.; Li, D.; Tang, Z.; Wang, Y.; Chen, G.; Chen, H.; Brash, J.L. Blood compatible materials: State of the art. *J. Mater. Chem. B* **2014**, *2*, 5718–5738.
28. Jeon, O.; Song, S.J.; Yang, H.S.; Bhang, S.-H.; Kang, S.-W.; Sung, M.A.; Lee, J.H.; Kim, B.-S. Long-term delivery enhances in vivo osteogenic efficacy of bone morphogenetic protein-2 compared to short-term delivery. *Biochem. Biophys. Res. Commun.* **2008**, *369*, 774–780.
29. Jeon, O.; Song, S.J.; Kang, S.-W.; Putnam, A.; Kim, B.-S. Enhancement of ectopic bone formation by bone morphogenetic protein-2 released from a heparin-conjugated poly(L-lactic-co-glycolic acid) scaffold. *Biomaterials* **2007**, *28*, 2763–2771.
30. Weber, M.; Steinle, H.; Golombek, S.; Hann, L.; Schlensak, C.; Wendel, H.P.; Avci-Adali, M. Blood-Contacting Biomaterials: In Vitro Evaluation of the Hemocompatibility. *Front. Bioeng. Biotechnol.* **2018**, *6*, 99.
31. Tatsumi, K.; Ohashi, K.; Matsubara, Y.; Kohori, A.; Ohno, T.; Kakidachi, H.; Horii, A.; Kanegae, K.; Utoh, R.; Iwata, T.; et al. Tissue factor triggers procoagulation in transplanted mesenchymal stem cells leading to thromboembolism. *Biochem. Biophys. Res. Commun.* **2013**, *431*, 203–209.
32. Gleeson, B.M.; Martin, K.; Ali, M.T.; Kumar, A.; Pillai, M.G.-K.; Kumar, S.P.G.; O'Sullivan, J.; Whelan, D.; Stocca, A.; Khider, W.; et al. Bone Marrow-Derived Mesenchymal Stem Cells Have Innate Procoagulant Activity and Cause Microvascular Obstruction Following Intracoronary Delivery: Amelioration by Antithrombin Therapy. *STEM CELLS* **2015**, *33*, 2726–2737.
33. Coppin, L.; Sokal, E.; Stephenne, X. Thrombogenic Risk Induced by Intravascular Mesenchymal Stem Cell Therapy: Current Status and Future Perspectives. *Cells* **2019**, *8*, 1160.
34. Laurens, N.; Koolwijk, P.; de Maat, M.P. Fibrin structure and wound healing. *J. Thromb. Haemost* **2006**, *4*, 932–939.
35. Olczyk, P.; Mencner, L.; Komosinska-Vassev, K. The role of the extracellular matrix components in cutaneous wound healing. *BioMed Res. Int.* **2014**, *2014*, 747584.
36. Stegen, S.; van Gastel, N.; Carmeliet, G. Bringing new life to damaged bone: The importance of angiogenesis in bone repair and regeneration. *Bone* **2015**, *70*, 19–27.
37. Ye, J.; Coulouris, G.; Zaretskaya, I.; Cutcutache, I.; Rozen, S.; Madden, T.L. Primer-BLAST: A tool to design target-specific primers for polymerase chain reaction. *BMC Bioinform.* **2012**, *13*, 134.
38. Kibbe, W.A. OligoCalc: An online oligonucleotide properties calculator. *Nucleic Acids Res.* **2007**, *35*, W43–W46.